Mechanistic Modelling of Microscale Chromatography

Nick Whitelock

Industrial Supervisors

Dr. Mari Spitali & Dr. Razwan Hanif

Academic Supervisor

Dr. Vladimir Zivkovic

A thesis presented for the degree of Engineering Doctorate in

Biopharmaceutical Process Development

Biopharmaceutical & Bioprocessing Technology Centre, School of Chemical Engineering and Advanced Materials, Newcastle University

August 2021

For James, Pat and Sophie

Acknowledgments

There are too many people deserving of gratitude to give justice to here, so I shall mention just a small proportion without whom none of this would have been possible.

The staff of the School of Chemical Engineering and Advanced Materials at Newcastle University, are highly appreciated due to providing the training, support and direction needed to take on this work. In particular, my academic supervisors Dr. Vladimir Zivkovic, Dr Milan Mijajlovic and Dr. Moritz von Stosch, who, though joining the project late, provided a huge amount of ideas, enthusiasm and their valuable time. I have thoroughly enjoyed working with them and cannot adequately express how much their hard work, insight and advice has meant to myself and the project. Additionally, the administrative staff at Newcastle University, in particular Nikki Hawley, have always managed to provide much appreciated organisation of supplies, accommodation and meals for stressed students. The other students and teaching staff at Newcastle maintained a jovial atmosphere, and somehow made learning often obtuse, unintuitive concepts a fun experience. I remember fondly many good times in the Toon, and am glad for the friends and experiences I made there.

Without the stipend and course fees provided by the EPSRC, I could not have undertaken this course, and will be forever grateful for the funding and opportunities I received.

I owe a debt of gratitude to UCB, who provided the materials, location and direction of this project, in particular, Dr. Mari Spitali, whose patience and encouragement was unwavering, if not always merited. Dr. Razwan Hanif has provided a free reign to explore well outside of the project remit with a lot of support and ideas. Additionally, a number of people have contributed ideas that have turned out to be fruitful, including Chris Morris, Mark Pearce-Higgins, Didier Philippe and Neil Watson. The welcome afforded to me by all the staff in the downstream process development group at UCB was highly appreciated.

I would never have completed this without my friends and family, who have tolerated having the same conversation with me for the past few years; Sophie Porret who has missed evenings, weekends and holidays as I focussed on this work (and managed to make a beautiful son whilst I struggled through a thesis!), my grandmother, Pat, has been a constant inspiration and is very sorely missed, and finally my father Chris, who has been a continual source of sage advice, no matter how often it was ignored.

Contents

List of Figures

List of Tables

Symbols and Abbreviations

a280 - Absorbance of 280nm radiation, measured in Absorbance Units

A_x - Absorbance at wavelength x

AcO - Acetone

AEX - Anion Exchange

ANOVA – Analysis of Variance

AU - Absorbance Units

BTC – Breakthrough Curve

CCCF- Clarified Cell Culture Fluid

CEX - Cation Exchange

CHO – Chinese Hamster Ovary

CPP - Critical Process Parameter

CQA - Critical Quality Attribute

CSTR – Continuous stirred tank reactor

CV – Column Volume

Da - Dalton

DBC - Dynamic Binding Capacity

DLVO - Derjaguin-Landau-Verwey-Overbeek

DMF – Dimethyl Formamide

DoE - Design of Experiments

EBC – Equilibrium Binding Capacity

ED – Equilibrium Dispersive

EMG - Exponentially Modified Gaussian

Fab - Antibody-Antigen binding fragment

FDA – US Food and Drug Administration

FPLC - Fast protein liquid chromatography (interchangeable with HPLC in some applications)

HCP - Host Cell Proteins

HEK – Human Embryonic Kidney

HETP - Height Equivalent to a Theoretic Plate

HPLC – High performance/pressure liquid chromatography

HTPD - High Throughput Process Development

ID- Internal Diameter

IEX - Ion Exchange Chromatography

IgG - Immunoglobulin class G

IP – Intellectual Property

LHS -Liquid Handling System

M - Mole/L

mAb – Monoclonal antibody

Mol = 6.022×10^{23}

mAb - Monoclonal Antibody

MSS - MabSelect SuRe

MSSLX – MabSelect SuRe LX

NaCl – Sodium Chloride

PABA – Para (4)-aminobenzoic acid

PCA - Principal Component Analysis

PES- Polyethersulfone

PFR – Plug flow reactor

PLS - Projection to Latent Structures/Partial Least Squares

PLW – Post load wash

PrA - Protein A

PTM – Post translational modification

QbD - Quality by Design

R^2 – Coefficient of determination

RMM – Relative Molecular Mass

SMA – Steric Mass Action

UCB - Union Chemique Belge

UV - Ultraviolet

Mechanistic Model Terms

c- Mobile phase concentration

d_p – Particle diameter

D_{ax} – Axial Dispersion Coefficient

D_L – Apparent axial dispersion Coefficient

D_M - Molecular diffusivity

D_p – Pore diffusion Coefficient

H – Height Equivalent to a Theoretical Plate (see HETP)

k_{ads} – Adsorption rate

k_{des} – Desorption rate

k_p – Partition coefficient

K_{eq} - Langmuir equilibrium constant

k_f- Film diffusion coeffient

R_p - Particle radius

Re- Reynolds number

s - Second

Sc – Schmidt number

Sh – Sherwood number

q_{max} -Maximum adsorption capacity

k' – Retention coefficient

k_f – Film diffusion coefficient

M - Molar mass

q – Stationary phase concentration

Q – Volumetric flowrate

R_p – Particle radius

u – Interstitial flow velocity

V_x - Volume, relating to system x

v – Superficial flow velocity

β – Pore fraction (subscript p for particle, b for bed)

ε - Molar Extinction coefficient (subscript wavelength) or porosity (subscript b for bed, p for particle, t for total and eff for effective particle porosity)

λ – Wavelength

τ – Bead tortuosity or characteristic time

ϒ – Coefficient for Ruthven's axial dispersion correlation

υ – Kinematic Viscosity

EMG Terms

h – EMG peak height

μ_g - Gaussian Peak Position

σ_g - Gaussian Peak Width

τ - Exponential decay coefficient

HETP Terms

a - Peak width right of centre

b – Peak width, left of centre

h - Peak Height

HETP – height equivalent to a theoretical plate (see H).

M_n - n^{th} statistical moment

N – Plate count

μ - First absolute moment

σ^2 – Variance/second absolute moment

As - Asymmetry

$W_{1/2}$ – Peak width at half maximum

Abstract

Microscale chromatography as an experimental tool has shown much utility in process development due to reduced material consumption and ease of parallelisation which are of major benefit when compared to conventional lab-scale studies. Microscale columns are commonly used in early process development where the most impactful decisions, such as choice of unit operation, purification strategy, resin, and the choice of candidate are made with limited resources and knowledge. Understanding the behaviour of microscale chromatography and better applying the knowledge gained from microscale studies to large scale chromatography may allow faster, more efficient and more robust early process development, and therefore more effective processes once a bioprocess is fully developed and products commercialised. It is the overall aim of the project to develop a model to determine large scale mass transfer parameters describing a lab-scale chromatographic process from microscale data, and allow one to simulate and optimise large scale separations whilst enjoying the benefits of reduced resource consumption of the microscale domain.

From the outset, characterisation of the differences between lab-scale columns operated on a conventional Fast Protein Liquid Chromatography (FPLC) system and microscale columns on a robotic Liquid Handling System (LHS) was performed. Determining the common metrics of column performance, HETP, asymmetry and experiment-to-experiment or column-to-column variation between columns and experiments provides an understanding of some of the key differences between lab-scale and microscale column formats with regards to system, scale and data quality, as well as providing an opportunity to optimise the experimental design of microscale experiments. This was performed through evaluating methods of improving resolution, including fashioning rigs to use microscale columns on a conventional system, evaluating various tracer substances and evaluating a novel strategy of pre-filling collection plates.

Investigations into ascertaining the dynamic binding capacity (DBC) of IgG to Protein A resin using microscale data has been performed with 3 microscale column volumes at several residence times using the high throughput system, and repeated at lab scale, with further work into understanding the effect of intermittent flow on resin: target interaction by mimicking the microscale operation on a larger system.

This effort has led towards data used to calibrate a mechanistic model of chromatography at both lab scale and microscale with the intention of predicting lab scale behaviour. By correcting for scale, operational and flow effects, one may predict large scale performance through calibrating a model with microscale data, enabling better process understanding with reduced material consumption.

Impact Statement

It is hoped the work presented here may aid in others for better understanding microscale chromatography, as well as how to improve the data obtained when running microscale experiments. A number of minor contributions to the field of microscale chromatography have been highlighted, through some novel experimental techniques such as improved resolution due to plate pre-filling, by improving the range of flowrates achievable on a liquid handling system by implementing intermittent flow, investigating the impact of otherwise unavoidable intermittent flow with a conventional chromatographic system, improved HETP tracer selection, and a comparison across multiple column volumes, IgG subtypes, chromatographic systems and flow regimes, as well as implementing intermittent flow within a mechanistic model framework for microscale chromatography.

This work has been presented in talks at multiple conferences, including international (HTPD 2017, Toledo) and national (IChemE BESIG YR, 'best presentation', 2017 winner), and has changed their ways of working at the parent organisation and improved the level of understanding they can obtain from these novel, high throughput systems.

On a more personal level, the time spent on this project and working in UCB was an invaluable experience, enabling a career that went into supervising pilot scale purification of mAbs at a contract manufacturer of monoclonal antibodies and leading downstream processing operations and development for a gene therapy manufacturer for AAV, lentiviral and adenoviral therapies. The skills learnt as part of this project allowed a few novel approaches to the latter work, including using the EMG equation for peak deconvolution to best assess the performance of separating full and empty AAV capsids by ion exchange in the face of highly variable analytics, a series of models to better predict filtration flux decay and improving viral titration by using the Poisson distribution, all of which were supported by the need for improved mathematical and bioprocess understanding, project management and other expertise developed during this project. Indeed, I feel very fortunate to have undertaken this project as I continued a career in mechanistic modelling of chromatography with world leaders in the field, and owe my much of my expertise, experience and companionship (including my new family) what I discovered as part of this project.

1 Introduction

1.1 Project Motivations

A trend in the process industries, especially biopharmaceutical production, is the need for increased process understanding (Gronemeyer *et al.,* 2014), considering the high cost of development (PhRMA, 2016), the regulatory pressures and benefits of being first to market emphasising rapid, cost effective and robust process development. In early process development, when processing decisions have the most impact, resource is often scarce, which can lead to non-optimal processes to ensure timely delivery of material. Microscale experimentation, coupled with highly automated, parallel liquid handling workstations provide ways of obtaining process understanding with reduced material, labour and time consumption, though the operational and design differences must be understood and corrected for if the results at this scale can be representative of larger scales, such as the conventional laboratory, pilot and manufacturing scale.

It is the aim of this project to develop a better understanding of microscale protein A chromatography in an industrial setting, with the purpose of creating a model for translating results across these scales, leading to increased process understanding with reduction in resource consumption.

1.2 Biopharmaceuticals

Biopharmaceuticals are medicinal products synthesised using biological systems and are typically proteins, nucleic acids, or whole cells. The FDA defines them as "any virus, therapeutic serum, toxin, antitoxin or analogous product applicable to the prevention, treatment or cure of diseases or injuries of man" (Code of Federal Regulations, 2018) though there a variety definitions in parlance, some of which exclude blood, antivenom, hormones, vaccines and other therapies that are directly extracted from natural sources, rather than genetically engineered organisms (Rader, 2008). Depending on this distinction, human therapeutic biopharmaceutical manufacture can be over thirty years with manufacture using genetically modified organisms, or a hundred years old considering penicillin productions, or if stretching the definition, thousands with the inclusion of alcohol manufacture through yeast fermentation.

Distinct from the far more established, chemically synthesised small molecule drugs, therapies derived from transgenic cell culture have shown much promise in the past few decades. Development on biopharmaceutical production has been a major area of research; from the humble beginnings of penicillin manufacture in repurposed items such as hospital bedpans (Bud, 2007) merely a century ago, the industry now invests over $50B into biopharmaceutical development annually, directly employs over 800,000 people, has over 500 FDA approved products with over 7,000 products in development, representing over 20% of total pharmaceutical

sales worldwide (PhRMA, 2016). One of the largest classes of approved biopharmaceuticals are antibodies, with their market is expected to value $137-220 billion by 2022 (Grilo & Mantalaris, 2018).

1.2.1 Antibodies

Antibodies (Ab), also known as immunoglobulins (Ig) are a superfamily of glycoproteins, imperative to the function of the adaptive immune system. They are produced, *in vivo*, by blood plasma cells and provide humoral immunity to the host. They function through binding to complimentary partners, antigens, which are often cell surface markers of bacteria, viruses or a range of other adventitious agents (Brekke & Sandlie, 2003), leading to neutralisation, agglutination, precipitation of the pathogen or activation of the complement system, and protection from disease.

The huge diversity, specificity and selectivity of these molecules make them very appealing drug candidates, offering fine control and modulation of biological pathways, and therefore disease, that smaller compounds simply cannot (Buss, 2012). These therapies represent the most prevalent class of biopharmaceutical (Walsh, 2014), with dozens of currently approved drugs, and over 300 in development (Ecker *et al.,* 2015).

Monoclonal antibodies as therapeutic entities is a relatively new phenomenon compared to conventional, small molecule drugs; the first of its class receiving market approval by regulatory agencies in 1986 with Orthoclone, a CD3 binding IgG_2 indicated against kidney transplant rejection (Starzl & Fung, 1986, Meijer *et al.*, 2003) whilst natural antibodies had been known of for many decades, it was only with modern genomic techniques and developments in hybridoma technology, in which an antibody producing B cell is hybridised with an immortal cancer B cells to form an effective production system, that they became viable candidates for therapy (Liu, 2014).

The synthesis of these molecules is a monumental task when contrasted with typical, small molecule therapies; their complex structure with many thousands of functional groups and chiral centres ensures that production through chemical means is infeasible, meaning one may only manufacture these entities with a biological system with the highly sophisticated machinery which cells possess. Monoclonal antibodies require post translation modifications (PTMs) for their therapeutic function, especially glycosylation, to eliminate immunogenic responses otherwise expected from incompatible glycosylation patterns. This means that mammalian expression systems, such as Chinese Hamster Ovary (CHO) and Human Embryonic Kidney (HEK) cells are the typical expression systems due this innate ability to perform PTMs, impossible for the higher producing yeast and microbial expression systems (Spadiut *et al.* 2014).

In vivo, a plethora of different antibodies, with many different structures and associated sequences, are produced; a polyclonal mixture, meaning isolation and expression of a single type is not exhibited in nature and

must be created. There is significant heterogeneity across antibody types by species; typically antibodies are discovered using non-human animals, such as mice, and then must be modified to remove the non-human regions (the Fc region and scaffold) and replace them with motifs expressed in human antibodies, a process aptly named 'Humanisation'; one cannot use the initially discovered antibody or hybridoma for production of pharmaceutical antibodies for humans without risking severe immunogenicity. Typically, this is achieved using a chimeric intermediate with the murine variable region grafted to a human Fc region, though other technologies such as phage display are also widely employed (Liu, 2014).

Modern antibody therapies are typically produced through biotechnological means, with genetic modification, cell culture and sophisticated processing to manufacture these drugs. The discovery and development of each compound is a highly expensive endeavour, taking many years and an average of well over a billion pounds per approved molecule (Shaughnessy, 2012). In order to reimburse the huge investments such candidates require, process development must lead towards manufacturing processes that can produce sufficient yields and throughputs to meet demand, whilst being economically promising allowing for remuneration, and therefore funding of further drug development.

1.3 Monoclonal Antibody Production Processes

Therapeutic monoclonal antibodies, whilst incredibly diverse in specificity and function, are typically manufactured using a similar process. For the wide array of drug candidates; the method of discovery, cell lines used, and physicochemical properties are often similar across the entire class of compounds. Companies often operate a general platform for most stages of drug discovery and development, such as discovery, candidate screening, cell line development and production. Every currently approved monoclonal antibody is an IgG, which, excluding the antigen binding regions, are largely similar in terms of mass, charge and physical structure (Shukla *et al.,* 2007).

Many biopharmaceutical manufacturers operate platform processes; that is, a generic process that is then tailored to and optimised for each specific candidate. This enables faster process development, with the equipment, staff, facilities and expertise in place to quickly bring a candidate drug to production, assuming it 'fits', or performs well within the platform. When a new drug can bestow a maximum of twenty years patent protection from filing, and may take 10 years to develop, every day saved in process development means significant remuneration (Mohs *et al.*, 2017). This is possible due to similar cell lines and cell line and media development strategies for each candidate leading towards similar upstream processing challenges, and the similar physicochemical properties, such as size and isoelectric point meaning that often only relatively small adjustments are typically made to an existing downstream processes to develop a new drug, rather than designing a new process *ab initio*.

A well-publicised production process is the 'A-MAb' case study, which was commissioned by a consortium of biopharmaceutical manufacturers, and describes a general process which is widely adopted by the industry for the production monoclonal antibodies using modern practises and paradigms (CMC Biotech Working Group, 2009). This general process for antibody manufacture is the use of suspension cell culture for product synthesis, cultured within bioreactors, followed by extraction of the product through a clarification train typically consisting of centrifugation and a series of filtration steps of reducing coarseness, multiple modes of chromatography and buffer exchanges as shown in Figure 1.1.

Cell culture, production and primary recovery is considered the realm of upstream processing (USP), with downstream processing (DSP) responsible for transforming a broth of cells, debris and product into a highly refined, concentrated, pure drug substance. Platform mAb production processes are often similar, with two or three orthogonal (exploiting different physicochemical properties) chromatographic steps, two orthogonal viral clearance steps and buffer exchanges for conditioning and formulation, and can be classed into upstream processing activities and downstream processing, in which the molecule is captured from harvest material, 'polished' to remove reaming impurities and then concentrated and formulated into a buffer to form drug substance.

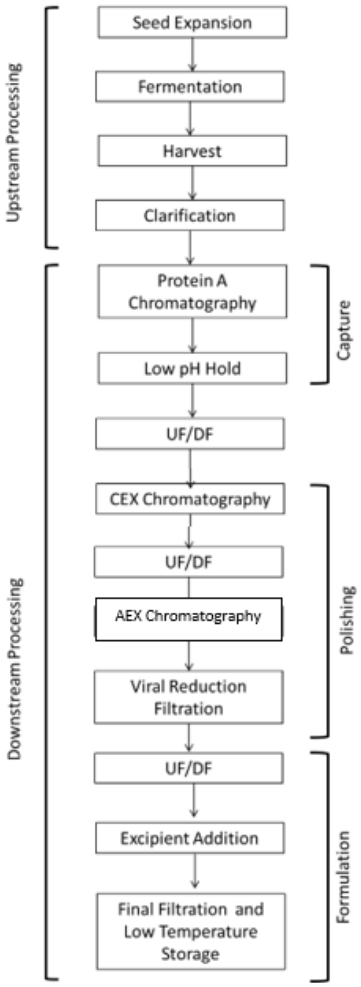

Figure 1.1 - A general mAb process, as described in the A-MAb case study (CMC Biotech Working Group, 2009)

1.3.1 Upstream Processing

Upstream processing of biopharmaceuticals concerns ensuring the cell culture is maintained in an optimal state, growing to a suitably cell density, maintaining high cell viability and producing antibody with expected and consistent quality, yield and impurity profile. It is during this stage that the cells grow, multiply and express protein. In a typical process, small bioreactors or flasks are inoculated, from a cell bank, with genetically modified cells which proliferate in media, with larger bioreactors then inoculated with the cell culture fluid from previous vessels until a suitable scale is reached through a seed train, enabling the required quantities of material to be expressed. Upstream processing is a vast discipline, with the goal of producing large amounts of high-quality, consistent product, using a myriad of bioreactor types, control regimes, media and cell lines. Suffice to say, however, upstream processing whilst ensuring the actual manufacture of the product, it is highly time intensive, expensive and a major source of process variation, and often the largest factor introducing product variability and affecting product quality (Hutchinson, 2014).

Monoclonal antibodies are expressed extracellularly, meaning no disruption of the cell membranes is required, whereas antibody binding fragments (Fabs) expressed in microbial system require some periplasmic disruption through shear forces, sonication or enzymatic attack. Extraction is accomplished by separating the cells and large particles from the media, typically through centrifugation or depth filtration. If required, flocculants can be added to aid aggregation of particles and therefore their clearance, though addition of this must be validated for clearance during the process, and risks product binding to the flocculants, reducing yield. Cells and large debris form a pellet during centrifugation, with the product remaining within the fluid phase, or supernatant, for further processing (Gottschalk, 2017).

The supernatant is filtered to remove remaining large particulates, with some processes utilising centrifugation for further solids removal whilst reducing the required filtration area. Ultrafiltration may be employed to concentrate the product, reducing volume handling required for downstream processing, which is most often employed in processes producing very low concentration of product within the bioreactor to better utilise expensive chromatographic resin, improve binding capacities, easier facility fit and reduced processing time. Once clarified and treated, the material should be free from cells and large particles, containing an expected and consistent concentration of monoclonal antibody, though also containing a plethora of host cell proteins, DNA fragments, endotoxins, aggregates, virus particles, media components and other product related and process related impurities that require removal (Staby *et al*., 2017).

1.3.2 Downstream Processing

Downstream processing concerns purifying and formulating the product. Purity and efficacy requirements are strict; these products are typically intended to be introduced into diseased, possibly immunocompromised people. Concentration, purity and recovery should be consistent throughout a production campaign, and due to

the expensive nature of the product and process, time and material consumption must be minimised whilst maintaining quality. A downstream process train will have a variety of unit operations, demanding each to be well optimised and controlled to ensure excessive product is not wasted to cumulative loss and that quality is maintained. The standard unit operations are described in Figure 1.1, and are typically classed into filtration to remove solids and virus particles, ultrafiltration for product concentration, diafiltration for buffer exchange (Houp, 2009), and chromatography for clearing impurities. The order, nature and efficacy of these unit operations varies from process to process, and it falls into the responsibility of downstream processing to be able to cope with any variation introduced by upstream processing, such as feed concentration, impurity profile and volume to consistently provide product of expected quality and recovery.

1.3.2.1 Chromatography

A difficulty with purifying antibodies is that they are expressed in low concentrations within the media, though thanks to improvements in upstream development, this has improved significantly in the past few decades (Li *et al.*, 2010), with ten grams per litre (1% (w/v)) considered a high titre, or concentration, which is less than 1% (w/w) of feed material. The products are mixed with a wide array of impurities, from lipids and DNA to viruses and media components, and are fragile molecules. These compounds are sensitive to thermal, pH, shear and biochemical degradation, and must be kept free from adventitious agents. These impurities, such as host cell proteins and viruses, could prove to be infectious or raise an immune response, and must be reduced to proven acceptable levels before formulation. It is chromatography that typically performs these activities, from capture of product from feedstock, to purifying and polishing out any process or product related impurities.

Chromatography is considered the workhorse for manufacture of most biopharmaceuticals, especially monoclonal antibodies (Kelley, 2007). It is a separation technique, where a multicomponent mixture is partitioned into stationary or mobile phase based upon properties of the components and adsorber, such as isoelectric point, hydrophobicity and size (Guiochon *et al.,* 2006). Often multiple, orthogonal chromatographic steps are used as part of a process, with the vast majority of the host cell proteins (HCP) and DNA are cleared through these steps, with orthogonal processing ensuring separation occurs by at least two separate physical phenomena, often electrostatic, size and chemical affinity. In addition, chromatography often serves as a powerful analytical technique, with a variety of formats used in every aspect of drug development, from product and impurity quantification, identification and characterisation. Analytical chromatography will often employ the same physical processes and chemistries as preparative chromatography, and largely differs on scale, throughput and of course, application.

There are many forms of chromatography, from the simple thin layer chromatography to more complicated arrangements such as two-dimensional and multimodal chromatography. These can operate in bind and elute mode, whether product is bound, washed and eluted after contaminants, or flow through mode (Lacki, 2018, Collins, 1997), in which contaminants bind and product flows through the column. A monoclonal antibody

process will typically use several techniques (Table 1.1), though most employ a capture in bind and elute mode, and DNA clearance through anion exchange chromatography in flow-through mode.

Table 1.1- Description of some of the major chromatographic chemistries employed in monoclonal antibody purification

Separation Mechanism	Example Chemistry	Comments	Mode
Cation Exchange (CEX)	Sulfopropyl ligand	Negatively charged ligand binds positively charged target or contaminants	Both flow through and bind-elute
Anion Exchange (AEX)	Quaternary ammonium ligand	Positively charged ligand binds negatively charged target or contaminants	Both flow through and bind-elute
Hydrophobic Interaction (HIC)	Phenyl ligand	Hydrophobic ligand interacts with hydrophobic patches on target or contaminants	Both flow through and bind-elute
Affinity (AC)	Recombinant Protein A ligand	Target or contaminants binds with high affinity and selectivity to functional groups of ligands through hydrogen bonding.	Typically bind-elute
Mixed mode/Multimodal (MMC)	Ceramic Hydroapatite Matrix	Target or contaminants interact through a variety of mechanisms, including ion exchange, hydrophobicity and affinity	Both flow-through and bind-elute
Size Exclusion (SEC), Gel Filtration (GF) or Gel Permeation (GP)	Matrix provides separation ability, not ligand	Large molecules elute early, as cannot access the full volume accessible to smaller molecules. Separation upon size (hydrodynamic volume) and steric hindrance. Rarely used in commercial processes due to small sample volumes, low flowrates and dilution of product.	Flow through

Chromatography can be a time-intensive unit operation, due to slow flowrates to preserve bed integrity, reduce shear, meet pressure limits and to ensure the chemical processes have adequate time for separation, as mass transfer is often a limit to efficiency for protein chromatography. Resin beads are constantly being developed to withstand faster flow and exhibit greater binding capacities and lessened kinetic resistances, thus offering faster cycling, more efficient cycles and enhanced throughput, with other offerings such as membrane and monolith technology designed to improve kinetics and therefore unit operation throughput by improving mass transfer (Orr *et al.,* 2013).

1.3.2.1.1 Affinity Chromatography

Affinity chromatography functions through separating components by relative affinity, or selectivity for binding to a ligand (Costa & Cabral, 1991). This affinity is achieved through selective, reversible interactions, such as hydrogen bonding or coordinate covalent bonding, with components with high affinity for the ligand being retained within the column, whilst the remaining, unbound components continue to flow and exit the column.

Affinity chromatography is frequently used in the purification of proteins; recombinant research proteins are often 'tagged' with a poly-histamine chain of residues, which coordinates to nickel or cobalt within a column as immobilised metal affinity chromatography. This is later eluted with a competitor to the nickel, typically imidazole, with many other impurities removed. This same approach is used with a variety of other tags, including Strep-tag, maltone binding protein, and chitin binding protein amongst others (Lichty *et al.,* 2005). An issue with introducing affinity tags to therapeutic proteins is that they may be immunogenic and therefore must be demonstrated to be tolerated and safe to be given to patients or must be removed and purified out before formulation. Therefore, affinity tag introduction to therapeutic proteins is discouraged, with not a single therapeutic protein with an affinity tag currently approved by the FDA (Dozier & Distefano, 2015), whereas Fc-fusion proteins are relatively common, this does not serve as an affinity tag for the purposes of purification but for biological action (Ogasawara & Alexander, 2019).

However, affinity is still a highly valuable mechanisms for separation of monoclonal antibodies even without introducing exogenous tags to the target. The adaptive immune system has existed for over 500 million years (Flajnik & Kasahara, 2010), providing nature a significant head-start in developing methods of preferentially binding antibodies. Protein A, Protein G and Protein L are all examples of bacterial proteins which have evolved to bind and sequester antibodies, conferring the pathogenic bacteria resistance to their host's immune response. These proteins, immobilised on resin beads, preferentially bind antibodies, interacting with the Fc region for A and G, and the Fab region for protein L, without the need to introduce any non-therapeutic moiety to the protein.

1.3.3 Bioprocess Development

Thanks to progress by process development, biopharmaceutical manufacture has advanced from paltry amounts of penicillin manufacture under a century ago, to now multiple tons of therapeutics, representing billions of pounds in revenue (Ecker *et al.*, 2015). Cell line development has reached a point where one can express up to ten grams of product per litre of culture for well-developed lines, a three log improvement in 20 years (Li *et al.,* 2010). Process development concerns ensuring consistent product quality, optimal yields, process robustness and throughput, minimising cost of production, whilst contending with this increase in titre, competition and increasing regulatory expectations.

Protein biopharmaceuticals are highly expensive to produce, costing up to tens of thousands of pounds per gram (Brian, 2009) in stark contrast to small molecule drugs, which are often manufactured for a fraction of a penny per gram (Hill *et al.,* 2018). Therefore, being able to determine, test and validate a process quickly, and robustly, is a major driver in bioprocess development. The cost of a process is especially important towards to end of a products' intellectual property protection in which competition is imminent. Even with many years of IP protection, costs of goods can easily mean a therapeutic is unprofitable, even if best in class, due to the presence of cheaper alternatives. Biosimilars, that is, generic versions of biopharmaceuticals whose patents have expires,

have already entered the market, including for mAbs (Raedler, 2016). Early in process development, cost is also a major factor, as there is significant chance of failure during trials, minimising the economic risk of this is crucial, often through simultaneous development of other candidates to mitigate the risk by hedging a pipeline into many separate therapies. Considering the costs of development, benefits of being first to market, and time-limited protection to IP, rapid and agile process development is crucial. Even a decade ago, every day a blockbuster drug is delayed from market; several million dollars is lost in opportunity alone (Sun, 2010).

With the advent of Quality by Design (QbD), multivariate statistical analysis and highly automated laboratory systems, both the need and the ability to gather ever more data became increasingly apparent (Rathore & Winkle, 2009). Optimising, characterising and implementing a bioprocess can be incredibly expensive, dwarfing manufacturing costs of small molecule drugs, further motivating innovation in bioprocess research and development (Farid, 2007).

1.3.4 Quality by Design

Quality by Design (QbD) is defined by the FDA as "*a systematic approach to development that begins with predefined objectives and emphasizes product and process understanding and process control, based on sound science and quality risk management*" (FDA, 2009). It is an approach to process development that relies on product and process characterisation, with statistical modelling and whole process understanding used to aid process control, to reduce waste and ensure consistent product quality and supply.

It is a paradigm born from the pharmaceutical industries' excessive levels of waste, frequent batch failures and poor process control under the previous paradigm of Quality by Testing (QbT). In some cases, waste of product was as high as 50% of total batches (Rathore & Winkle, 2009), and often the industry could not acceptably demonstrate scale-up, or adequately explain batch failures. These issues threatened a consistent supply and increased the cost of these medications, and the FDA was receiving more new drug applications each year and risked not being able to regulate them all effectively if their resources were stretched further.

Need for change was clear, and the FDA responded with the Quality by Design imperative. This prioritised process and product understanding, modelling and characterisation, through continual improvement, holistic, risk-based approach to process development, in which a process would be studied for sources of variation, and how to control variation in such a way to lead to consistent product quality. Rather than being concerned with a single unit operation or parameter at a time, with processes being inflexible reactive affairs relying on product testing for release, a process would instead be viewed as a whole, with development becoming more proactive to face anticipated challenges, with better process understanding, process analytics, control strategy and robustness, reducing failure rates, wastage and regularity oversight.

Critical Quality Attributes (CQA's) of the drug, the properties of the product that affect the quality and efficacy of the therapy, such as impurity levels, potency and post translational modifications, must be finely controlled during manufacture. These attributes are linked to Critical Process Parameters (CPP's), parameters in the process that must be well understood and managed, such as buffer composition and process temperature, through experimental results and modelling with rigorous risk assessment. A product design space, a multidimensional space of the acceptable CQAs, is defined as a target product profile (TPP). Assuming a product falls within the boundary of this design space, it is within specification, and the process is controlled. A process design space is constructed for each unit step built from the CPPs and represents the area in which the process can still be controlled to meet desired quality.

Animal studies, clinical results, product characterisation and historical data are used to define the CQAs, with data, risk modelling and statistical understanding used to correlate the CQAs to CPPs. Clinical data may show the maximum dose of HCP before any adverse effect shown, and data from other drugs may form part of this criteria. This means that rather than tight specifications determined under the Quality by Testing paradigm, with poor understanding of process inputs and how they affect quality, the priority is knowing the ranges in which a process can meet this quality, and adequate process understanding and control strategies in place to ensure these ranges are adhered to. This also demonstrates that process control, and processes operations are not necessarily static, but that the process may be adjustable within this design space to account for external sources of variability.

1.3.4.1 Statistical Understanding

Process development under the QbD paradigm requires a substantial amount of process and product understanding. Bioprocesses are complex affairs and measuring the effect of even a single factor on the quality of the product and process overall requires significant investigation, and therefore investigating a combination of factors makes this endeavour exponentially more difficult. With many unit operations, each with a multitude of controlled and uncontrolled parameters, optimisation represents a significant experimental burden. Statistical techniques allow one to identify and quantify relationships and model complex processes to improve process understanding, and with a suitable statistical understanding of the data, the experimental requirement can be reduced through models with relatively fewer experiments performed to validate a model.

Univariate approaches, such as altering a single factor at a time and measuring a response would be prohibitively time, material and cost intensive when applied to optimising a bioprocess, as only a single factor may be evaluated at a time, and others needing fine control. This approach would fail to show any higher order interactions amongst variables, running the risk of optimising within a local optimum specific to the starting assumptions, rather than a global optimum for the entire system. This approach also fails to demonstrate a holistic understanding of a bioprocess.

1.3.4.2 Multivariate *Analysis*

Multivariate analysis techniques are of great utility in process development. Design of Experiments (DoE) is often employed in bioprocess development for condition screening, optimisation, robustness testing and modelling (Mandenius & Brundin, 2008). DoE is a statistical framework for planning of experiments and interpretation of systems to investigate as many conditions in as fewer experiments as practicable, specific to the model used. For a DoE investigation, many factors are changed simultaneously to set levels with one or more response measured, with both an understanding of the effect of a single factor on the system, and also the relationships and interplay between factors. There are many formats, the most suitable depending on the investigation at hand, the desired level of understanding and the experimental limitations. Full factorial designs have each controlled variable investigated at two or more levels, meaning a total number of experiments increases exponentially and grows to a large number of experiments with modest amounts of levels and factors. Fractional factorial designs require fewer experiments, at the expense of omitting higher order interactions between variables. Whilst this allows investigations to take place that would be otherwise too time intensive, the parameter estimations are more prone to error, and main effects are often indistinguishable from interactions between variables (Gunst & Mason, 2009). Parameter choice and level selection must be carefully considered to minimise experimentation whilst ensuring enough data is obtained to adequately understand the system under investigation. The results from DoE studies are usually displayed in contour or surface plots through response surface methodology, which involves fitting polynomial surfaces to the data (Whitcomb & Anderson, 2005). A common use of this is to identify 'sweet spots', or optima, of the experimental space, for further investigation and analysis.

Regardless of the design type, for bioprocesses, which may have a plethora of CPP's to investigate across many unit operations, the necessity for considerable numbers of experiments remains, producing large quantities of data. Multivariate statistical tools such as principal component analysis (PCA), and projection to latent structures (PLS) are useful tool to reduce the complexity of multidimensional data through combining many dependant variables into few, independent variables through linear transformations (Maitra, 2008, Malmquist & Danielsson, 2004). This has shown much use, ranging from chemometrics (Trygg *et al*., 2007) to clinical trial evaluation (Bekke-Hansen *et al.,* 2012), and are powerful tools for the reduction of dimensions within data, and therefore easier data interpretation and better process understanding.

1.3.4.3 Mechanistic Modelling

The above statistical approaches rely on empirical data for pattern identification and therefore provide little ability for extrapolation, as relationships outside the measured data can only be speculated, though interpolation is possible as the data may be generalised into a linear or polynomial function. In contrast, mechanistic modelling offers, through applying the physical principles and fundamental relationships involved, a method of accurately describing the mechanics of a systems and therefore extrapolating outside of a measured

response space, whilst also better understanding within this space through their basis in first principles of fluid dynamics, transport phenomena and thermodynamics. For most mechanistic models, statistics are also used in order to calibrate these models, an example is calibration or validation though measuring a goodness of fit metric. One could consider a mechanistic model to be an extension of a statistical model, in which known scientific correlations and principles are applied to a dataset, to reduce experimental burden and increase confidence in extrapolating outside of the initial dataset (Pandey *et al.,* 2017).

However, the requirement for such stringent mechanistic understanding can inhibit their implementation; with chromatography, there is such a wide variety of parameters and complex relationships that can affect the behaviour of the process, such as the resin-protein, protein-solvent and solvent-resin interactions, their rates, and their individual properties (Hanke & Ottens, 2014). Models are merely an approximation of a process, and the precision can vary significantly based upon the model type, training data and system complexity, though if the assumptions are valid, and the model describes the process accurately, it demonstrates a better process understanding than statistical modelling alone, being derived from established principles rather than merely an approximation of data. Mechanistic models relevant to chromatography, will be discussed in greater depth in Chapter 6.

QbD aligned process development is increasingly important for ensuring safe, consistent and economical production of therapeutic antibodies; whilst regulatory pressures, cost drivers, increasing candidates count and increased throughput and impurity burden from upstream processing are an ever present challenge, paradigms such as using platform processes, statistical and mechanistic modelling and the wide variety of chromatographic techniques available make better processes and process understanding possible under these conditions. However, with the multitude of parameters to test, the experimental burden is increasing, and novel methods must be employed to ensure the data requirement can be achieved, and the understanding is robust enough to best evaluate, operate and optimise a process to provide crucial medications to those that rely upon them at a consistent quality and acceptable cost.

2 Introduction to High Throughput Process Development

2.1 High Throughput Process Development

Highly automated liquid handling systems becoming more ubiquitous, reliable and economical has facilitated the advent of high throughput, microscale experiments in process development, allowing a greater extent of experimental space to be investigated with reduced material, time and labour consumption. With modern robotic liquid handling systems multiple independent experiments can be performed simultaneously and in parallel with very little manual input, with high precision, and lower material requirement than has been possible with conventional experimentation.

With early process development, material availability and process understanding are limited, whilst decisions concerning process operation and design parameters must be made, thus screening a large experimental space pairs well with a platform process, such as monoclonal antibody purification, and supported by ever increasing R&D costs and proportionately fewer drugs in a pipeline being approved each year (Fishbaum, 2011). Due to the 90% chance of a product entering Phase I trials failing to meet approval (Harrison, 2016), devoting much expense to a single IgG in early process development is risky, therefore products may enter the market and reach patients with an uneconomical, non-optimal process when approved.

Microscale, high throughput techniques are well used in the pharmaceutical industry; high throughput screening is frequently used to identify favourable characteristics from many molecules during candidate discovery, with often more than 100,000 assays performed daily on a single system (Bader *et al*., 2018, Attene-Ramos *et al*., 2014). Cell line development is often performed with microtiter plates, for screening productivity, and microscale bioreactors, such as the AMBR 15 and AMBR 250 ranges are often used for investigating culture and process quality, respectively (Baumann & Hubbuch, 2017).

With downstream processing, as with other areas of process development, robotic systems have shown much utility. From increasing assay throughput, such as ELISA, western blot, PCR and spectrometry, modern systems also allow filtration, mixing, centrifugation and chromatographic steps to be mimicked on the microscale, and investigated with a high throughput approach (Hubbuch, 2012).

2.1.1 Microscale Chromatography Formats

For chromatography there are a variety of resin formats and chemistries available for purifying monoclonal antibodies in the microscale domain (Chattre & Titchener-Hooker, 2009). Resin filled tips, resin filled plates and microscale columns, such as the Atoll RoboColumn series (Atoll, 2013), are increasingly employed for process development.

With resin filled tips, a device is connected to the aspiration tips on the liquid handling system arms. The tips contain the resin under investigation, with fluids, such as equilibration, load and elution buffers aspirated through the device and dispensed into microtiter plates. Microtiter batch plates are typically 96-well format with small volume of resin within, held in position above a filter membrane with pore sizes significantly below the average resin particle diameter. Buffer and load material are aspirated on top and drawn through onto 96 well plates through vacuum or centrifugation, allowing collection in a plate beneath the filter plate and operating the entire plate like many separate columns.

Both formats are extensively used for screening chromatographic conditions (Wenger *et al.,* 2007, Hanke & Ottens 2014, Feliciano *et al.,* 2016), the pipette chromatography tips offering superior fractionation, as one can take multiple fractions merely by moving the tips across a plate, rather than changing collection plates entirely. However, this is to the detriment of throughput, with 8 resin reservoirs per liquid handling system rather than 96 for the batch plates. Fluid handling is different for both; the batch plates flow is difficult to control, as a vacuum or centrifugation must be applied to create the required pressure differential for the working fluid to transverse the resin, and must be stopped to change collector plates, and therefore collect fractions. The micropipette tips operate in a bidirectional manner and can dispense or aspirate a limited volume at a time due to machine limitations, which may significantly affect their representation of scale. The batch plates range down to 2 µL resin volume and pipette tips in the order of 300 µL. These formats have demonstrated good approximation of lab-scale columns for HCP, aggregate clearance and recovery for Protein A chromatography, when compared at lab-scale equipment (Chattre & Titchener-Hooker, 2009).

2.1.1.1 Microscale Columns

Miniaturised columns, however, offer an improved tool for chromatographic process development for many investigations (Lacki, 2012). While batch plates and tips are well used in screening buffers, products and resins, their inherently different flow regimes, geometries and data collection abilities limit their usefulness, whereas microscale columns attempt to mimic lab scale columns more closely, allowing investigations into resolution, gradient elutions amongst other experiments typically performed. Miniaturised columns, such as the Atoll MiniColumns series, are available with resin volumes of 50 µL to 600 µL, with an internal column diameter of 5 mm and bed heights from 2.5 mm to 3 cm (Atoll, 2013). They are available prepacked with a wide variety of resins, working in a downflow mode and compatible with a range of liquid handling platforms; hand pipetted varieties, which offer a low-cost access to microscale chromatography, centrifuge operated types, typically up to a 384 well format, and liquid handling system operated columns. Both hand pipette and centrifuge operated types offer benefits, such as a high throughput and no need for an expensive liquid handling system, they present difficulties in controlling and maintaining a constant, defined flow rate, which is often of high importance to chromatographic studies, as well as requiring considerable manual intervention. Additional problems are associated with fraction collection, and performing more complex investigations, such as gradient operations which require precise and controlled liquid handling to sufficiently mimic larger scale behaviour.

Miniaturised columns designed for use with automated liquid handling systems have a demonstrated ability to mimic full chromatographic processes in microscale and parallel when combined with a liquid handling system (Britsch *et al*., 2008, Evans *et al*., 2017, Treier *et al*., 2012a, Benner *et al*., 2019, Khalaf *et al*., 2016, Keller *et al*., 2017). These columns operate by dispensing liquid, such as buffer and load material, through the inlet at the top with a liquid handling system, with an O-ring preventing fluid from leaking out the inlet. The liquid handling system dispenses liquid, at controlled flowrates through the column and effluent is collected within 96 well plates that shuttle along underneath the columns, allowing twelve fractions per column per plate. These systems can change and read plates, using an integrated plate moving arm and UV plate reader, as well as prepare assays, clean plates and prepare buffers from stock solutions without manual intervention.

As with both conventional lab-scale columns, which range in the order of millilitres, and these microlitre columns the geometry is cylindrical, and similar with regards to aspect ratio (except for 50 µL and lower columns, in which diameter is greater than length), with expected similar packing density to in-house packed columns at scale. However, the bed height is drastically changed, and as discussed below, this is likely to have significant effects on the separation. Additionally, there are a number of deviations between the scales, geometry, and method of use and data acquisition that must be considered, evaluated and if possible, mitigated.

2.1.2 Scale Considerations

Scaling of downstream processing is not a new science, and is a common activity during process development, transferring from lab sized production to larger scale manufacture as a scale-up, for commercial supply or in-house material supply, or from large scale to smaller for the purposes of further process development or troubleshooting, as a scale-down model (Sofer & Hagel, 1997). Chromatographic columns are typically scaled from lab-scale investigations to pilot and production scale using volumetric expansion, in a radial direction. The radius of a chromatographic column is increased, from the order of a few millimetres at lab-scale, to meters at pilot and production scale whilst the axial dimension typically remains constant. This ensures the bed height, and thus the superficial fluid velocity, residence time and both fluid and bed pressure remain similar. There are small deviations in fluid flow with this approach, due to a difference to the volume to column surface area ratio, the wall effect seen with respect to packing density and fluid velocity at the boundary between the column interior and wall, as well as resin beds often losing structural integrity with increasing diameters (Tran *et al.,* 2007). The method of operation between lab-scale and above is very similar, with FPLC machines of increasing flow capacity used, typically with similar software and configurations, though with higher volume processing capabilities through use of increasingly larger pipe bore, collection vessels and larger pumps.

Lab-scale columns are available with resins that can be packed manually or bought prepacked. Many can be disassembled; parts replaced, repacked and reassembled easily, and are well established in industry and academia, and therefore have a myriad of papers and books detailing their use, characterisation and limitations (Rathore *et al*., 2003, Schmidt-Traub, 2006, Carta & Jungbauer, 2010). Their associated systems have been used

and developed for decades, and offer fine fluid control, on-line pressure, UV, temperature and conductivity measurements, and fractionation, with straightforward automatic use through sequential 'scouting' runs possible on several systems, and automatic buffer preparation with binary or quaternary pumps with stock solutions.

With a lab-scale and larger columns, the dead volume, the volume of fluid in the flow path of the system not the column, is typically minimal compared to the column and thus the system rarely significantly impacts results, though, with smaller columns this can be an important consideration (Kaltenbrunner *et al.,* 1997). Additionally, with buffers suitably covered, the entire system is static and closed, with no moving parts, except for pump pistons, directly interacting with the column matrix or fluid, and no evaporation or fluid loss within the system possible if properly prepared.

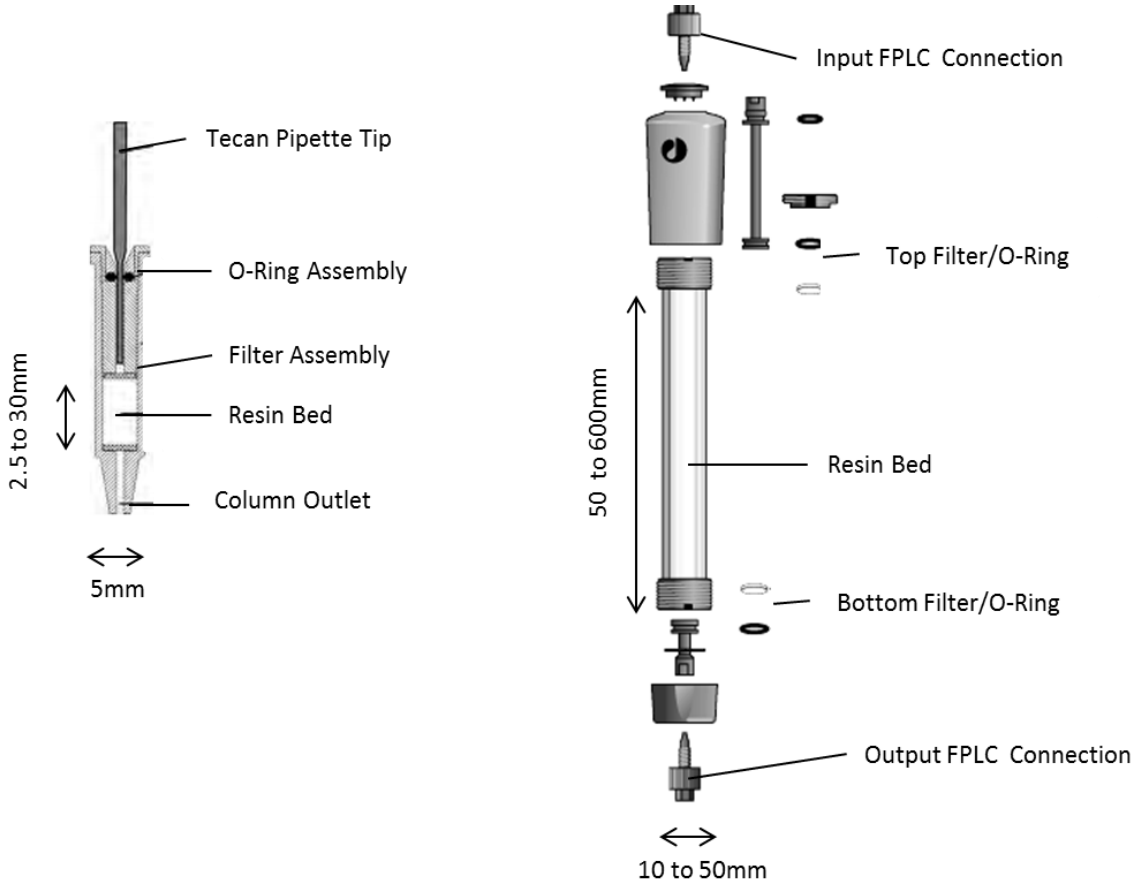

Figure 2.1 - Diagrams of a microscale column, compared to a conventional lab-column. Of note are the changes in dimension, method of use and geometric differences. Images adapted from Wiendahl et al, 2008 and GE Healthcare

2.1.2.1 Design Differences

Whilst typical lab-scale columns are well established, with fine fluid control, microscale columns and are not operated in a closed environment, with buffers exposed to the air during operation. They are relatively new phenomenon when compared to conventional columns, with the patent filed in 2006 (Schroeder, 2006), and therefore do not have the benefit of extensive literature or understanding. The nature of liquid handlers and the columns, with a single experiment using multiple buffer types and columns, simultaneously, precludes operating them in a fully closed system. Though when paired with a liquid handling system (LHS), they offer precise fluid control, they exhibit a number of differences due to their geometry (Figure 2.1). The volume within the column inlet is variable with regards to needle placement; 2 mm above the bed is suggested by the manufacturers, though columns move during use and the column cradle often does not lie completely flat and may be moved by the operator. This small variation, of only a few millimetres, can be a significant proportion of a 50 µL column. The inlet and outlet void are the only dead volume within the system, with no tubing, as on a FPLC system, to delay and holdup fluid.

The inlet assembly has an O-ring and filter, both of which can be prone to degradation, and cannot easily be replaced. The higher surface area to volume ratio at this scale lends itself to significant wall effects, where the fluid at the radial boundary of the column is static; poor flow may affect column packing and material distribution, and thus column efficiency, with some papers suggesting that the distributor cap on the top of the column in ineffective at maintaining plug flow (Chhatre & Titchener-Hooker 2009). This is very pronounced at this scale, where the diameter of the column at 5 mm is only a few times larger than typical resin beads, which are commonly in the range of 50 to 100 µm, a consideration when packing effects can extend to up to 50 particle diameters (Farkas & Guiochon, 1997). Additionally, if any component interacts with the column wall material, it will be greatly pronounced at this scale considering the far higher surface area to volume ratio in the microscale domain. As already implied, the different bed heights must be considered, as must flow rate. At constant bed heights, such as typically employed during scaling from pilot scale to commercial manufacturing, the flow rate can be scaled as a constant linear flow velocity, which ensures both the flow velocity and the time the material spends resident in the column, the residence time, remain constant regardless of scale. At different bed heights, as must be used during in microscale chromatography to maintain a similar geometry, mitigate the wall effect and match volumes adequately, this it is impossible to scale both factors simultaneously, meaning one must choose to either scale for linear flow velocity or residence time, depending of the separation and desired performance (Rathore and Sofer, 2012). For instance, separations which are more kinetically limited, such as affinity separations, the bed-height is of less importance, and therefore scaling for residence time desired, whereas for more hydrodynamically driven separations, such as size exclusion (Rathore & Velayudhan, 2002, Lacki, 2012), column efficiency is key, and therefore linear flow velocity has a larger impact. The European Union's Committee for Proprietary Medicinal Products (CPMP) has highlighted bed heights as a key parameter to be considered to determine the validity of a scale-down chromatographic model (European Medicines

Evaluation Agency, 1995). Regardless of which scaling strategy, all process volumes (e.g. Loading, washing, elution lengths) are typically scaled for a number of column volumes (CV).

With bind-elute chromatography of proteins, kinetic resistances often dominate, meaning scaling flowrates such that the material spends equal time within the column is often the most prudent approach. This provides equal opportunity for interaction with the resin at each scale, and is the simplest strategy for scaling, assuming the rate limiting step is not velocity dependant. Whilst for some experiments, such as investigating bed compression, scaling for linear flow velocity may be pragmatic. The fluid control on a Tecan EVO 200, the LHS used in this study, is precise but cannot pump at a rate slow enough for some applications, especially with columns with very small bed heights combined with chromatography with long residence times. The minimum sustained flowrate the system can maintain is 0.8 µL s^{-1} which corresponds to a linear flowrate of 15 cm h^{-1} on a 5mm diameter column, a maximum residence time of one minute for a 2.5 mm bed height with a 50 µL column.

2.1.2.2 Operational Differences

The mechanisms by which these columns are operated are vastly different; on an FPLC system, pumps and valves ensure constant flow for the entire operations. With an LHS, however, the maximum volume per aspirate-dispense cycle is limited by the volume of the pipette, often to 1 mL. This means during a typical chromatographic run the pipette tip would enter and exit the column many times. It is possible, however, using suitable liquid class settings, to load the pipette with a gradient, or sequence of buffers, with a capillary storage within the pipettes and air gaps preventing mixing. Though a gradient must be prepared earlier, rather than mixing between two pumps as on a FPLC, they are possible to achieve with a series of steps, though is merely an approximation of the smooth gradient easily achievable with FPLC systems. While this reduces the need for constant mechanical interaction with the column, this movement, and its associated deviations with column pressure, as well as interrupted flow whilst aspirating more fluid, mean the scale operation is not wholly mimicked. More flow interruption is introduced with a plate change; it can take several seconds to store a generated plate and fetch a new one, during which the flow must stop to prevent wasted effluent. This interrupted flow increases the effective residence time and must be properly assessed if residence time is to be effectively investigated.

Additional difficulties arise from the fact that unlike traditional FPLC chromatography, an LHS is an innately open system. All buffers, load material and effluent lie open to the ambient air rather than closed containers, for ease of pipetting, introducing the risk of evaporation or interaction with the environment. Additionally, as eluate forms as drops on the column outlet, and fall at random intervals, aliquot size cannot be finely controlled. There is also substantial risk of a drop falling while a plate is absent, or in motion, thus not falling into a well to be measured, introducing error loss and presenting difficulties in establishing a mass-balance.

The way data is collected is intrinsically different; with modern FPLC systems, UV, pH, conductivity, pre and post column pressure and temperature are all continuously monitored with in-line sensors, with fractions taken optionally. With a microscale LHS set up, all data is gathered through collection of effluent in fractions on a 96 well plate. These are read for absorbance at a high throughput for radiation of wavelengths of 230 nm to 1,000 nm and can have a variety of assays performed upon them. However, conductivity and pH measurements must be performed one at a time, in a highly manual manner with specialised probes, highlighting that whilst DSP development can be ported onto a high-throughput device, it is best matched with an equivalent leap in analytical throughput to enjoy the increase in experimental capability.

Due to the fact these fraction sizes are limited to the drop size at minimum, resolution is poor when compared to a 12 µL flow cell with a high sampling rate, as is typical on FPLCs, used in conjunction with a larger column. Resolution is often further limited by the minimum working volume of the collection plate for spectrometric determination, which is typically in the order of over 50 µL. Unlike FPLC system, there is no associated chromatogram processing software commonly used for microscale column paired with UV absorbance measurements in a 96 well format, meaning manual processing is typical. Due to the vast quantities of data the system is capable of producing, data must be processed in a high throughput manner.

Diederich and Hubbuch (2017) have detailed and evaluated a large number of possible error sources when performing microscale separations with respect to analysis through UV absorbance, system pipetting accuracy and intermittent flow. They have highlighted that the systems are generally accurate with regards to pipetting, improving with increased volume, though emphasised the importance of accounting for the variability of microtiter plates and intermittent flow. Different molecules behaved inconsistently with regards to flow regime, with some showing no difference between continuous and intermittent flow, and others deviating significantly , typically the largest molecules had the greatest effect. This highlights the importance of establishing the differences on a case-by-case basis for both molecule, and nature of the study, such as breakthrough, elution or pulse tests, and is why intermittent flow in particular is focussed on later in this work.

Each of these highlighted differences with respect to operation and scale shall be explored with respect to typical experiments likely to be performed on these columns, for the purposes of understanding, and if possible, mitigating, the effects of these scale and system deviations to better perform high-throughput experiments and to improve interpretation of microscale data.

3 Microscale Protein A Capture

3.1 Introduction

Protein A chromatography typically serves as the first chromatographic operation in downstream processing of mAbs, in which product is isolated and concentrated from crude fermentation broth. Recombinant Protein A, produced in bacteria, is immobilised onto beads, usually consisting of porous polysaccharides such as agarose and dextrose, though a variety of formats are employed, including silica and mesoporous plastic (Schmidt-Traub, 2006). This matrix proves support, whereas the Protein A provides the resin its function through physicochemical selectivity and affinity of the Protein A domains to the Fc region of IgG. Antibodies preferentially bind to these ligands in solution, out-competing host cell proteins which often cannot bind, or only bind weakly through hydrophobic interactions or electrostatics rather than the highly favourable hydrogen bonding networks mediating immunoaffinity binding (Yang *et al*., 2003). These weakly bound contaminants are largely washed off in a low pH buffer, low salt buffers, high salt buffers or a combination thereof (Post Load Wash, PLW) by shielding the electrostatic or hydrophobic interactions between contaminants and ligand, or contaminants and product. After impurities are eliminated, the pH is lowered to disrupt the binding between target and ligands to elute the purified antibody (Elution). The column is regenerated, and any remaining species washed off in a stronger acid buffer (Strip, Regeneration or Post Elution Wash) and cleaned in a solution (for base tolerant Protein A this is typically sodium hydroxide) after a number of cycles to remove bioburden and to solubilise contaminants, as a Clean in Place (CIP) operation. At the end of a cycle the column is either discarded (for single use columns), stored in a bacteriostatic storage solution, or re-equilibrated for further cycles.

Protein A ligands offers favourable separation ability for many IgG's, offering over 99% impurity clearance and high recovery in a single operation, and also a large concentration factor (Gottschalk, 2017). For this reason, chromatographic capture of product by Protein A is typically the first chromatographic steps in downstream processing of monoclonal antibodies. This has the benefit of removing most impurities early, reducing risk of chemical and biochemical degradation of the product by the impurities, also removing the burden of further processing such components. Unlike ion exchange (IEX) or Hydrophobic Interaction Chromatography (HIC) steps, adsorption is tolerant of loading buffer pH and conductivity, and the elution conditions (low pH) allow facile and efficient viral clearance by holding material in the acidic environment for a set duration, denaturing enveloped viruses.

Protein A does have several limitations; the Protein A may leach from the resin into the material (Carter-Franklin, 2007), which must be tested for and clearance validated due to the immunogenicity of Protein A (Palmqvist *et al.* 2002). The resin is typically highly expensive, as it is manufactured using recombinant protein, with costs over 50% higher than other commercially relevant resins, selling over $15,000 per litre (Rathore *et al.,* 2015) with a

process column of over one meter in diameter, as is often used in commercial scale, consuming over $1M in Protein A alone (Follman, 2004).

As the ligand is a recombinant protein, it is sensitive to pH, thermal, and biochemical degradation, therefore requiring both gentle conditions but also efficacious cleaning regimes. The resin beads are also vulnerable to excessive pressure, though modern Protein A resins offers significantly improved pH tolerance, resistance to leaching ligand, and ever more binding capacities.

Due to the efficacy of this step, the high cost of resin and the risk of contaminants, such as Protein A, introduced into the process, optimisation of this step is crucial to effective IgG downstream processing. Therefore, establishing a scale-down approach will enable the benefits of microscale HTPD, such as increased experimental space and reduction in time, material and labour consumption, and more effective processes to be established. It is the aim of this chapter to investigate scaling down Protein A separation and explore limitations regarding column resolution and consistency, by evaluate the performance of the capture of two IgGs on a 200 µL microscale column platform.

3.2 Materials

3.2.1 Preparation of Load Material

IgG A (IgG_1) and IgG B (IgG_4) clarified cell culture fluid (CCCF) was available from prior pilot scale fermentations, in which the cell culture fluid had been clarified by centrifugation followed by a series of filtration steps. This CCCF was then filtered through polyethersulfone (PES) membrane with a pore size of a 0.45 µm with pH and conductivity measured. As for all of this work, IgG aliquots were available frozen at -80 °C, which were defrosted at 4 °C for 24 hours, bought to room temperature before experimentation, and mixed to ensure homogeneity. Titres were provided by Protein A HPLC measurement.

3.2.2 Buffers

For each antibody and experiment, a number of buffers were freshly prepared for each experiment (Equilibration, Post Load washes, Elution (low pH), Strip, CIP and storage buffers). These were filtered at 0.22 µm before use and stored at room temperature. Buffer composition is provided in Table 3.1.

Table 3.1 - Buffers used in Protein A capture for IgG A and IgG B

Buffer	Composition	pH
Equilibration	100mM Sodium Phosphate	7.0
Wash	100 mM Sodium Phosphate (IgG A and B) 100 mM sodium phosphate + 500 mM Sodium Chloride (IgG B)	7.0

Elution	100mM Sodium Citrate	3.5
Regeneration	100mM Citric Acid	2.1
CIP	100mM Sodium Hydroxide	High

3.2.3 Microtiter plates

96 well UV transparent, flat bottomed, microtiter plates were provided by Corning, USA, of two volumes. Full area plates, with a working volume of 75 µL to 200 µL were available, as were half-area plate', by the same manufacturer, with working volumes of 25 µL to 125 µL. The diameter ranged from 7 mm per well for full area, and 5 mm for half area plates.

Additionally, deep well plates were also used if excessive volumes were being sampled. These are not UV transparent, so samples from these plates were often transferred to smaller plates after mixing for measurement.

3.2.4 Liquid Handling System

For most of the liquid handling performed, a Tecan Freedom EVO 200 system was used, one of three available on site. A photograph and the specific layout of used modules is shown below (Figure 3.1). 8 stainless steel tips, connected to 1mL pipettes were used to introduce fluid to the columns. These were connected to a liquid handling arm (LiHa), which was able to move in x, y and z directions, with each tip able to be independently operated in the y and z axis, and in unison along the x-axis, and dispense at different flowrates. The system is capable of sustaining flowrates from 0.8 µL s^{-1} to over 1 mL s^{-1}. A robotic manipulator arm (RoMa) moved microtiter plates across the deck to the integrated plate reader, cradle or storage blocks, and operated the waste tray. A Te-Stack module provided the capability to rapidly store over a dozen plates on two stacks, and a Te-Chrom module allowing microtiter plates to be shuttled underneath a column cradle to collect effluent. A Tecan Infinite 200 PRO plate reader was used to measure absorbance from plates of radiation of wavelengths between 230 nm and 1 µm with a dynamic range up to 2.3 AU. The system was programmed using the proprietary Tecan software, EVOware, which allowed processes to be performed by creating a script describing operations. A limitation of the software and system is that operations could not be performed in parallel but sequentially, meaning that an operation, such as dispensing fluid, had to be interrupted whilst another operation, such as retrieving a microtiter plate, was performed.

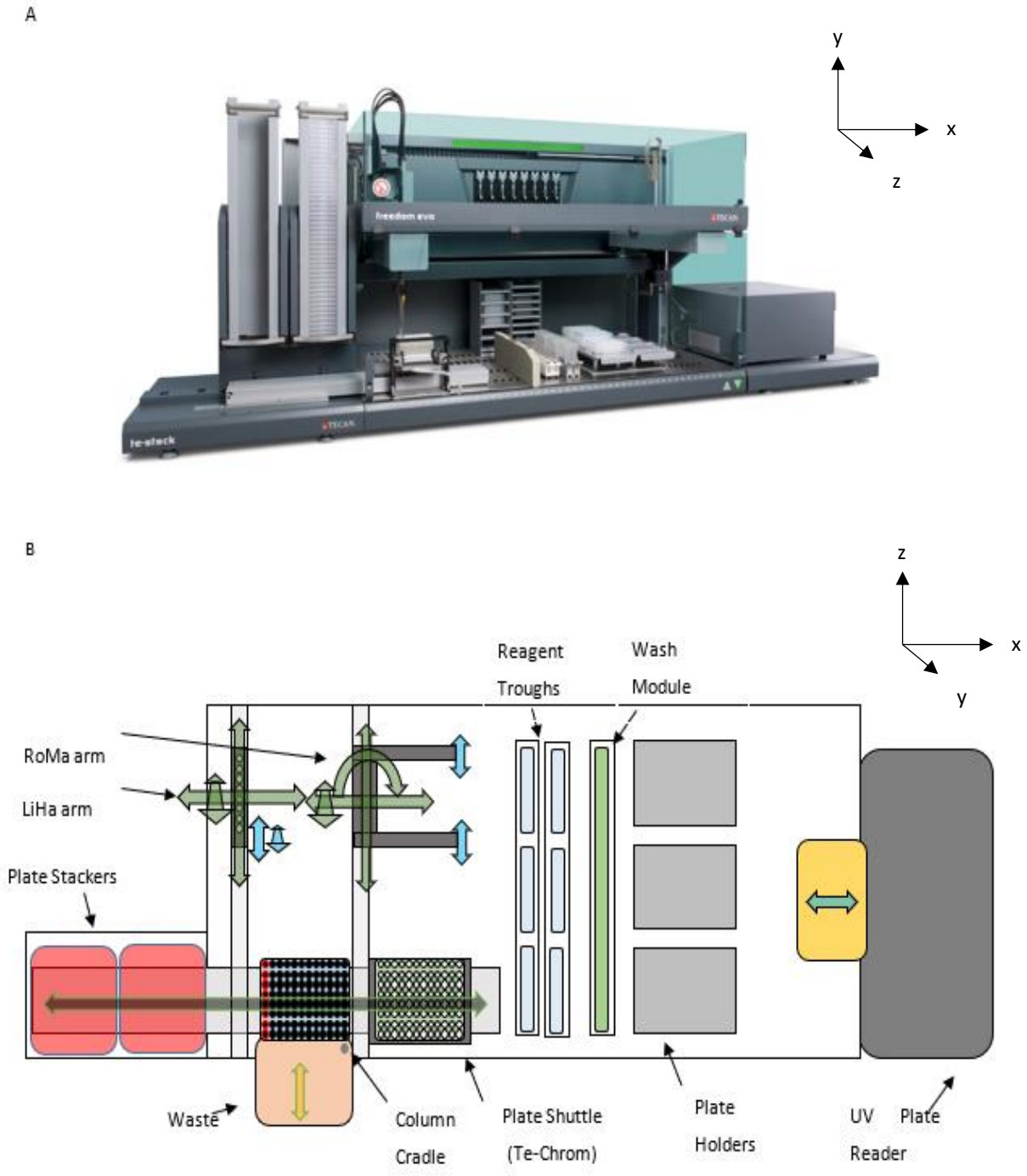

Figure 3.1- Diagrams of the Tecan Freedom EVO 200 Workstation. ***A*** *– Photograph of the configuration used,* ***B*** *- Schematic Representation in a top-down view, with green arrows indicating external degrees of freedom, and blue represent internal; i.e. The RoMa arm can move spatially in 3 dimensions, rotate in one plane, and move its claws in one dimension.*

3.2.4.1 Columns

Eight 200 µL Microscale columns were used with bed heights of 1 cm and internal diameters of 5 mm, purchased pre-packed with recombinant Staphylococcal Protein A resin (MabSelect SuRe). This is an agarose matrix with base tolerant recombinant Z-domain of Protein A allowing high binding capacities and ability to use caustic cleaning without denaturing the ligand.

3.3 Methods

3.3.1 Microscale Protein A Capture of an IgG_1 and an IgG_4 from feedstock

The microscale chromatographic operations followed that at large scale, in that a number of column volumes of equilibration buffer were dispensed down the columns, immediately followed by loading the feed material to a defined load challenge of 30 g L^{-1}, followed by one wash step for IgG A (IgG_1) with equilibration buffer, and two for IgG B (IgG_4), including a high salt buffer. Columns were eluted, regenerated and cleaned, with storage solution flushed across the columns at the end of each set of experiments. IgG A and B had differing titres, so the volume to be loaded was tailored to each IgG to meet 30g L^{-1}.

Equilibration, cleaning and storage flow through fractions were discarded, the other operations effluent was collected in UV transparent plates. Between each fluid change, the tips were thoroughly washed in water using the integrated wash module. 8 columns were operated in parallel, with each column subject to identical conditions. The general procedure is given below (Figure 3.2).

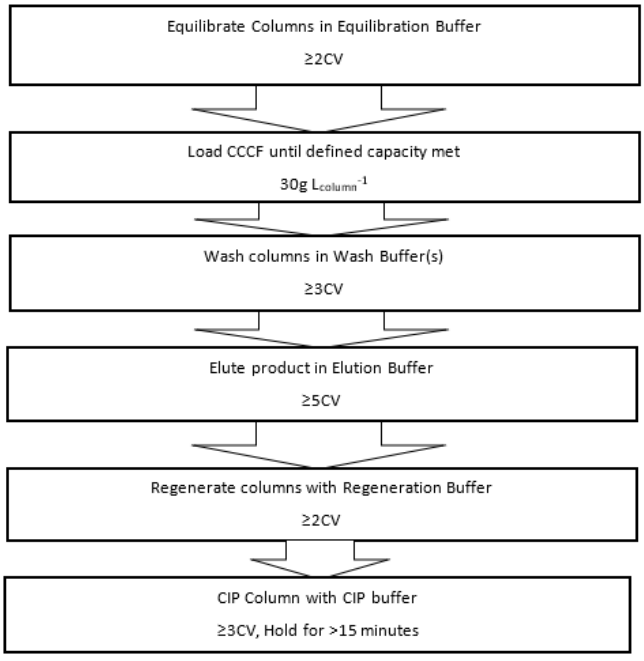

Figure 3.2 - Process description diagram of the protein A chromatography process used in this study

3.3.2 Scaling Strategy

Due to the reduced bed height of these microscale columns compared with conventional, lab-scale columns used otherwise used on this process (1 cm vs 20 cm), one must decide which flowrates best approximate the larger scale system. Residence time scaling, in that the same time for fluid to pass along the length of the column regardless of scale, was used, a typical strategy when comparing columns of different bed heights in bind-elute of proteins (Rathore & Velayudhan 2002, Kidal & Jensen, 2006) due to minimising differences arrising from mass-transfer limitted separations.

A volumetric flowrate of 0.83 µL s^{-1} was employed, providing an effective residence time of 240 s for the entirety of the chromatographic separation, the same residence time as that used for conventional scale columns. A 15 minute hold step is employed during the CIP to aid efficacy. These process runs were repeated at a number of fraction volumes, keeping all other parameters constant between runs. Either half-area plates or full area plates were used for fraction collection and analysis.

3.3.3 UV Spectroscopy

All microtiter plates were analysed through measuring UV absorbance at 280 nm, 900 nm, 977 nm, corresponding to protein concentration, a non-absorbing wavelength and aqueous volume, respectively. Standard curves for these plates were generated, in which 12 volumes of fluid (available protein A eluate and CCCF for each IgG and elution buffer) were dispensed into the wells (75µL to 200 µL for full area plates, 25µL to 125µL for half area plates), and then UV absorbance for each well determined at wavelengths of 280nm, 900 nm and 977 nm. A linear regression was performed for each of the UV absorbance values at each wavelength (280 nm and 977 nm – 900nm) using Microsoft Excel (Figure 3.3).

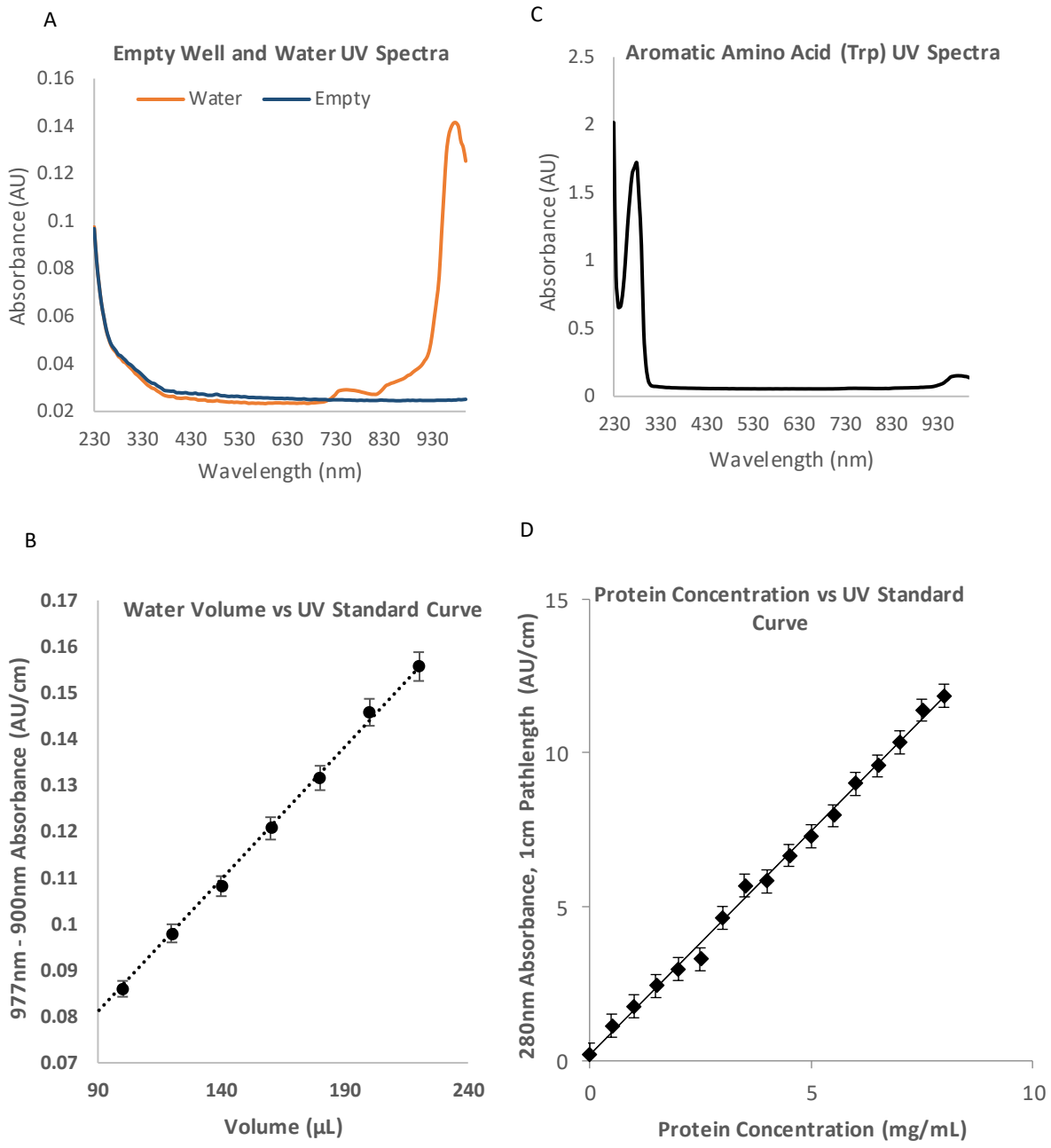

Figure 3.3 UV Calibration Curves for microtiter plates. ***A*** *- The UV spectra of an empty well compared against a well filled with water.* ***B*** *- Well containing aromatic amino acid (tryptophan) with absorbance peak at 280nm, blanked with water, demonstrating 977nm and 280 nm are the strongest absorbing wavelengths.* ***C*** *- a typical calibration curve of 977nm absorbance vs plate volume and (D) 280nm absorbance adjusted to 1cm pathlength for a water and protein solution of known concentration, respectively*

3.4 Data processing

3.4.1 Treating Microtiter Plate Data

The microtiter plates generated were measured for UV absorbance at 280 nm, 900 nm and 977 nm in each well. Using the raw values, the background absorbance of the plates was subtracted, and the 977 nm and 900 nm readings were used to determine the path length, and therefore the volume within the wells with reference absorbances, and the following equation [3.1]

$$\frac{(A_{977,sample} - A_{900,sample}) \times r_{mm}^2 \times \pi \times reference\ length_{mm}}{(A_{977,reference\ length} - A_{900,reference\ length})} = V\ (\mu L) \qquad [3.1]$$

280 nm radiation is strongly absorbed by proteins due to the aromatic amino acid residues of tryptophan, tyrosine and phenylalanine. 977 nm corresponds to a strong absorbance peak in water, whereas 900 nm is chosen as a blank to correct for anomalous and background absorbance; this range is not usually strongly absorbing in biological molecules (McGown, 1998). As 977nm absorption is temperature dependant, an isosbestic point away from the 977 nm peak maximum, such as 900 nm, is often measured so that absorbance values do not change with respect to temperature (McGown & Hafeman, 1998). As all UV measurements were taken in a climate-controlled lab, this was not thought to be important, but was collected nevertheless.

The absorbance readouts were concatenated together into a single file, forming a pseudo-chromatogram. Graphs were plotted of the cumulated volume (x-axis), against 280 nm absorption, corrected for plate absorbance, and transformed into the signal for a 1 cm path length, thus being invariant to fraction volume and representative of concentration. Errant values were removed by selecting for 'nonsense' volume measurements, such as negative volumes and volumes more than 5 times the average volume, with both the volume and 280 nm readings removed from this data.

3.5 Results and Discussion

Initially, 150 µL fractions were collected during these experiments, which exhibited clear peaks for the load and elution operations, though the poor resolution meant one could not clearly discern a consistent, isolated peak for the 'strip' fractions (Figure 3.4). Slight asymmetry of the elution peaks was evident in the smaller fractions for IgG A and IgG B, respectively, which became far more evident as one increased the resolution to 50 µL per fraction.

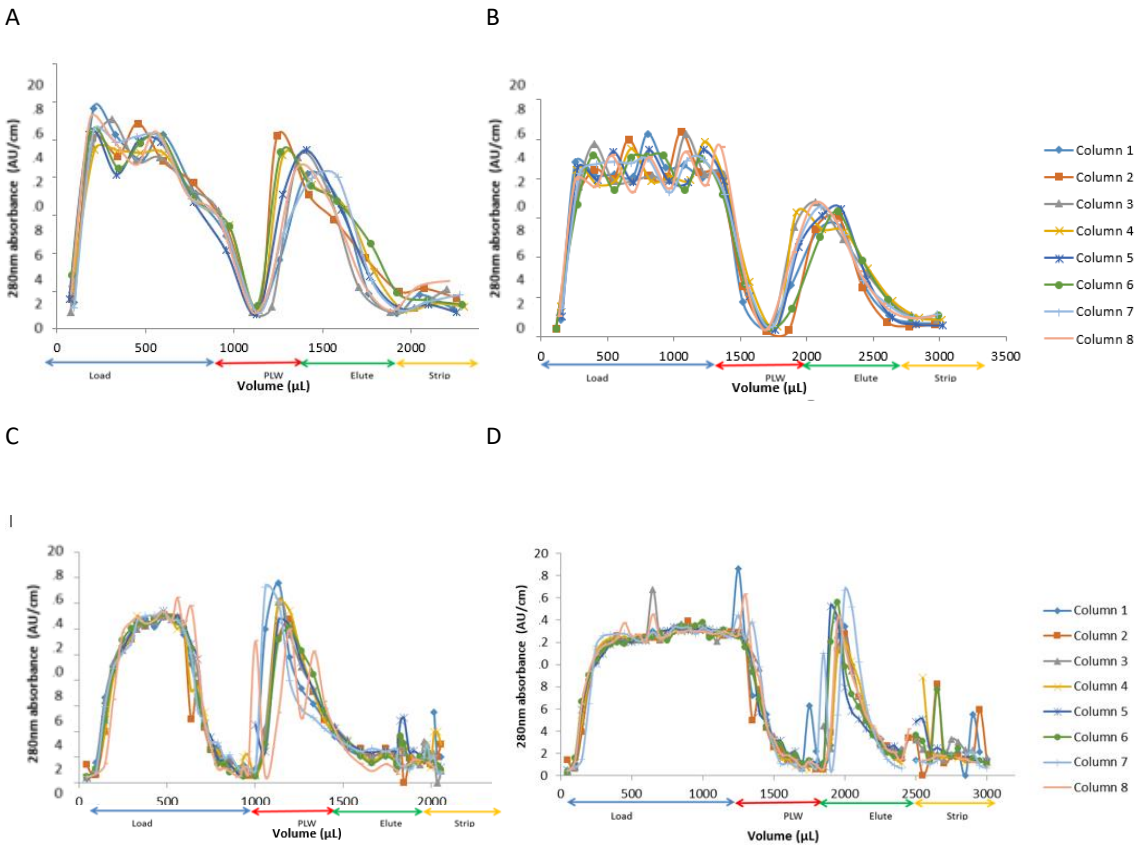

Figure 3.4- IgG - Protein A pseudo-chromatograms generated using full area UV transparent plates showing improvement in resolution but increase in noise with decreasing fraction size ***A*** *– IgG A at 150 µL fraction volume,* ***B*** *– IgG B at150 µL fraction volume,* ***C*** *-IgG A at 50 µL fraction volume****, D*** *– IgG B at 50 µL fraction volume.*

At fractions of 50 µL and below, the data was of very poor completeness (Figure 3.4); the fractions were significantly below the working volume of full well plates (75 µL), and therefore the effluent, rather than forming a flat meniscus, would form a droplet on one side of the well. This meant that the single point of absorption in the middle of the plate did not represent the contents and provided errant readings, either measuring very little absorbance (suggesting empty wells), and specular reflection measuring significantly higher absorbances than possible with absorbance alone. For some experiments the majority of data points were omitted. Using a half-area plate mitigated this effect, and fractions were reduced to beneath this value, demonstrating superior resolution (Figure 3.5), as well as maintaining the similarity for the larger scale, historical data.

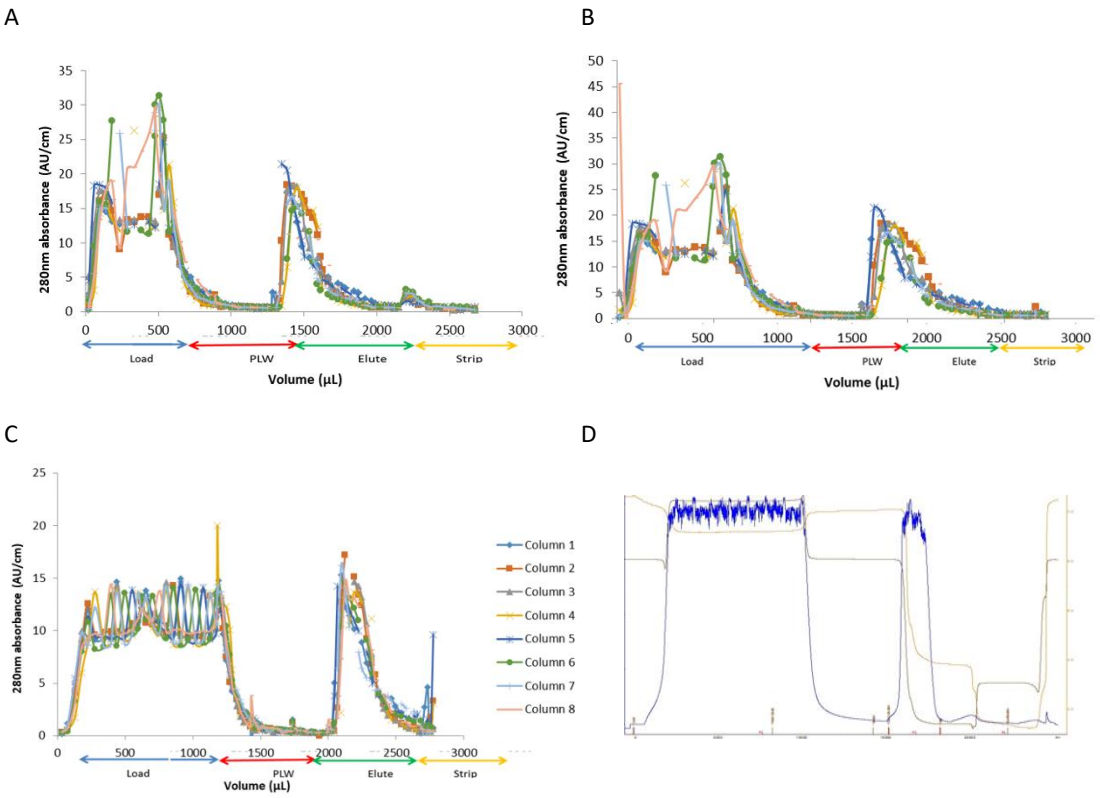

*Figure 3.5 - IgG - Protein A pseudo-chromatograms generated using half area UV transparent plates **A** – IgG A with 40 µL fractions, **B** -IgG A with 25 µL fractions, **C**- IgG B with 25 µL fractions. One can see improved resolution though with increasing gaps within the data. **D** – IgG A at larger scale (historical data) showing qualitative similarity to the microscale separation*

Processing removed errant readings through a series of checks for possible values for volume and corrected 280 nm absorbance, as incorrect readings often gave very high, or negative values due to inaccuracies in either pathlength or 280 nm absorbance. These errant values were thought caused through two mechanisms; firstly, the aliquots being of too small a size to image through being below the minimum resolvable volume due to the meniscus effects, leading to non-central beam paths and reflection of UV radiation. Additionally, as the absorbances are processed as UV absorbance corrected to a 1 cm path length, to equate to a metric correlated to concentration and to remove any variation caused by wells being unevenly filled, at small volumes this calculation became more error prone as relative error increased, though absolute error may have remained the same.

Choosing a suitable fraction volume meant that one could better resolve peaks, though often at the expense of losing material (Table 3.2); at very small fraction volumes, effluent could not be measured through either increased movement of collection plates leading towards more missed drops or through drops forming within wells. This meant that more structure within the data could be observed, at the cost of completeness.

Table 3.2 - Measure of resolution and volume loss, as a function of fraction size, measured volume determined by 977nm – 900nmm absorbance, and dispensed volume is determined by the method on the LHS

Fraction Size (µL)	Data Points Per Chromatogram	Volume Loss (Measured volume by UV absorbance compared to dispensed volume)
150 (with full area plates)	20	9%
100 (with full area plates)	30	14%
50 (with full area plates)	60	29%
40 (with full area plates)	75	43%
40 (with half area plates)	75	21%
25 (with half area plates)	120	33%

3.5.1 Elution Comparability

To investigate the consistency of elution between columns and experiments, repeats were performed and assessed for IgG A and B with only elution fractions collected. A 40 µL fraction volume was chosen collected on a half area plate and performed for IgG A alone.

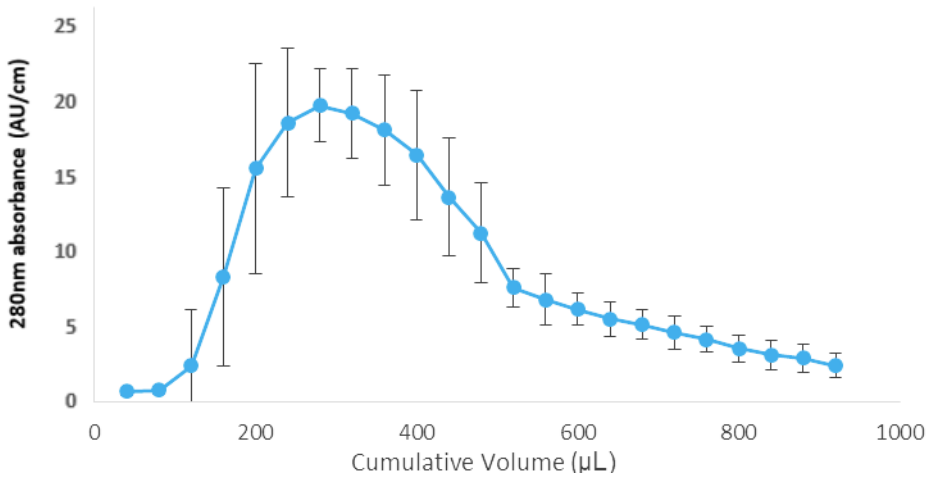

Figure 3.6 - Elution Chromatograms for 8 columns across 5 runs, demonstrating typical variation between responses

Variation in elution peaks was observed (Figure 3.6), though with a consistent, significant shoulder on the tail. No trends between columns or experiments were identified that lead towards a consistent difference in peak profile. The peaks were integrated, and the total amount of collected IgG calculated. The average recovery was

72%, which, accounting for the volumetric loss (Table 3.2), means an expected actual recovery of 94%, a typical value for protein A chromatography (Fahrner *et al.*, 2001, Pabst *et al.*, 2018).

A

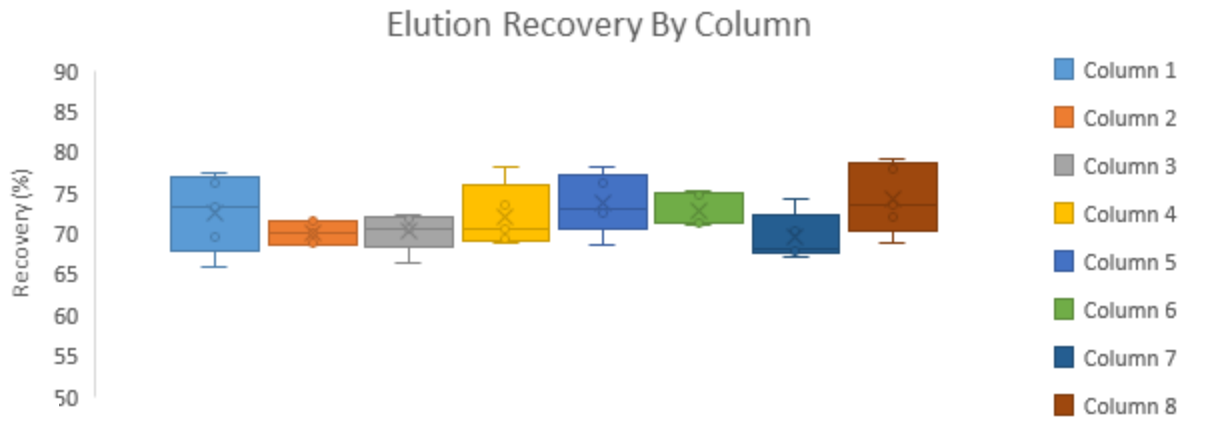

B

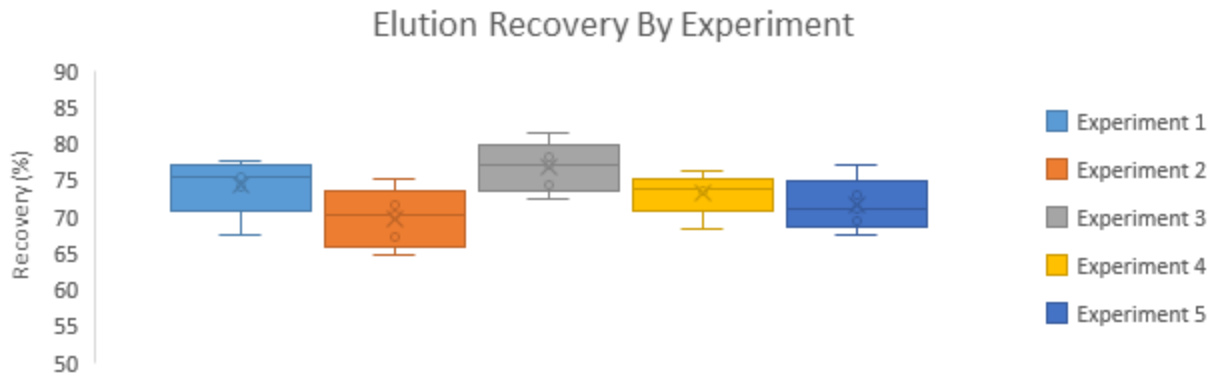

Figure 3.7- Box and Whisker Plots of recovery and variability of microscale column elution, for run-to-run and column-to-column variability; ***A*** *– Average for each column measured over 5 experiments;* ***B*** *– Average for each experiment measured over all 8 columns*

Similar variations in recovery were observed both between columns during a single experiment and between identical columns during separate experiments (Figure 3.7). One can surmise that it is the system itself, such as the intrinsic low signal to noise in the microscale domain and stochastic nature of drop formation that are responsible rather than lot-to-lot variability of the columns themselves; the columns, whilst variable between experiments, seem to be comparable in terms of elution efficiency across an average of 5 runs with 8 columns. This was confirmed with one-way ANOVA, in which for data grouped by either experiments or column failed to show any significant difference (with a F-critical value greater than F value, and a P value greater than 0.5 for both structures). A point to note is that these columns are from the same manufacturing batch, and therefore true lot-to-lot variability may actually be greater between adsorber and column lots than what has been reported here.

3.5.2 Discussion

Performance on microscale columns for a capture of two IgG's by Protein A chromatography was assessed by UV spectrometry alone, with no analysis of impurity clearance. Poor resolution was observed initially, and therefore fraction volume was investigated to for resolution and completeness. Whilst poor recovery was observed, this is likely due to experimental limitations in which collection plates failed to determine fractions, either due to working volume limitations or drops missing the well and correlated with total volume loss across the entire separation. Interestingly, the elution peaks demonstrated a consistent shoulder (3.5 CV for a pool of >80% of total eluate product), likely due to packing effects (Kaltenbrunner *et al*., 1997), significantly more than is expected from larger scales, both in this process, and similar processes in literature (Pabst *et al*., 2018). This increased pool volume has been reported by others (Kiesewetter *et* al., 2016, Keller *et al*., 2019), and therefore charactering these columns may be able to better explain this discrepancy.

4 Column Characterisation

4.1 Introduction

Because of the ever-increasing regulatory pressure of proving the efficiency, quality, safety and reproducibility of purification of biopharmaceuticals and the associated equipment and consumables, chromatographic columns should be qualified before use to ensure expected performance, as well as monitored for resin reusability and column equivalency. This is of particular importance when scaling column bed heights, as resolution and efficiency will vary significantly. Column qualification is commonly performed on lab-scale and larger columns to evaluate packing quality, though with microscale column being a modern development, there is few published methods for qualifying these columns.

4.1.1 HETP and Asymmetry

HETP (Height Equivalent to a Theoretical Plate) determination with a non-binding tracer is a common metric of column efficiency. It is a measure of the axial dispersion of material along a column and describes column resolution, with its roots in fractional distillation in which the name was coined (Peters, 1922). A well packed, homogenous column should have a small theoretical plate height, though this is wholly dependent on the resin, bed characteristics, pore size, packing quality, tracer, solvent and flowrate used (Rathore *et al*., 2003).

$$HETP = A + \frac{B}{u} + (C_s + C_m) \cdot u \qquad [4.1]$$

HETP values are highly dependent on flow rates, as shown by the Van Deemter equation [4.1], in which *u* represents linear flow velocity, A is Eddy-diffusion parameter, B the Diffusion Coefficient, and C represents the resistance to mass transfer of analyte between mobile phase (C_m) and stationary phase (C_s). Resistance to mass-transfer dependant dispersion correlates linearly with flowrate (C term), as it represents the time taken to for material to transport to stationary phase, diffusion related dispersion (B term) is reduced with higher flowrates, as low flowrates provide more time in which the analyte diffuses, whilst eddy dispersion (A term), caused by channelling and non-ideal packing, is unaffected by flow rate. HETP values are determined from a pulse response, which can be directly measured (Figure 4.1), or inferred from a step change response (Figure 4.3).

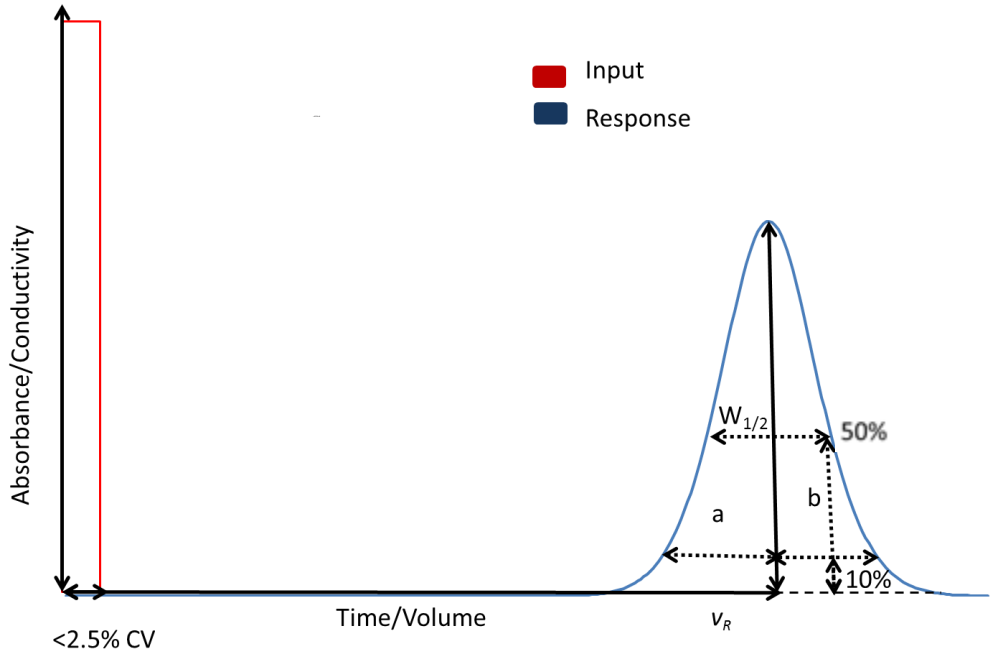

Figure 4.1- The derivations of HETP and Asymmetry parameters from a pulse or differentiated frontal experiment

A tracer experiment, performed by injecting a small pulse of noninteracting material, is the typical approach to determined HETP. A well packed column with many theoretical plates should generate a symmetric, gaussian response, with typical As value between 0.8 and 1.4 (Rathore *et* al., 2003), determined with [4.2]. While an ideal column has an asymmetry value of 1.0, bed irregularities, unfavourable fluid flow and components external to the column will increase asymmetry considerably (Helling *et al.* 2013), as will prohibitively slow mass transfer (Jeansonne, 1990).

$$A_s = \frac{b}{a} \qquad [4.2]$$

4.1.2 Determining HETP Parameters from Response

For plate count determination with a peak response and using the peak width approach, two parameters are needing determination from the response, a retention time or volume (v_R or t_r), and the width at half height ($w_{1/2}$) in time (subscript t) or volume (subscript v) [4.3] with HETP then determined through [4.4]. The remaining parameter is the column length, which is known beforehand. These parameters can be determined directly from the peak with ease at sufficient resolution, however, with poor resolution data, the sparseness of points means that a single reading may be far away from the true peak maximum and midpoint, meaning one must interpolate these values, introducing error inversely proportional to resolution. In addition, considering that a highly

asymmetric peak can mean the peak maximum and retention time differ significantly (Schmidt-Traub, 2006), as seen with the difference between mean residence volume and peak maximum/retention volume (Figure 4.2).

$$N = 8\ \ln(2) \times \left(\frac{v_R}{w_{1/2}}\right)^2 \qquad [4.3]$$

$$HETP = \frac{L}{N} \qquad [4.4]$$

Under these conditions, accurately calculating HETP may better use another approach; by using the method of moments, a statistical approach that allows estimation of population parameters. Determining these moments may be performed with a number of approaches, including approximating the peak with a mathematical function.

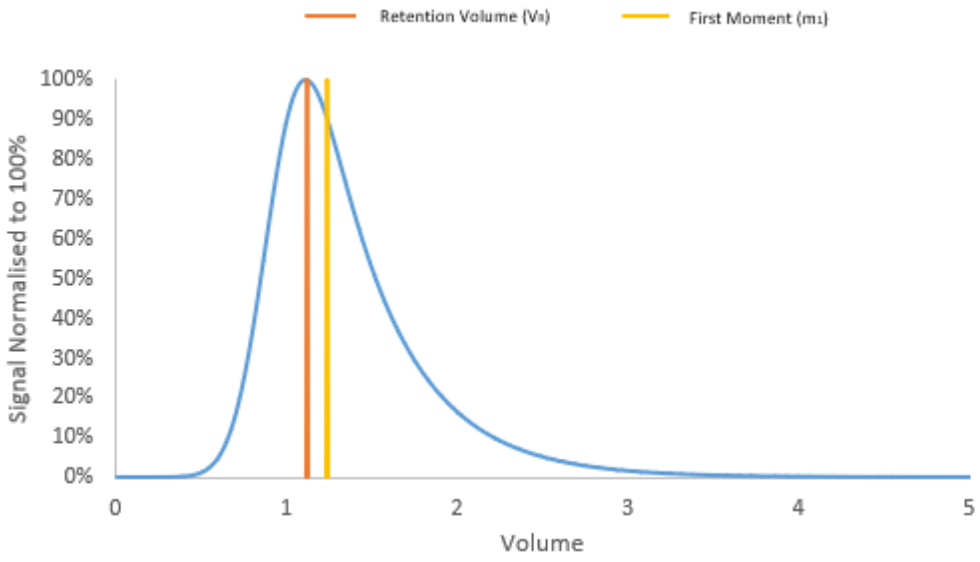

Figure 4.2 – Demonstration that peak maximum (mode), retention volume and average (mean) retention Volume, or first moment, differ with asymmetric peaks, adapted from Dyson, 1998.

4.1.2.1 Fitting a Distribution to Data

One method for analysing and comparing chromatograms is through fitting an equation, curve or distribution to the data. This has several benefits, rather than analysing a multitude of data points, each chromatographic peak can be reduced to a function with a small number of parameters, allowing direct comparison of these

parameters, and therefore performance between systems columns and resins. For lower resolution data, it allows an estimation of the true data structure, and interpolation of results, based upon expected peak shape.

There are several functions one can apply to describe chromatographic peaks, with over 90 described by Di Marco and Bobi (2001). Splining and fitting polynomials is simple, and requires no initial knowledge or estimation of parameters, though noise and errors will introduce bias into the model. These are very poor approximations of chromatographic peaks, with very large numbers of terms needed to fit well, and often leads to over fitting in which the random error is included in the model, preventing effective interpretation of the data. Fitting with a known function that describes chromatogram peaks offers a method of modelling peaks based upon expected characteristics whilst not excessively modelling error. As discussed, an ideal chromatographic peak is a symmetric Gaussian (Coning & Swinley, 2019, Kadjo *et al*., 2017), however, due to mixing within the system, mass transfer resistance, poor packing and material gradients in the column, where the column is not entirely homogenous, chromatographic peaks are often asymmetric, or skewed (Rathore *et al.,* 2003).

Asymmetric Gaussian functions are often used to account for tailing or fronting, which are Gaussian functions convoluted with another function, often an exponential decay curve to account for wash-out kinetics. Whilst the Poisson distribution describes chromatographic plate theory, which is highly asymmetric at lower occurances, with a large number of theoretical plates, as typically seen in preparative chromatography, this is closely approximated by the symmetric Gaussian distribution (Said *et al.,* 1982), though this may not be a valid assumption for small bed heights considering reduced plate count leading towards this asymmetry.

Of the many asymmetric functions describing chromatographic peaks, of note are the log-normal, Edgeworth/Cramér series and the Gram/Charlier series, though the exponentially modified Gaussian (EMG) is the widely for chromatographic analysis due to its good peak approximation, few parameters and correlation of these parameters to measurable properties of the peak (Kalambet *et al.,* 2011). This is highly beneficial for fitting poor completeness, microscale data; the fewer parameters means one can fit them with fewer data points, and the correlation to easily measurable parameters, such as peak width and height, providing robustness and confidence in the fit (Foley, 1987).

4.1.2.2 Fitting EMG function to data

The EMG equations can take many forms, though for the purposes of this, a single definition, provided below [4.5] is used. For fitting an EMG function, the x-axis and y-axis of raw data is typically fed into an optimisation regime, or curve fitting tool. The algorithm will typically vary the parameters in to maximise a goodness of fit statistic between the equation and data, trying to find a combination of parameters that best describes the data.

$$f(x; h, \mu_g, \sigma_g, \tau, y_0) = y_0 + \frac{h\sigma_g}{\tau}\sqrt{\frac{\pi}{2}} \cdot e^{\left(\frac{1}{2}\left(\frac{\sigma_g}{\tau}\right)^2 - \frac{x-\mu_g}{\sigma_g}\right)} \cdot erfc\left(\frac{1}{\sqrt{2}}\left(\frac{\sigma_g}{\tau} - \frac{x-\mu_g}{\sigma_g}\right)\right) \quad [4.5]$$

HETP values may be derived through two methods, from interpolating the modelled peak widths at greater resolution or through integration and moments analysis of the peak.

A moment is a quantitative measure of the shape or characteristics of a function. There are infinitely many moments that can be determined through the general identity in [4.6] though only the first four are typically used in chromatographic analysis as estimation of these moments becomes more error prone with increasing order, and higher order moments do not lend themselves to intuitive interpretation.

$$m_n = \frac{\int_0^\infty v^n \cdot c(v)\ \mathrm{d}v}{c(v)\ \mathrm{d}v} \quad [4.6]$$

$$m_0 = \int_{-\infty}^{\infty} v^0 \cdot c(v)\ \mathrm{dv} = A \quad [4.7]$$

$$m_1 = \mu_v = \frac{\int_0^\infty v \cdot c(v) \cdot \mathrm{d}v}{\int_0^\infty c(v) \cdot \mathrm{d}v} = \mu_G + \tau \quad [4.8]$$

$$m_2 = \sigma_v^2 = \frac{\int_0^\infty (v - \mu_v)^2 \cdot c(v) \cdot \mathrm{d}v}{\int_0^\infty c(v) \cdot \mathrm{d}v} = \sigma_G^2 + \tau^2 \quad [4.9]$$

$$m_3 = \frac{1}{m_0}\int_0^\infty v^3 \cdot c(v)\ \mathrm{dv} = 2\tau^3 \quad [4.10]$$

The zeroth moment corresponds to total peak area [4.7], the first moment the mean residence time or volume [4.8], the second moment the variance [4.9], and the third skewness of the peak [4.10]. Further moments correlate to distortions of the peak, and typically have lesser contributions to chromatographic peak shapes.

$$N = \frac{\mu_v^2}{\sigma_v^2} \quad [4.11]$$

Using this approach, HETP can be redefined in terms of the first absolute moment (μ), the variance (σ^2) [4.11]., providing a measure of plate count whilst better accounting for peak asymmetry. The relative contributions of the system and column to band broadening can be considered additive (Schmidt-Traub, 2006, Carta & Jungbauer, 2010, Brooks *et al.*, 1988 and Grinias *et al.,* 2015,) one can consider the measured first moment ($\mu_{measured}$) and variance, $\sigma^2_{measured}$, to be the summation of the column first moment and second moment ($\mu_{measured}$ or σ^2_{column}) and external contributions ($\mu_{external}$ or $\sigma^2_{external}$), the variance introduced by the system and by the variance introduced by the injection volume (σ^2_{inj}) [4.12 and 4.13]. This allows better comparison between scales, as external volume can be considered, and corrected for, when determining HETP values. The exponential decay component of band broadening, τ, is not additive, so therefore asymmetry cannot be accounted for in external volumes with this approach (Kaltenbrunner *et al.* 1997).

$$\sigma^2_{measured} = \sigma^2_{column} + \sigma^2_{external} + \sigma^2_{inj} \quad [4.12]$$

$$\mu_{measured} = \mu_{column} + \mu_{external} + \mu_{inj} \quad [4.13]$$

Additionally, one can also estimate the band broadening and retention caused by the injection itself [4.14 and 4.15].

$$\mu_{v,inj} = \frac{V_{inj}}{2} \quad [4.14]$$

$$\sigma^2_{v,inj} = \frac{V^2_{inj}}{12} \quad [4.15]$$

At lab-scale and above, the protocols for performing both frontal and pulse experiments are well established. Though each resin manufacturer may specify slightly different parameters such as flow rate, tracer substance, concentration and volumes, as well as detection method, the general protocol is usually very similar; using a pulse of detectable, non-adsorbing material, occasionally step change instead for transition analysis, flowed

through the column at constant velocity with the response measured. Within the microscale domain, however, the literature is not nearly as extensive.

It is known the wall effect can alter packing densities and dispersion, which would be especially pronounced at microscale (Susanto *et al*., 2008, Knox *et al*., 1976, Roberts & Carta, 2020), with HETP subject to this, meaning such a method could help to determine and quantify differences experienced across scales. Knox & Parcher (1969) reported that the wall boundary extended to up to 30 particle diameters, whereas Farkas & Guiochon (1997) reported 50 particle diameters. Regardless of which value is most appropriate, with mean particle diameter of 85 µm, this effect will extend across the entire bed diameter of microscale columns of only 5 mm diameter and therefore is a very important consideration. It is the aim of this chapter to develop methods for testing HETP and asymmetry of microscale columns in order to assess how representative of larger columns they are, and whether HETP can be further used as a test of microscale column performance or as a means to determine model parameters.

4.2 Established Methods

4.2.1 Large scale

The pulse method is the most common method of determining HETP, with a small volume of analyte, such as salt or a UV absorbing tracer is introduced onto a pre-equilibrated column at a defined superficial flow velocity, commonly in the order of 30 - 100 cm h^{-1}. HETP values can be derived from the response (Figure 4.1). The volume of analyte introduced differs between resin manufacturers, though most suggest no greater than 2.5% of column volume such that the subsequent peak variance is through dispersive effects alone, rather than composed largely of the initial tracer injection. Ideally, this injection should approximate a Dirac delta function (of zero width but non-zero area), though in practicality the volume must be large enough to ensure a sufficient signal is obtained (Schmidt-Traub, 2006). Additionally, many constrain the tracer to consist of a reasonably low concentration of analyte compared to running buffer, typically less than 1% (w/v), to reduce nonidealities due to variations in viscosity or flow (Rathore *et al.,* 2003). The column is then pumped with equilibration buffer at the same flow rate, and a response measured using conductivity or absorbance of the resulting effluent.

4.2.1.1 Pulse Method

The column to be assessed is equilibrated with the buffer of choice, typically the same as the process equilibration buffer. The tracer is introduced, and the process buffer is again flowed down the column, with the effluent monitored.

One may account for the dead volume, or extra-column volume, of the set-up, as may greatly influence analysis, which can be performed running a pulse through the system without a column. One can then account for this

dead volume by removing the peak position without column from the pulse data performed with a column, though this will not account for broadening in the system, which can be achieved with mechanistic modelling (Chapter 6 and 7) or through moments analysis, though as described, moments analysis will not account for additional peak asymmetry. Ideally, one should choose a system with the lowest dead volume and must also ensure the pulse volumes handled by the system are accurate. This is not typically a concern for larger scales, but with small scale this is an important consideration.

4.2.1.2 Frontal Method

The frontal method is very similar, with a pre-equilibrated column being pumped with the equilibration buffer with the addition of an analyte, the tracer buffer. Rather than a small pulse, this buffer is continuously pumped at the defined flow until the tracer is apparent in the output. This data is commonly available in manufacturing, in which step changes are often performed in the process, and therefore may give an insight into column performance over a campaign without requiring additional qualification experiments (Larson *et al*., 2003) through measuring transition in conductivity between buffers. As with pulse methodology, the tracer concentration must be considered as this may impact the resultant values (Lettner *et al.,* 1995). Care should be taken to ensure the buffer switch is as fast as possible. In this investigation, for suitable sized columns, large sample loops filled with analyte buffer were used for small columns, rather than a separate buffer inlet, to ensure this fast step. As with the pulse method, the dead volume should be accounted for, if not avoided as much as possible. The resulting chromatogram is then differentiated with respect to time or volume, with the differentiated signal forming a peak (Figure 4.3). However, because of two different buffers in contact, there could be an effect on mixing not apparent during pulse injections, as well as a reduction in signal due to the requirement to differentiate the incoming signal. Some have reported a significant difference in HETP estimation through these two different methods (Lettner *et al.,* 1995).

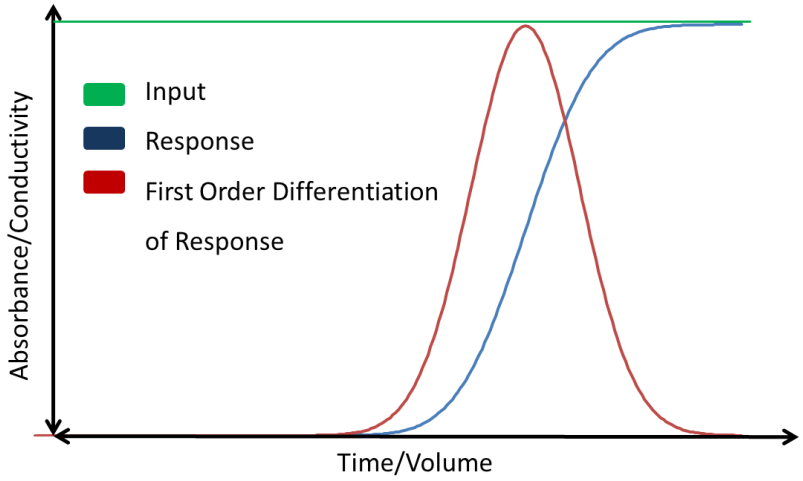

Figure 4.3 - Obtaining a pulse trace from a frontal experiment through differentiation

4.2.2 Methods on Microscale Columns

These protocols, being well established, are facile to follow for the vast majority of columns at lab-scale and greater. Difficulties arise where the system is of a separate scale to the column of interest, such as HETP testing a small lab scale column on a lab scale system with significant dead volumes. These issues can be mitigated by either using a system better suited to the scale concerned, or by removing as many sources of dead volume as is practicable, as well as through analysis with the method of moments, though this is less perfreable than avoiding the phenomenon experimentally. This may be achieved using sample loops of appropriate size to avoid mixing of analyte within the system before introduction to the column.

For microscale columns several complexities arise. Firstly, the physical design of the column; whereas typical lab-scale columns allow direct plumbing to a FPLC system through threaded connectors, microscale columns do not possess such adaptors and are operated by pipette.

Two companies who had published results of HETP testing microscale column were contacted, the column manufacturer (Repligen, formally Atoll), and the resin manufacturer (Cytiva, formally GE Healthcare), for information on how they performed their microscale column characterisation. The column manufacturer kindly forwarded their own internal data, demonstrating that they had used a liquid handling system. The resin manufacturer had fashioned a rig with which to attach a microscale to a conventional FPLC system, though did not provide their data.

4.2.2.1 HETP analysis using a liquid handling system (column manufacturer (Repligen) method)

The column manufacture suggested mimicking a HETP experiment entirely on an LHS. This configuration presents a number of issues seen with their data; poor resolution meant their fitting was not robust, the weak UV signal meant a 25% CV pulse was employed, a 10-fold increase compared to convention. Figure 4.4 exhibits this data, with a total of 10 data points, and significant noise.

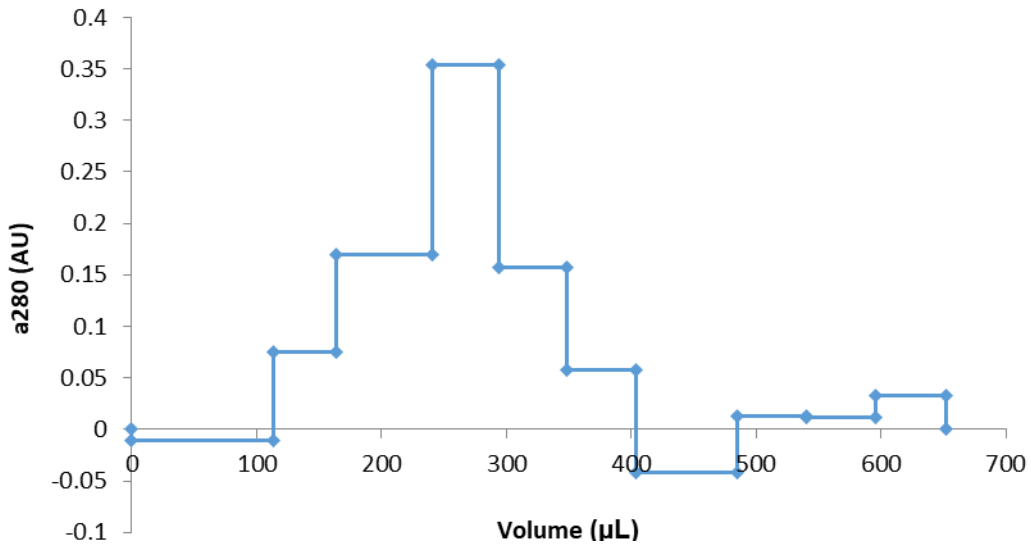

Figure 4.4 - Microscale column manufacturers In-house HETP data, with which they used to HETP qualify the columns. 12 Data Point per column, 66 µL (0.33 CV) fraction size, courtesy of Repligen (formally Atoll GmbH)

4.2.2.2 HETP analysis using a FPLC system (resin manufacturer (Cytiva) method)

Whereas testing on a liquid handling system is the most straightforward, experimentally, for microscale columns, the resin manufacturer had performed HETP by building a rig to allow connection of the microscale column to a conventional FPLC machine, though did not provide raw data, but did confirm in correspondence that this was the approach they had used. This provides all the benefits FPLCs bring, in that it is a closed system, with continuous fluid control and online monitoring, as well as providing high resolution with a UV flow cell volume of a few microliters on smaller FPLC systems, demonstrated in the provided chromatograms (Figure 4.5).

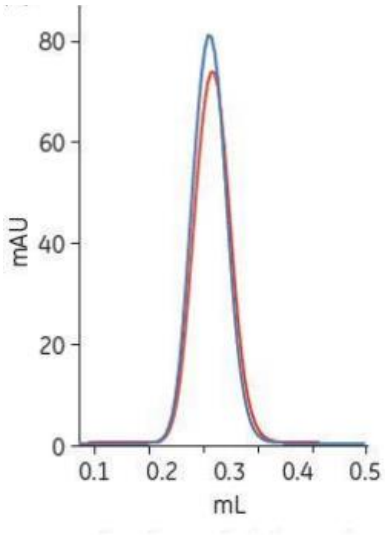

Figure 4.5 - Resin Manufacturers in-house HETP data , courtesy of Cytiva (formally GE Healthcare), with two repeats (blue and red) of a 200 µL column. Of note is the increased retention volume (>1 CV), likely due to hold-up volume of their system. Obtained from GE Healthcare.

4.3 Materials

4.3.1 Buffers

The primary buffer used for this work is the established in-house HETP running buffer (100mM Sodium Phosphate, pH 7.0), with different HETP spiking buffers, each with a small concentration of UV active component or salt.

4.3.1.1 HETP Tracer Buffers

A number of analytes were tested for use in HETP, with their compositions below (Table 4.1). Analytes were selected initially from available compounds in the lab (DMF, AcO, AcON, NaCl, Cystamine) and tested for absorbance, with further analytes acquired (PABA, Trptophan, Cystamide). These compounds were selected based upon strong UV absorbance, lack of toxicity and volatility. All analytes were titrated to a pH of 7.0 ± 0.05 with phosphoric acid or sodium hydroxide to ensure constant pH.

Table 4.1 - Composition of HETP Analyte Buffers

Analyte	Composition
Sodium Chloride (NaCl)	100mM Sodium Phosphate + 0.5 M NaCl
Acetone (AcO)	100mM Sodium Phosphate + 1% (v/v) AcO
Acetonitrile (AcON)	100mM Sodium Phosphate + 1% (v/v) AcON
Dimethylformamide (DMF)	100mM Sodium Phosphate + 1% (v/v) DMF
Phenylalanine (Phe)	100mM Sodium Phosphate + 5mM Phe
Toluene	100mM Sodium Phosphate + 0.1% (v/v) Toluene
Tryptophan (Trp)	100mM Sodium Phosphate + 5mM Trp
Cystamide	100mM Sodium Phosphate + 5mM Cystamide
1,4 Aminobenzoic Acid (PABA)	100mM Sodium Phosphate + 5mM PABA

4.3.2 Equipment

As before, the Tecan Freedom EVO 200 was used, though this time with larger (600 µL) microscale columns with an internal diameter of 5 mm and a bed height of 3 cm. A conventional FPLC system (AKTA Pure 25) was also used, paired with a HiScale column (GE Healthcare), and manually packed with 58 mL of Protein A resin (MabSelect SuRe, GE Healthcare), with a bed height of 29 cm and internal diameter of 1.6cm. The FPLC systems enabled continuous pH, conductivity, UV (190 nm to 700 nm wavelength), and pressure measurement.

4.3.2.1 Microscale Column to FPLC Rigs

In order to benefit from the online measurements that a FPLC system affords, a number of approaches were tried to attach microscale columns onto a FPLC. Two rigs were fabricated, the first using silicone tubing and larger connectors which were adhered to a spare Tecan LiHa tip, which in turn was pushed into a microscale column. This was followed by more rubber tubing, secured with zip-ties (Figure 4.6A); the second rig used capillary tubing (Figure 4.6B), of internal diameter of 0.25mm rather than the conventional tubing of diameter 0.15 mm, to reduce system pressure, and smaller connecting parts were used. The loops were secured directly above the LHS tip, and the column was integrated into the system by forming a screw-thread on the column outlet by forcibly twisting the columns into a conventional FPLC female screw thread adapter.

The minimum volume able to be handled by the system was 10 µL in 10 µL increments, motivating a different route to be taken if 12 µL (2% of a 600 µL column volume) was to be handled reliably and accurately. To ensure the system injected correct columns of analyte solution, custom loops were fabricated by cutting lengths of PEEK tubing (GE Healthcare). Capillary tubing of 0.15 mm internal diameter was used, a length of 68 cm contained 12 µL of fluid. This was confirmed by weighing empty tubing and weighing again when filled with water. Volumes were within error of the balances used (± 0.5 mg).

The set-up was not ideal; there was significant dead volume (450 µL for rig 1, 290 µL for rig 2, determined by filling with water and measuring the mass difference, likely an error prone estimate), ideally the rubber tubing needed replacement by capillary tubing to reduce mixing within the tube. Care was taken to minimise leaks, though they often occurred due the inherently insecure connections. The additional back pressure (0.3 MPa) also put further strain on the column, at faster flowrates the column would separate at the inlet as the housing could not withstand the pressure. Additionally, the limitations of testing a single column at a time meant it became quite time consuming; while effort was made to optimise and streamline testing through planning sequential experiments, going from simultaneously testing eight columns to one was detrimental to throughput.

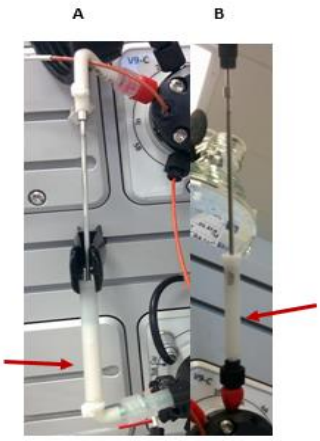

*Figure 4.6 – Rigs for connecting microscale columns to a FPLC system **A** - The first rig, **B** the second rig, demonstrating a reduction in volume by removing rubber tubing and excess connections. Red arrows highlight the columns*

4.4 Experimental Methods

4.4.1 Ascertaining UV Spectra

100 µL of analyte were pipetted into a Corning 96 well UV transparent flat-bottomed microplate and placed in the Infinite 200 PRO plate reader. Absorbances were measured in 5nm increments from 230nm to 1µm wavelengths. Data was plotted to form spectra. Again, background measurements were taken and corrected for at every measured wavelength against an empty well.

4.4.2 Pulse Tests

Pulse tests, in which a small volume of non-adsorbing material was flowed down columns were commonly performed over the course of the project, namely for HETP determination here and column bed characterisation in Chapters 6 and 7. Described below is the general methodology for performing these experiments.

4.4.2.1 Pulse tests using an LHS

Resolution in 96-well plates can be poor, due to the minimum working volumes of the plates used (schematic in Figure 4.7, described in Chapter 3). Beneath this minimum working volume, the effluent forms a ball within the well, meaning the single point UV absorbance is subject to specular reflection, and the single point does not represent the average contents of the well, or the droplet is entirely outside the path of the radiation. With an even meniscus, however, assuming the contents are homogenous, one can measure the absorbance, path length and therefore calculate the concentration by applying the Beer-Lambert law [4.16]. A strategy of prefilling the wells to above this working volume, and then accounting for this additional volume in processing was attempted as a means of acquiring better resolution by avoiding the minimum working volume limitation.

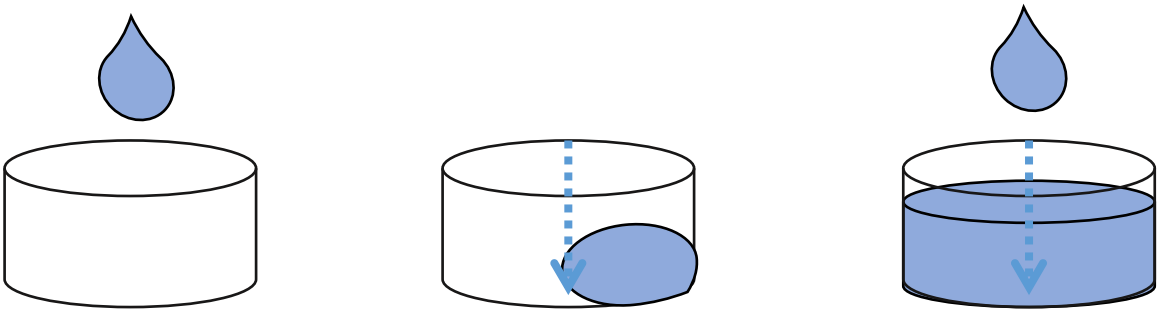

Figure 4.7 - Demonstration of well pre-filling, exhibiting how an even meniscus, and therefore accurate measurements can be achieved by pre-filling wells

The plates used (Corning 96 well UV transparent flat-bottomed microplates) were filled with running buffer to the working volume (100 µL) before use. These plates were then stacked, with an empty plate on top as a barrier to evaporation, in the plate stackers on the LHS before use. For the first dispense cycle, 930 µL of running buffer was aspirated, followed by a 2% CV pulse of analyte solution (12 µL) and another 8µL of running buffer. This ensured that the analyte solution was immediately followed by running buffer without waiting for another aspiration cycle and preceded by a small amount of running buffer minimise additional analyte remaining on the tip surface, which could affect the peak. The running buffer was dispensed along the columns at a linear flow velocity of 60 cm h^{-1}, higher than the manufacturers guidelines of 30 cm h^{-1} (GE Healthcare, 2011a), but used in-house to save time as well as being safely within the flow capability of the LHS. The time moving the plates was not considered, though is expected to be <10 s in total for the vector settings used. Fractions were collected every 25 µL in pre-filled plates. Up to two aspiration-dispense cycles were used, corresponding to a total of 3 CVs of fluid for a 600 µL column, read over 6 plates, meaning 72 fractions for column per run. Columns were used in 8-fold replicates. Smaller columns were subject to a single aspiration cycle. The plates were then measured for absorbance at 977 nm, 900 nm and 280 nm using the plate reader, for single point absorbance measurements, with data then processed with the standard curve approach, detailed in the previous chapter.

4.4.3 HETP tests on an FPLC

To avoid mixing in the system as much as possible, before introduction of the analyte buffer to the column, different pumps were used for equilibration buffer and the running buffer, with a system wash occurring in-between, except for the microscale columns, in which the analyte was introduced by the sample loop for pulse tests (12 µL and 2 mL loop volumes), and sample pump for frontal tests at large scale, largely for system dead volume mitigation and greater volume accuracy. All experiments at all scales were performed at a superficial flow velocity of 60 cm h^{-1}. Equilibration volumes were increased from 5 CV to 10 CV to account for the increased contribution from system volume for microscale columns and avoid system mixing dominating results.

4.4.4 Calibration Curves

As before, calibration curves were generated for the analytes and buffers used, for accurate volume and UV absorbance measurement. The FPLC has a UV cell of constant volume, so no volume calibration had to be performed, however, the linear range of the detector was measured to investigate the linearity absorbances, thus allowing the Beer-Lambert law to be valid [4.16], in which absorbance is linearly correlated to the concentration of UV active material and path length. Samples of too high absorbance cannot have their concentration accurately measured without reducing the pathlength or concentration, as too few photons are detected to accurately determine absorbance (Wormell & Rodger, 2013). There are many other physical processes leading to deviations from Beer-Lambert behaviour, such as concentration dependant intermolecular interactions and sample inhomogeneity, which will be ignored due to the low concentration of PABA used (5

mM), significantly below the aqueous solubility in standard conditions of 40 mM (Yalkowsky & Yan, 2003), and that relatively high absorbances are measured before deviation from linearity is observed (Figure 4.8) means these effects were not further considered.

$$A(\lambda) = \varepsilon_\lambda \cdot c \cdot L = \log\left(\frac{I_0}{I}\right) \qquad [4.16]$$

To assess this range in which concentration of UV active material and 280 nm absorbance were related linearly, the system was flushed with UV inactive buffer (deionised water). A gradient of UV active buffer (5mM para-amino benzoic acid (PABA), 0 to 100% over 500 mL) was then applied, to observe at which 280 nm values the relationship deviated from linearity. Linear regression was performed for 280 nm absorbance values under 1000 mAU, and the resulting line equation used to extrapolate the theoretical absorbance at higher concentration of PABA. This adjusted 280 nm absorbance was then compared against the experimental 280 nm absorbance. As a test for the accuracy of this value, a literature value of the extinction coefficient of PABA was used to determine the theoretical absorbance at a given concentration. The system being used has a UV path length of 2 mm, and the extinction coefficient at 280 nm (ε_{280nm}) of PABA has been interpolated, with a linear approximation, from a literature dataset to be 5455 M^{-1} cm^{-1} (Grammaticakis, 1951).

The conductivity was also measured to ensure that the pumps were operating correctly, as PABA imparts conductivity to the buffer. No significant deviation from linearity (< 5% relative error) was exhibited at absorbance below 2,000 mAU (Figure 4.8), with significant increases in deviation between expected absorbance and measured above this value. The resulting graph allows a correction of the absorbance for saturated signal for PABA, though as the measured absorbance plateaus at 2600 mAU, this approach may only provide an improvement of 500 mAU, from 2000 mAU to 2500 mAU, and should not replace diluting the sample to be within the linear range, though will be used here to account for any excessive absorbance. The adjustment from measured absorbance to theoretical absorbance will also become very error prone as the plateau region is approached. The molar extinction coefficient value of PABA can be determined with the calibration curve, and differs by less than 5% to the reported value in literature (ε_{280nm} literature = 5455 L M^{-1} cm^{-1}, ε_{280nm} determined through linear regression = 5331 M^{-1} cm^{-1}), which can be explained by different lots of PABA and small errors in preparation.

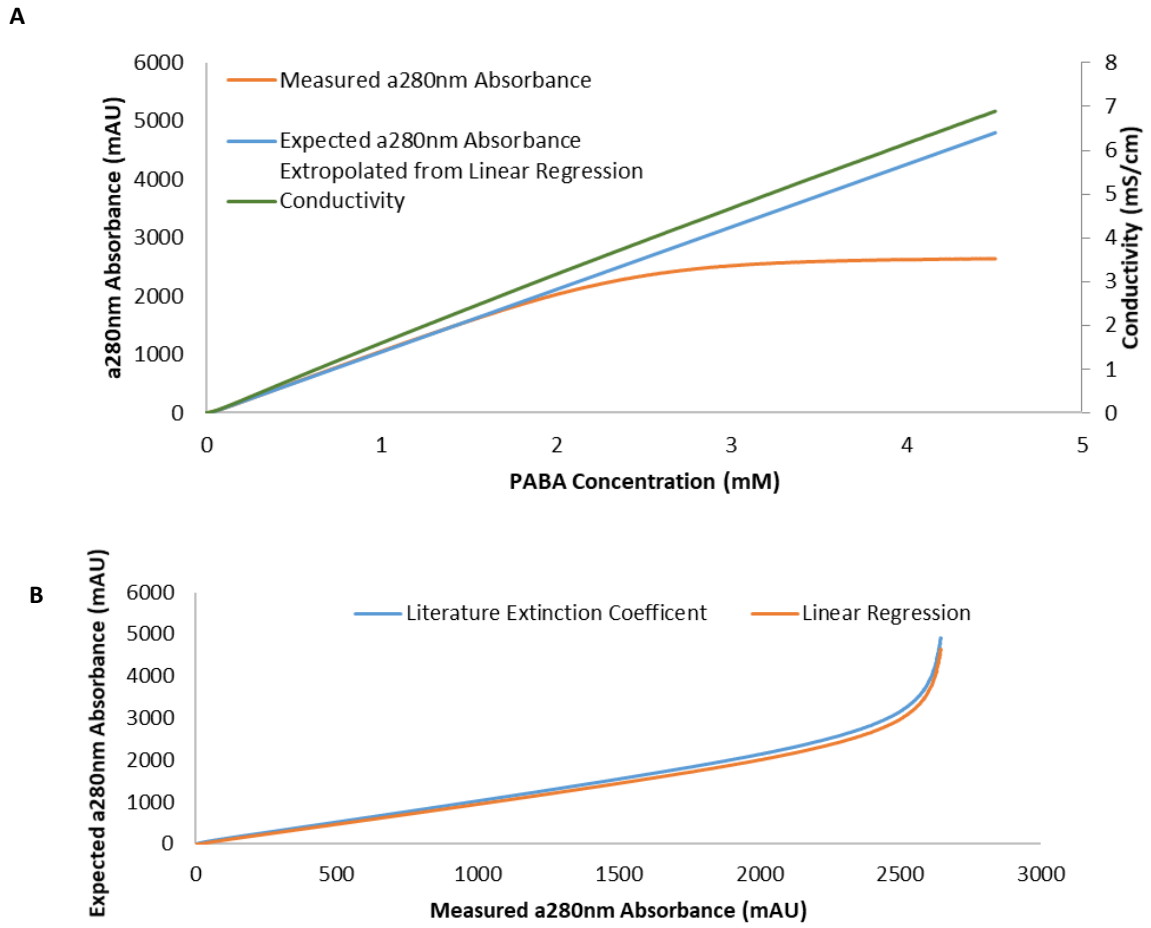

Figure 4.8- Calibration curves for UV saturation estimation and correction. ***A*** *-Calibration curve of 280nm absorbance vs increasing concentration of UV active buffer (from 0 to 5mM PABA over 500mL at 5 mL/min) demonstrating linearity between concentration and UV absorbance beneath 2000 mAU, with less than 5% difference between the expected and measured absorbances.,* ***B-*** *Measured absorbance value when compared against the expected value, by either using literature extinction coefficient (blue) and that determined by the linear regression (orange).*

4.4.5 Drop Size Determination

Experiments to determine the average drop volume from microscale columns were performed through UV absorbance. 96 well plates were prediluted (100 µL), measured for volume, and then passed under the columns under normal operation collecting drops of effluent. The volume of effluent was determined by measuring the difference in volume within the wells before chromatography and afterwards, through 900 nm corrected 977 nm absorbance. The fraction volume was set on the LHS to be 15 µL, which was considered to be well below the drop size, estimated using a manual pipette to be in the order of 30 µL. Wells were prefilled with buffer to ensure each drop was resolved, as each drop was additional to a volume that met the minimum measurable volume. A script in MatLab was written, which selected for volumes at least 5 µL above the measured prediluted volume and removed them from the dataset, such that small variations within aspirated volumes could be ignored entirely.

4.4.6 Measuring FPLC Dead Volume

Extra-column, or system, volume can greatly impact results of HETP tests especially at small scale, determining this volume was considered crucial for column evaluation and future modelling. Measuring the dead volume was performed by equilibrating the system with an equilibration buffer and determining UV absorbance. Once a steady UV signal was achieved, the system was then filled with UV active buffer (1% v/v Acetone) at a defined flowrate, and the response measured, until the UV signal stabilised. Additionally, for pulse tests, one can account for dispersion of the analyte material before, or after, introduction of the material onto the column. As the pulse material is stored within a sample loop, which is not in line with the system for the breakthrough runs. This experiment is performed identically to the pulse tests described above, but with a small length of tubing replacing the column. One can see a highly asymmetric peak (Figure 4.9A)., indicating significant mixing within the system rather than the rectangular pulse that would occur in an ideal system. When compared by differentiating a step response into a peak (Figure 4.9B), or by integrating a pulse response peak into a step response, two notable differences are seen, an increase in offset but reduction in peak width for the step response, likely due to the difference of flow path in this configuration. This suggests that dead volume determination should be tailored to the HETP being performed, both for flowrate but also system configuration.

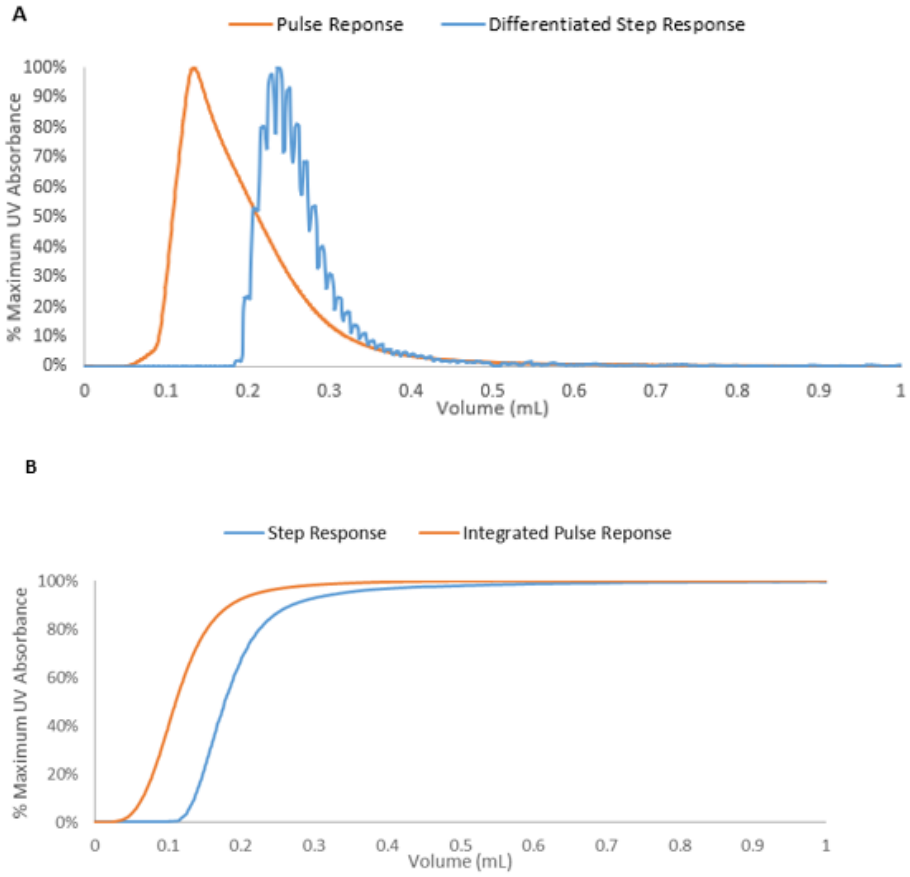

Figure 4.9- Comparison of Step vs Pulse methods of dead volume determination, ***A*** *– Compared by processing a step response into a pulse by differentiation, of note are the artefacts introduced by the procedure the oscillations are caused by amplifying the noise in the raw data, and the increased offset but reduced dispersion for the step response* ***B-*** *Both approaches compared by processing a pulse response into a step response by integration. Both approaches were processed by normalising the Y axis to percentage of maximum signal*

4.4.7 Data Treatment

For all HETP results, the volume was corrected such that the volume was measured from the midpoint of injection. The data then had baseline conductivity or 280 nm absorbance removed, and if required, the chromatogram was differentiated by calculating the difference in conductivity or 280nm absorbance for each subsequent volume/time point. If absorbance exceeded 2,000mAU, but was less than 2,500mAU, a correction was performed as detailed in section 4.4.4. The statistical moments were determined through the above identities[4.5 to 4.9], with the integrals determined through the trapezium or Simpsons rule (Misra *et. al*, 2019), or through fitting the EMG function and processing of the determined EMG parameters. EMG parameters were fitted using a least-squares curve fitting method.

4.5 Results and Discussion

Initial work was focussed on improving the resolution of the resultant HETP peaks. Whereas others have taken approaches including transferring eluate material from an oversized plate into a smaller, 384 plate with reduced minimum working volume (Evans *et al.* 2017), though not directly used for HETP determination, the additional time in regards to material transfer, and requiring additional plates meant other methods of improving resolution and signal were investigated. The work by Osberghaus *et al*., (2012), in which a pulse experiment was repeated with an offset was ruled out due to significant losses of liquid through missed drops meaning the peaks often overlapped, rather than a true offset, though ideally this should have been further evaluated.

4.5.1 Drop Volume Determination

In order to optimise fraction size with the aim to improve data density, if trying to elute single drops, an understanding of the drop size distribution is required, as well as seeing drop size variability among the columns. Using the prefilling approach, 18 plates were analysed to determine the drop size from microscale columns.

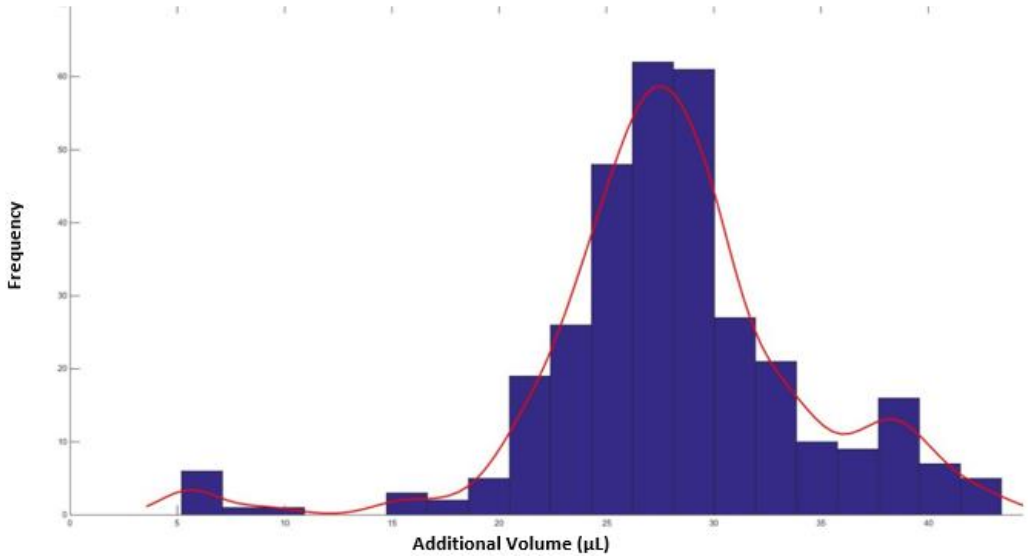

Figure 4.10 – Histogram (2 µL bins) of measured drop volume distribution with 18 plates,

The mean drop size was 28.1µL, with a standard deviation of 6.1µL (Figure 4.10). From 1728 wells measured in the experiment, only 1093 had the required volumes for selecting for volume determination indicating a drop had been collected, a well occupancy of 62%. Total mass retention was measured at 22,550 µL (±132µL) across all runs, measured from 25,920 µL dispensed by the machine, representing a 13% loss, likely down to plate changes and shuttles leading to these lost drops. This a significant improvement compared to the mass retention without using the pre-filling technique, which averaged more than twice the volume loss at comparable resolution (Table 3.2).

The impact of the volume loss varies experiment to experiment; experiments such as HETP analysis, where constant flowrate is required, may suffer more lost drops due to the need to minimise flow interruption and use many plates to capture as much data as possible. Low resolution investigations using fewer wells is likely to lose a lot less fluid, due to fewer plate changes and shuttles per volume of fluid, as well as being able to implement a pause before plate changes, reducing drop loss. Column variability was shown to be small, both between runs and between columns. All drop size averages appeared similar for all runs, columns and column positions (Table 4.2). One way ANOVA confirmed no significant difference between either individual experiments nor columns.

Table 4.2- Drop size measurements from microscale columns, A – For each column, with 5 experiments per column B – For each experiment, with 8 columns per experiment

A

Column	Mean Drop Volume (µL)
1	31.1 ± 8.3
2	30.3 ± 7.9
3	31.4 ± 10.1
4	30.1 ± 11.6
5	30.8 ± 9.2
6	31.2 ± 9.8
7	34.2 ± 12.5
8	32.0 ± 7.6

B

Experiment	Mean Drop Volume (µL)
1	29.3 ± 7.3
2	30.3 ± 11.2
3	35.1 ± 9.4
4	31.4 ± 7.5
5	32.3 ± 3.8

4.5.2 HETP resolution improvement

Initially, the column manufacturer's method of a 25% CV pulse was performed, though using a 600 µL column, rather than the 200 µL columns used by the manufacturer, for the purposes of improved resolution; a larger column increased the number of possible fractions by a factor of 3 with no other modifications.

Using 25µL fractions, such that it is just beneath the average drop volume, with the pre-filling strategy, resolution was greatly improved, with 72 data points per column, however, the data has significant noise (Figure 4.11), and it was not possible to fit an EMG distribution with any degree of confidence.

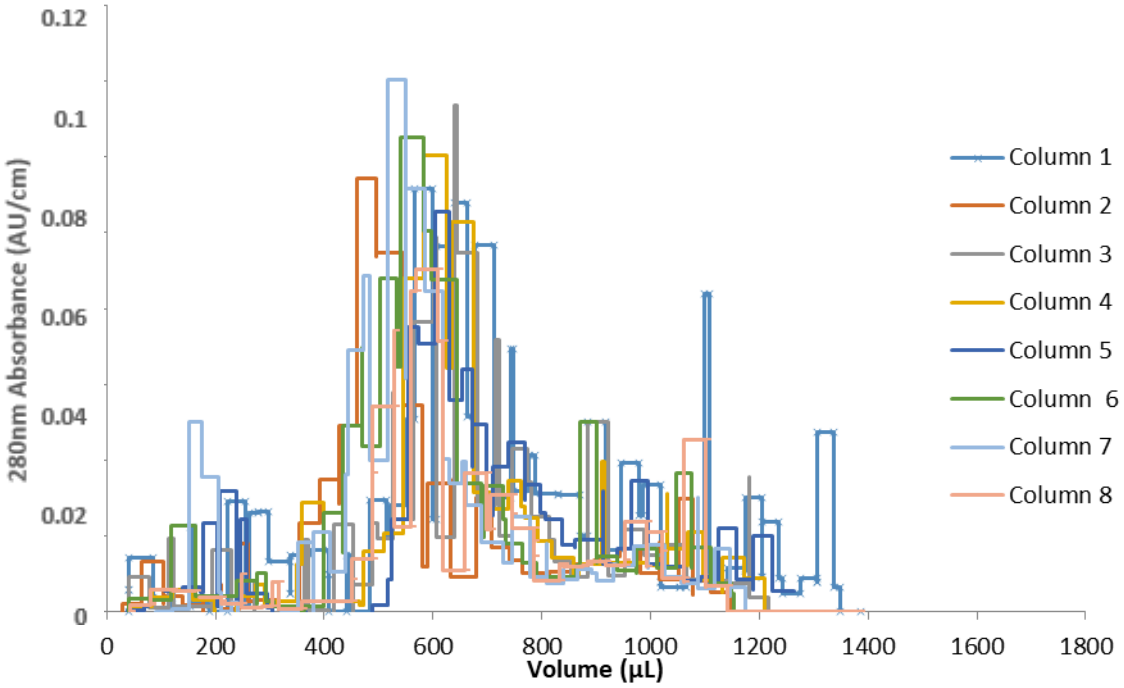

Figure 4.11 - HETP Pulse with 600 µL columns with column manufacturers protocol and improved resolution, 25% CV pulse of 2% (v/v) AcO

The source of poor signal was investigated. Acetone readily evaporates at room temperature, so the impact of this was quantified. Two plates filled with phosphate buffer of volumes 50 µL to 300 µL, and acetone concentration of 0% to 2% (v/v) were monitored over 5 hours, one subject to UV absorbance read every 5 minutes, the other at the beginning and end of the experiment. Considering liquid level alone, Figure 4.12A demonstrates that evaporation was insignificant, even at these greatly extended timescales. Additionally, evaporative losses were comparable for both the continuously read plate, and the one left on the deck, showing

the UV reader does not significantly affect evaporation over multiple reads. Linear regression showed total evaporative loss was on the order of 80 nL to 150 nL per minute for 50 µL to 300 µL starting volumes respectively. The change of evaporation with well fill volume can be explained by both the frustum geometry of the wells meaning greater volumes have slightly more surface area, as well as less shielding from the ambient airflow by the headspace of air for less filled wells.

280 nm measurements, however, did exhibit a significant decay (Figure 4.12B) with respect to time. Acetone has a boiling point of 56°C (Haynes, 2014), and a high vapor pressure at standard temperatures and ambient pressure (Dean & Lange, 1999). Over the course of the experiment, absorbance at 280 nm of the acetone containing samples followed an exponential decay curve, with a half-life of 45 minutes. The plates and solutions are expected to be exposed to the environment for a similar amount of time during normal operation, suggesting this is a significant source of error in HETP tests with acetone on microscale columns. On a closed FPLC system, this evaporation is negligible, hence the common use of acetone as a tracer at this scale without issue.

A

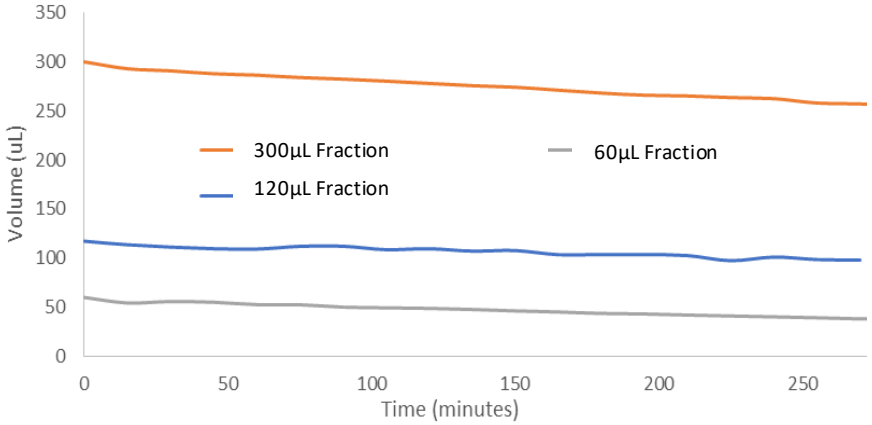

B

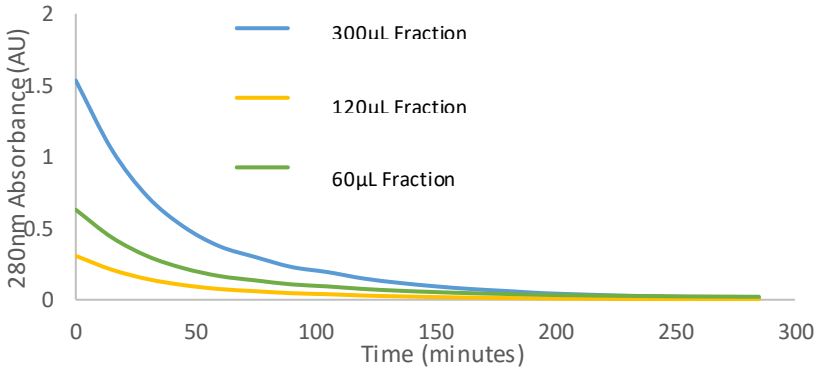

Figure 4.12 – Measurement of microtiter plates filled with solutions of 300 µL, 120 µL and 60 µL of 2 % (v/v) acetone measured every 5 minutes for 5 hours. ***A*** *– Volume decay over time determined by 977 nm and 900 nm absorbance* ***B*** *– Acetone loss over time determined by 280 nm absorbance*

4.5.3 Analyte and Method Selection

Due to the volatility of acetone and the open nature of microscale chromatography, the use of acetone as the analyte on LHS runs was discounted. In order to find a suitable spiking agent, UV spectra were taken of all easily accessible reagents with the criteria of strong UV absorbance, reduced volatility and minimal toxicity. These included the organic solvents dimethylsulphoxide, dimethylfuran (DMF), acetonitrile and toluene. Organic powders, such as cystamine hydrochloride, tryptophan, para-aminobenzoic acid (PABA), phenylalanine and tyrosine were also investigated, and acetone and sodium chloride served as a standard. UV active salts, such as Sodium Nitrite, would have also been worth evaluating, but were not considered at the time.

Toluene was excluded early, as it readily dissolved the plastic plates at concentrations enough to strongly absorb UV. Dimethylformamide, PABA and Tryptophan all exhibited strong absorbance, with the latter two being diluted to 0.5 mM for spectral measurement to prevent saturation of the detector and were subsequently corrected to 5 mM per the Beer-Lambert law [4.16].

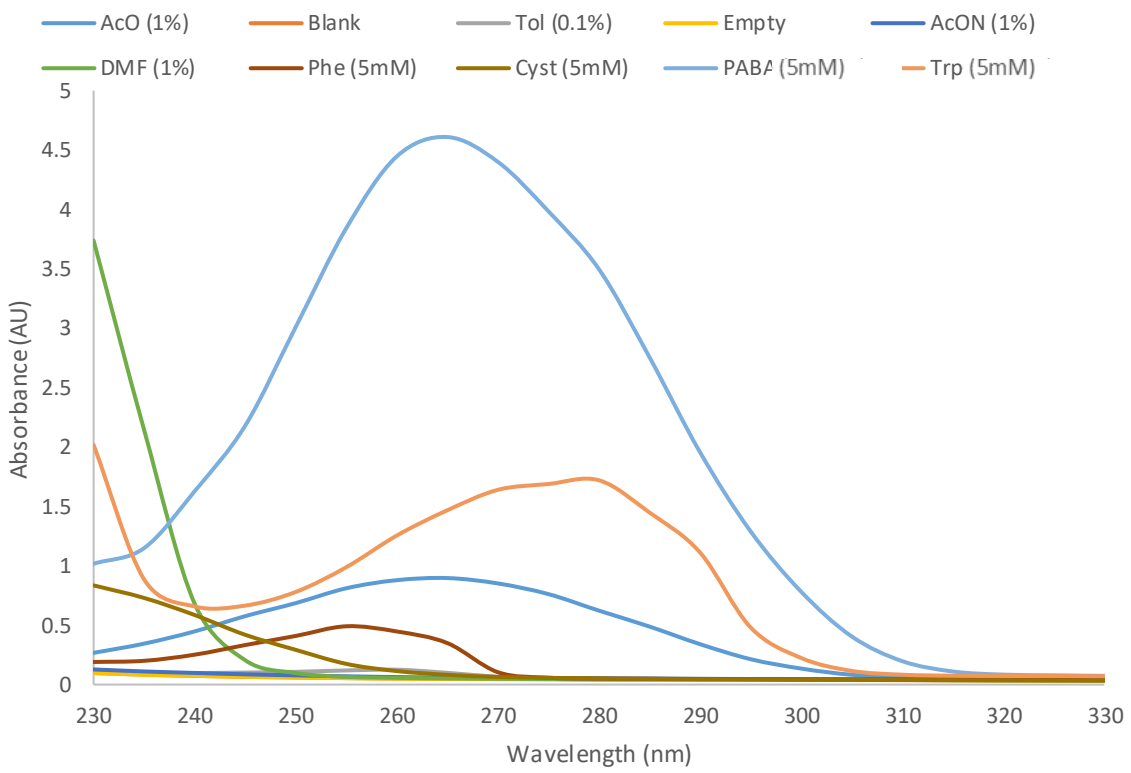

Figure 4.13 - Spectra of candidate HETP analytes; PABA and Tryptophan were diluted to 0.1 mM in order to avoid saturating the detector, and the spectra corrected from this diluted sample using the Beer-Lambert law

4.5.3.1 *Large Scale Screening*

A large lab scale (58 mL) column with a 29 cm bed height, packed with Protein A resin (MabSelect SuRe), was used in conjunction with an FPLC system. Several HETP pulse experiments were performed, with NaCl, Acetone, DMF, Tryptophan and PABA as the analyte, and a frontal separation of NaCl. Concentrations were standardised to 5 mM for PABA and Tryptophan, 1% (v/v) for acetone and DMF and 0.5 M for salt, and a 2% CV volume pulse of material used for all pulses.

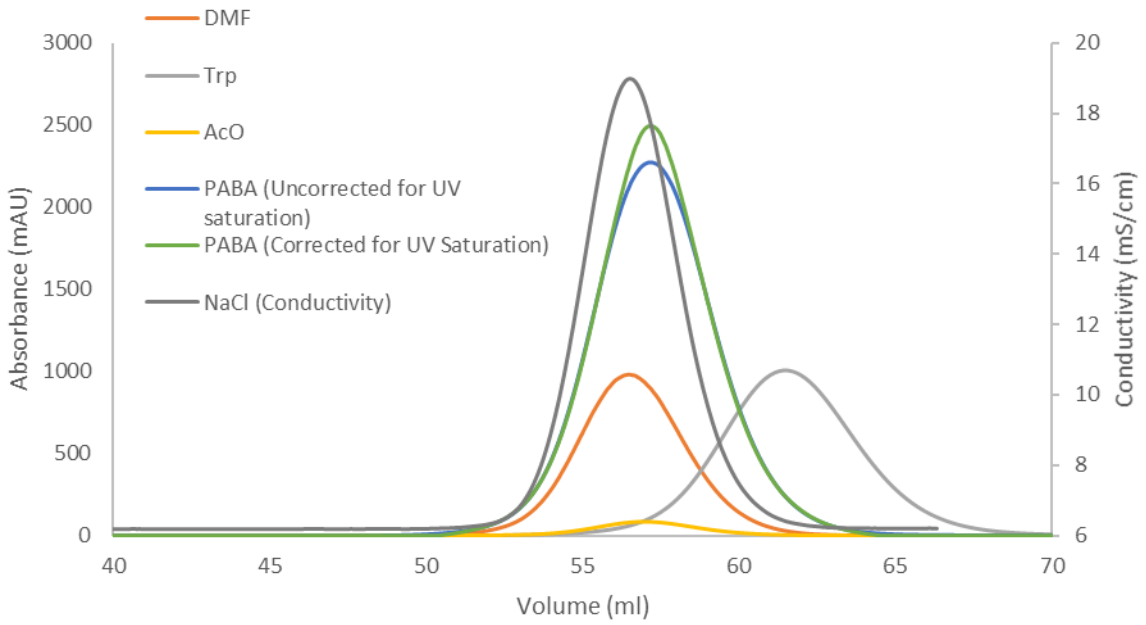

Figure 4.14 - HETP Chromatograms for candidate analytes on large scale (58mL) column. For NaCl, conductivity is the relevant signal, for other analytes, 280nm absorbances were taken. The PABA was adjusted using the calibration curve, showing a slight increase in peak height compared to the non-corrected data.

NaCl, acetone and DMF co-eluted, whereas PABA showed some retention by the column and Tryptophan demonstrated a strong retention and fronting (Figure 4.14). DMF had strong UV absorbance and equivalence to NaCl and Acetone derived HETP and EMG parameters (Table 4.3), it is toxic to humans (Kim & Kim, 2011), limiting its suitability. PABA was corrected for UV saturation, though this had no impact to the increase to retention time, it has decreased peak width slightly.

Table 4.3 - HETP parameters at lab-scale using selected analytes. HETP parameters were determined by EMG fitting, and the method of moments approach as well as measurement from peak width at half height and retention volume. n = 3.

Analyte	First Moment (CV)	Second Moment (CV^2)	Plates per Meter (Peak Width Approach) (m^{-1})	Plates per Meter (Method of Moments Approach) (m^{-1})	Asymmetry	Peak Signal
Acetone	0.983 ± 0.007	1.02E-03 ± 2.84E-05	4878± 7	3377± 6	1.10± 0.02	0.083 AU ± 0.0043
Sodium Chloride (Pulse)	0.974 ± 0.006	9.64E-04± 2.32E-05	5333± 9	3462± 8	1.12 ± 0.02	18 mS/cm ± 0.01
Sodium Chloride (Smoothed, Differentiated Frontal)	0.976 ± 0.004	1.09E-03 ± 2.80E-05	5095± 7	3008±5	1.04± 0.01	n/a
DMF	0.974 ± 0.005	1.02E-03 ± 3.11E-05	4270± 5	3254± 3	1.12± 0.02	1.05 AU ± 0.02
PABA (UV, saturation corrected)	0.986 ± 0.005	1.09E-03± 2.84E-05	3445± 6	2991 ± 5	1.13± 0.02	2.3 AU ± 0.03
Tryptophan	1.06 ± 0.005	1.22E-03 ± 3.22E-05	3199 ± 8	3151 ± 6	0.91± 0.03	1.12 AU ± 0.01

Minimal differences between numerical integration with either Simpsons or the Trapezium rule (Kalambet *et al.,* 2018), and EMG determination of the moments were observed, so have not been reported. As adequate fittings were observed using the EMG/Method of Moments approach, and as it better approximates efficiency regardless of peak asymmetry (Carta & Jungbauer, 2010), this approach was solely used for comparisons across scales rather than using the peak width at half height, though this was associated in an increase of plate height. Additionally, using the method of moments, one could remove the system contribution to band broadening and residence time extension, though for this scale of column the impact of system would be negligible, as system volumes were less than 1% of the total volume, so has not been performed here.

PABA was selected as the analyte of choice; whilst it exhibited the poorest HETP results in terms of plate number, it is non-toxic, being a common UV blocking agent in suntan lotion (Patel *et al*., 1992), has very high absorbance at low concentrations, and elutes in similar volumes to NaCl and Acetone whilst exhibiting similar asymmetry. Another benefit is that PABA his a solid at room temperature with a melting point above 180°C, meaning evaporation would be a non-issue. Though the peak width is the second largest after tryptophan, even after saturation correction, the asymmetry was comparable to the conventional analytes, NaCl and acetone.

Additionally, unlike DMF, PABA has some prior mention in literature as being used as an HETP analyte (Rathore *et al.*, 2003).

Frontal runs were tested, to investigate their suitability to determining HETP and asymmetry parameters. While the HETP and asymmetry values were representative of the conventional pulse test, there was significant noise introduced (Figure 4.15). As the data is processed by plotting the difference between a measurement and subsequent measurements, small deviations are greatly amplified, and the total signal is reduced. While this technique does have merit due to it being rather straightforward to perform, with less manipulations than a pulse and availability of data during normal operation, it's intrinsically noisy nature means that at microscale data is unlikely to be reliable due the nature of amplifying errors by differentiating the data, though the EMG parameters remained similar between the two approaches (Table 4.4). At large scale, one has the benefit of having a large number of data points that one can use to smooth the data, using a filter or other methods, and reducing this noise. With microscale data, and the scarcity of data points per experiment means there is a high risk of losing the structure and information within the data by smoothing and should therefore be avoided where possible.

Table 4.4 - Comparison of EMG parameters for Differentiated Frontal and Pulse HETP Tests, demonstrating good similarity between methods (Pulse, and Differentiating a Frontal Experiment). Tau is the parameter with the largest deviation, being significantly higher for frontal runs, all other parameters are more consistent.

	Differentiated Frontal Response	Pulse Response	% Difference Between Approaches
σ (CV)	0.0234	0.0229	2.18%
μ (CV)	0.971	0.967	0.41%
T (CV)	0.0129	0.0141	9.30%

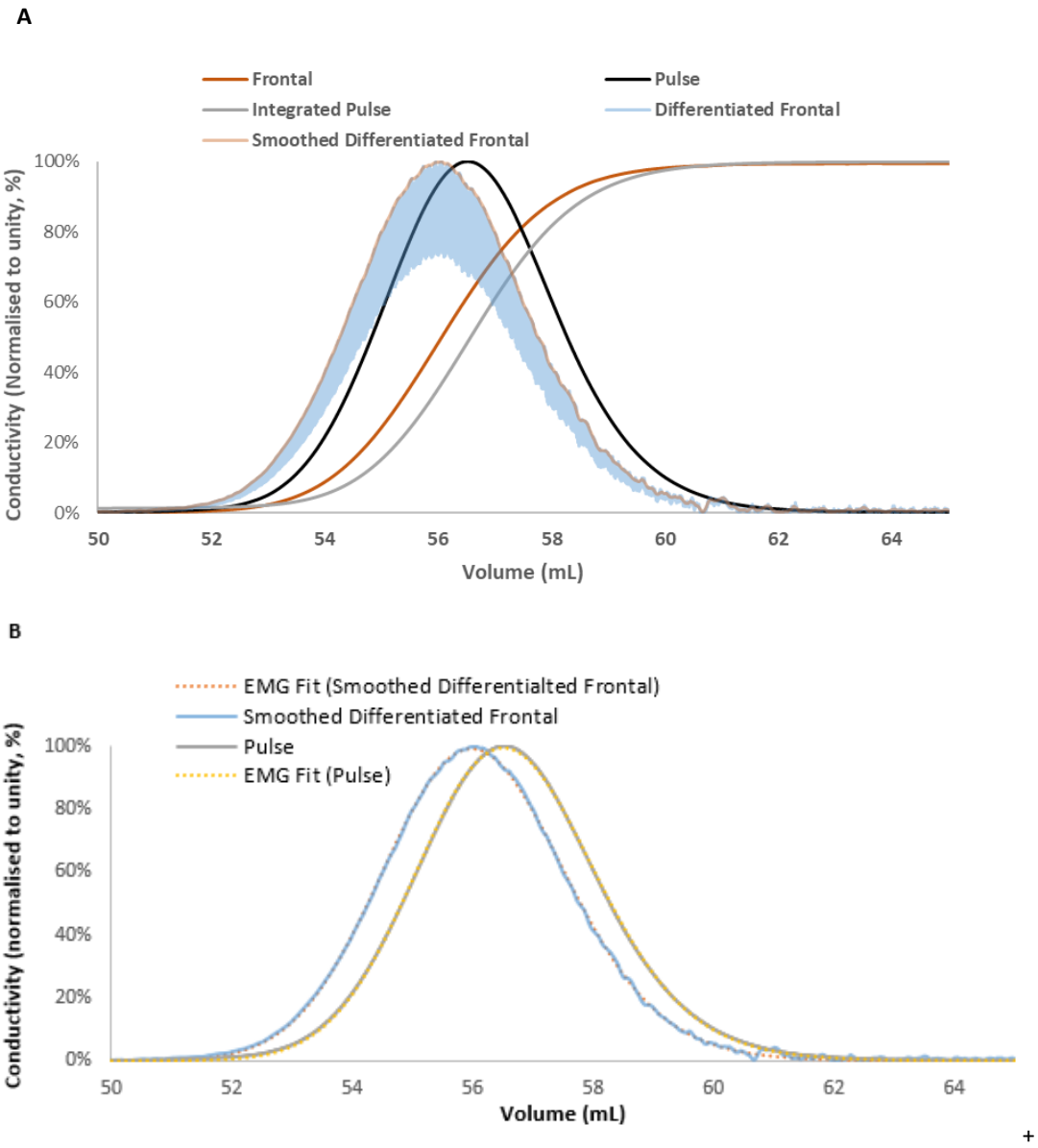

Figure 4.15- Comparison of frontal and pulse HETP tests. ***A****- Frontal and Pulse HETP chromatograms at large (58 mL) scale, with raw frontal and pulse, and integrated pulse and differentiated frontal data, exhibiting increased noise, which has been reduced using smoothing (window of 0.05 mL).* ***B*** *– EMG fits of the raw pulse and differentiated frontal data, demonstrating a good quality of fit. The significant offset between the approaches is likely caused by difference in flow path, considering the similarity in volume with the difference in dead volume estimation*

4.5.4 HETP analysis using a liquid handling system (column manufacturers method)

Below is an example of a HETP run (Figure 4.16), using a 600 µL column, and a 2% CV pulse of 5 mM PABA, and a fitted EMG distribution, and fitting parameters and HETP metrics are shown in Table 4.5. One-way ANOVA did not show any significant differences between metrics for across individual columns nor individual experiments.

A

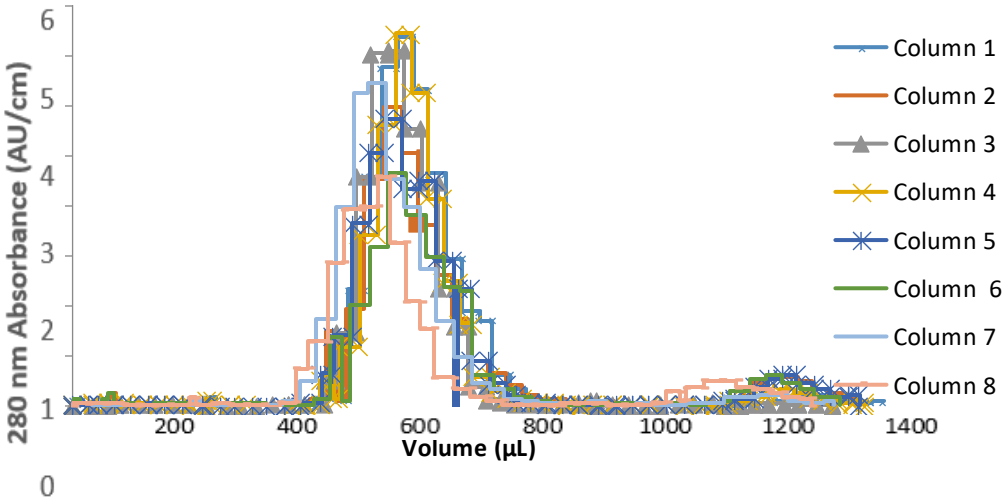

B

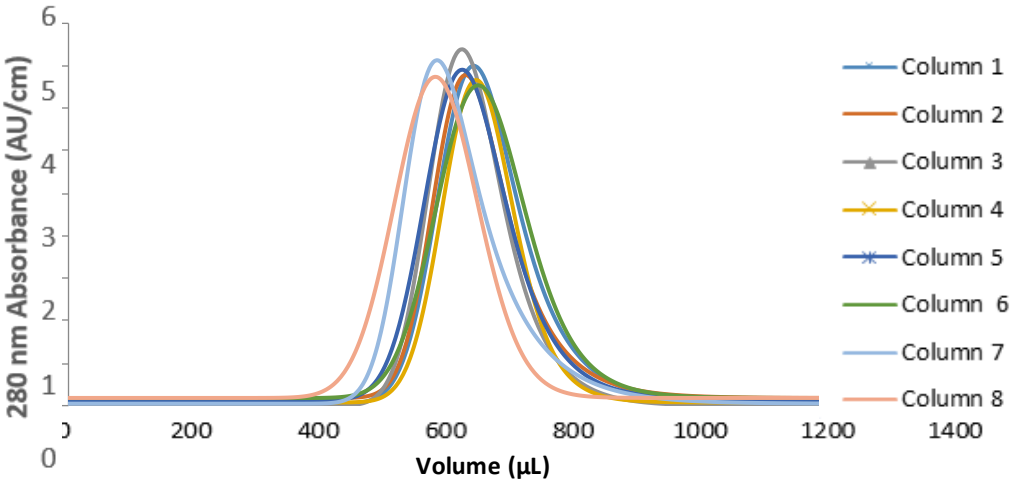

Figure 4.16- Experimental data and EMG fit for 600 µL columns with PABA pulse. A-Experimental data for 8 columns. B - The EMG equation fit of the data demonstrating significant retention volume shifts, but similarity in peak width

Table 4.5- HETP and EMG fitting parameters for LHS derived data with a, 600 µL column, 5mM PABA 2% CV Pulse. A- Average Performance per column over every experiment (n = 5), B – Average performance per experiment over every column (n = 8)

A

Column	EMG Mean (µ (CV))	EMG Width (σ, CV)	EMG Skew (τ, CV)	Plates per Mete (Method of Moments) (m^{-1})	Plates per Meter (Peak Width) (m^{-1})	Asymmetry (As)	R^2
1	1.01 ± 0.05	0.080 ± 0.011	0.12 ± 0.01	2068 ± 301	2282 ± 243	1.88± 0.73	0.97 ± 0.02
2	0.99 ± 0.06	0.077 ± 0.004	0.11 ± 0.02	2233 ± 208	2341 ± 27	2.24 ± 0.72	0.91 ± 0.04
3	0.99 ± 0.02	0.084 ± 0.002	0.09 ± 0.02	2597 ± 668	2649 ± 185	2.10 ± 0.63	0.97 ± 0.02
4	1.02 ± 0.03	0.075 ± 0.008	0.09 ± 0.01	3161 ± 359	3267 ± 288	1.99 ± 028	0.94 ± 0.08
5	0.89 ± 0.03	0.069 ± 0.004	0.15 ± 0.04	1366 ± 159	1366 ± 185	2.72 ± 0.92	0.93 ± 0.06
6	1.08 ± 0.05	0.091 ± 0.006	0.06 ± 0.01	3538 ± 341	3573 ± 421	1.33 ± 0.99	0.96 ± 0.03
7	0.91 ± 0.00	0.077 ± 0.008	0.13 ± 0.00	1558 ± 252	1589 ± 193	2.07 ± 0.75	0.94 ± 0.09
8	0.93 ± 0.04	0.106 ± 0.000	0.05 ± 0.00	2309 ± 586	2425 ± 225	2.75 ± 0.59	0.98 ± 0.01

B

Experiment	EMG Mean (µ (CV))	EMG Width (σ, CV)	EMG Skew (τ, CV)	Plates per Mete (Method of Moments) (m^{-1})	Plates per Meter (Peak Width) (m^{-1})	Asymmetry (As)	R^2
1	1.06 ± 0.05	0.075 ± 0.007	0.13 ± 0.00	2096 ± 411	3113 ± 416	2.749 ± 0.78	0.94 ± 0.05
2	1.01 ± 0.00	0.080 ± 0.002	0.11 ± 0.02	2260 ± 172	2321 ± 186	1.758 *± 0.52*	0.97 ± 0.01
3	0.97 ± 0.00	0.074 ± 0.011	0.09 ± 0.01	2759 ± 121	2521 ± 143	1.927 *± 0.59*	0.96 ± 0.03
4	1.02 ± 0.01	0.083 ± 0.002	0.09 ± 0.02	2740 ± 237	3225 ± 253	2.29*± 0.69*	0.99 ± 0.03
5	0.94 ± 0.05	0.066 ± 0.002	0.15 ± 0.04	1475 ± 277	3609 ± 302	1.98 *± 0.62*	0.94 ± 0.05

A secondary, smaller peak was visible after the second, on all runs (Figure 4.16). This was surmised to be a small amount of additional analyte introduced with the second aspiration cycle, possibly due to residual amount of tracer still present on the pipette tip, as the widths at half height were similar. This peak is entirely separately resolved, and therefore does not affect HETP determination and was not fitted by the EMG equation.

Microscale data demonstrated worse results than seen at lab-scale; with increased plate height and variability between runs (Table 4.5) The poorer HETP results are to be expected, the wall effect will dominating at smaller scales, worsening packing efficiency, with others also reporting greater band broadening on microscale columns (Susanto *et al.*, 2008, Osberghaus *et al*, 2012, Benner *et al*., 2019, Keller *et al.*, 2017).

A total overall asymmetry of over 2 is double the measured asymmetry value at lab-scale and would fail a column for use in production. It is thought the high asymmetry could be due to mixing within the column inlet; a 12µL dispense with significant variation in the pipette tip position could mean the analyte solution mixes significantly with running buffer before introduction to the column, and therefore introduce highly asymmetry into the inlet. Additionally, this may be an artefact of the small plate count; in which an ideal column would be better represented by a Poisson distribution, which is highly asymmetric at small rate parameters.

4.5.5 Small Scale HETP analysis using an FPLC (Resin manufacturers method)

4.5.5.1 Small Lab scale (1mL) and Microscale columns (600 µL) on an FPLC

By making a rig to fashion the microscale columns onto a FPLC like the resin manufacturers (Figure 4.5), it was possible to generate an HETP response, though with significant shouldering of the peak (Figure 4.17A), which prohibited fitting the EMG function accurately. This led to the development of the second rig to reduce the internal volume, and reduce the system contributions. The second rig produced less asymmetry in the resulting HETP peaks and allowed the fitting of an EMG function with good quality of fit. Three runs with the same column were performed to test for variation between runs, with very little variation exhibited between repeats (Figure 4.17B).

A

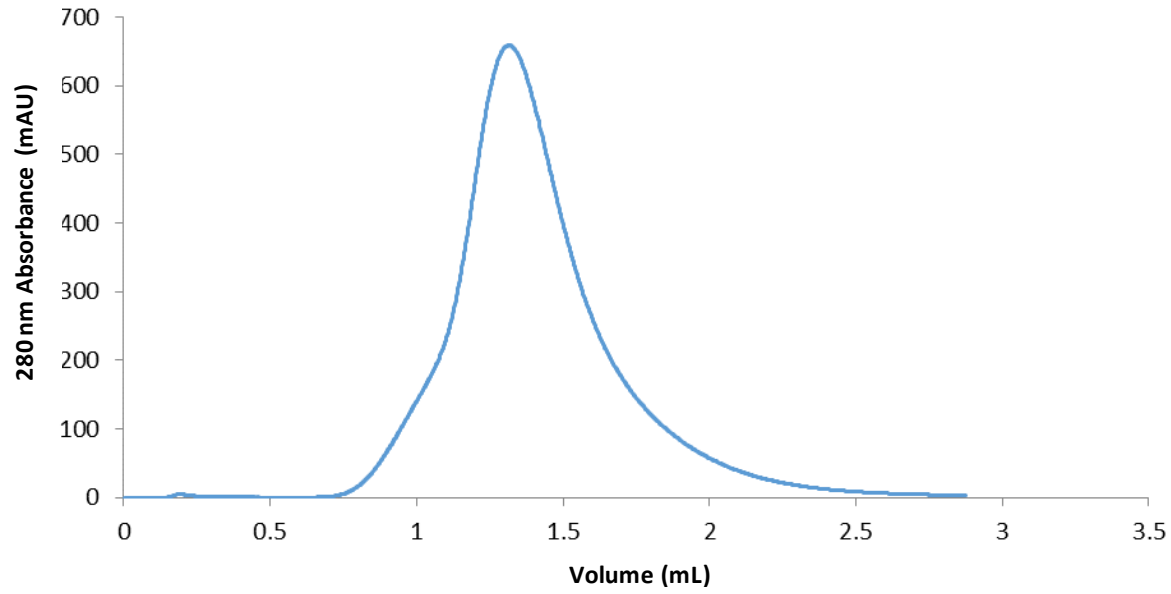

B

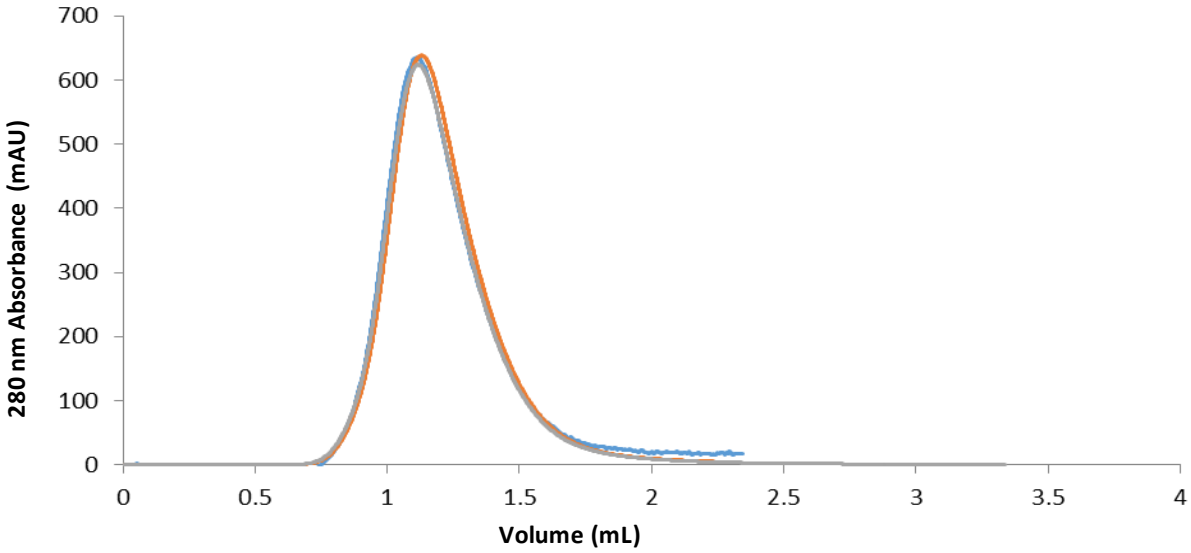

Figure 4.17- Peak responses from using 600 µL columns and rigs to attach them to a conventional FPLC. ***A*** *– The first rig, demonstrating a high degree of shouldering and increased retention volume.* ***B*** *– Three repeats with the second rig, with reduced internal volume and reduction in shouldering, and retention volume.*

Due to the still highly asymmetric and poor HETP results, a prepacked 1mL column was tested, which has a bed height of 25 mm, and a diameter of 7 mm. This was largely to see the effects of small scale HETP testing on a FPLC system using a column designed for such a system, thus avoiding issues arising due to the rig. Additionally, the column coming prepacked from the manufacturer meant we could assume the column to be packed well,

even if HETP results, likely caused by dead volume evidenced by the asymmetry and retention time being above the column volume, suggested differently. Figure 4.18 shows the good quality of fit for the EMG equation.

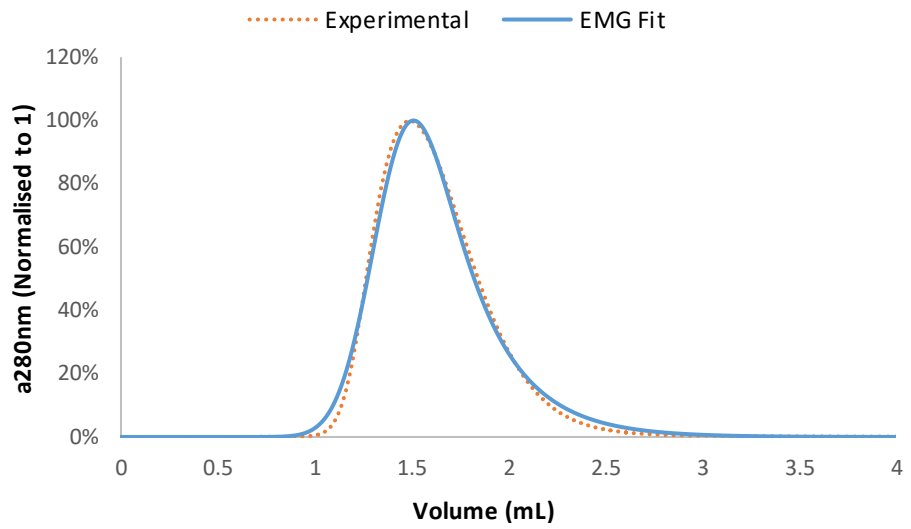

Figure 4.18 - 1mL Column PABA Pulse HETP, demonstrating large asymmetry and a retention volume greater than column volume, both phenomena suggesting the large dead volume of the chromatographic system is influencing the response significantly

4.5.5.2 Dead Volume Correction

Using the method of moments, one can separate the effects of external and internal peak position and broadening by adjusting the first and second moments with those of the system volume alone. In order to do this, the first and second moments of a pulse test without a column were determined, at the flowrate used for the pulse tests (equivalent to 60 cm h^{-1} for the 58 mL, 1 mL, 600 µL columns at 0.2mL/min, 0.4mL/min and 2.0/mL min respectively). A good quality of fit was observed (Figure 4.19) for all flowrates.

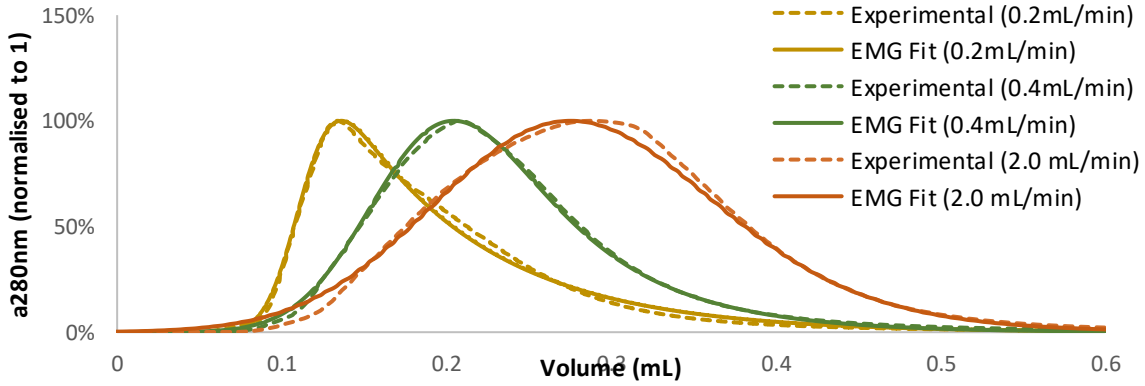

Figure 4.19 - Pulse test without column, and the EMG fit. For the flowrates used for HETP tests Pulse used 5mM PABA, 20 µL injection.

With the EMG parameters, the first and second moments were determined, shown in Table 4.6. These values may then be used to correct for system induced band broadening and changes to the peak location, affording a better measure of plate count for the column alone, similar to the work by Grinias et al.(2015). However, the system volume of the column parts (frits, etc.) for the large (58 mL) column was not determined, and considering the large bore of the tubing, is likely to be a few millilitres, but a small fraction of the total column volume.

Table 4.6 - The EMG Parameters and First, second moments of pulse tests without columns and the associated variances and retention volume of the injections, used to correct for dead volume effects

Column Volume (mL)	**0.6**	**1**	**58**
Column ID (mm)	5	7	16
Column Bed Height (cm)	3	2.5	28
Flowrate (mL/min)	0.2	0.4	2
σ_{system} (mL)	0.02	0.04	0.07
μ_{system} (mL)	0.11	0.17	0.24
τ_{system} (mL)	0.0847	0.0642	0.0556
First moment of system ($m_{1,\ system}$, mL)	0.13	0.21	0.31
Second moment of system band broadening ($m_{2,\ system}$, mL^2)	0.0076	0.0057	0.0080
Injection Volume (mL)	0.012	0.020	1.16
$\sigma^2_{injection}$ (mL^2)	1.20E-05	3.33E-05	1.05E-01
$\mu_{injection}$ (mL)	0.006	0.01	0.58

Table 4.7 -HETP values and fitting parameters comparing microscale column on LHS, microscale column on FPLC, small lab scale column on FPLC and large lab scale column on FPLC using PABA as the tracer, with and without dead volume correction using method of moments, demonstrating similarity. 3 repeats for each experiment, normalised to column volume

Experiment	Column Length (cm)	EMG Mean (μ, (CV))	EMG Width (σ_g, (CV)	EMG Skew (τ) (CV)	Plates per Meter (Peak Width) (m^{-1})	Plates per Metre (Method of Moments) (m^{-1})	Plates per Meter (Corrected for Dead Volume) (m^{-1})	Asymmetry (As)	R^2
600 µL Column LHS	3	0.978 ± 0.063	0.082 ± 0.012	0.100 ± 0.034	2554 ± 739	2316 ± 749	n/a	1.795 *± 0.22*	0.96± 0.05
600 µL Column FPLC	3	1.661 *± 0.027*	0.167 *± 0.008*	0.181 *± 0.042*	*1972 ± 31*	1862 *± 30*	2223± 58	*1.812 ±0.17*	0.99± 0.01
1mL HiTrap, FPLC	2.5	1.357 *± 0.071*	0.163 *± 0.002*	0.174 *± 0.012*	2083 *± 7*	1649 ± 7	1365± 11	2.02 *±0.112*	0.99 *± 0.01*
58mL HiScale, PFLC	29	0.972*± 0.012*	0.029*± 0.003*	0.018*± 0.009*	3445± 6	2991 ± 5	2875± 27	1.13± 0.02	0.99 *± 0.01*

Fitting and HETP statistics for the prepacked 1mL column, the 600 µL microscale column on the LHS, and on the FPLC are shown with and without dead volume correction (Table 4.7), with the method bringing the HETP for the 600 µL columns more comparable between LHS and FPLC systems. This suggested that the poor results seen were a consequence of the scale; mixing dominating the response and leading to increased plate height and asymmetry, rather than the columns being of a worse pack. By accounting for system volume, plate counts in the small scale were more aligned with a large-scale lab column, but still exhibited increased plate height, in line with what others have reported for microscale columns used on an LHS (Susanto *et al.* 2008). Interestingly, the 600 µL columns actually measured improved plate height and asymmetry, compared to the 1 mL column designed for such the FPLC system, though the reduction in plate height may be an artefact of the dead volume of the rig, which was not accounted for in moments analysis.

4.5.6 Discussion

Characterising microscale column on a FPLC is a superior method for data quality and consistency when compared to performing these experiments on an LHS; with better signal to noise ratio, completeness of data, reproducibility and simplicity of processing (Table 4.7). The dead volume contributions to peak position and width, however, limit the reproducibility to scale even with correction; a dedicated, low dead volume system could show far more promise by minimising the system volume. The large dead volumes of the system, apparent by the larger retention volumes, increased variance (both gaussian and exponential) meant that dilution and mixing dominated results through band broadening and shifting true retention and peak width values; by correcting the first and second moments with theoretical variance of the tracer, the response of the system and using a known distribution that models chromatographic peaks well, the EMG equation, one can account for low resolution data. Using the EMG and method of moments approach has allowed responses to be determined with better precision for the LHS system and demonstrated similar results between LHS and FPLC, though uncertainty in the data prevents a precise determination.

Issues with handling small volumes of fluid on a system not designed for such a task were resolved, with volumes controlled down to a precision of under 10 µL with custom sample loops of a desired volume. Performing experiments with small columns (1 mL) designed for use on conventional systems showed high asymmetry , comparable to the microscale column, which could not be corrected for using the method of moments approach, with high asymmetry also present on data generated using the LHS. Previous issues with the evaporation and poor signal were successfully resolved by screening tracer candidates, with PABA demonstrating both strong UV absorbance, safety in handling and lack of volatility. Whereas some differences with regards to HETP parameters, exacerbated by the high absorbance of PABA (adjusted with the use of a standard curve for UV saturation), the impact of this was assumed identical between scales. Further analysis could benefit this, including loading differing volumes and concentrations of PABA to see whether any differences are an artefact of overloading.

Performing HETP experiments in high throughput is possible, even if the results are more variable. The coefficients and parameters derived are comparable to those on the FPLC in regard to peak asymmetry and plate height, with the benefit of being far higher throughput. The method development has enabled a significant improvement to resolution, such that 12 µL injections of material are able to be resolved in enough detail to fit a probability distribution function commonly used in chromatographic characterisation.

Whilst it has been shown that resolution of the system can be driven far compared to the column manufacturers data (Figure 4.4), to dropwise levels on a liquid handling system (Figure 4.16), to a very high resolution using an FPLC (Figure 4.17), there are significant deviations at scale. Asymmetry deviates compared to large lab scale, and this is apparent in high resolution data. It is hoped it has been demonstrated that this may be due to scale differences rather than system, with small lab-scale columns showing similarly poor characteristics. Dead volume correction has been successful in reducing this disparity, and suggests that this should be accounted for when scaling results. Additionally, the liquid handling system and microscale column in combination exhibit far more variation between equivalent experiments in terms of yield, retention times and peak shape than the FPLC-lab-scale column counterparts. Attempts have been made to explain and mitigate the source of these errors, such as small deviations in volume, evaporation, low signal, lost drops and operational differences, as well as the reduced amount of data per column per experiment, though further analysis will be performed to better assess microscale column performance with respect to protein adsorption, and eventually using mechanistic models to provide a mathematical insight into these differences.

5 Dynamic Binding Capacity

5.1 Introduction

The binding capacity of a column is an important metric for chromatographic process economics, determining throughput, cost of goods and the required material and scale of operation. This value is determined by how much mass of a specific component can bind per unit volume of resin, with typical values for affinity chromatography in the range of tens of grams of counterligand per litre of resin for monoclonal antibody processing (Gottschalk, 2017).

There are two main metrics of this capacity; the static binding capacity (or equilibrium binding capacity, EBC); that is, the maximum amount possible to bind assuming an arbitrarily large residence time, when equilibrium is reached. This is possible when there is ample opportunity for every possible binding site to be occupied and represents the maximum possible degree of product binding with that feed material, which may be determined by using a frontal approach, or by batch adsorption.

In reality, due to the very high surface area to volume ratio of industrial bioprocess resins, the tortuous pore network and large target molecules means a significant proportion of these binding sites are hidden, or shielded, by being within poorly accessible pores in the resin, or affected by the binding of product at proximate sites blocking interaction. These less favourable binding positions will take considerably longer time to become occupied due to these resistances to mass transfer. One can access more available sites by increasing residence time, though to reach the maximum capacity is usually prohibitively time and material consuming, and therefore expensive, so a resin binding capacity must be tested under real world use, with a set residence time and concentration, within a packed bed, and determined as a dynamic binding capacity (DBC).

This is commonly accomplished with product continuously loaded on to the column at a set residence time, for a suitable load volume until product is seen breaking through the column (Hahn *et al.,* 2005), as a breakthrough curve (BTC) analysis [5.1], or the experiment may continue to provide an EBC value by loading until saturation [5.2]. The volumes may (Pabst et al., 2018) or may not be (Carta & Jungbauer, 2010) adjusted with subtracting dead volume of the system, and/or the holdup volume of the column which may be then further adjusted to account for column porosity and accessible hold-up volume.

$$DBC_{10\%} = \frac{C_F\, V_{10\%}}{V_C} \qquad [5.1]$$

$$EBC = \frac{\int (C_F - C_v) dv}{V_c} \qquad [5.2]$$

A breakthrough of 10% of the loading concentration is the conventional measurement for the dynamic binding capacity of the particular adsorbate, resin and residence time, though this can vary and is a compromise between a high signal and to minimise product consumption, and if often lowered in cases where the process is set to remove a particularly unpleasant impurity (Carta & Jungbauer, 2010). This value then has a safety margin applied for use, usually around 80%, such that a column is challenged with 80% of the known $DBC_{10\%}$ amount to avoid the risk of product wastage in the effluent.

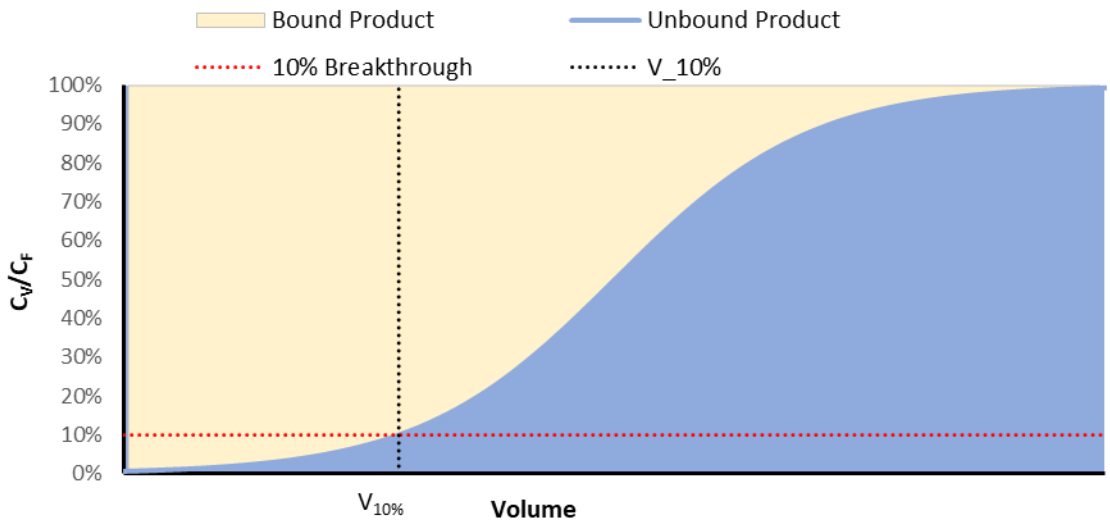

Figure 5.1- Schematic of Dynamic Binding Capacity (DBC) determination using the frontal method, and the Equilibrium Binding Capacity (EBC). The vertical line intersecting the effluent concentration at 10% of feed concentration represents the 10% breakthrough volume, which may then be used to determine the $DBC_{10\%}$ value, and the integral of the bound volume (in yellow) can be used to determine the equilibrium binding capacity through [5.1]

The residence time optimisation is important; bioprocess resins can be very expensive, especially for Protein A, and thus any reduction in requirement is promising economically. As process duration is also an important factor, therefore the operation should be a compromise between maintaining acceptable capacity and time. Because of the high cost of resin, time and material requirement, being able to perform DBC experiments in a

microscale, high throughput manner provides a significant benefit for early process development, especially considering the high material consumption of breakthrough experiments.

5.1.1 Microscale Breakthrough DBC

Many groups (Wenger, 2010, Benner *et al*., 2019, Susanto *et al.,* 2008, Osberghaus *et al.,* 2012 Wiendahl *et al.*, 2008, Diederich & Hubbuch, 2017) have described some deviation from lab-scale to microscale with interrupted flow, due to aspiration-dispense cycles, and plate changes affecting results. The static flow, inherent to high-throughput chromatography, leads to a higher effective residence time; it can take many seconds to swap a plate, greatly increasing binding opportunity for the following fractions, and a reduction of product within the effluent. This is apparent on breakthrough experiments in which kinetic limitations are the leading cause of nonideality rather than thermodynamics, leading towards a saw-tooth motif, as exemplified with Wiendahl *et al*., 2008 (Figure 5.2). Interestingly, in theory this should lead towards a greater DBC value, though others have reported both an inconsistent increase and decrease in expected DBC (Wiendahl *et al*, 2008), and a decrease alone (Welsh *et al*., 2014), suggesting there are several other factors at play when scaling the separation onto microscale columns. As the nature of intermittent flow varies from experiment to experiment, based upon a number of factors such as fraction volume, machine specification and feed concentration dictating the flow profile, the impact of this needs to be assessed on a case-by-case basis.

While the LHS can operate at multiple flowrates, to run different flowrates simultaneously is prevented by nature of the aspiration-dispense cycle, as all pipette tips cannot move independently across the width of the plate but can only do so in unison (Figure 3.1) limiting the duration of the experiment to a single aspiration volume, with different fraction volumes. Additionally, any multiple-speed aspirations must be coded using the machine language manually, as the software doesn't provide this functionality natively. In short, while multiple flowrates are possible for certain kinds of experiments, such as elution studies, this is not practical for breakthrough experiments, so all investigations were performed in 8-fold parallel. One could test multiple feed streams, or column types in one experiment with ease with this system, still providing a valuable avenue for high-throughput DBC determination.

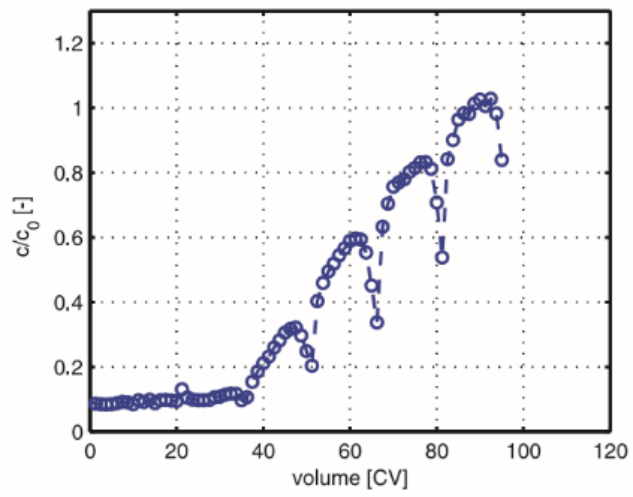

Figure 5.2 - A typical breakthrough DBC experiment performed on an LHS, demonstrating the saw-tooth effect of interrupted flow (Wiendahl, 2008)

The chapter aim is to test the viability of an LHS-Microscale Column system to rapidly find the binding capacity of novel compounds on a variety of microscale column volumes and flowrates, and to enable optimisation of the system with regards to data quality, material use and time.

5.2 Materials and Methods

5.2.1 Materials

5.2.1.1 Load Material

Purified material was available, in which the IgG (IgG A, an IgG_1) had been treated as for the prior Protein A-microscale work (clarified), and subject to three chromatographic separations (Protein A Affinity, Anion Exchange and Cation Exchange), providing a highly pure product. This was then diluted to match the expected titre of load material (4.7 g L^{-1}). Typically crude material would be used for DBC determination, though purified material used here meant one could use UV alone for concentration determination.

5.2.1.2 Microscale Columns

Robocolumns were obtained in three volumes; 50 µL, 200 µL and 600 µL, prepacked with a Protein A resin (MabSelect SuRe LX) . These had bed heights of 2.5 mm, 10 mm and 30 mm respectively, with internal diameters of 5 mm.

5.2.1.3 Lab-scale Columns

4.7 mL HiScreen columns (Cytiva) were obtained, also prepacked with a Protein A resin (MabSelect SuRe LX). These had bed heights of 10cm and internal diameters of 0.77cm. These are the smallest columns most process development activities are conventionally performed upon with a view to immediate scaleup, as two of these columns in series has comparable bed height to typical production scale columns at 20 cm.

5.2.2 Methods

5.2.2.1 Frontal Experiments

Before use all columns were equilibrated in >10CV of Equilibration Buffer, with effluent collected in waste. Upon equilibration, load material is introduced to the columns at a defined flowrate, with effluent being collected in 160 µL fractions in full area UV transparent microtiter plates for a total of 20 CV, corresponding to a load challenge of over 90mg mL^{-1}, significantly above the published capacity of up to 70 mg mL^{-1} (GE Healthcare, 2011b). For retention times under 240 s for 200 µL columns and below, the system was not capable of maintaining such low flowrates, so wait operations were programmed in; for every small dispense at high flow, the system was halted for a finite time, to average out the flow and maintain a set residence time (Table 5.1).

Table 5.1 - Volumetric flowrates used and associated wait commands to meet residence times for 3 volumes of microscale column on a LHS. Pauses are evened out across the experiment, occurring every 10 seconds of flow (values shown are averaged per column volume of material collected). 50 µL columns required this intermittent flow strategy to meet all desired residence times, whereas 600 µL columns did not require this strategy at all.

	Effective Residence Time (s)					
	480		**240**		**160**	
Column Volume	Volumetric Flowrate (µL s^{-1})	Wait duration (s CV^{-1})	Volumetric Flowrate (µL s^{-1})	Wait duration (s CV^{-1})	Volumetric Flowrate (µL s^{-1})	Wait duration (s CV^{-1})
50 µL	0.82	420	0.82	180	0.82	100
200 µL	0.82	240	0.82	0	1.25	0
600 µL	1.25	0	2.5	0	3.75	0

After sample application, columns were then washed in equilibration buffer (>3CV) with material then eluted with elution buffer (>3CVs), again with eluate being collected in 160 µL fractions, followed by a strip buffer for 3CV s, then finally cleaned and stored as appropriate. All plates were measured at 280nm with absorbance corrected for background signal, and DBC was determined [5.1].

5.2.2.2 *Probing Interrupted Flow*

In order to assess the impact on interupted flow on DBC, a FPLC method was created incorporating the same interupted flow as seen on the LHS, accounting for plate changes and aspiration cycles at a given number of column volumes of material loaded. To determine the duration of these interruptions the LHS was set to perform 10 operations, in sequence, of the processes which lead to interupted flow; plate changes and aspiration cycles, while the duration was timed. The position of these halts is determined by the volume of the aspiration-dispense cycle and the flowrate during loading.

The plate changes were found to take 10.3 seconds each, whereas an aspiration cycle took 42.7 seconds, occuring at every 3.2 and 1.6 column volumes respectively for a 600 µL column. This averages to an effective residence time of 30 s, in addition that defined by the flowrate. This regime was then mimicked on a lab-scale column on a conventional FPLC, with the column volume increased, but residence time maintained.

5.2.2.3 *Determining Breakthrough UV Absorbance*

In order to define breakthrough absorbance for each antibody for the LHS, load material was pipetted in a UV transparent microtiter plate in a series of dilutions (from 125% of the standard concentration of feed material to a buffer blank) with a fraction volume of 160 µL. This was then measured for 280 nm, 900 nm and 977 nm absorbance on a plate reader with linear regression performed on the concentration and volume to 280 nm absorbance. Using this relationship, 10% breakthrough was defined as the 280nm absorbance corresponding to 10% of the feed concentration. Linear regression was also performed as a quality test, though the higher concentration fractions (100% C_F and above) were omitted, as significant plateau is apparent, suggesting reaching the limit of the detector.

To perform the same on an FPLC, in which the volume is not a variable due to the fixed flow cell, buffer was flowed in the system, and then replaced with load material until stable UV signal achieved, and then flushed again with buffer. 10% breakthrough was considered as 10% of the difference between load material 280 nm absorbance and 280 nm absorbance of running buffer (Figure 5.3). UV absorbances were safely in the dynamic range of the detector, meaning 10% breakthrough values calculated this way would not be subject to error with respect to UV saturation, and would not need adjustment.

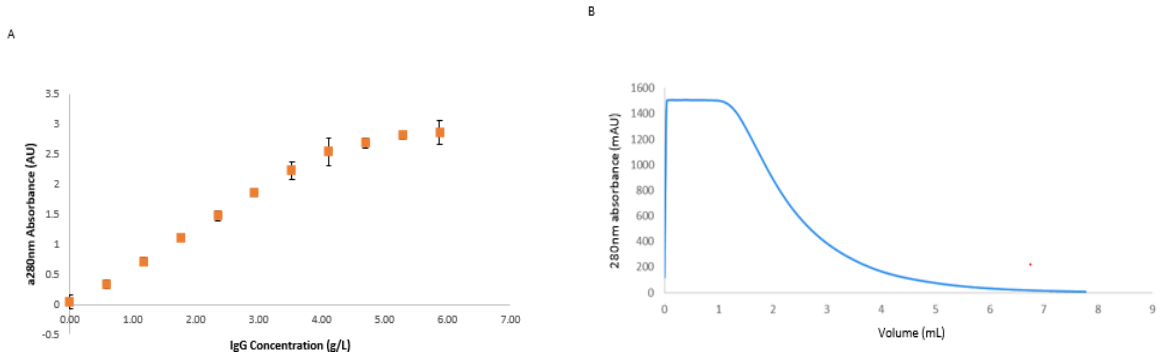

*Figure 5.3 – Determination of $DBC_{10\%}$ absorbance vales for LHS and FPLC . **A** – LHS; The determination for material in microtiter plates was determined using a range of dilutions of feed material, from 125% (this material was under diluted compared to that used for loading the columns) to 0% of the feed concentration of 4.7 mg mL^{-1}. **B** – FPLC; The system was equilibrated in load material (4.7 mg/mL), before being washed with UV transparent buffer. The absorbance at 10% value was determined at 10% of the difference between protein solution and buffer absorbance.*

5.3 Results and Discussion

As before, work was performed to assess the method, scalability and variability of microscale columns when for determining breakthrough capacity. The three available volumes of microscale column were assessed, 50 µL, 200 µL and 600 µL.

5.3.1 Comparing $DBC_{10\%}$ and Column Volume

One can see that a clear sawtooth motif was exhibited on the resulting chromatograms for 200 µL and above, with 50 µL columns not exhibiting this (Figure 5.4), as no plate changes nor aspiration cycles were necessary considering the volumes of feed required needed to meet a suitable load challenge. For the 600 µL and 200 µL column, larger 'troughs' in the curve correspond to plate changes with an aspiration cycle, whereas the smaller troughs are associated with aspiration cycles without a plate change. These same experiments were performed at scale, in order assess how representative these breakthrough curves are to larger scale columns.

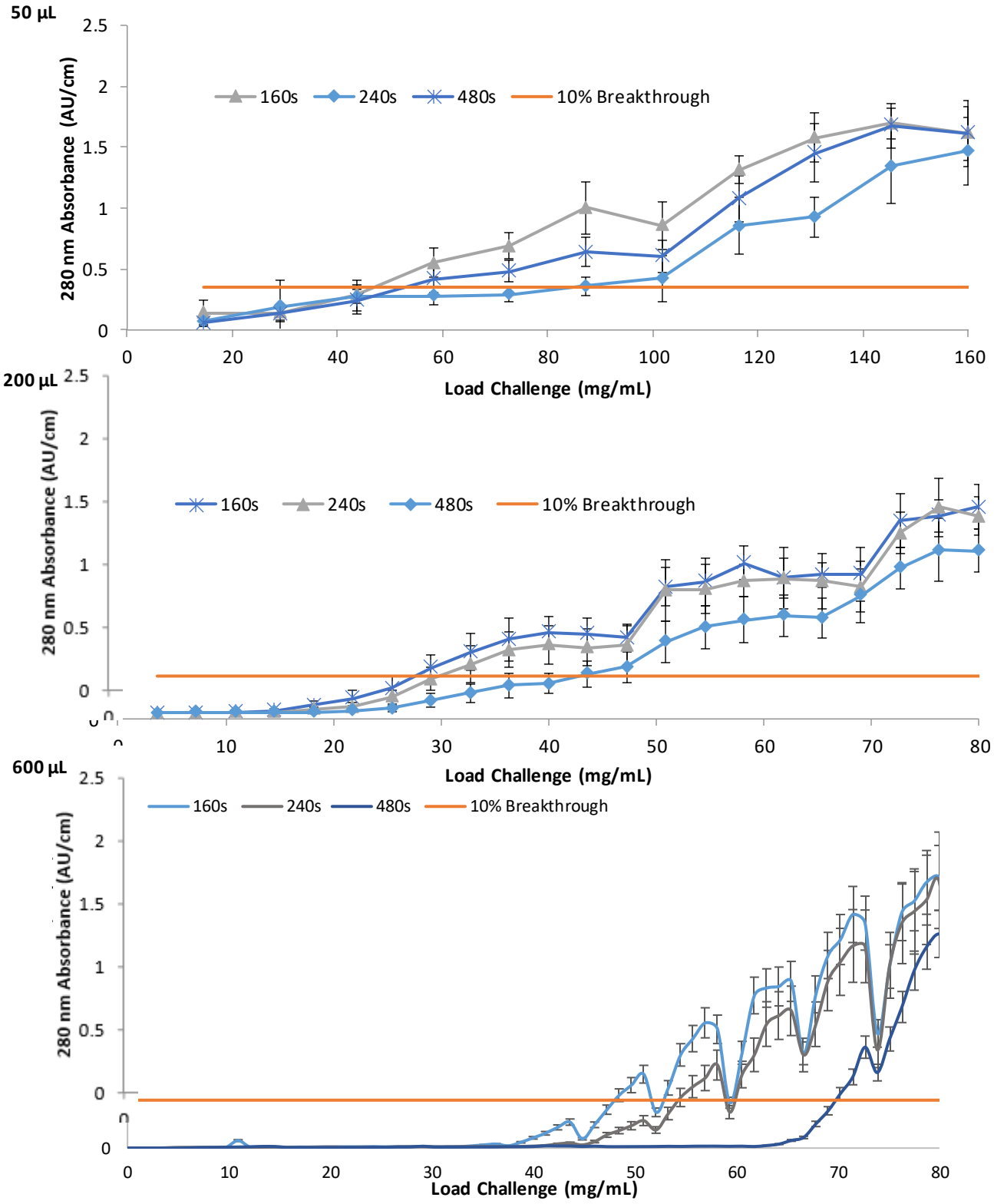

Figure 5.4- Breakthrough Curves for three microscale column volumes at three residence times for three volumes of microscale columns, demonstrating the saw-tooth motif for the 200 µL and 600 µL columns. The 50 µL columns were subject to a higher load challenge due to the sparse data density allowing over 160 mg/mL load challenge on a single plate.

For the breakthrough points for 200 µL columns and 600 µL columns, the troughs were ignored, and a trend plotted between the peaks; this removed the difficulty of analysing multiple breakthrough points but had to be tested to see whether this was a suitable approach for best interpreting the equivalent residence time without intermittent flow.

5.3.2 Assessing the Impact of System and Flow Regime

In order to obtain lab-scale results, so as to see how representative microscale DBC is to larger scale, a 4.7 mL column packed with the same Protein A resin was used for DBC studies. Residence time was set to be identical, regardless of column length, a typical approach (Benner *et al*., 2019, Welsh *et al*, 2016), as was load challenge and feed material as for the LHS experiments. A clear residence time- breakthrough position relation is exhibited (Figure 5.5) across all repeats (n = 3).

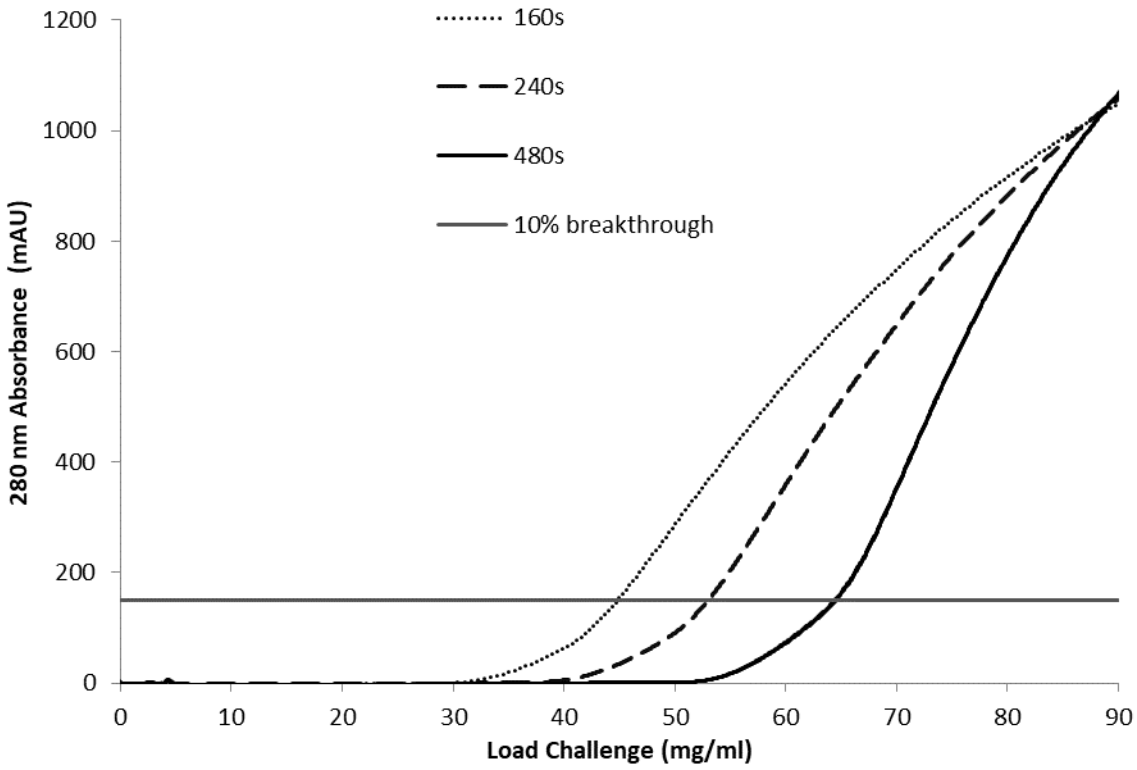

Figure 5.5- 4.7mL $DBC_{10\%}$ breakthrough curves at multiple residence times, demonstrating significant residence time DBC relationship

Using the second 'rig' described during the HETP work (Chapter 4), DBC experiments were performed using a microscale column operated on a FPLC machine as a control to see whether deviations between the large scale data and microscale was due to the system differences, or the columns alone.

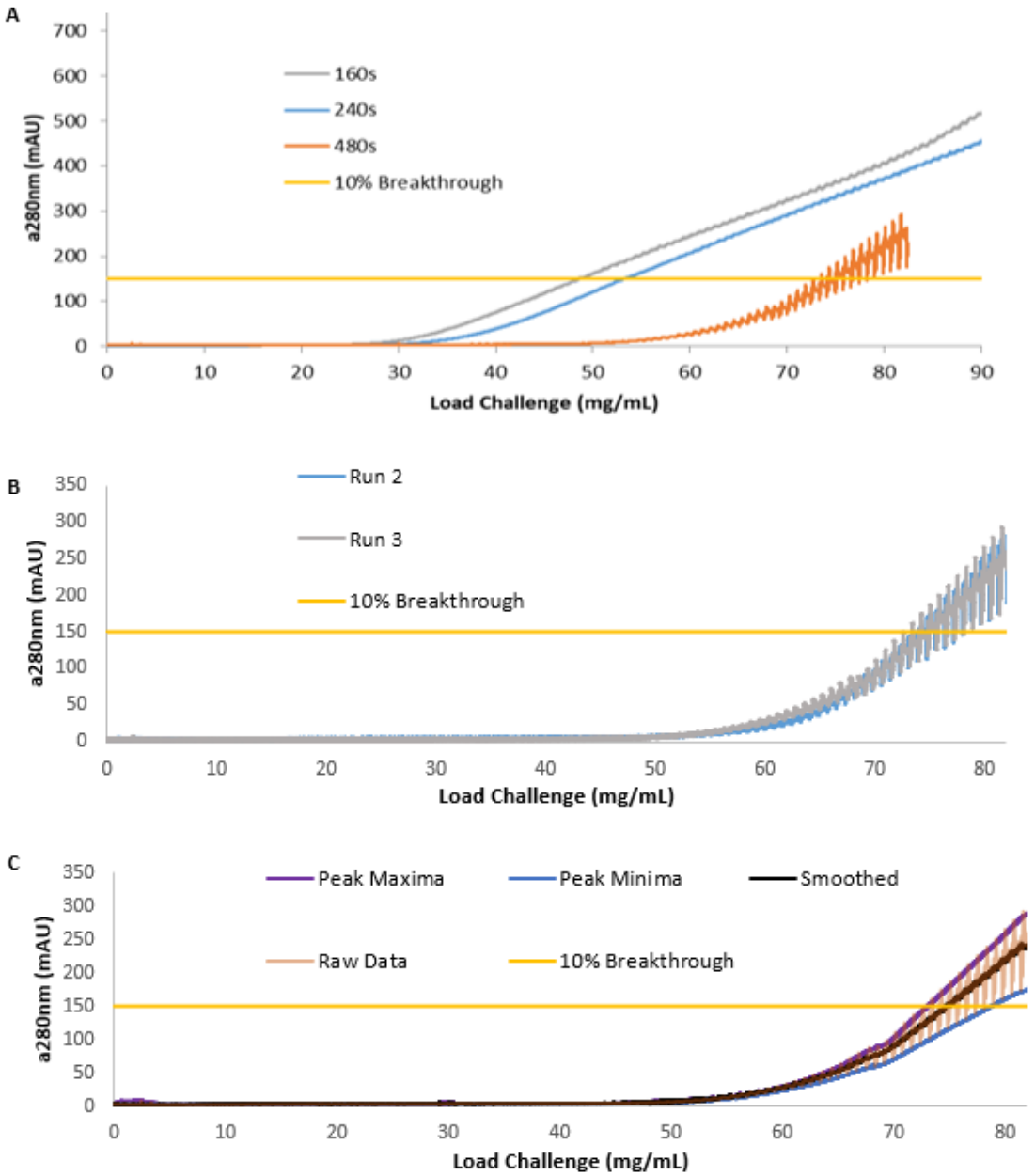

Figure 5.6 - DBC experiments performed on 600 µL columns and second rig. ***A -*** *$DBC_{10\%}$ at multiple retention times. At 480 s, the breakthrough curve demonstrates oscillatory behaviour, likely due to pressure spikes for the slow speed of the pump affecting the UV spectrometer, or possibly air within the pumps, though would not explain the otherwise stable baseline, and the fact this behaviour persisted even after a thorough purge of the system.* ***B-*** *2 further repeats of the 480 s residence time run, showing the oscillatory behaviour persists even after a thorough purge of the system and column* ***C-*** *Visual comparison on ambiguity of breakthrough position for an oscillating curve, in which one may determine the breakthrough point by either taking the raw data, the peaks maxima/minima or by smoothing the oscillations*

At the 480 s residence times, the 600 µL breakthrough curve on the rig demonstrated oscillatory behaviour which persisted across purges of the system (Figure 5.6); this may be due to being at the lower limit of the speed the systems pumps could maintain, or air being introduced through the handmade nature of the rig leaving potential dog-legs in the flow path. This meant 10% breakthrough could be determined much in the same was for the microscale systems as on an LHS, through smoothing the entire curve, or taking the trend between the troughs or peaks. Either approach will impact the measured $DBC_{10\%}$ value. In the above data, when taking the maxima, minima and a smoothing function over 1mL, the values are 73, 75 and 78 mg/mL respectively.

Due to the higher resolution, the fact it more closely approximates a lab-scale column, and the lower variability between runs, columns and therefore a clearer DBC-residence time relationship, 600 µL appeared to be the most appropriate DBC determination, though at a cost of higher material consumption, as well as still not being a perfect representation of the equivalent residence time at scale (Table 5.2) due to an increase in dynamic binding capacity. As expected, one can mimic lab-scale breakthrough experiments well on microscale columns on both systems (LHS and FPLC) with somewhat comparable results, though greater amounts of variation plague interpretation with the LHS compared with FPLC as they did with column qualification.

Table 5.2-Comparison of FPLC and LHS Derived $DBC_{10\%}$ values

Column Volume	4.7mL	50 µL	200 µL	600 µL	600 µL
System	FPLC	LHS	LHS	LHS	FPLC
Retention Time (s)	$DBC_{10\%}$ (mg/mL)				
480	64 ± 0.1	85 ± 14.3	44 ± 8.7	71 ± 1.9	73 ± 1.4
240	53 ± 0.1	55 ± 9.2	30 ± 7.4	58 ± 2.4	60 ± 0.3
160	44 ± 0.1	39 ± 11.6	28 ± 10.5	48 ± 2.3	47 ± 0.5

Additionally, the impact of the system volume was assessed by taking the holdup volume determined in Chapter 4 with a step change of UV active buffer (Figure 4.9) for the system, or by the pulse tests without column, of which provide an estimate of under 0.3 mL. Considering the larger volumes of fluid used until a response is measured, with a HETP pulse occurring within 1.5 CV of feed compared to over 90 CV being required with the DBC determination, this has a far lower impact, with at most an overestimation of $DBC_{10\%}$ by 0.3 g L^{-1} using this system. For the microscale column operated on a FPLC, the holdup volume of the system was more significant, introducing up to 4 g L^{-1}, when accounting for both system and rig volume.

To assess the impact on interupted flow on DBC results, a FPLC method was created incorporating the same interupted flow as seen on the LHS, applied to lab-scale columns.

A

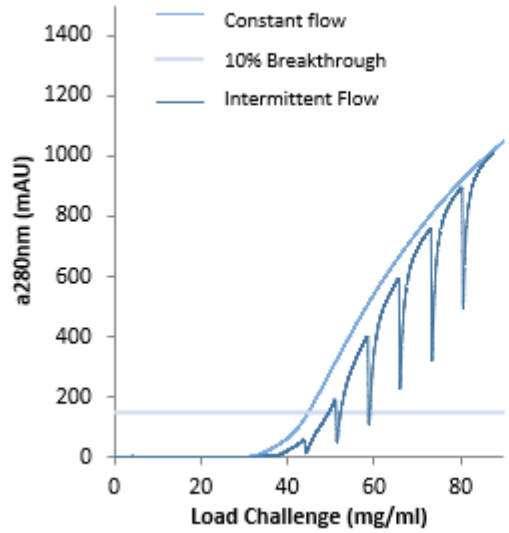

B

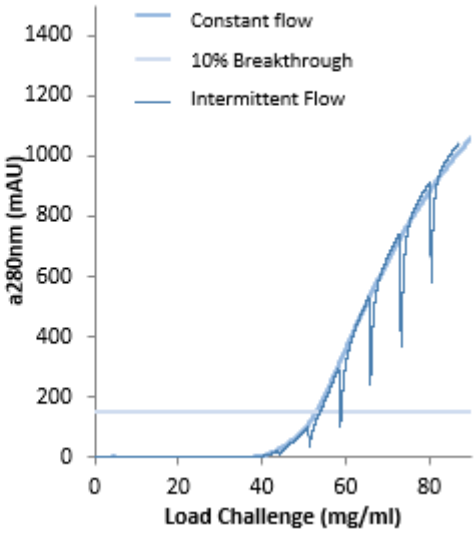

C

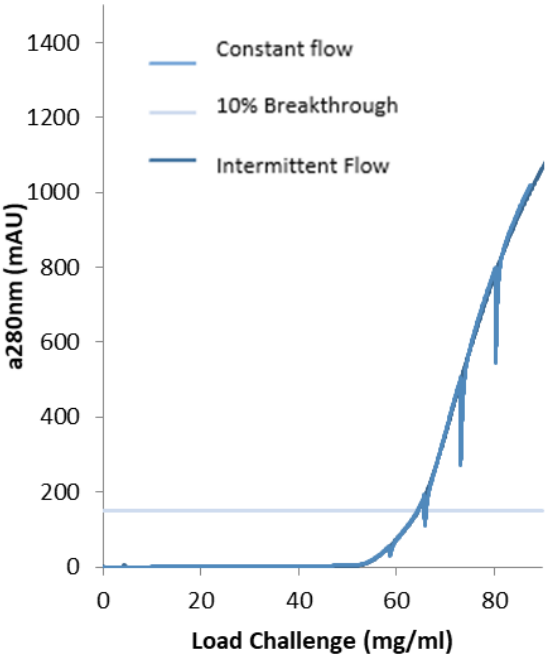

Figure 5.7– Comparison of uninterrupted, and interrupted flow, with lab scale column on a FPLC system

A – 160 s residence time

B - 240 s residence time

C- 480 s residence time

It was seen that, at higher residence times, the intermittent flow had very little impact on breakthrough position, whereas for lower residence times, interrupted flow was significant (Figure 5.3), with the saw tooth motif seen with microscale breakthrough performed with a LHS. This is expected, as the 30 s of increased residence time is a far larger proportion of 160 s than of 480 s, a 19% increase compared to 6%, which is apparent in the comparison between flow regimes (Table 5.3).

Table 5.3 - Comparison of Interrupted and Continuous flow $DBC_{10\%}$ values. n = 3

Residence Time	Continuous Flow $DBC_{10\%}$ (mg/mL)	Interrupted Flow $DBC_{10\%}$ (mg/mL)
480 s	64 ± 0.1	64 ± 0.1
240 s	53 ± 0.1	55 ± 0.0
160 s	44 ± 0.1	51 ± 0.2
130 s	37 ± 0.1	45± 0.1

To investigate whether the effect can be mitigated by reducing the flowrate, an experiment was set up with a residence time of 130 s, accounting that the 30 s of interrupted flow per column volume would increase the effective residence time to 160 s.

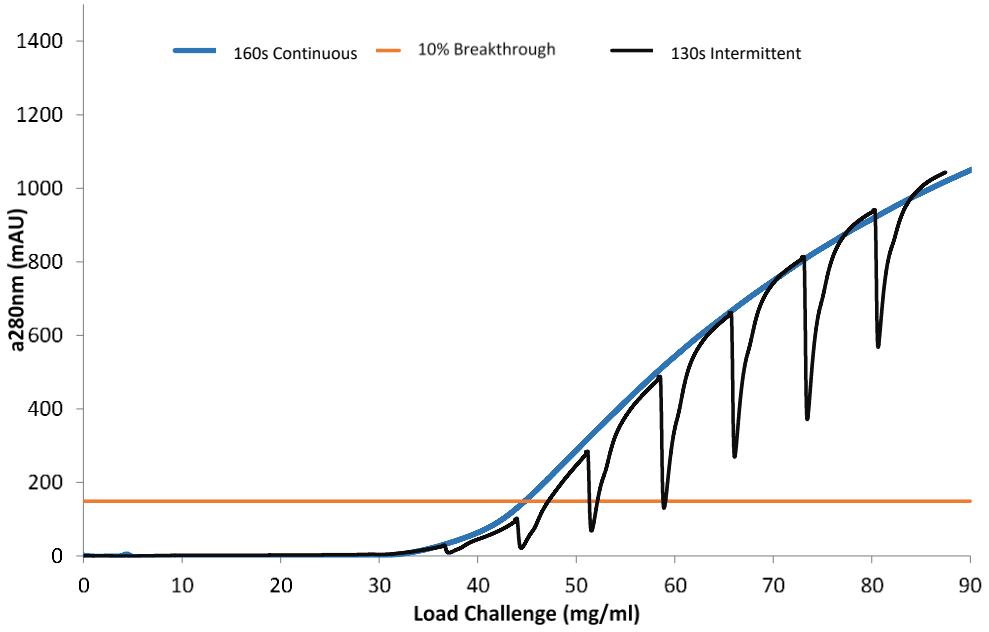

Figure 5.8 - Comparison of uninterrupted, and interrupted flow on breakthrough curves for 160 s residence time continuous flow and 130 s interrupted flow, with 30 s pauses , demonstrating one can mitigate intermittent flow somewhat by altering the flow velocity to account for pause time, though the measured 10% value is still not representative, the profile appears to match better than without this adjustment.

The experiment with 130 s residence time, subject to the same interrupted flow regime demonstrates better similarity to the 160 s continuous condition both in term of breakthrough profile, with improved similarity to the continuous $DBC_{10\%}$ value (Figure 5.8), though still exhibits some significant differences. The breakthrough profiles match best towards the end of the saw-tooth motif, with the final data points before a trough having the greatest similarity between intermittent and continuous flow, with greater differences exhibited immediately after a trough. This supports the hypothesis that the effective residence time, including the robot manipulation time, can account for some of the differences observed between an LHS run and a continuous FPLC run, but will not fully resolve these differences, and that taking the first breakthrough value, rather than subsequent or smoothed value, is the most appropriate approach.

5.4 Discussion

Binding capacity studies have exhibited similarity between microscale and lab-scale chromatography, though with the increased variability experienced as with HETP determination, with the notable trend that 600 µL microscale column have demonstrated a higher breakthrough capacity per unit volume compared to lab scale, whereas the other column volumes exhibit both higher and lower capacity, from longer to shorter residence time respectively. One must consider the entire system, the contribution of diffusion, wall effect and liquid handling at scale, before interpreting any results obtained on the system as representative of larger scale breakthrough. Being able to determine these differences, measure them and simulate them may be the first step to mitigating them, and better understanding microscale data and how it can describe larger scale separations. It is clear that intermittent flow leads towards increased breakthrough capacity when tested at lab scale, due to reduction in kinetic limitation due to increased effective residence time, though there are several other factors potentially impacting differences at scale, and intermittent flow alone would not explain any increase in binding capacity for the longer residence times, as seen with no significant increase with the lab-scale system. An approach in which an “average” residence time was tested when accounting for intermittent flow showed promising results when evaluated on an FPLC for shorter residence times. Further extending the tested flowrates could have also been promising, in which the linear velocity was matched between scales rather than the residence time.

Other potential factors influencing different behaviour at scales may include other mass transfer resistances, possibly dependant on linear flow velocity and reduced column efficiency, the effect of fractionation compared to continuous measurement and the interpretation of true breakthrough position that require a greater level of understanding. It is with this goal that mechanistic modelling was to be performed on the system, with a view to better interpolate between sparse datapoints, to interpret intermittent flow and the impact on mass transfer and therefore performance of the IgG - Protein A capture across scales and systems.

6 Calibrating a Mechanistic Model of IgG Breakthrough of Protein A at Lab scale

6.1 Introduction

Chromatography is often labour, time and materially expensive, with experiments often taking several hours, consuming valuable feed material, buffers and resin, all of which may be in poor supply, or prohibitively expensive. For a conventional chromatographic process, considering the dynamic action of chromatography and myriad of underlying physical mechanisms, to optimise all parameters for the purposes of improving throughput, robustness, product quality, or some combination thereof, requires a great deal of experimentation. Despite the cost of experimentation, the multitude of process parameters, influence of material quality attributes and regulatory pressures, chromatography must be well understood, and well controlled to maintain robust, optimal processes and a consistent supply of essential drug substance for patients.

Process optimisation and characterisation can be a significant undertaking, even for high-throughput process development and design of experiments; often one cannot optimise all chromatographic process parameters with experimentation alone in an efficient manner, but may rely on a mechanistic modelling approach for better process understanding (Lacki, 2018, Shekhawat & Rathore, 2019, Kumar & Lenhoff, 2020). A mechanistic model reduces the number of experiments, but does not eliminate the need for experimental data, as an accurate model often requires calibration through experimentation to determine model parameters. A strategy of using calibration data, engineering correlations and mechanistic modelling to better understand and simulate a process will be employed in this work to develop a modelling workflow.

6.2 Model formulations

There is a plethora of approaches for mechanistically modelling separations of vastly differing complexities since their inception a century ago (Bohart & Adams, 1920). This includes simple models in which only bulk adsorption from mobile to stationary phase is simulated (Bak *et al.,* 2007), approaches in which every individual particle within the system is modelled as a discrete system and through a molecular dynamics approach (Pasti *et al.*, 2016), and computational fluid dynamics simulations in which the material distribution and flow in three dimensional space and time is simulated (Sharma *et* al., 2011, Jungreuthmayer *et al.*, 2015, Ghosh *et al.*, 2013, Fang, 2009). The choice of models should be performed by considering the assumptions that can be made while accurately describing the system, the experimental requirements and feasibility, and computational burden, tailored to the level of process understanding required.

All mechanistic models considered share similarities, in that two distinct processes are simulated; the movement of mobile phase material through the column (transport), and transfer and accumulation of material between

mobile and stationary phase (adsorption), what separates them is what assumptions are made and which mechanisms are simulated to model transport and adsorption behaviour. The ideal model, or equilibrium model only simulates material partitioning as the isotherm dictates, ignoring all other mass transfer resistances (Felinger & Guiochon, 2004). Whilst typically poor at predicting peak shape, for retention time prediction and estimation of displacement effects these models can be powerful tools and provide a simple method of determining the most favourable separation possible as there can be no improvements over thermodynamics (Gu, 1995).

Plate models approximate a chromatography column as a series of stacked plates, each with complete, instantaneous mixing within the plate but slower transfer between the plates. It is these plates that are assumed for HETP determination, and unlike ideal models, this class of model can simulate dispersion, proportional to the height of these plates. These models lump all sources of band spreading into a single metric, the plate height (Velayudhan & Ladisch, 2006), and therefore cannot distinguish between competing mass transfer resistances, nor simulate the complex balance of multiple mass transfer resistances, or the mass transfer resistances changing with respect to one another or time. Therefore, this class of models has limited predictive ability (Guiochon *et al.,* 2006).

Rate models are a broad class of models and include rate terms or expressions describing the rate of material movement and accumulation against a mass transfer resistance. As with previous classes of models, they exist in a variety of formats, differing by their base assumptions. The Equilibrium-Dispersive (ED) model includes terms describing *effective* axial dispersion, often used to account mass transfer resistance causing band broadening, and the Lumped Kinetic model includes a single kinetic term which describes a summation of all mass transfer resistances in addition to axial dispersion. These models, despite their assumptions, have described IgG binding to Protein A, with Bak *et al.,* predicting the initial breakthrough curves of rabbit Ig binding to a range of Protein A resins using an ideal model with Langmuir kinetics (Bak *et al.,* 2007), as has Katoh (Katoh *et al.*, 2007), Teeters described aggregate clearance with a lumped kinetic model to find optimal process conditions (Teeters *et al.,* 2009), with Ng *et al.,* using an Equilibrium Dispersive model with Langmuir kinetics to also optimise a Protein A capture (Ng *et al.,* 2012).

The General Rate Model (GRM) is a more rigorous model, simulating convection, axial dispersion, mass transfer resistances and adsorption equilibria or kinetics (Schmidt-Traub, 2006), meaning that for systems without a single rate limiting step but many, or with few theoretical plates, the general rate model is more suitable than other models (Guiochon *et al.,* 2006). There are a number of distinct mass transfer processes and related resistances which are simulated in the GRM, which is a system of two partial differential equations (PDE), one describing material flow within the interstitial volume of the column [6.1] and one describing the material distribution within the interstitial volume of the resin particles [6.2].

$$\frac{\partial c}{\partial t} = -u\frac{\partial c}{\partial z} + D_{ax}\frac{\partial^2 c}{\partial z^2} - \frac{3\,k_f}{\beta_c\,r_p}\left(c - c_p\,\big|_{r=r_p}\right) \quad [6.1]$$

$$\frac{\partial c_p}{\partial t} = -D_p\left(\frac{\partial^2 c_p}{\partial r^2} + \frac{2\,\partial c_p}{r_p\,\partial r}\right) - \frac{1}{\beta_p} \quad [6.2]$$

The general rate model accounts for convection within the column, with *u* representing interstitial velocity, which is related to superficial velocity, v [6.3]. β_p and β_c represent accessible pore fraction for the bed [6.4] and particle [6.5] and are defined in relation to the porosity of the respective environments (porosity being the fraction of void volume to total volume). Superficial velocity is often used as a metric of flow in bioprocess development, which is defined as the volumetric flowrate when divided by the cross-sectional area of the column, describing the flow velocity of an empty column subject to ideal plug flow. This is often used in place of the interstitial velocity, as one is not often able to calculate nor consider the pore fraction of the column when measuring flowrate. Interstitial velocity is the more appropriate term when modelling mass transport inside the column, which accounts for the space accessible to the fluid, and is therefore higher than the superficial flow velocity.

$$u = \frac{v}{\varepsilon_c} \quad [6.3]$$

$$\beta_c = \frac{\varepsilon_c}{1 - \varepsilon_c} \quad [6.4]$$

$$\beta_p = \frac{\varepsilon_p}{1 - \varepsilon_p} \quad [6.5]$$

The differential equation over the particle stationary phase within pores ($\frac{\partial q_i}{\partial t}$) represents the accumulation and transfer of material between pore interstitial volume and stationary phase; i.e. the sorption between mobile and stationary phase within the bead. This term is defined by which adsorption model, or isotherm, is chosen.

This simulations are subject to initial and boundary conditions, and have been described by Guiochon *et al.,* (2006). The set of intial conditions establishes the column intersitial volume, the particle void volume and stationary phase are all free from absorbing material at the beginning of the simulation [6.6 to 6.8 respectively]. Boundary conditions at the inlet [6.9] often take the form of the Danckwerts boundary conditions (Danckwerts,

1953) which dictates that the inlet mobile phase concentration (c_{in}) is determined by convection and dispersion (D_{ax}), with systems with relatively small contributions of axial dispersion, such as preparative chromatography, able to simply this expression to ($c(t, z=0) = c_{in}$). The inlet function is often taking the form of a rectangular pulse, with frontal simulations performed by setting the injection time (t_{inj}) to the duration of the experiment [6.10]. For the outlet condition, only convective transport is considered [6.11].

$$c(t=0,z)=0 \quad [6.6]$$

$$c_p(t=0,z,r)=0 \quad [6.7]$$

$$q(t=0,z,r)=0 \quad [6.8]$$

$$c(t,z=0)=c_{in}(t)-\frac{D_{ax}}{u_{int}}\cdot\frac{\partial c(t,z=0)}{\partial z} \quad [6.9]$$

$$c_{in}(t)=\begin{cases} c_{feed} & t \le t_{inj} \\ 0 & t > t_{inj} \end{cases} \quad [6.10]$$

$$\frac{\partial c(t,z=L)}{\partial z}=0 \quad [6.11]$$

6.2.1.1 *Mass Transfer Processes*

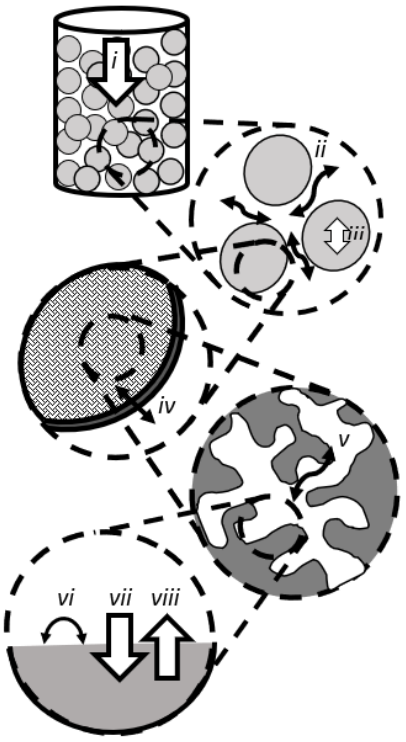

***Figure 6.1- Visual Representation of the significant mass transfer processes modelled in chromatography**, with I being convection, ii and iii axial dispersion in the interstitial column volume of drug product or resin particles, respectively, iv demonstrates diffusion across the film surrounding resin particles, and v representing diffusion of product within the pores. vi, vii and viii represent the diffusion across the surface of the resin bead, and adsorption and desorption, respectively.*

There are a variety of mass transfer parameters simulated in the general rate model, exhibited graphically in Figure 6.1. These can be classified into diffusion, convection and adsorption processes. Convection is the axial movement of the mobile phase through the column caused by an external force. it is responsible for the introduction and removal of mobile phase material from the column, achieved by applying a pressure differential across the column. Axial dispersion in the interstitial zone of both mobile phase material and resin particles follows Fick's laws of diffusion in most implementations of a general rate model, though more complex schemes such as the Stefan-Maxwel laws are used when diffusion requires greater understanding (Graham & Dranoff, 1982, Tao *et al*., 2011). For many models, this dispersion term is neglected, as for most implementations at preparative chromatography, axial dispersion has a negligible (<1%) effect on column performance for bed heights above 10 cm (Felinger & Guiochon, 1995).

Film diffusion is the transfer across the laminar, stagnant film surrounding the resin beads, and is often not rate limiting as the resistance of material transport within the pores, intraparticle transport, often dominates. There are several contributors to effective intraparticle transport, such as molecular diffusion, Knudsen diffusion, convection and surface diffusion (Guiochon *et al*., 2006). For preparative chromatography of macromolecules within micropores, however, typically it is molecular diffusion that dominates, whereas microporous resins may have some contribution of convection, though typically very little (Schmidt-Traub, 2006). Macroporous supports, however, can see significant contribution by convective flow (Frey *et al*., 1993). Electrostatic interactions between the support and protein, diffusion of small molecules within the solid itself and surface diffusion have all been described for polymeric ion exchange resins, and often leads to paradoxical results, in which effective pore diffusion is greater than molecular diffusion alone, suggesting further mechanisms affecting phenomena (Carta & Jungbauer, 2010). An effective pore diffusion coefficient is often used in models describing affinity chromatography on porous resins without such an artefact (Horstmann & Chase, 1984, Pabst *et al*., 2018, Hahn *et al*., 2005, McCue *et al*., 2003), accounting for the Fickian diffusion of material, with the driving force proportional to the concentration gradient, within a tortuous pore network and approximating every contribution to intraparticle flow within this metric.

The relative contribution of mass transfer resistances depends entirely on the system studied, though for preparative protein chromatography, with resin particles of radius greater than 5 µm, which represents the vast majority of preparative chromatography resins, pore diffusion and external film transfer represent the kinetic rate limiting step for most cases (Schmidt-Traub, 2006), with pore diffusion often the main contributor. For some cases in which pore diffusion dominates and the adsorption is highly favourable and fast, the distribution of bound material within the bead follows a shell progressive uptake mechanism (Carta & Jungbauer, 2010), facilitating an assumption of the system to a shrinking core model (Bowes & Lenhoff, 2009, Ruthven, 2000) .

6.2.2 Adsorption

Adsorption is the often reversable process in which material binds from the intraparticle mobile phase to the stationary phase, through a number of physical processes, such as van der Waals and dipole-dipole interaction, hydrophobic interactions and hydrogen bonding (Sun & Yang 2008). Adsorption models describe the relative affinity and capacity of adoption, with a selection described in Table 6.1 and a schematic given in Figure 6.2.

Table 6.1 - A selection of single component isotherm models often used in simulating preparative chromatography. c is mobile phase concentration (c_s that of the modifying species), K_{eq} is the equilibrium constant, q is stationary phase concentration and q_{max} the stationary phase capacity.

Model	Equation	Model Notes	Usage Notes
Linear	$q = K_{eq} \cdot c$	Simple model, stationary phase concentration proportion mobile phase concentration only.	Valid where column is loaded far below capacity, such as analytical chromatography. Often used to describe binding of contaminants, or other species where capacity is unlikely to be challenged.
Langmuir	$q = \frac{q_m \cdot K_{eq} \cdot c}{1+(K_{eq} \cdot c)}$	Accounts for binding site occupancy through maximum capacity (q_m) term	Most widely used for single component adsorption, many variations exist (Kinetic formulations, competitive versions, mobile phase modulators, etc.)
Steric Mass Action (SMA)	$q = \frac{c}{K_{eq}} \left(\frac{c_s}{\Delta - (v + \sigma)c}\right)^v$	Δ is the total ionic capacity of stationary phase, σ is the steric factor (accounting for blocking of binding sites), and *v* is the characteristic charge (for maintaining electroneutrality of the system/desorption of salt)	Most commonly applied to ion exchange processes, as steric inhibition and charge conservation are applied.

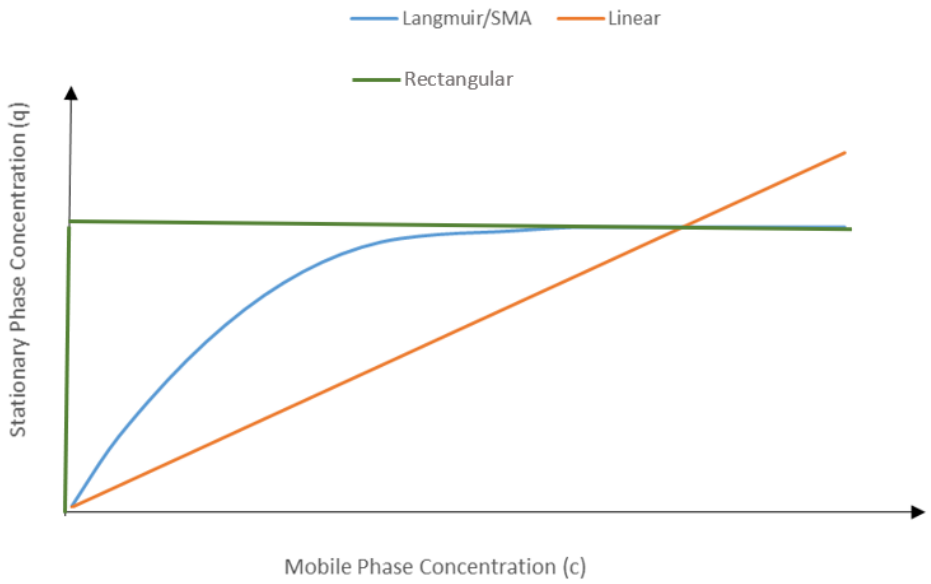

Figure 6.2 - Visual Representation of three common isotherms. Both SMA and Langmuir exhibit a maximum capacity term, which is reached when the stationary phase concentration plateaus. Linear isotherms however have no such limiting capacity and therefore the concentration of material transferring into the stationary phase continues unlimited; this is useful for analytical chromatography and modelling impurity clearance for polishing steps, as capacities are rarely reached in these applications. Rectangular isotherms assume binding is infinitely favourable, with all available binding sites able to be occupied at all nonzero mobile phase concentrations.

Adsorption models are typically classed into two distinct groups; equilibrium models and kinetic models, Equilibrium models assume that the distribution of material between stationary phase, or isotherm, is achieved instantaneously, whereas kinetic models assume both binding and unbinding have finite rates and are therefore time dependant. The fast rate of binding for Protein A to IgG Fc domains as evidenced by large second order rate constants and high equilibrium constants (Saha *et al.* 2003), slow rates of pore diffusion and relatively large particle diameters mean binding kinetics are often insignificant (Carta & Jungbauer, 2010, Horstmann & Chase, 1984, McCue *et al*., 2004), though will be important for less conventional systems, such as monoliths and membranes which exhibit less prohibitive mass transfer resistances due to their structure enabling convective mass transport to binding sites and therefore require accurate estimation of adsorption kinetics to describe the system adequately (Boi *et* al., 2007).

An adsorption isotherm describes the relationship between mobile phase and stationary phase for the system; for small molecules it is commonplace to determine adsorption behaviour using base thermodynamic principles (Heeter & Liapis, 1998), and incorporating structure-activity relationships, such that one can predict the adsorption process by the species' structure and composition alone. However, considering the large mass, complexity, variety of adsorption mechanisms, and structural complexity and heterogeneity of proteins, determining macroscopic models, though often tedious, provides simple approximations whilst not modelling the innate complexity and variability of molecular dynamics (Carta & Jungbauer, 2010). Simplified models based

on physicochemical properties, such as colloidal models, have shown some utility for protein chromatography, especially when describing ion exchange (Kumar & Lenhoff, 2020), possibly reducing or removing the need for any experimental adsorption data to calibrate a model (Ladiwala *et al*., 2005), including for mAbs – protein A systems to predict a suitable elution pH (Ishihara *et al*., 2005).

Of equilibrium models, the linear isotherm is one of the simplest, in which it assumes bound and unbound material has a set distribution (K_{eq}), which is met for all load challenge. This simple assumption describes single component binding at very low load challenges, as for analytical chromatography, well, and has been used to describe contaminant binding (Ng, *et al.,* 2012) for preparative application. However, in preparative chromatography of high titre products, where resin utilisation and throughput are important considerations, processes are designed to run close to column capacity where the number of available binding sites is material is introduced diminishes. In order to account for this, other adsorption models include a maximum capacity term to describe site saturation. The rectangular isotherm is another simple model, in which the equilibrium constant is assumed to be unimportant, with the only parameter being this maximum capacity which may be met for all load concentrations.

The Langmuir isotherm is perhaps the most ubiquitous in modelling protein chromatography (Ganetsos & Barker, 1993, Fornstedt *et al.* 2016). It may be derived through kinetic (Patiha, *et al.*, 2018) and thermodynamic (Bird, 1933) approaches, and describes a reversible, homogenous monolayer adsorption of a single component to homogenous, singly occupiable ligands. It assumes no interaction between components, that all binding sites are equivalent and singly occupied. Whilst the Langmuir isotherm is widely used to describe protein binding, in reality, each one of these assumptions is demonstrably untrue; proteins often aggregate leading to multilayer binding, the binding sites and proteins do vary in size and energy in part due to conformation changes and variability. Wildtype protein A possesses 5 distinct binding sites for IgG (Jansson *et al*., 2006), the proteins can occupy more than a single binding site, a single binding site can bind multiple proteins, and protein s do interact with great complexity, often varying with concentration. However, for a simple approximation, Langmuir often suffices to explain macroscopic adsorption behaviour (Latour 2014).

There are a number of variations applicable to the Langmuir isotherm in use for modelling chromatography; if more than one molecule is being simulated, competitive Langmuir allows for each molecule to bind to sites with differing equilibria, modelling competitive adsorption between the species. The assumptions are made that the capacity is the same for each species, which is likely untrue, as well as not simulating interactions between species. Nonetheless, such models have shown use in IgG purification, with many applying this approach to separating aggregates from monomeric proteins or other contaminants (Norde 1996, Close *et al.,* 2014b, Zhang *et al*., 2019, Nilsson 2005).

Additionally, one can extend the Langmuir isotherm to simulate two or more distinct sites for binding, the Bi-Langmuir isotherm. This allows individual capacities and equilibria for each binding site and assumes that it is competitive binding between the two. Whilst most systems have more than one binding sites, with even high affinity systems such as IgG and Protein A exhibiting many (Borg *et al.,* 2014, Da Silva *et al.* 2019, Dimartino *et al*., 2015, Perez-Almodovar & Carta, 2009a), the Bi-Langmuir is critical if the relative contribution of these sites are similar; if one binding site is far more active than another, the isotherm can be approximated with a single binding site for most of the operation, though would fail to correctly describe saturation behaviour.

If binding is moderated by the presence of another factor such as salt or pH, the Langmuir isotherm is often extended further, to include 'Mobile Phase Modulators'. The binding of protein to ion exchange resins, hydrophobic interaction resins or affinity resins is largely determined by mobile phase pH (Sandoval *et al*., 2012) and ionic strength (Guélat *et al*., 2012), which can be simulated much the same way the target molecule can, with mass transfer resistances and capacities. The equilibrium values are often charged as a function of mobile phase modulator concentration (Karlsson *et al*., 2004b).

The Steric Mass Action (SMA) isotherm models other phenomena, such as steric hindrance of the binding sites by species, competitive exchange of species and ions (Chen *et al*., 2006, Brooks & Cramer, 1986), and charge conservation. Each component, such as protein and salt are given a characteristic charge, and a steric component describing the blocking of binding sites by the molecules size. This isotherm has shown great utility in simulating ion exchange processes (Kumar *et al.,* 2015).

The kinetics of binding for many preparative chromatographic operations are not rate limiting, instead transport processes determine performance. (Müller-Späth *et al.,* 2011) though for cases with adsorption kinetics, rate terms can be used instead. This approach is also often used with simpler models, such as the lumped rate and ED formulations, to account for some kinetic effect not included in the model (Ng *et al*., 2012). In these cases, the values for binding rate have no physical meaning, but account for mass transfer not accounted for with transport alone, so limit potential for model extrapolation. With regards to IgG capture by Protein A chromatography, as in most types of affinity chromatography, the equilibrium constant is rather favourable with dissociation constants in the nanomolar range (Carta & Jungbauer, 2010, Yang *et al.,* 2003, Reader & Shaw, 2017, Wilson *et al.*, 2010). One can assume a rectangular isotherm, which is well supported in literature for high K_{eq} values in general and notably for Protein A – IgG systems, which it is used to describe adsorption behaviour with a shrinking-core model (Zhang *et* al., 2015, Pfister *et al.* 2018, Weinberg *et al.*, 2017, Bankston *et al.,* 2008, Bergander *et al.*, 2008, Baur *et al*., 2018, Wenger, 2010, Subramanian, 2004, Lopes da Silva *et al*., 2019, Perez-Almodovar & Carta, 2009a, Sheth, 2009, Steineback *et al*., 2016, Shi *et al*., 2020). Even in cases where the adsorption is not strictly rectangular, the assumption is often useful to describe such systems (Ruthven, 2000).

6.2.3 Mass Transfer Parameter Correlations

Many engineering correlations have been published for estimating mass transfer resistances applicable to chromatography and may be developed upon an experimental and/or theoretical basis (Wang *et al*., 2005), though are often inaccurate compared to empirical determination of mass transfer resistances.

6.2.3.1 Axial Dispersion

Axial dispersion is the bidirectional movement of material axially within the interparticle space. Two phenomena are responsible for this: molecular diffusion of the protein, and eddy dispersion [6.12]. Several correlations are used to estimate this, including Ruthven (1984), in which the total axial dispersion correlated to molecular diffusivity and non-idealities through the geometric constraints of γ_1 and γ_2 usually set to 0.7 and 0.5, respectively [6.12]. De Ligny (1971) expanded the second term to include influence by molecular diffusion, based upon Gidding's (1959) random walk analysis [6.13] , Chung & Wen (1968) have also reported an empirical correlation [6.14] in which molecular diffusion was omitted entirely, which is a robust assumption for large molecules and faster convection.

$$D_{ax} = \gamma_1 D_m + 2\gamma_2 r_p u \qquad [6.12]$$

$$D_{ax} = \gamma_1 D_m + \frac{5\, r_p\, u}{1 + 4.4\, D_m \,/\, (r_p\, u)} \qquad [6.13]$$

$$D_{ax} = \frac{2 r_p\, u \varepsilon_b}{0.2 + 0.011\, Re^{0.48}} \qquad [6.14]$$

Molecular diffusivity (D_M) of a protein in aqueous solution can be estimated by the correlation of Polson, 1950, [6.15], though Tyn's (Tyn & Gusek, 1990) and He's (He & Niemeyer, 2003), correlations have shown much reduced error between experimentally determined values, though require estimates of gyration radius of IgG, viscosity or other measurements. The molecular diffusivity of dextran follows the correlation by Frigon *et al.,* 1983 [6.16]. In addition, one can also determine the molecular diffusion of the material chromatographically by determining the variance of a small pulse injection with and without the flow stopping for a defined duration (Pathak & Rathore, 2016, Shaw & Schy, 1981), with a peak parking approach.

$$D_M(m^2\ s^{-1}) = 2.74\ \times 10^{-9}\ M^{-\frac{1}{3}} \quad [6.15]$$

$$D_M(m^2\ s^{-1}) = 7.04\ \times 10^{-9}\ M^{-0.47} \quad [6.16]$$

One can determine effective axial dispersion experimentally, by performing HETP tests and defining apparent axial dispersion (D_L) by plate height, H, through a simple identity [6.17] though this is a combination of all mass transfer resistances, rather than dispersion in the interstitial bed volume alone, though this is often sufficient for simple models (Guiochon *et al.,* 2006).

$$D_L = \frac{H\ u}{2\ \varepsilon_c} \quad [6.17]$$

6.2.3.1 Film Diffusion

$$Sh = \frac{k_f d_p}{D_m} \quad [6.18]$$

$$Sh = \frac{k_f d_p}{\varepsilon_c} Re^{\frac{1}{3}} Sc^{\frac{1}{3}} \quad [6.19]$$

The film transfer rate, or external mass transfer rate, can be estimated through hydrodynamic principles. To estimate film thickness, or resistance to diffusion, a practicable approach to correlate the dimensionless numbers, through the Sherwood (Sh) number [6.18 and 6.19], the ratio of convective to diffusive transport, and the Schmidt number , Sc, the ratio of momentum diffusivity and mass diffusivity [6.20].

$$Sc = \frac{\upsilon}{D_m} \quad [6.20]$$

The flow within chromatographic columns is usually very laminar, with very low Reynolds numbers (Re), considering the slow flow velocities and small particle diameters [6.21], sometimes characterised as Stokes flow (Costa & Cabral 1991).

$$Re = \frac{d_p\ \varepsilon_c\ u}{\upsilon} \quad [6.21]$$

Additionally, one may use the correlations for k_f from Kataoka *et al.,* (1972) [6.22] which is valid for flow with Reynolds numbers up to 100, or Wilson and Geankoplis (1966) [6.23] for flow regimes with Reynolds numbers between 0.0015 and 55. Both correlate film diffusion to the cube root of interstitial velocity.

$$k_f = 1.165u^{\frac{1}{3}}\left(\frac{r_p}{D_m}\right)^{-\frac{2}{3}}\left(\frac{1-\varepsilon_b}{\varepsilon_b}\right)^{\frac{1}{3}} \quad [6.22]$$

$$k_f = 0.687u^{\frac{1}{3}}\left(\frac{\varepsilon_b r_p}{D_m}\right)^{-\frac{2}{3}} \quad [6.23]$$

6.2.3.2 Pore Diffusion Coefficient

Pore diffusion is often the rate limiting mass transfer resistance in preparative chromatography of proteins, owing to the relatively large bead diameter, highly tortuous pore networks, relatively large molecules and the lack of convective flow within the pores. Due to the favourable binding Protein A:IgG exhibits and literature on other systems describing the adsorption of IgG and protein A through a shrinking core model, this is likely to be a critical mechanism to model quality. The magnitude of diffusion is highly dependent on the pore network, size distribution and heterogeneity of the intraparticle space, and is therefore often difficult to predict. Indeed, four distinct mechanisms contribute to pore diffusion; molecular diffusion, Poiseuille flow, Knudsen diffusion and surface diffusion (Guiochon *et al.,* 2006).

A number of identities of pore diffusion are available; the Mackie and Meares correlation (1955) was developed to describe diffusion in ion exchange media and is a poor approximation of macromolecule diffusion as it does not take molecule sterics, nor pore structure into account [6.24]. Brenner and Gaydos (1977) introduced this capability with their correlation [6.25] assuming cylindrical pores, and accounts for tortuosity (τ) and steric hindrance.

$$D_p = \frac{\varepsilon_p}{\left(2-\varepsilon_p\right)^2} D_m \quad [6.24]$$

$$D_p = \frac{\varepsilon_p k_p D_m}{\tau} \quad [6.25]$$

Resin tortuosity is rarely measured but assumed to be between 2 and 6 for most commercial resins (Gu *et al.,* 2013), and is a measure of how much the pores diverge from a perfect cylinder. The values of k_p correlate to size exclusion effects, which may vary during column loading (Gutenwik et al., 2004, McCoy & Liapis, 1991, Clark et al., 1985). τ must be determined experimentally, either by an inverse method (Kempe *et al*., 2006), or by microscopic methods, such as confocal microscopy (Green & Perry 2007, Carta *et al*., 2005 Hubbuch *et al*., 2003). Other have determined the resistance to pore-diffusion for IgG on a Protein A resin with batch adsorption (Bergander *et al.* 2008, Traylor *et al*., 2014), and some report that this value varies significantly with protein concentration (McCue *et al*., 2003, Hahn *et al*., 2003 Horstmann & Chase 1989), though Perez-Almodovar & Carta (2009a) demonstrated that the concentration dependancy of pore diffusion was mitigated when accounting for finite adsorption rates.

6.2.3.3 Porosity

Column porosity and total porosity can be determined experimentally through pulse experiments with penetrating and non-penetrating analytes. Total porosity (ε_t) is related to column porosity (ε_c) and particle porosity (ε_p) through [6.26].

$$\varepsilon_t = \varepsilon_c + (1 - \varepsilon_c)\varepsilon_p \qquad [6.26]$$

With a small tracer injection, akin to HETP tests, total porosity may be determined as the proportion of void volume to total volume, or the retention volume of the material divided by the volume of the column used. One can repeat this experiment with a molecule that cannot penetrate pores, such as Dextran Blue 2,000,000, with a molecular mass of 2 x 10^6 Da and a molecular radius that prevents pore transport in many media, the column, or bed porosity is determined as above. This approach can be applied more rigorously, in which analytes of known steric size are applied, allowing the size-distribution of pores to be determined (Pabst *et al*., 2018, Perez-Almodóvar & Carta, 2009a).

6.2.4 Adsorption Isotherm Determination

There are a number of experimental approaches to determining which adsorption isotherm is most appropriate and the values of the relevant parameters, including static, frontal and perturbation methods (Seidel-Morgenstern, 2004). Frontal experiments, in which the concentration of response measured, using the inverse method in which adsorption parameters are fitted to the model either in breakthrough (Pan *et al.*, 2005) or elution analysis (Rudt *et al.* 2015), though these often have to rely on assumptions that mass transfer is not limiting, or have been well described. A common approach for isotherm estimation is static, or batch adsorption

determination due to the small material consumption and easier interpretation when performed in microtiter plates, in which a defined volume of resin, usually in the order of microlites, is equilibrated in feed material of varying concentrations or volumes (Bergander *et al*., 2008). Equilibration must be achieved, usually by incubating and agitating the mixture for several hours. One can also perform analogous experiments in which a column, rather than microtiter plates, is saturated with material. This leads to greater material consumption, but better accuracy (Gu *et al.,* 2013, Ng *et al.,* 2012) when compared with microtiter plate methods. In the batch adsorption approach, a range of load challenges is tested, with a plot of stationary phase concentration and mobile phase concentration generated by measuring the concentration of material present in the interstitial space compared to the material bound to the resin, enabling the fitting of an appropriate adsorption isotherm.

For isotherms with a mobile phase dependency, such as the SMA isotherms dependence on salt concentration, or extended Langmuir isotherms with Mobile Phase Modulators, such as pH or temperature, one can perform these experiments with a differing concentration of mobile phase modulator, or different pH's (Kasche *et al.,* 2003). This approach can be applied to columns, where one can perform frontal analysis or measure material retention under a gradient of inhibiting species (Rudt *et al*., 2015).

6.3 Model Fitting with the Inverse Method

A common approach of parameter determination is the inverse method, in which an algorithm varies model parameters, and compares the modelled process it to experimental data. This algorithm then iterates through the landscape of allowed variables to minimise the error between model output and experimental data, eventually finding a set of optimal values. Care must be taken to avoid finding a local minimum in lieu of the global minimum; the search space increases exponentially with parameter number, and these values of each parameter can vary by orders of magnitude and interact in similar ways; an unfavourable isotherm can mask a larger binding capacity and kinetic effects are often difficult to isolate. A number of previous groups have used genetic algorithms (Müller-Späth *et al.,* 2011, Osberghaus *et al.,* 2012, Treier *et al.,* 2012b) and artificial neural networks (Wang *et al.,* 2017a) to improve fitting confidence.

The objective function, or optimised value, is often the sum of squared error (SSE), which is the difference between all experimental and simulated data points, squared [6.27]. This ensures all errors are positive and means the optimisation will tend to discriminate against outliers to a greater extent than just measuring an absolute error.

$$SSE = \sum_{i=1}^{n} (Experimental_i - Simulated_i)^2 \qquad [6.27]$$

As simulations and experiments are often performed with varied number of data points, the mean square of error (MSE) is used [6.28]. For this approach, the y-axis is often scaled the same for all simulations, for instance, scaling to inlet concentration or maximum absorbance, rather than 280 nm absorbance or protein concentration.

$$MSE = \frac{SSE}{n} \qquad [6.28]$$

6.4 Mechanistic Model Applications

Mechanistic modelling of chromatography has been applied to many bioprocess development activities, across the full range of development stages, from determining the best order of unit operations (Nfor *et al*., 2013) to process validation (Degerman *et al.,* 2009, Close *et al.*, 2014b, Rischawy *et al*. 2019) and performing root cause analysis at manufacturing scale (Wang *et al.*, 2017b).

Process optimisation is a common application for mechanistic models, in which the chromatographic process is optimised for a combination of factors, such as purity, throughput and recovery, across both a single chromatographic step (Lienqueo *et al.,* 2009, Karlsson *et al*, 2004b, Hahn *et al*, 2014, Orellana *et al*., 2009, Shene *et al*., 2006), but also two or more linked together (Nfor *et al*., 2013, Pirrung *et al.,* 2019, Pirrung *et al.,* 2017, Huuk *et al*., 2014*)*, in which the performance of the first step on the performance on the second is evaluated, optimised or assessed for robustness (Westerberg *et al.*, 2013). Process parameters, such as load challenge, buffer composition, pooling criteria and flowrates can be easily changed as boundary conditions in the model framework, with the model then predicting process quality. If the objective function is not well defined, a Pareto optimisation may be performed, generating a multidimensional Pareto front (Gétaz *et al.,* 2013, Joshi *et al.,* 2017). Often robustness, rather than each individual factor, is of importance, so the remaining factors such as recovery, purity and throughput, are often then imposed as constraints rather than objectives. Several groups have applied this approach for evaluating the robustness of an operation and specifying a design space (Degerman *et al*., 2009, Jakobsson et al., 2005, Jakobsson *et al.,* 2007 , Westerberg et al., 2012, Borg *et al.*, 2014, Kaltenbrunner *et al.*, 2007, Close *et al*., 2014a), with others using this approach to develop a control strategy in the face of process variability (Close *et al*., 2014b, Steinebach *et al.*, 2016).

Adsorber selection is another activity in which mechanistic models have shown much utility, in which an optimised process on one adsorber may be compared against an optimised process of another (Nfor *et al*., 2011), rather than benchmarking on an arbitrary process. Additionally, comparing mass transfer across different adsorber types has been performed, from mixed mode (Nfor *et al.,* 2011, Zhang *et al.*, 2019), ion exchange (Stable *et al*., 2017), and affinity (Pabst *et al*., 2018, McCue *et al*., 2003) systems. The reusability of protein A resin has also been extensively modelled (Shekhawat *et al.,* 2018, Behere *et al.,* 2018, Feidl *et al.,* 2020), and

mechanistic models have even been used for the development of chromatographic supports (Ndocko *et al.*, 2011).

Evaluating the impact of scale is another application which exploits a mechanistic model's ability to account for different systems, geometries and flow velocities. Mollerup *et al*. (2007) optimised a process with a reaction dispersive model and accounted for the differing flow velocities and bed heights, successfully predicted scale deviation from 8 mL to 55.6 mL. Rischawy *et al* (2019) predicted behaviour of a 3 L column with a model calibrated at 16 mL, with Ghosh *et al*. (2014a) successfully predicting behaviour of membrane chromatography from 5 mL to 140 mL. This work was explored further (Ghosh *et al*., 2014b), by scaling from an 80 µL cartridge to a 1.2 L device. Numerous other groups have calibrated models with microscale columns to predict lab-scale, or larger scale, behaviour, and these will be discussed further in the following chapter.

Determination of adsorber capacity for the purposes of optimisation is widely employed. Due to the high cost of Protein A resin compared to other formats, this is typically a major incentive for optimisation (Perez-Almodóvar & Carta, 2009b). Pabst *et al.,* (2018) conducted an extensive study of 12 Protein A resins with 9 Fc-containing proteins, including Fc fusions proteins, monospecific and bispecific monoclonal antibodies, using batch adsorption (1.25 mL scale) and breakthrough (10 mL scale) to describe breakthrough behaviour and optimise productivity. Ghose *et al*. (2004) optimised a dual flowrate loading strategy, in which the column is loaded at a faster flowrate for the initial portion of the load block, with the flowrate reduced later to improve both capacity and productivity. Interestingly, their data demonstrated a sawtooth motif on the transition between flowrates, which the model described well. Ng *et al,* (2012) employed a lumped rate model to optimise the protein A capture of IgG, and then furthered this work by expanding into a multiple-column chromatography system (2014), with Pfister *et al.,* (2017) & Pagkaliwangan *et al.* (2018) approaching a similar project of optimising continuous capture of IgG by Protein A. Kaltenbrunner *et al*., (2016) described breakthrough behaviour using the cumulative form of the EMG equation to characterise the profile, and used empirical transition functions to predict behaviour across residence times, load concentrations and column lengths.

As the nature of the optimisation regime, data quality and known parameters are of importance, mechanistic modelling shall be applied to the capture of an IgG by Protein A at lab-scale with the view to eventually scale the model to simulate and better interpret microscale data. It is hoped this initial system of models will provide an understanding of which mass transfer resistances are important. Calibrating a model with the ability to simulate, and therefore predict, the flowrate dependency of IgG breakthrough shall be attempted for capture step in order to better understand the requirements to build sufficiently accurate models, and the best practice to understand and apply the information gained to model building, calibration and interpretation.

6.4.1 Published Parameters of IgG-Protein A Chromatography Mechanistic Models

Modelling chromatography is an expanding science, with ever new methodologies, model formulations and techniques available. There have been several papers that have applied mechanistic models of varying types to the problem of characterising IgG binding to a Protein A column for various purposes, with some of the relevant parameters displayed below (Table 6.2). All of these systems have been subjected to different feed material, IgG subtypes and resins, and due to the specificity of model parameters to the whole system, these therefore cannot be directly compared, though should serve as suitable initial estimates. Of note are Pabst *et al*., (2018), who compared many different adsorbers, including MabSelect SuRe LX with a general rate model and a Langmuir isotherm with breakthrough data, Hahn *et al*., (2005) evaluating MabSelect SuRe with batch update experiments and determination of pore diffusion assuming a rectangular isotherm and with an analytical model, and Perez-Almodóvar & Carta, 2009a evaluated MabSelect with a shrinking core model, a pore diffusion model and a heterogenous binding model. This highlights the variation in modelling methodology, calibration data and parameters for even models for a relatively focussed application, Protein A capture of mAbs, in the total landscape of preparative chromatography.

Table 6.2 - Published Mass Transfer Parameters of IgG Binding to a Protein A Column

Parameter	Value	Reference
Bed porosity (ε_b)	0.38-0.45	McCue *et al.,* 2003, Hahn *et al.,* 2005, Pabst *et al.,* 2018, McCaw *et al*., 2014
Particle porosity (ε_p)	0.46-0.98	McCue *et al.,* 2003, Hahn *et al.,* 2005, Pabst *et al.,* 2018, Horstmann & Chase, 1986,
Effective particle porosity for IgG (ε_{eff})	0.34 -0.7	Hahn *et al.,* 2005, Pabst *et al.,* 2018
Maximum binding capacity of column (Q_{max})	30-70 g/L	McCue *et al.,* 2003, Hahn *et al.,* 2005, Pabst *et al.,* 2018, Horstmann & Chase, 1986, McCaw *et al.,* 2014, Ng *et al.,* 2013 Perez-Almodóvar & Carta, 2009a
Langmuir equilibrium Constant (K_{eq})	$10^7$to 10^9 M^{-1}	McCue *et al.,* 2003, Hahn *et al.,* 2005, Pabst *et al.,* 2018, Horstmann & Chase, 1986, McCaw *et al.,* 2014, Ng *et al.,* 2013, Liu *et al.,* 2015
Langmuir association rate constant (k_a)	10^3-10^6 M^{-1} s^{-1}	Wilson *et al.*, 2010, Yang *at al.*, 2003, Reader & Shaw, 2017, Hahn *et al.* 2005, Pabst *et al.,* 2018, Bak *et al.*2007
Pore Diffusion Coefficient (D_p)	0.5 - 5.1 x 10^{-11} m^2 s^{-1}	Hahn *et al.,* 2005, Horstmann & Chase, 1986, McCue *et al.,* 2003, Pabst *et al.,* 2018, Perez-Almodóvar & Carta, 2009a
Molecular Diffusivity of IgG (D_M)	3.7 x 10^{-11} m^2s^{-1}	Tyn & Gusek, 1990
Film Diffusion (k_f)	3x 10^{-6} - 4 x 10^{-6} m s^{-1}	Horstmann & Chase, 1986, Hahn *et al.,* 2005

6.5 Materials and Methods

6.5.1 Mathematical Methods

A rate model of chromatography was used for all column simulations, using MatLab and the module "Chromatography Analysis and Design Toolkit" (CADET), which is a fast and accurate solver for the general rate model of chromatography, using a finite volume scheme (Leweke & von Lieres, 2018). This software functions using its own external simulator, using MatLab to formulate the model. MatLab was used extensively, both to call the CADET simulations, for data handling as well as some simulations not handled in CADET natively, such as dead volume simulation. Latter versions of CADET than used for this work, however, do now include mixing simulation through continuously stirred tank reactor (CSTR) and plug flow reactor (PFR) models.

6.5.1.1 Dead Volume Simulation

Dead volume was approximated by ideal plug flow reactors [6.29], to account for delay, in series with a continuous stirred tank reactor [6.30], accounting for dispersion, though this may also be achieved by using many CSTRs in series, though may lose the physical significance of the volumes (Mo & Jensen, 2016). This PFR and CSTR approach has been employed to simulate or determine dead volume in chromatographic systems for multiple systems (Montesinos-Cisneros *et al.* 2007, Yang & Etzel, 2003, Ghosh *et al.* 2014, Sarfert & Etzel, 1997, Boi *et al.*, 2007, Dimartino *et al*, 2011a). The volumes for this were determined with a least squares approach using pulse or step responses without a column inline. Whilst any combination of CSTR's can simulate band broadening (Kumar *et al.* 2015), a combination of both a PFR and CSTR was used to maintain physical meaning of the volumes. Microscale column are assumed to have unmeasurable volume and therefore set to zero, due to no external volume to the column, with internal volumes, such inlet chamber being highly variable with respect to column position, and other items such as column distributor not able to be easily measured.

$$c_{out}(t) = c_{in}(t - \frac{V_{PFR}}{Q}) \quad [6.29]$$

$$V_{CSTR}\frac{\partial c}{\partial t} = Q\,(c_{in} - c_{out}) \quad [6.30]$$

6.5.2 Dead Volume Determination

Obtaining dead volume calibration data was performed by equilibrating the system with water. Once a steady signal was achieved, the machine was then pumped with UV active buffer (1% v/v Acetone) at a defined flowrate, and the response measured, until the UV signal stabilised, with the volumes a single PFR and CSTR determined through a least-squares fit of the response. For determining the dead volume for the system configuration during tracer introduction, an additional CSTR was modelled to improve approximation of the pulse, by accounting for

dispersion of tracer before introduction to the rest of the system, with data obtained with a 100 µL pulse. This process was repeated for all volumetric flowrates used in this study (Figure 6.3). A offset was observed between flowrates, suggesting another uncontrolled factor was influencing behaviour, possible valve switching times though this was not further investigated as by simulating this effect, any impact would be mitigated. Fortunately, peak areas were comparable between flowrates, with no consistent trend when compared against flowrate.

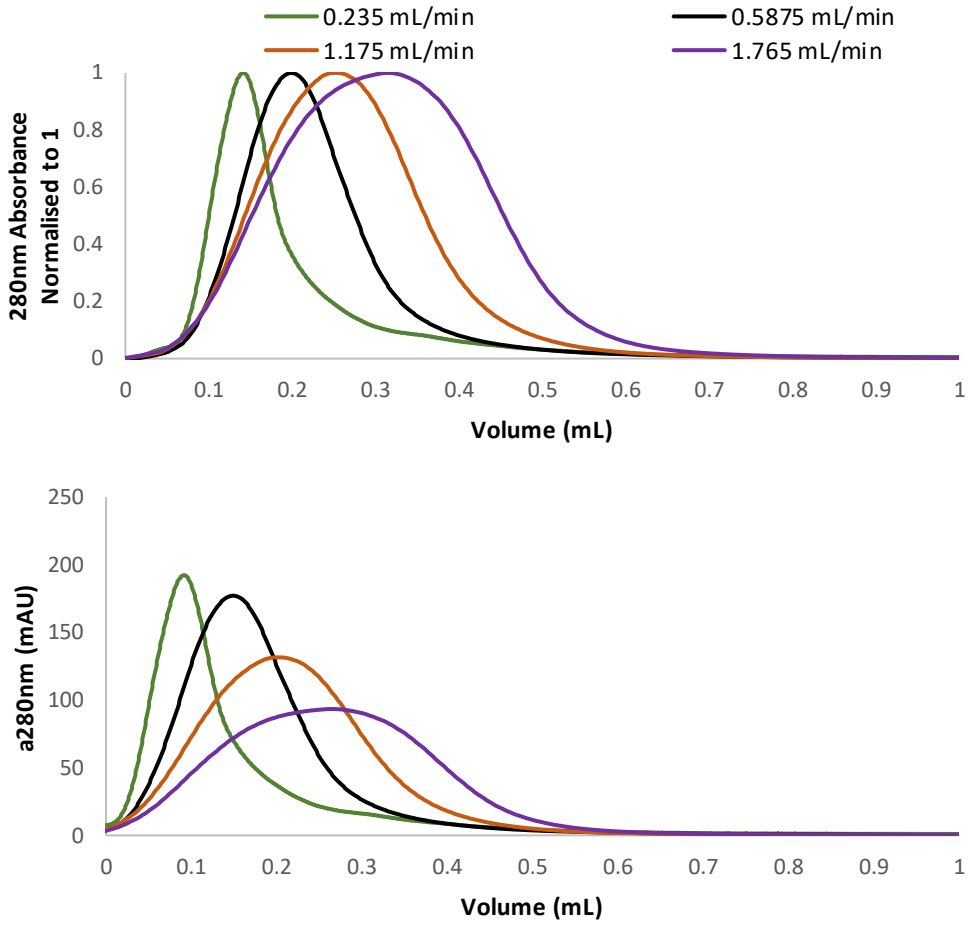

Figure 6.3- System pulse responses at 4 residence times, demonstrating the increased peak offset and width with increased flowrate. Amplitude has been normalised to 1 for ease of interpretation for the top plot, with raw 280nm absorbance values for the bottom plot demonstrating comparable peak areas despite a variation in peak position

In order to separate pre- and post-column mixing, a column was fully equilibrated in UV active buffer, and taken out of the flow path of the system as the system was flushed entirely in UV transparent buffer. After the absorbance had baselined again the column was brought back inline and flushed with buffer at defined flowrates, and the response measured, and a single PFR and CSTR volume determined corresponding to the column valve, post column tubing and UV flow cell. The pre-column CSTR and PFR are then modelled upstream of the column, with their outputs serving is the inlet boundary condition for the column model when combined with the step or pulse methods. Additionally, moments analysis was used to determine the first moments of the peaks, and correcting for dead volume, separate to the using the inverse method, to serve as estimates of

porosity and dispersion for pulse tests, using the same approach as employed in Chapter 4. This work could not use the data from Chapter 4 alone, as different flowrates were employed, different adsorber type and a different system configuration with larger injections (100 µL) used in the prior work.

6.5.3 Optimisation Regimes

An inverse method was used in order to fit the mass transfer parameters to experimental data, based upon simulating the system with an estimate of mass transfer parameters, obtained from literature or known correlations, with the results of the simulation then compared to experimental data. Constrained optimisation was used in MatLab to vary, and therefore calibrate these mass transfer parameters with the function *fmincon* using the interior points algorithm (Byrd *et al*., 1999).

6.5.4 Parameter Estimation

There are a large number of parameters one has to determine to simulate the General Rate Model. Many parameters are known beforehand, such as column length, particle diameter, flowrate of the mobile phase and feed concentration, and therefore do not need to be calibrated, however, most parameters must be determined experimentally or through correlations. Estimations are used to initialise the model; these are altered when the model is fully calibrated, with bounds to keep computational burden acceptable. For some parameters the limit is straightforward, i.e. the porosities must have a value between 0 and 1, whereas other parameters can vary significantly, often by multiple orders of magnitude. Values taken from the published works (Table 6.2) are taken for many of the initial estimates.

6.5.5 Adsorption Isotherm Parameters

As a typical Langmuir isotherm is implemented without accounting for adsorption or desorption rates, two parameters are required, q_{max} and K_{eq}, though this was also tested by also initialising for an adsorption rate (k_{ads}), with the desorption rate being this value divided by the adsorption equilibrium constant, K_{eq}. As previously described (Horstmann & Chase, 1984, McCue *et al*., 2003, Carta & Jungbauer, 2010, Pabst *et al*., 2018), the finite rate of adsorption is often insignificant compared to other mass transfer resistances for preparative protein, so is sometimes omitted when describing Protein, A chromatography. q_{max} was also estimated through product data (GE, 2012a) to be 70 g L_{bed}^{-1}, which was comparable with literature values (Pabst *et al*., 2018)

In this work, batch adsorption plates were also used, in which 800 µL volumes of various concentrations of material (0 to 4.7 g L^{-1}) was left to equilibrate for 6 hours on resin slurry plate of 20 µL resin volume, following the manufacturers protocol. Data was interpreted through applying the Langmuir isotherm to also estimate K_{eq} and q_{max}. Saturation experiments were performed in which material of a known concentration was fed onto a column until the breakthrough reached feed concentration.

6.5.6 Mass Transfer Parameter Initialisation

There are a large number of mass transfer parameters estimations to make; these serve as initial guesses for the parameters of the model before they are calibrated with experimental data, or are constraints to limit the optimisation window, reducing computational burden and reducing the risk of optimising away from the true values.

The film diffusion coefficient, k_f, can be one of the mass transfer rate limiting steps for chromatography (Deyl *et al.,* 1975), and therefore could have a significant impact on simulations and model quality, though it is unlikely to be the rate limiting step in IgG-Protein A chromatography. Typically, correlations are used for determination of this, or through using the inverse method. Film diffusion is dependent on interstitial velocity, so will change with scale. D_p is the pore diffusion coefficient, which is often reported to be rate limiting, and should be particularly significant for this system (Carta & Jungbauer, 2010). The molecular diffusivity value of IgG ($3.7x10^{-11}$ m^2s^{-1}) served as an upper bound, and an initial estimate made at 10^{-12} m^2s^{-1}. Pore surface diffusion was assumed to be insignificant, as the highly favourable IgG – protein A interaction meant that protein unbinding was a rare occurrence in loading conditions, which is required for surface diffusion. Therefore, this parameter was given a value of zero and not varied during model calibration. D_{ax}, the axial dispersion coefficient, is also reported in literature. This is occasionally omitted from models (Pabst *et al*., 2018, Bowes & Lenhoff, 2011, Carta & Jungbauer 2010), as for preparative scale chromatography it is often insignificant, though for smaller scales it can have an impact. With the eventual aim to scale down the models, considering the different flow regimes and reduction in plate counts, accurately determining this parameter was considered important (Roberts & Carta, 2020, Marek *et al*., 2018). Column and particle porosity are also reported in literature, as is *effective* particle porosity (ε_{eff}), which accounts for the size exclusion phenomena that large molecules, such as IgGs, face when diffusing within a constrained pore network. Estimates for these values for IgG binding this Protein A resin were reported by Pabst *et al.,* (2018) of 0.7 to 0.4, and by Hahn *et al.,* (2005) of 0.52.

6.5.7 Model Calibration Data

The accuracy of a model is wholly dependent on the accuracy of the parameters; therefore, it is crucial to determine these parameters with as much precision and accuracy as possible and improve upon the initialised values. For this, a number of approaches were used (Table 6.3) to better develop a workflow and to determine which experiments were necessary. Data was separated into calibration and validation sets, to build and test the model. As with the binding capacity investigation, all experiments were performed with purified protein, so that one could determine concentration directly from the chromatogram, rather than having to perform additional experiments, such as size exclusion HPLC and Protein A HPLC. This does limit the validity of the model to describe adsorption of crude material, whereas models calibrated with crude material have been employed, though require offline analysis to quantify material (Bak *et al*.,2007, Pirrung *et al*., 2018).

Table 6.3 – Experiments used to calibrate the Mechanistic Model of Protein A binding an IgG

Experiment Type	Probing Material	Conditions	Parameters Varied
Breakthrough	Drug product (binding)	One concentration (4.7 gL^{-1}), five residence times (160 s, 240 s, 480 s)	q_{max}, k_f, D_p,
Breakthrough	Drug product (binding)	One residence time (240 s). three concentrations (2.3 g L^{-1}, 4.7 gL^{-1}, 7.5 g L^{-1})	q_{max}, K_{eq}
Pulse	Drug product (nonbinding)	Four residence times (160 s, 240 s, 480 s, 1200 s)	ε_{eff}, k_f
Pulse	PABA	Four residence times (160 s, 240 s, 480 s, 1200 s)	ε_t, ε_p
Pulse	Dextran	Four residence times (160 s, 240 s, 480 s, 1200 s)	ε_c,D_{ax}

In order to minimise the possibility of fitting the model to a local optimum, experiments were optimised in batches; a single parameter may be estimated through a large number of experiments in a sequential manner. Moments analysis was employed as an insight into parameter estimation separate of the mechanistic model inverse method.

6.5.8 Bed Porosity Determination with Dextran 2,000,000

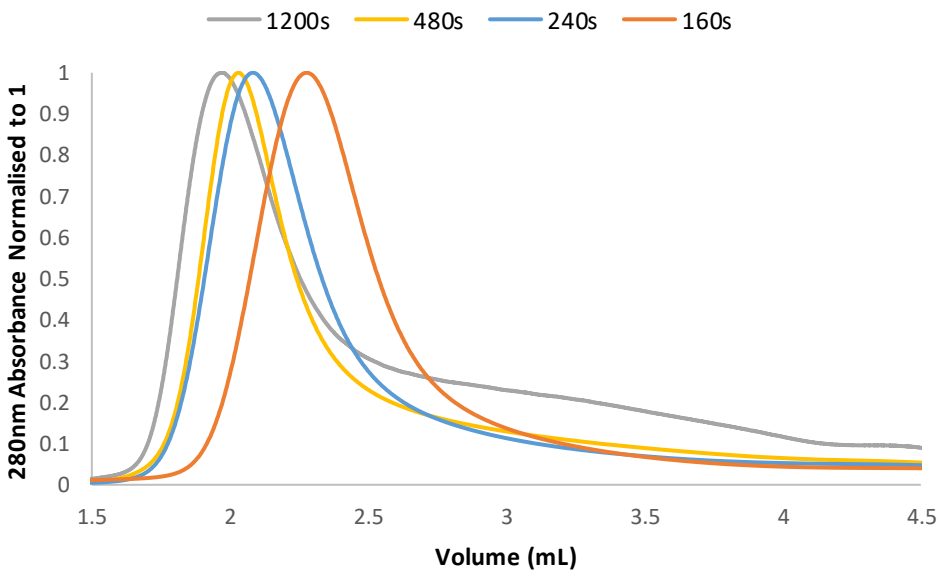

Figure 6.4- Dextran pulse data at multiple residence times, peak absorbance normalised to 1

The experimental data (Figure 6.4) was obtained for four flowrates, with 100 µL pulses of Dextran 2,000,000 (5 g L^{-1}) in solution with 100mM sodium hydroxide, to prevent binding to the resin. This data was scaled for a peak maximum amplitude of unity for convenience, reducing differences across tracer absorbance and differences in tracer volume, and due to the nature of these chromatograms having a single peak, the peak position, width and skew was of importance, rather than amplitude.

Moments analysis was performed at all flowrates for all residence times, with and without a column, and corrected for dead volume through fitting the EMG equation and determining the first moment of the peaks for all residence times. Integrating the peak numerically, without using the EMG equation was thought to be error prone due to the strong shouldering of the peaks, as well as potentially posing a problem when low resolution data were to be assessed.

To evaluate whether the model could estimate the bed porosity through the inverse method, the data was used to calibrate a model directly with the inverse method. For the simulations of dextran pulsed through the column, a number of parameters were estimated initially. Dextran was assumed to not adsorb in the experimental conditions, the adsorption model was omitted. Particle porosity (ε_p), pore diffusion coefficient (D_p) and Film Diffusion Coefficient (k_{eff}) were set to zero to account for dextran's assumed inability to penetrate the pores, leaving the bed porosity (ε_b) and axial dispersion (D_{ax}) to be optimised by fitting to the calibration peak position and width. Initial estimates of the molecular diffusivity and axial dispersion were taken from literature and using correlations.

6.5.9 Total porosity determination using PABA

As with Dextran, a moment approach by application of the EMG equation was employed. Film and pore diffusion coefficients were set arbitrarily high, with particle porosity and axial dispersion being the optimised variables.

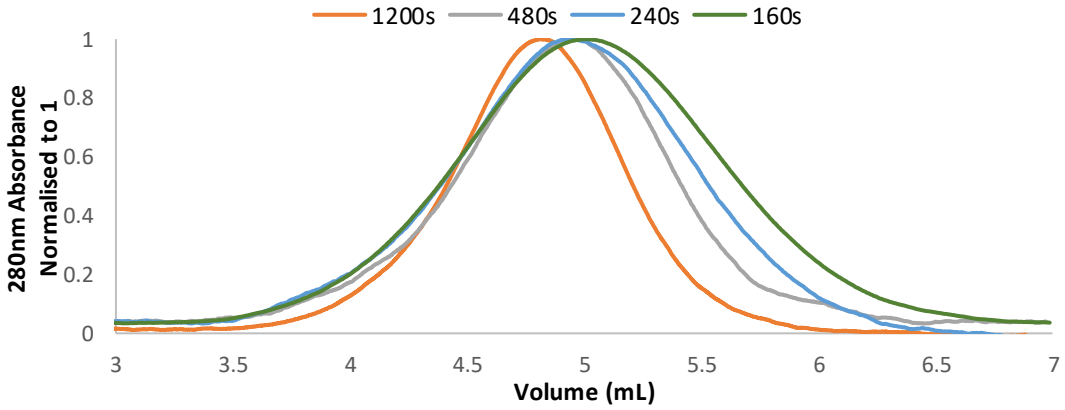

Figure 6.5 – PABA Pulse Experiments, at multiple residence times

As with dextran pulses, a moments analysis was used, as was the inverse method, with all peak absorbance scaled to 1 (Figure 6.5). Total porosity was determined as the dead volume corrected first moment, with particle porosity then calculated [6.26].

6.5.10 Accessible Particle Porosity with nonbinding IgG

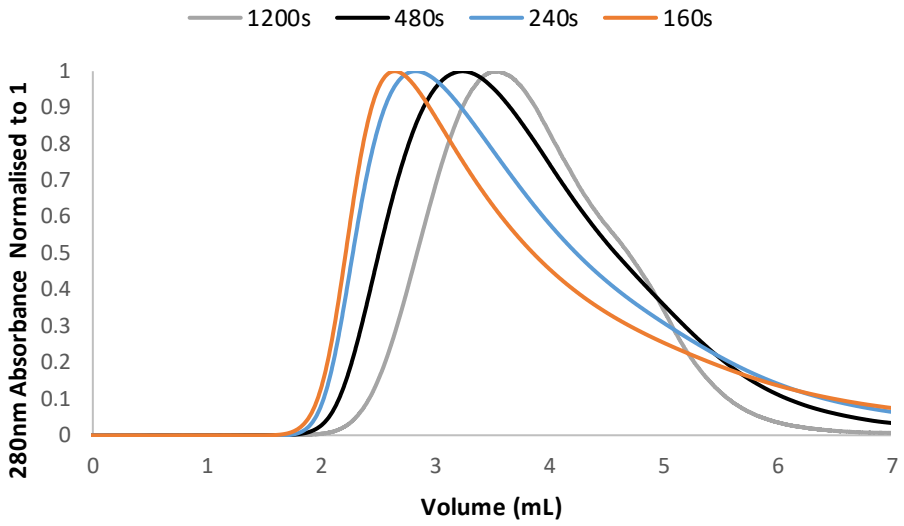

Figure 6.6 – Pulse of IgG in nonbinding conditions at multiple residence times

Non-binding drug substance was pulsed through the column at multiple flowrates, in order to determine the effective particle porosity, the fraction of the resin particles accessible by drug product, and as an initial estimate of axial dispersion and pore diffusion. One can see a clear correlation between residence time and peak maxima (Figure 6.6). Binding was prevented by lowering the pH of the feed material to elution conditions, with a pH of 3.5. Analysis was performed as for dextran and PABA pulses, with the added evaluation using a reduced HETP-v curve slop to determine pore diffusivity parameter, using the relationships shown below [6.31 to 6.36], in which h is reduced plate height, v' is reduced interstitial velocity, v is superficial velocity, and has been adapted from Carta *et al*., 2005, Perez-Almodóvar & Carta, 2009a, Gritti & Guiochon, 2006); the intercept of this plot can determine the axial dispersion coefficient correlation [6.35], if one assumes it is strictly correlated, linearly, to interstitial velocity.

$$h = \frac{HETP}{d_p} \qquad [6.31]$$

$$v' = \frac{u\, d_p}{D_m} \quad [6.32]$$

$$k' = \frac{\mu - V_0}{V_0} \quad [6.33]$$

$$V_0 = \varepsilon_b V_c \quad [6.34]$$

$$h = 2\,\gamma_2 + \frac{1}{30}\frac{\varepsilon_b}{1-\varepsilon_b}\left(\frac{k'}{1+k'}\right)^2\left(\frac{10}{Sh} + \frac{D_m}{D_p}\right)v' \quad [6.35]$$

$$HETP = \frac{L\sigma^2}{\mu^2} = \frac{2\,D_L}{v} + \frac{2\,\varepsilon_b}{1-\varepsilon_b}\left(\frac{k'}{1+k'}\right)^2\left(\frac{d_p}{6k_f} + \frac{d_p^2}{60\,D_p}\right)u \quad [6.36]$$

6.5.11 Determining Model Parameters with Breakthrough Data

6.5.11.1 Breakthrough at multiple feed concentrations

Breakthrough Experiments were performed as for chapter 5, in which a column was washed and loaded with differing concentrations of IgG A feed material (2.3, 4.7 and 7.5gL^{-1}), and loaded to a maximum concentration of 90gL^{-1}. For determining the breakthrough absorbance and concentration of material, the UV flow cell was blanked with buffer, then washed with protein solution, and UV absorbance obtained, then concentration and breakthrough percentage calculated based upon the UV calibration curve, as per the previous chapter. All columns were subject to CIP, regeneration and equilibration before use.

6.5.11.2 Breakthrough at Multiple Residence Times

Multiple residence times were also probed on the IgG Protein A system during breakthrough, as during chapter 5, with and without intermittent flow. In addition, the standard process residence time, 240 s, was overloaded significantly to explore any behaviours arising at these load challenges and for observation of the saturated breakthrough profile.

6.6 Results and Discussion

6.6.1 Dead Volume Determination and Simulation

Initial work was performed to assess the contribution of dead volume on resultant chromatograms; as relatively small volumes of columns are used (4.7 mL), the system volume could be significant and affect model validity, though would also serve as a proof of concept for further work performed on smaller columns.

Both step change responses and pulse responses were obtained at a variety of residence times and were subject to analysis through two means. Through inverse-fitting with mechanistically modelling with plug flow reactors and continuously stirred tank reactors, for the purpose of introducing and correcting for this within the mechanistic modelling framework, and through determining the first moments with the EMG equation for better estimating column porosities. For the EMG approach, good fittings were observed for all flowrates (Figure 6.7), though for faster flowrates a poorer description of the peak front was apparent than for the peak tail, in which material appeared to elute before the injection, likely a limitation of using the EMG equation to characterise pulse responses.

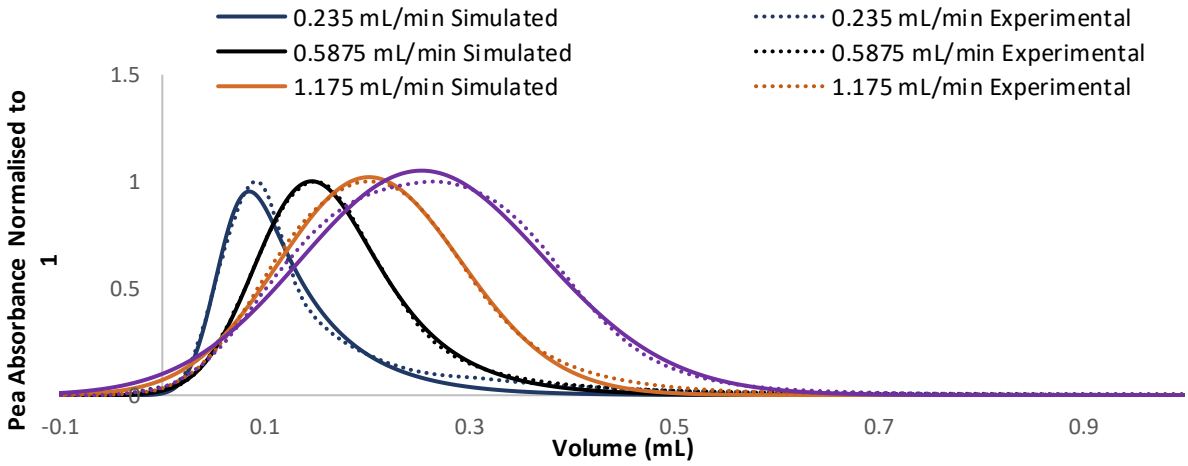

Figure 6.7 – Pulse Response and EMG Fits for Dead Volume Determination at 4 flowrates. X -axis plotted as volume, as retention time or load challenge have no physical basis in the system.

For step change simulation, a single PFR and CSTR in series model was employed for determining total system volume and post-column volume, whereas for pulse tests an additional CSTR of the same volume was introduced to account for dispersion of the material within the loop valve on the system, with better quality of fits observed. Improved fittings were also found when applying two CSTR's for modelling the step response, as others have reported (Boi et al., 2007) due to two CSTR's ability to approximate a sigmoidal breakthrough, though adequate fittings were observed without. Additionally, the post column dead volume was estimated by flowing a saturated column (1% (v/v) Acetone) into a system containing water alone, with CSTR and PFR volumes estimated.

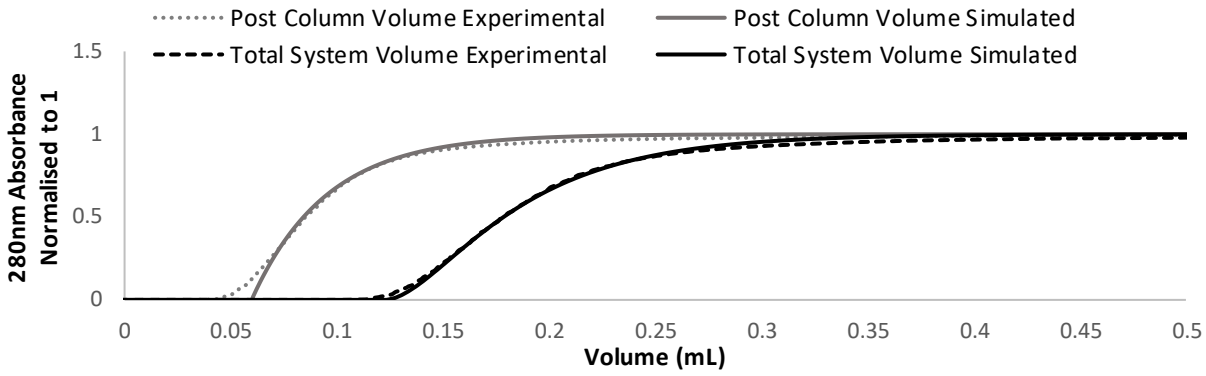

Figure 6.8- An example step response and CSTR/PFR simulation of system with UV active buffer and PFR-CSTR model for total system volume (black) or post column volume (grey), demonstrating a good fit but poor approximation of early breakthrough.

For the pulse response, poor fittings were observed with only a single CSTR with PFR modelled, though acceptable with two CSTRs (Figure 6.9). As expected, better fittings were observed when introducing yet another CSTR, bringing the total to three, but the fits were adequate with two CSTRs and a PFR with less complexity, and therefore was used for modelling system volume. The CSTR volumes were as the post and pre-column CSTRs.

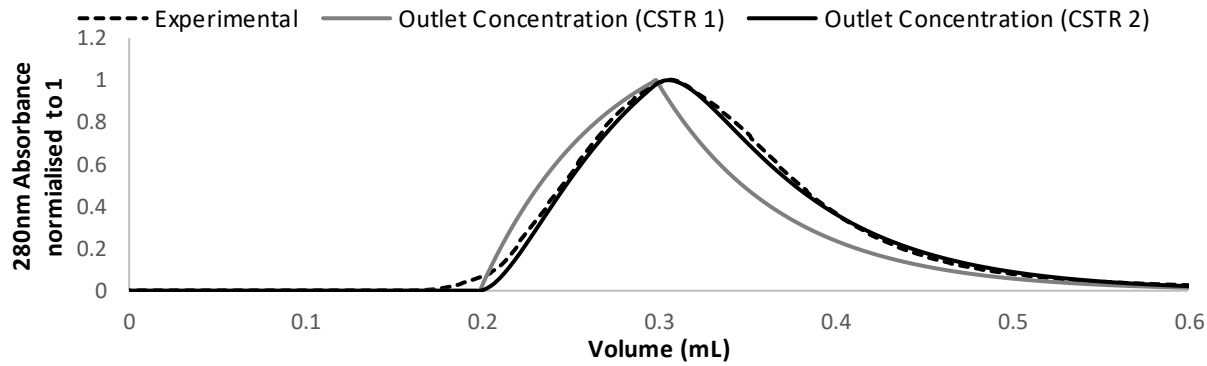

Figure 6.9- A pulse response of system with UV active buffer and PFR-CSTR-CSTR model

One can see comparability between system volumes measured by both the method of moments and inverse method (Table 6.4), in which dead volume appears to increase with flowrate; this is likely due to system limitations such as valve switching time, as other have not reported such a phenomenon (Boi *et al.*, 2007). The post column volume was significantly smaller than the total dead volume determined by CSTR and PFR fitting of step responses, and within possible errors of the total system volume. Therefore post-column mixing was ignored for peak fitting with in which the total variation in post column volume will impact porosity determination by less than 1%, whereas total column mixing should describe the additional broadening and lag introduced by the system, regardless of position in the flow path.

The total system CSTR and PFR models can describe the flow effects well enough for incorporation in a mechanistic modelling workflow, and good EMG fits, and therefore first moments can be obtained for better estimating porosities, with each approach providing better estimated than neglecting dead volume entirely. For the CSTR + PFR approach, the post column model could be applied at any point by adjusting the total system model into pre-column mixing and post-column mixing, able to account for fine structure in a response arising from the column. Of the two methods of fitting, CSTR/PFR and the EMG equation, the EMG approach exhibited better quality of fit, which follows logically, considering the greater number of parameters needed to describe the EMG and wide applicability to describe chromatographic peaks. These peaks typically exhibit more complexity to describe than two CSTR's and a PFR with a total of three parameters between them, and typically require significantly more CSTR's modelled in series to approximate a peak shape well described by the EMG (Mo & Jensen, 2016).

The CSTR and PFR models failed to show a consistent total volume across the various flowrates, likely due to the limitation of the system seen in the raw data, in which the peaks shifted with regards to flowrate. However, as these successfully described the pulse response, they were integrated into the model, in which either the pulse or step configuration as simulated based upon the nature of the data.

Table 6.4 – Simulated CSTR and PFR volumes, EMG parameters and first and second moments used to model system contributions to brand broadening for step responses and pulse injections at multiple flowrates. Uncertainties were calculated from standard deviation of parameters across three repeats

Residence Time Equivalent (s)	1200	480	240	160
Flowrate (mL/min)	0.235	0.5875	1.175	1.7625
σ (mL)	0.023 ± 0.001	0.0465 ± 0.002	0.0841 ± 0.003	0.112 ± 0.006
μ (mL)	0.0582 ± 0.002	0.1079 ± 0.003	0.1702 ± 0.007	0.2118 ± 0.008
τ (mL)	0.062 ± 0.002	0.0617 ± 0.002	0.0364 ± 0.002	0.0473 ± 0.001
First Moment (mL)	0.121 ± 0.003	0.1697 ± 0.008	0.2066 ± 0.007	0.2591 ± 0.009
Second Moment (mL^2)	0.0072 ± 0.000	0.0154 ± 0.001	0.0303 ± 0.001	0.0471 ± 0.002
Combined CSTR Volume (pulse response, mL)	0.082 ± 0.004	0.104 ± 0.005	0.172 ± 0.007	0.204 ± 0.009
PFR Volume (pulse response, mL)	0.083 ± 0.001	0.125 ± 0.006	0.126 ± 0.005	0.132 ± 0.006
Total Volume ($CSTR_{1,2}$ + PFR, pulse response, mL)	0.162 ± 0.002	0.229 ± 0.010	0.298 ± 0.012	0.336 ± 0.017
CSTR Volume (step response, mL)	0.071 ± 0.003	0.087 ± 0.004	0.103 ± 0.005	0.11 ± 0.005
PFR Volume (step response, mL)	0.053 ± 0.001	0.054 ± 0.002	0.075 ± 0.004	0.083 ± 0.004
CSTR Volume (post column, step response)	0.041 ± 0.001	0.084 ± 0.004	0.079 ± 0.003	0.091 ± 0.004
PFR Volume (post column, step response)	0.013 ± 0.000	0.015 ± 0.001	0.023 ± 0.001	0.032 ± 0.002
Total Volume (CSTR + PFR, step response)	0.124 ± 0.006	0.141 ± 0.007	0.178 ± 0.007	0.193 ± 0.008

6.6.2 Porosity Determination

6.6.2.1 Bed Porosity Determined with a Dextran Pulse

When performing pulse experiments of Dextran 2,000,000, initially a concentration of 0.5gL^{-1} was employed; this was increased to 5gL^{-1} on both systems due to poor signal experienced with the latter microscale experiments. Dextran pulses were found to bind to the Protein A column, prohibiting porosity determination. McCaw *et al.* (2007), used 7M urea when using a similar Protein A resin to prevent binding, though as urea is a powerful denaturant, risking effecting the Protein A ligands and prohibiting binding experiments, other agents were screened. It was found that 100mM NaOH was enough to inhibit binding without the risk of deteriorating the adsorber, as this is a manufacturer recommended buffer used for CIP of the resin. The quick nature of pulse tests, with only two column volumes of effluent measured, meant the column wasn't in a caustic solution for extended periods.

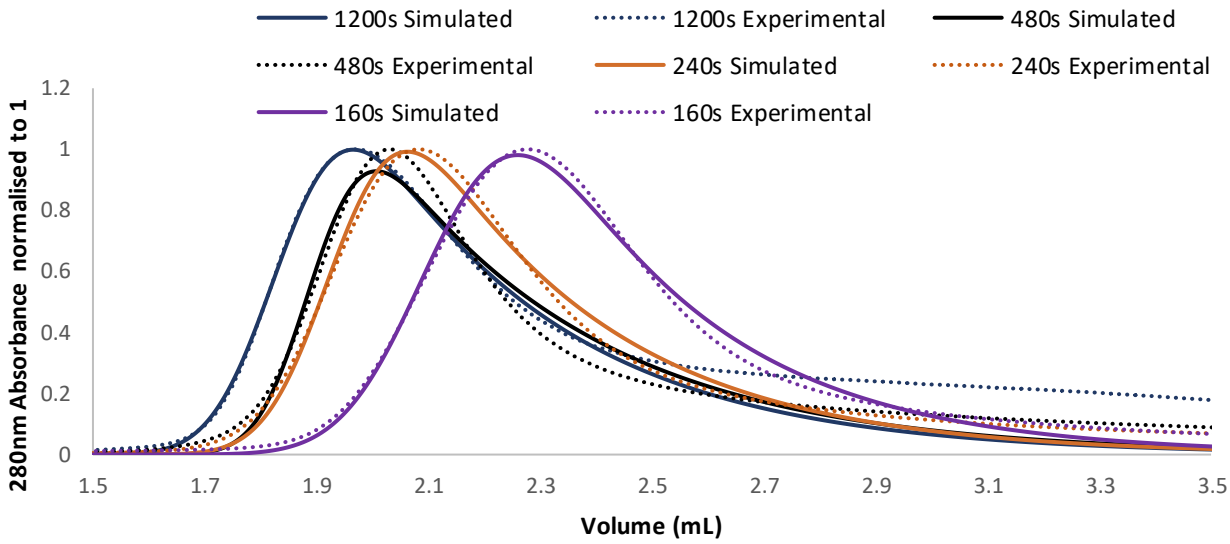

Figure 6.10 – Dextran Pulse Experiments and EMG Fits for 4 residence times, demonstrating large amount of tailing affecting EMG fitting

From the responses, at all flowrates, though in particular with slower flow, significant shouldering of the peak is observed, perhaps due to interaction with the pore network, ligands or particles; the dextran reagent used would have a mass distribution, rather than a single species of exactly 2,000,000 Da (Qader *et al.*, 2011), and both the particles and pores in chromatography media also have a significant size distribution (Hagel *et al.*, 1996, Pabst *et al.*, 2018), suggesting some slow partition of the smaller fractions of dextran into the larger pores may explain the high asymmetry. EMG fits were acceptable for all but the highest residence time, as the EMG equation could not fully approximate the high degree of tailing (Figure 6.10).This inability of the EMG equation to describe the high degree of tailing has previously been reported (Schweiger *at al.*, 2017 Gritti & Guiochon,

2012), and likely due to the lack of physical basis of the equation; tailing caused by thermodynamic effects does not follow EMG behaviour (Guiochon *et al*., 2006).

Without system volume correction, the optimised values for porosity increased with flowrate; this is likely to be the contribution from system effects, and the differing flow regimes or system limitations leading to deviations as seen with the dead volume responses. When corrected for, the flowrate dependency was no longer apparent and the porosities at all residence times were within the range found in literature, of 0.38-0.45, with significantly less of the variation between flowrates as without correction (Table 6.5).

Table 6.5 -EMG Parameters, moments analysis and inverse mechanistic model fit of the dextran peaks, demonstrating that correcting for system improves consistency across residence times. D_L was calculated using [6.17]. Uncertainties were measured as standard deviations from 3 repeats.

Residence Time	1200	480	240	160
Flowrate (mL/min)	0.235	0.5875	1.175	1.7625
Method of Moments				
σ (mL)	0.0944 ± 0.003	0.0765 ± 0.001	0.0956 ± 0.003	0.124 ± 0.002
μ (mL)	1.8396 ± 0.068	1.8947 ± 0.012	1.9376 ± 0.037	2.118 ± 0.049
τ (mL)	0.36 ± 0.0012	0.3872 ± 0.0041	0.3457 ± 0.0021	0.3213 ± 0.013
First Moment (Measured, mL)	2.1997 ± 0.004	2.2819 ± 0.009	2.2833 ± 0.005	2.4393 ± 0.015
Second Moment (Measured, mL^2)	0.1385 ± 0.00463	0.1558 ± 0.00021	0.1287 ± 0.00137	0.1186 ± 0.00257
ε_b (Without system volume Correction)	0.468 ± 0.019	0.4855 ± 0.013	0.4858 ± 0.008	0.519 ± 0.019
First Moment (With system and injection volume correction Injection, mL)	2.0295 ± 0.069	2.0623 ± 0.085	2.0267 ± 0.061	2.1302 ± 0.057
Second Moment (With system and injection volume correction Injection, mL^2)	0.1305 ± 0.002	0.1395 ± 0.001	0.0975 ± 0.002	0.0706 ± 0.003
D_L ($m^2\ s^{-1}$)	3.07 ± 0.09 x 10^{-7}	7.95 ± 0.03 x 10^{-7}	1.15 ± 0.08 x 10^{-7}	1.13 ± 0.04 x 10^{-6}
ε_b (With system volume correction)	**0.4318 ± 0.033**	**0.4388 ± 0.0029**	**0.4312 ± 0.0012**	**0.4532 ± 0.0062**
Inverse Method				
ε_b (Without system volume simulation)	0.4418 ± 0.005	0.4556 ± 0.019	0.4495 ± 0.018	0.4512 ± 0.007
D_{ax} (m^2s^{-1}) (Without system volume simulation)	1.90 ± 0.04 x 10^{-7}	5.54 ± 0.11 x 10^{-7}	9.76 ± 0.20 x 10^{-7}	1.62 ± 0.019 x 10^{-6}
ε_b (With system volume simulation)	0.4312 ± 0.002	0.4291 ± 0.002	0.4329 ± 0.008	0.445 ± 0.005
D_{ax} (m^2s^{-1}) (With system volume simulation)	2.69 ± 0.03 x 10^{-7}	5.08 ± 0.09 x 10^{-7}	1.14 ± 0.17 x 10^{-6}	1.68 ± 0.14 x 10^{-6}

As with moments analysis, correcting for system volume reduced the variability of bed porosity determination between flowrates (Table 6.5). Additionally, the Dextran peak can be better approximated by incorporating some arbitrarily low particle porosity (ε_p of 0.1), but a large kinetic resistance the partitioning into the bead through a small k_f or D_p value (Figure 6.11). Whilst interesting, this approach was not employed in model calibration, and particle porosity was assumed to be zero with respect to dextran for the sake of simplicity, therefore assigning all band broadening to axial dispersion alone in which D_L is equal to D_{ax}, though this is likely to artificially increase this value, as all transport resistances would be lumped within.

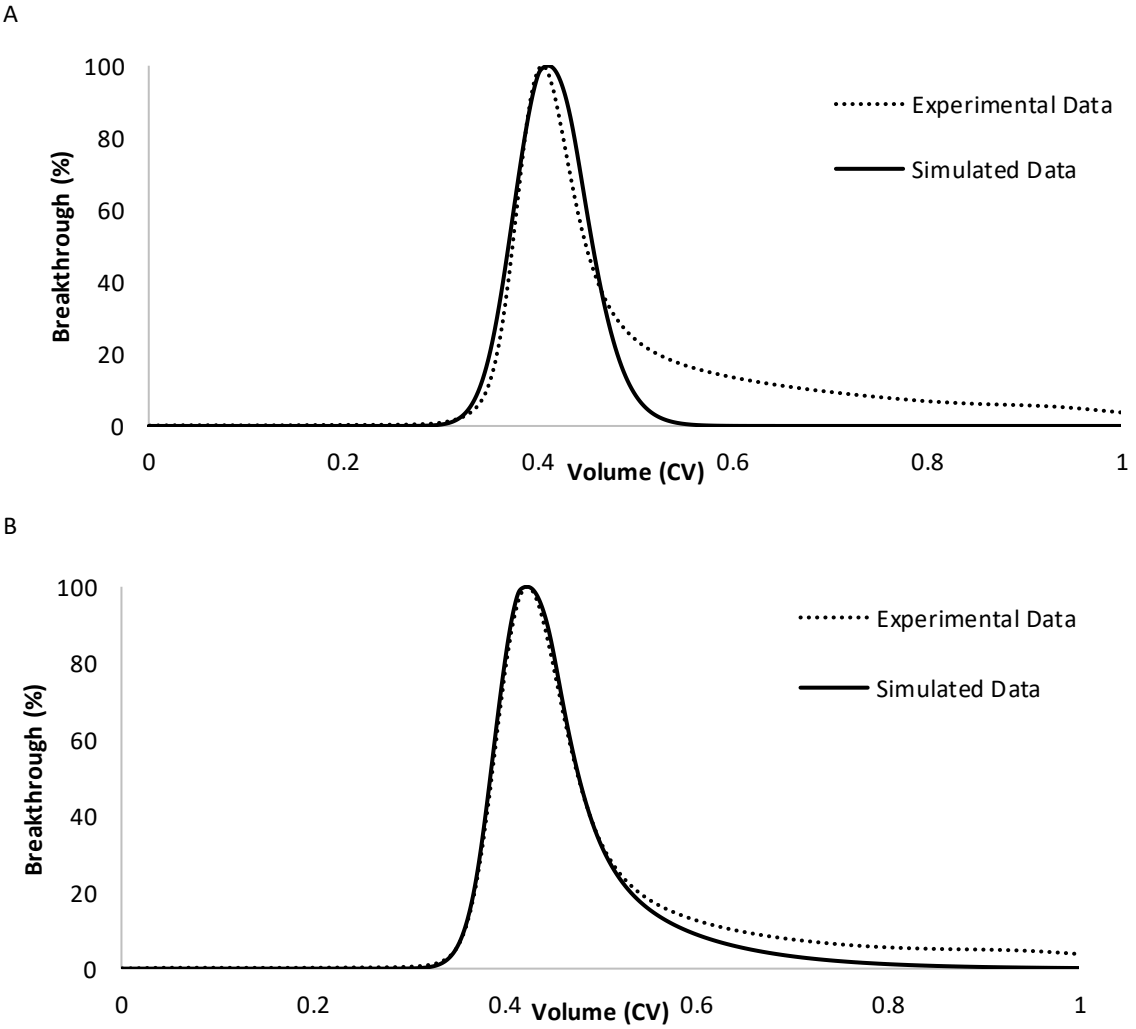

*Figure 6.11 – Dextran pulse and model fit, **A** – model fit where particle porosity was defined as zero, **B** - where particle porosity was non-zero (0.1), but a high resistance to mass transfer specified (low pore diffusion coefficient), demonstrating the tailing can be explained with a degree of particle permeability with slow rates of partition.*

To generalise the model further, for a multitude of flowrates, one can employ known engineering correlations. Using the Frigon correlation, a molecular diffusivity of Dextran 2,000,000 is determined to be 7.69 x 10^{-11} m^2 s^{-1}, within an order of magnitude to the experimentally determined value of 3.15 x 10^{-11} m^2 s^{-1} reported by Lebrun and Junte (1993).

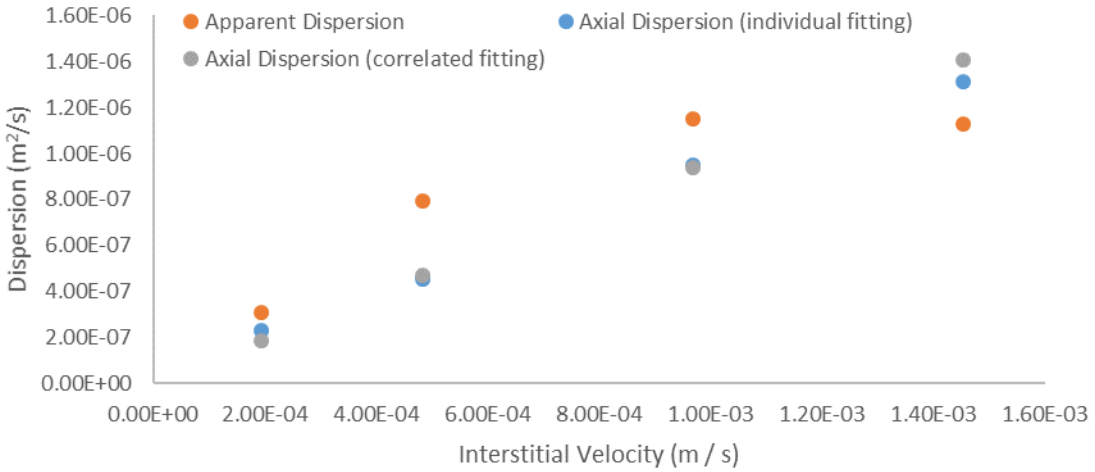

Figure 6.12- Axial Dispersion Coefficient, D_{ax} (from GRM fit, both individual and constrained by the correlation) and Apparent Dispersion, D_L (from EMG fit) vs Interstitial Flow Velocity of Dextran, demonstrating strong linearity, and some little contribution of an offset, suggesting molecular diffusion is not significant to band broadening for dextran pulses of residence time 480 s or less and that the HETP eddy dispersion term is dominant at these flowrates if no pore transport is assumed

Van Deemter, Ruthven and De Ligny's correlation specify that the axial dispersion coefficient linearly correlates to interstitial velocity with a constant contribution by molecular diffusion, and Chung and Wen specify no contribution of molecular diffusion, this is supported by the linear relationship measured to the fitted D_{ax} values (Figure 6.12), in which the apparent diffusion (determined with moments analysis and [6.17]) axial dispersion (by individual experiments) and axial dispersion (in which a linear correlation to flowrate was used) demonstrated similar trends. These values are of a similar magnitude to that determined with the Van Deemter methodology, though with improved linearity, likely due to the peak tailing significantly affecting EMG fit though not impacting GRM as greatly. Considering that the latter is more constrained in that the resultant chromatogram must be physically possible (e.g., at the outlet concentration is zero at time zero), it was assumed to be more reliable .

The used correlation for axial dispersion may then be reduced to a single relationship, how axial dispersion varies with flowrate, neglecting molecular diffusion. The experimental runs are then employed in a group to calibrate the model, with the relative axial dispersions set to follow this correlation. Molecular diffusivity will have a negligible impact on the axial dispersion for this system, and is therefore ignored (Susanto *et al.,* 2008), due to its low magnitude ($<10^{-10}$ m^2 s^{-1}). For this, the correlation of Ruthven is used, introducing the dimensionless, geometric constants y_2 from [6.12] (Ruthven, 1984). The model was then calibrated with this linear relationship with all residence times, instead of allowing freedom for each residence time.

Table 6.6 – Optimised Values for Axial dispersion Coefficients and Porosity for Dextran on a Protein A resin, when applying a correlation to generalise the model for several flowrates compared to fitting axial dispersion individually

ε_b	**0.434 ± 0.007**			
γ_2	4.90 ± 0.16			
Residence Time	160 s	240 s	480 s	1200 s
Using Correlation				
$D_{ax}(m^2s^{-1})$	1.88×10^{-7}	4.69×10^{-7}	9.39×10^{-7}	1.41×10^{-6}
Error (MSE, $\%^2$)	10.21			
Individually Fitting				
$D_{ax}(m^2s^{-1})$	2.32×10^{-7}	4.54×10^{-7}	9.48×10^{-7}	1.31×10^{-6}
Error (MSE, $\%^2$)	9.63			

Reasonable fitting was observed (Table 6.6) , with no improvement when also including the molecular diffusivity term. Porosities determined were of similar values published for this resin (0.96 from Pabst *et al*., 2018), though the bed porosity is determined by packing quality, and therefore likely to vary slightly between columns, or during the lifetime of use of a single column. Regardless of means of determination, whether through moments analysis or through fitting porosity through the inverse method, a bed porosity of 0.434 ± 0.001 was measured. Whilst this value is higher than reports by Pabst et al., (2018) with their own packed columns with a compression factor of 1.2, greater than the manufacturers recommendation of 1.1, and the porosity measured here is within ranges reported for similar resins (Yamamoto *et* al., 1977, Bowes *et al*., 2009).

6.6.2.2 *Total Porosity Determination with PABA*

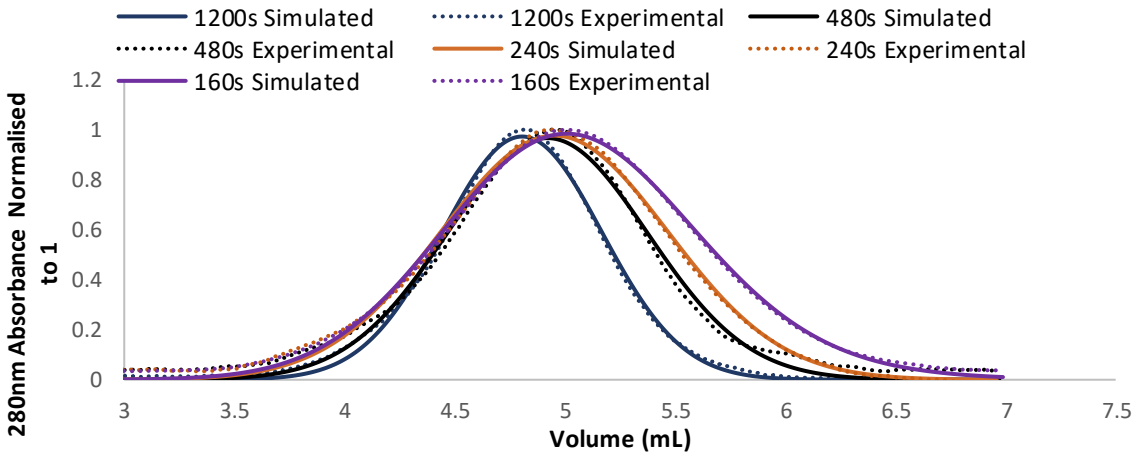

Figure 6.13 – PABA Pulse Experiments and EMG Fits for 4 residence times, demonstrating clear broadening of the peak at faster flowrates, and less tailing than observed with equivalent dextran responses

With PABA, a retention volume offset proportional to flowrate was observed, with slightly wider peaks (Figure 6.13), which may be an artefact of the system, as seen with the dead volume tests (Figure 6.7). Good EMG fits were obtained, with moments analysis further supporting the requirement for dead volume corrections (Table 6.7) , without it, particle porosities were fitted with physically impossible values (ε_p > 1), whereas after

correction, a value of 0.97 ± 0.01 was determined with good consistency across residence times. Though this is a rather high value for particle porosity, others have reported similar values for this resin (Pabst *et al*., 2018), with others reporting higher values for similar base matrices (Guan & Guiochon, 1996).

The inverse method was also followed to determine the particle porosity, and axial dispersion terms for PABA. Model formulation was similar to simulating the passage of Dextran through the column, in that binding terms were omitted, though unlike Dextran simulation, partitioning into the pores, pore diffusion and particle porosity were included in the model formulation. The values for k_f, the film transfer rate, was set arbitrarily high, as was D_p, the pore diffusion rate. The reasoning behind this was because PABA is a relatively small molecule when compared with proteins, with at least one log higher diffusivity when compared to IgGs (Vajda *et al.*, 2015), and therefore it was assumed that the mass-transfer limiting step would be convection of the material through the column, and that axial dispersion was the main contribution towards band broadening and therefore simulating a significant resistance to pore transport would impact any derived values for the particle porosity. Though a poor assumption, by performing multiple residence time experiments provides an insight into the validity of this. The same dead volume script for both pre-column and post-column mixing was also applied through simulating CSTR's and PFR.

Table 6.7 EMG Parameters and Moments analysis of the PABA peaks, demonstrating that correcting for system improves consistency across residence times, and ensures porosity values are physically possible

Residence Time	1200	480	240	160
Flowrate (mL/min)	0.235	0.5875	1.175	1.7625
Method of Moments				
σ (mL)	0.3617 ± 0.017	0.4543 ± 0.020	0.5147 ± 0.011	0.5217 ± 0.015
μ (mL)	4.788 ± 0.042	4.8664 ± 0.104	4.8343 ± 0.117	4.771 ± 0.137
τ (mL)	0.0182 ± 0.000	0.0243 ± 0.001	0.0183 ± 0.001	0.1814 ± 0.005
First Moment (Measured, mL)	4.8062 ± 0.017	4.8906 ± 0.021	4.8526 ± 0.012	4.9525 ± 0.02
Second Moment (Measured, mL^2)	0.1312 ± 0.00176	0.207 ± 0.01082	0.2653 ± 0.01369	0.3051 ± 0.01879
ε_t (Without system volume Correction)	1.0226 ± 0.038	1.0406 ± 0.026	1.0325 ± 0.018	1.0537 ± 0.030
ε_p (Without system volume Correction)	1.0397 ± 0.031	1.0712 ± 0.010	1.0569 ± 0.014	1.0942 ± 0.034
First Moment (With system and injection volume correction Injection, mL)	4.6352 ± 0.085	4.6709 ± 0.053	4.596 ± 0.139	4.6434 ± 0.136
Second Moment (With system and injection volume correction Injection, mL^2)	0.1231 ± 0.006	0.1908 ± 0.007	0.2341 ± 0.008	0.2572 ± 0.002
D_L (m^2 s^{-1})	5.55 ± 0.12 x 10^{-8}	2.12 ± 0.09 x 10^{-7}	5.37± 0.21 x 10^{-7}	8.67 ± 0.18 x 10^{-7}
ε_t (With system volume correction)	0.9862 ± 0.030	0.9938 ± 0.038	0.9779 ± 0.030	0.9879 ± 0.024
ε_p (With system volume Correction)	0.9758 ± 0.014	0.9891 ± 0.047	0.9612 ± 0.009	0.9789 ± 0.029
Inverse Method				
ε_p	**0.972 ± 0.003**			
y_2	2.8 ± 0.1			
D_{ax}(m^2s^{-1})	1.07 x 10^{-7}	2.68 x 10^{-7}	5.36 x 10^{-7}	8.04 x 10^{-7}

The values for bed porosity, as determined above, were introduced to the model, with axial dispersion correlation coefficient y_2 and particle porosity serving as the optimised values. Better fits were observed than with dextran considering the reduced tailing of the pulses. These values for both bed porosity and total particle porosity when determined using the inverse method agreed with published values for comparable Protein A resins (Horstmann & Chase 1989, Pabst *et al.*, 2018, McCaw *et al.,* 2014, Ng *et al.,* 2012, Teeters, *et al.,* 2009), the bed porosity is dependent on packing, whereas the particle porosity should be invariant to packing, under normal, noncompressive conditions. Interestingly, the measured and fitted values for axial dispersion were about half of the values for dextran, which does not follow logically with the model assumptions. PABA is assumed to be subject to intraparticle mass transfer whereas dextran was not, meaning PABA should have an increased apparent dispersion considering more sources of potential band broadening by the above assumptions. This reduction suggests that there was some other source of band broadening with the dextran

pulses, perhaps that the running buffer (100mM NaOH) was not sufficient to prevent all interaction between dextran and the adsorbent. Therefore, the PABA experiments are assumed to be more reliable in determining true axial dispersion, though the small increase in plate height as residence time is reduced does suggest there is some measurable kinetic resistance to PABA transport, even after dead-volume correction, though the contribution by eddy dispersion is the greatest source of band broadening at all the measured flowrates. A further concern is that from the screening of PABA and other HETP analytes (Chapter 4), PABA shows a slightly greater retention volumes than both other standard tracers, acetone and sodium chloride, though this difference was less than 2%, so has not been further considered.

6.6.2.3 Effective Particle Porosity Determination by IgG, nonbinding

To describe the effective, or accessible, porosity of a column, one can perform pulse experiments with non-binding product. This approach is widely used in size-exclusion chromatography modelling (Do *et al.,* 2011), in which it can be called 'effective particle porosity', or 'accessible pore volume fraction', and has been shown to describe size exclusion effects for other modes of chromatography well, including Protein A affinity (Hahn *et al.,* 2005, Pabst *et al.,* 2018, Perez-Almodóvar & Carta, 2009a).

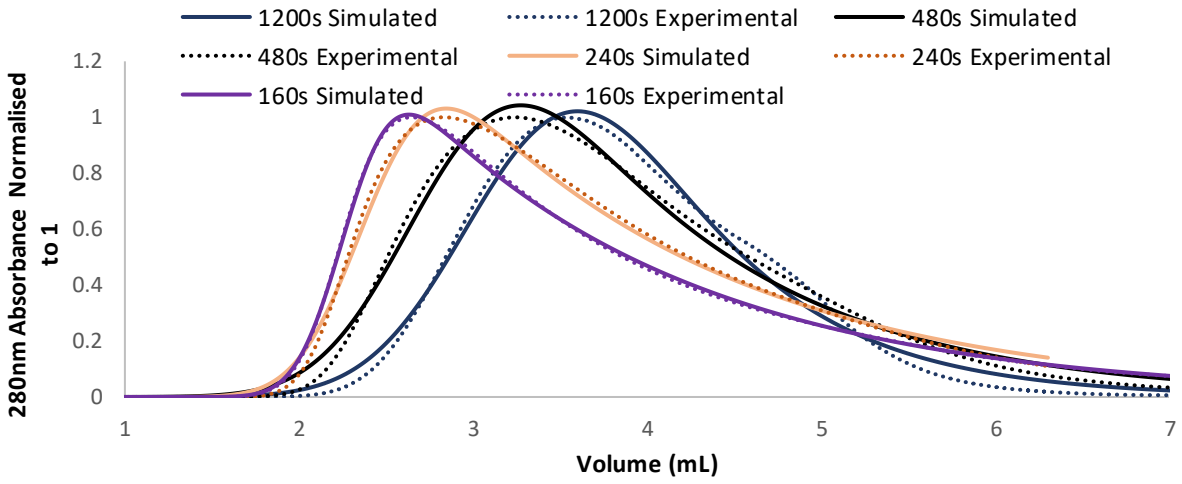

Figure 6.14 -Non-binding IgG Pulse Experiments and EMG Fits for 4 residence times, demonstrating peak maximum is correlated with residence time

From the raw data, one can also see a high degree of tailing in the pulse responses (Figure 6.14), increasing with flowrate, as well as variation in peak position, inversely proportional to residence time, the opposite to that observed with both dextran and PABA, and therefore contributions by system effects alone can be dismissed as the cause. Moments analysis, however revealed that the first absolute moment remained similar for all residence times, leading towards an effective particle porosity of 0.65 ± 0.03 (Table 6.8). This follows derivations of the general rate model, in which the first moment should be invariant to flow and not depend on any mass

transfer resistance, though defined by accessible volume, whereas peak variance will increase with every kinetic resistance (Schmidt-Traub, 2006).

This was further evaluated with a HETP analysis, in which one can correlate pore diffusion to the slope of a reduced HETP- reduced flow velocity chart (Figure 6.15), if assuming axial dispersion is strictly linearly correlated to flowrate, use the intercept to determine the factor [6.35 and 6.36] a similar approach as Carta *et al*., (2005), Perez-Almodóvar & Carta, (2009a) and Gritti & Guiochon, (2006). Standard deviations were calculated using the linear regression toolbox in Microsoft Excel.

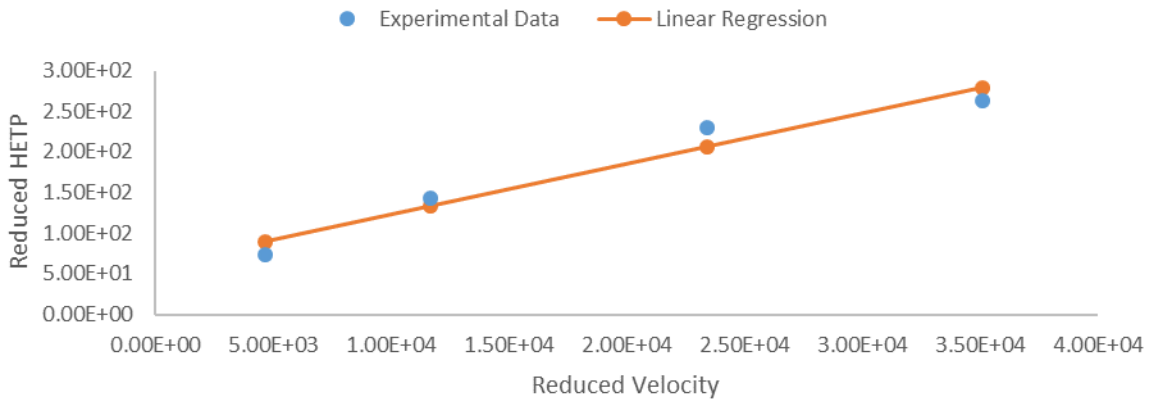

Figure 6.15 - Reduced HETP and Reduced Interstitial Velocity plot for non-binding IgG, used to estimate D_p and the linear relationship of D_{ax}

A significantly higher contribution of axial dispersion was determined with this approach, over double of that estimated with PABA, and higher than was measured with dextran. The small magnitude of the intercept, compared with the deviations from linearity exhibited in the data means difference is not necessarily robust, a value of y_2 as 0 is within the 95% confidence interval. This could be due to error compounded with this approach, both from fitting the EMG not accounting for significant tailing in the IgG pulse data and dead volume pulse data reducing confidence in this approach.

Table 6.8 – EMG Parameters and Moments analysis of the non-binding IgG peaks. The moments analysis, coupled with correcting for system volume reduces the variation in peak position compared to peak maximum alone.

Residence Time	1200	480	240	160
Flowrate (mL/min)	0.235	0.5875	1.175	1.7625
σ (mL)	0.5078 ± 0.0018	0.4564 ± 0.0096	0.3054 ± 0.0071	0.2187 ± 0.0025
μ (mL)	3.1436 ± 0.0014	2.743 ± 0.0293	2.3876 ± 0.0191	2.2697 ± 0.0418
τ (mL)	0.7947 ± 0.0099	1.235 ± 0.0135	1.6535 ± 0.0137	1.6444 ± 0.0231
Method of Moments				
First Moment (Measured, mL)	3.9383 ± 0.065	3.978 ± 0.08	4.0411 ± 0.072	3.9141 ± 0.109
Second Moment (Measured, mL^2)	0.8894 ± 0.00116	1.7336 ± 0.00000	2.8274 ± 0.00281	2.7518 ± 0.00144
ε_t (Without system volume Correction)	0.8379 ± 0.029	0.8464 ± 0.011	0.8598 ± 0.003	0.8328 ± 0.031
ε_p (Without system volume Correction)	0.7157 ± 0.022	0.7305 ± 0.016	0.7541 ± 0.027	0.7066 ± 0.023
First Moment (With system and injection volume correction Injection, mL)	3.7673 ± 0.145	3.7583 ± 0.087	3.7845 ± 0.170	3.605 ± 0.041
Second Moment (With system and injection volume correction Injection, mL^2)	0.8822 ± 0.015	1.7182 ± 0.041	2.7971 ± 0.023	2.7047 ± 0.109
ε_t (With system volume correction)	0.8016 ± 0.029	0.7996 ± 0.020	0.8052 ± 0.036	0.767 ± 0.020
$\varepsilon_{p,eff}$ (With system volume Correction)	0.6518 ± 0.030	0.6485 ± 0.028	0.6583 ± 0.026	0.5913 ± 0.006
D_p (Estimated through HETP analysis) m^2s^{-1}	$1.22 \pm 0.20 \times 10^{-11}$			
y_2 (Estimated through HETP analysis)	25.2 ± 19.1			
Inverse Method				
y_2	2.8 (assumed the same as for PABA, no improvement in model quality when unconstrained)			
D_{ax} (m^2 s^{-1})	1.07×10^{-7}	2.68×10^{-7}	5.36×10^{-7}	8.04×10^{-7}
k_f ($m\ s^{-1}$)	6.27×10^{-6}	8.51×10^{-6}	1.07×10^{-5}	1.23×10^{-5}
Sherwood Number	15.3	19.6	24.6	28.2
$\varepsilon_{p,eff}$	**0.65 ± 0.011**			
D_p (m^2 s^{-1})	$5.64 \pm 0.21 \times 10^{-12}$			
Error (MSE, $\%^2$)	3.31			

The same data was used for model calibration with the inverse method The values for the particle porosity of PABA was used as an upper bound for the optimisation regime, with the bed porosity set by the dextran pulse results. The film diffusion coefficient was estimated from the correlation of Wilson & Geankoplis (Equation 21) with a molecular diffusivity estimate of 3.7×10^{-11} m^2 s^{-1} (Tyn & Gusek, 1990). Particle porosity, pore diffusion and correlation-constrained axial dispersion were the optimised variables.

An approach in which the particle porosity was set to the value ascertained by PABA injections, with the remaining parameters (D_P, D_{ax}) given freedom, was performed to evaluate whether IgG porosity was the appropriate metric for describing IgG transport, or whether one could omit this experiment from the workflow. When ε_p was constrained to that determined by PABA injections, very poor GRM fits were observed when calibrating for all flowrates compared to allowing particle porosity to be calibrated for this component (Figure 6.16). The mechanistic model described the peak tailing better than the EMG could, though there was slightly poorer description of the peak front for the 160 s residence time. The parameters fitted by the model are in line with those in literature, with a pore diffusion coefficient similar to Pabst *et al.*, 2018, with no improvement to model quality by varying the y_2 value from that determined with PABA. This is a significant reduction in the pore diffusion coefficient determined by the HETP analysis, though is within the 95% confidence interval of this approach. Effective particle porosity was fitted as 0.65 ± 0.01, the same value as that determined through moments analysis of the dead volume corrected raw data, and within the ranges published by Pabst *et al*., (2018).

A

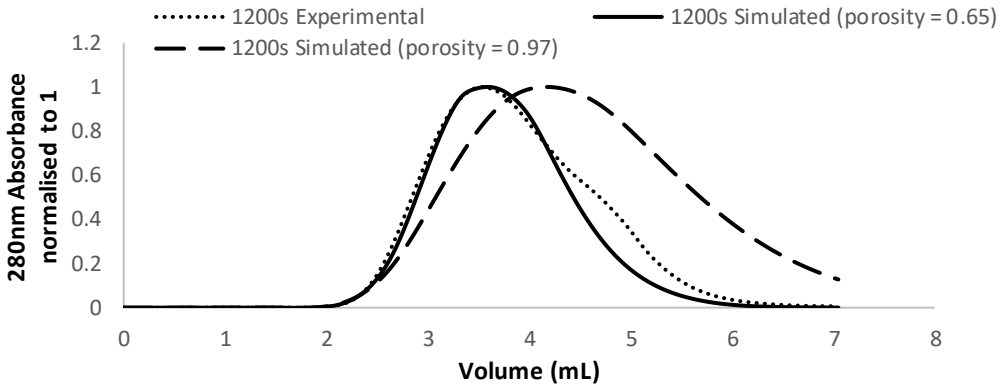

B

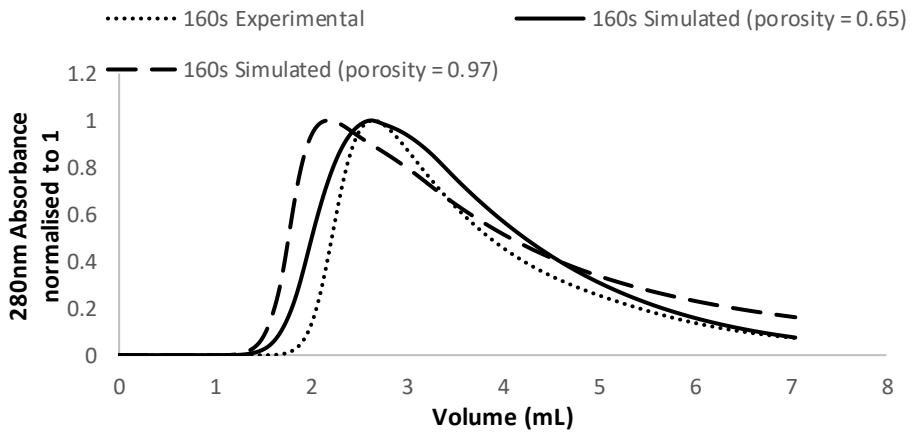

Figure 6.16- The fitting of the 1200 s (A) and 160 s (B) nonbinding IgG pulse with a single GRM formulation (describing 4 residence times; only the extremes are shown for clarity) through either allowing freedom ε_p of IgG, or through fixing ε_p of IgG to the same ε_p of PABA, demonstrating improved model accuracy by specifying a component specific effective particle porosity rather than assuming the full void volume is accessible, and that pore diffusion can account for the peak position-residence time relationship.

6.6.3 Isotherm Determination

Having calibrated the bed and column porosity, and axial dispersion coefficients, the adsorption model requires calibration to accurately describe breakthrough behaviour. A Langmuir isotherm has been used extensively (Horstmann & Chase 1989, Hahn *et al.,* 2005, McCaw, *et al.,* 2014, Pabst *et al*., 2018) to model Protein A binding IgG, and can also describe non-affinity systems well, when considering a single component only (Skidmore *et al.,* 1990, Kumar *et al.,* 2015). The binding rates of the IgG-Protein A are known to be high (Carta & Jungbauer, 2013, Saha 2015, Boi *et al*., 2007), the kinetic resistance to binding is unlikely to be significant in describing IgG breakthrough, however, by first establishing the equilibrium behaviour, one can later probe kinetic effects. Considering this highly favourable Protein A:IgG typically exhibits obtaining precision on the value of K_{eq} is unlikely to be crucial for model quality, whereas the value of q_{max}., the saturation concentration is likely to dominate.

Care must be taken when determining and interpreting q_{max} as there are many metrics of this, the capacity of the column or bed is the most commonly used, but this can also refer to the maximum capacity of the beads (considerably higher, as the column is not completely occupied by resin beads but has a significant interstitial fraction, determined here to be 0.43), and q_{max} of the gel which has an even greater amplification of q_{max} values considering the far larger pore fraction of the beads (determined here as 0.98 for small molecules, or 0.65 for IgG). q_{max} values in the model and isotherm have been adjusted to be the q_{max} of the column bed, and therefore being analogous to commonly determined EBC and DBC values for ease of interpretation.

6.6.3.1 Batch Adsorption

A

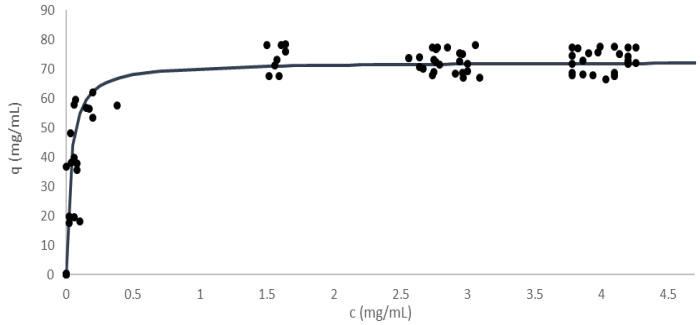

B

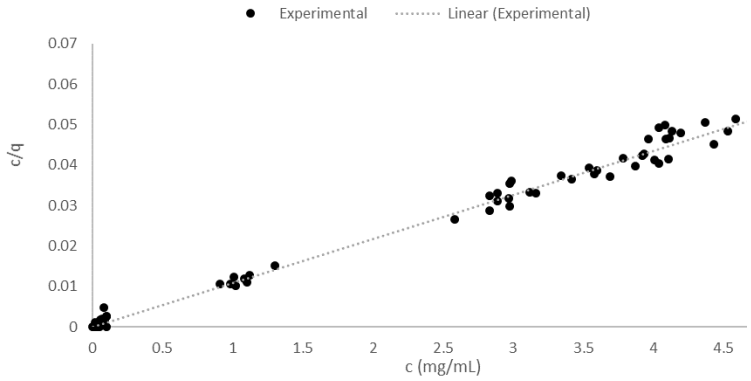

Figure 6.17- Experimental data and Langmuir Isotherm fit of IgG A binding to Protein A resin using equilibrium batch adsorption. q and c are stationary phase, and mobile phase concentration, calculated with absorbance measurements and with both load/wash effluent and elution concentrations. ***A*** *– Langmuir fit with least squares approach,* ***B*** *– Hanes-Woolf plot and linear regression.*

The isotherms for the IgG: Protein A were determined with batch adsorption with a 20 µ bed, under sufficient incubation (>6h) to ensure equilibrium is reached, including washes (1 mL) to remove non-specifically bound material. A single component Langmuir isotherm was used to interpret the data. The fit was achieved with both solver and least squares (Figure 6.17A), and through linearization with a Hanes-Woolf plot (Hanes, 1932) (Figure 6.17B). The Langmuir isotherm demonstrates very favourable equilibrium constant (K_{eq}), in line with literature values (Table 6.2). With the Hanes plot, K_{eq} values were not determinable, as the standard error exceeded the value of the y-intercept of the Hanes plot, though are clearly high considering the very low value for this intercept, suggesting a rectangular isotherm would also be valid. A q_{max} of 72.35 g L^{-1}, less than as determined through saturation experiments, though explainable through error in packed bed volume determination (a 20 µL bed volume has been extrapolated from), errors in protein concentration determination, as well as likely

different packing densities between the plates and columns, a common consideration with batch determination of isotherm (Carta, 2012, Bergander *et al.*, 2008, Bergander & Lacki, 2015).

6.6.3.2 The impact of Feed Concentration on Breakthrough

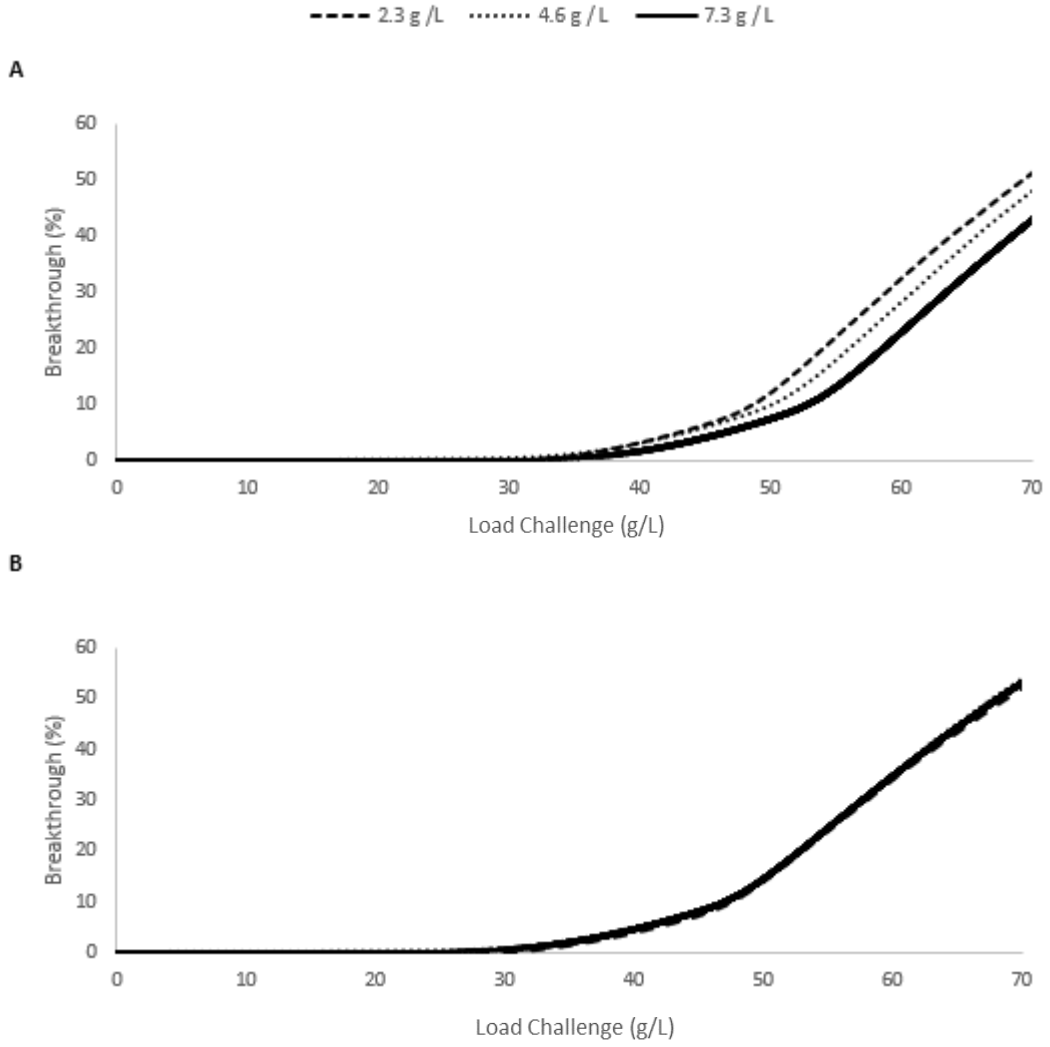

Figure 6.18 – Breakthrough Curves at Three Feed Concentration at 240 s Residence time. A – Without accounting for column holdup volume , B – With column holdup volume correction, demonstrating better consistency between feed concentrations

When comparing breakthrough between different feed concentrations, one can see a clear offset in breakthrough, which is removed when one accounts for the holdup volume of the column itself (Figure 6.18), here determined to be the total column volume accessible to IgG, calculated through the non-binding IgG pulses. Table 6.9 lists the corrected and non-corrected $DBC_{10\%}$ values, showing good constancy between feed concentrations, suggesting that the isotherm is not limiting capacity, and therefore is very favourable, which agrees with the batch adsorption determination and literature values. Others have reported a concentration-DBC relationship of IgG binding to Protein A by membrane technologies (Dancette et al., 1999, Boi et al,, 2013), though performed their experiments at for lower feed concentrations, further from the plateau region of the Langmuir isotherm where stationary phase capacity is not influenced by feed concentration.

Table 6.9 – $DBC_{10\%}$ Values determined at three feed concentrations, with and without adjusting for column holdup volumes demonstrating consistency in $DBC_{10\%}$ value regardless of feed concentration

Feed Concentration	Non-corrected $DBC_{10\%}$ (g L^{-1})	Corrected $DBC_{10\%}$ (g L^{-1})
2.3	51.6	49.7
4.6	53.1	49.4
7.3	55.8	50.0

6.6.3.1 Column Saturation and Modelling

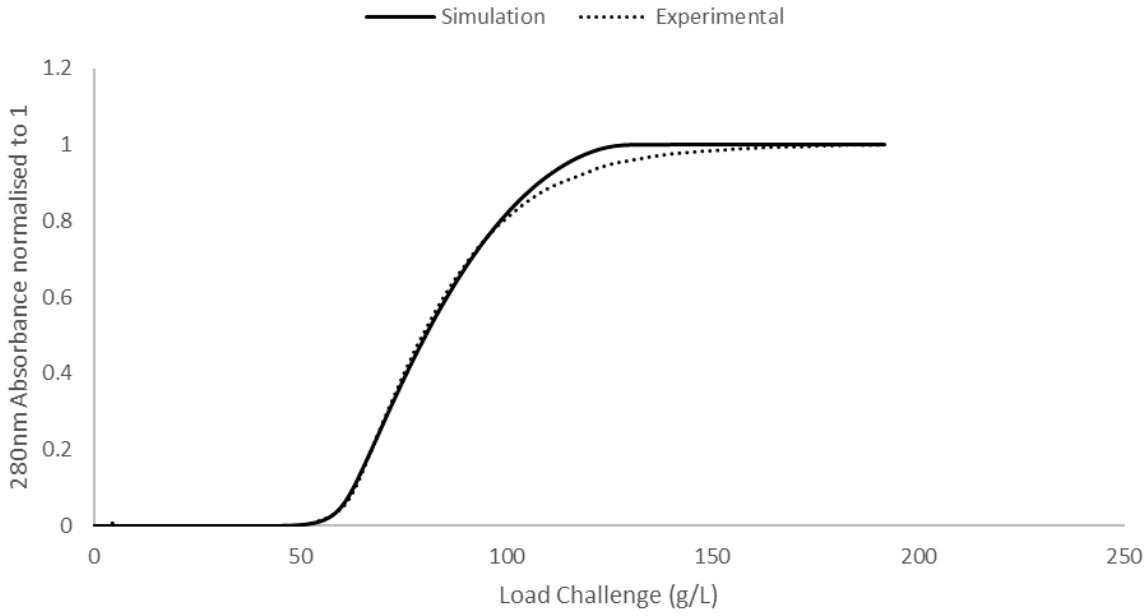

Figure 6.19 – Saturation Breakthrough and Model fit, used to determine the equilibrium binning capacity (EBC) of the column at a feed concentration of 4.7 g L^{-1}

Saturation experiments were integrated to determine the EBC at the feed concentration of 4.7 g L^{-1}, with the integral of the breakthrough subtracted from the feed amount and holdup volume of the column. Additionally, a model was fitted to evaluate what value of q_{max} would converge, with a good description of breakthrough behaviour (Figure 6.19). For this, the axial dispersion was assumed to follow the correlation used to describe the PABA pulses, and the bed porosities as described above, Pore-diffusion and the q_{max} parameters were left to vary to fit the data, with D_p fitting to a value of 3.52 x 10^{-12} m^2 s^{-1}, within an order of magnitude of literature values and that measured through non-binding IgG pulses. Good fits were observed for up to 80% of breakthrough, after which the model deviates from the experimental curve. This could be due to a number of reasons; changes in mass transfer resistances during the run, or possibly IgG-IgG interaction, which would falsely inflate the Langmuir capacity (Bruce & Chase, 2001). Other possible explanations include the increasingly restricted pore diffusion at high loading densities (Susanto et al., 2007), protein unfolding (McCue et al., 2008) heterogenous bead size distributions (Stone & Carta, 2007), the existence of more than one binding site with

different binding kinetics (Dimartino *et al*., 2015, Dimartino et al., 2011, Perez-Almodóvar & Carta, 2009a, Boi *et al*., 2007), displacement effects between aggregates and monomers (Hunter & Carta, 2001) , as well as a shrinking-core phenomenon followed by rearrangement of the adsorbate (Bowes and Lenhoff, 2011).

6.6.3.2 Comparison of methods

Table 6.10 details the q_{max}. EBC and K_{eq} values determined through batch adsorption, saturation and feed-concentration experiments, in which clearly the equilibrium is very favourable, as evidenced by literature, the negligible impact of feed concentration of capacity and the favourable partitioning during batch adsorption. For this work, the EBC determined through the saturations experiment is likely to be the most accurate descriptor of column capacity, as it is not subject to errors through poor volume determination and representation of bed packing as during batch adsorption.

Table 6.10 - Langmuir Isotherm values of IgG - Protein A, determined through batch adsorption, saturation and multiple feed-concentration breakthrough experiments

EBC estimated from integrating above chromatogram, saturation **experiment**	85.21 g L^{-1}
EBC estimated from integrating above chromatogram, saturation **model**	83.23 g L^{-1}
q_{max} estimated from batch adsorption (Langmuir)	72.35 ± 1.01 g L^{-1}
K_{eq} estimated from batch adsorption (Langmuir)	High (standard error was greater than fitted value)
K_{eq} estimated from multiple feed concentration breakthrough experiments	High (no significant impact on breakthrough profile at likely values)

The impact of these parameters on a model was tested by varying this parameter through several orders of magnitude, and measuring the impact on the error of the saturation model, using the estimate of D_p fitted with a single residence time; whilst this will not be as accurate as that fitted under multiple residence times, it is likely to be correct within 1 order of magnitude, whereas the adsorption parameters are being varied by multiple orders. One can see that the isotherm equilibrium constant, and adsorption rate do not impact the model unless brought to values significantly beneath that determined either from batch adsorption (for equilibrium constant), or literature values (Table 6.11), with no detriment to model quality if these values are increased. For the kinetic constant, this is logical, as characteristic times (τ) of adsorption, as with film transfer (r_p/k_f, <1s) are far smaller compared to pore diffusion (r_p^2/D_p, 10^2 to 10^3 s), convection (L/v, ~10^2s) and axial dispersion (L^2/D_{ax}, >10^4 s) (Bird *et al*., 2006). This observation supports reducing the isotherm to a rectangular isotherm with a single parameter, q_{max}, and not simulate finite binding kinetics, but assume that equilibrium is reached instantaneously, which is a relatively common assumption for this system (see section 6.2.2). This reduces the model to a transport dispersive model. This interaction is mediated by at a single site of IgG which is conserved across all subtypes of IgG, except IgG_3 (Van Loghem *et al.,* 1982), suggesting such a simplification would still be

useful for a variety of IgG subtypes. Whilst this is a simplification of the true adsorption behaviour, in which there is heterogeneity in binding and the presence of multiple, distinct binding sites, it is hoped this assumption will enable adequate description of breakthrough, which has otherwise been performed with an even simpler model, including a lumped Langmuir kinetic model by Bak *et al*.(2007), which was not able to describe the asymmetric breakthrough seen here, whereas Ng *et al*., (2012) surmised that it was the finite adsorption rates that led towards poor description of saturation behaviour for their Protein A breakthrough model; for better saturation description this resistance to binding would need to be included into the model.

Table 6.11 – The impact on varying the binding rate constant (k_{ads}, top) and equilibrium constant (K_{eq}, bottom) on model residuals describing IgG saturation breakthrough and literature values, suggesting that neither mass adsorption rate, nor equilibrium behaviour requires accurate estimates to describe breakthrough of IgG-Protein A at the expected ranges.

Adsorption Kinetics				
Error (SSE, %^{2})	τ (s)	k_{ads} (M^{-1} s^{-1})	k_{ads} (L $g^{-1}s^{-1}$)	Literature k_{ads}(M^{-1} s^{-1})
3.95	3.26E-02	1.00E+06	6.67E+00	8 x 10^3 to 3.5 x 10^5 (*Wilson et al., 2010, Yang at al., 2003, Reader & Shaw, 2017, Hahn et al. 2005)*
3.95	3.26E-01	1.00E+05	6.67E-01	
3.95	3.26E+00	1.00E+04	6.67E-02	
8.32	3.26E+01	1.00E+03	6.67E-03	
75.36	3.26E+02	1.00E+02	6.67E-04	
1040.2	3.26E+03	1.00E+01	6.67E-05	
2753.9	3.26E+04	1.00E+00	6.67E-06	
3379.7	3.26E+05	1.00E-01	6.67E-07	
3391.9	3.26E+06	1.00E-02	6.67E-08	
3391.9	3.26E+07	1.00E-03	6.67E-09	
Adsorption Equilibrium				
Error (SSE, %^{2})	K_{eq} (M^{-1})		K_{eq} (L g^{-1})	Literature K_{eq} (M^{-1})
3.95	1.00E+10		6.67E+04	$10^7$to 10^9 (McCue *et al.,* 2003, Hahn *et al.,* 2005, Pabst *et al.,* 2018, Horstmann & Chase, 1986, McCaw *et al.,* 2014, Ng *et al.,* 2013, Liu *et al.,* 2015)
3.95	1.00E+09		6.67E+03	
3.95	1.00E+08		6.67E+02	
3.95	1.00E+07		6.67E+01	
19.09	1.00E+06		6.67E+00	
322.67	1.00E+05		6.67E-01	
2299.2	1.00E+04		6.67E-02	
3247.3	1.00E+03		6.67E-03	
3378.4	1.00E+02		6.67E-04	
3379.7	1.00E+01		6.67E-05	

6.6.4 Fitting Breakthrough Data

6.6.4.1 Residence Time

Having determined the column, particle and effective porosities, the axial dispersion of the column, and reducing the adsorption model to rectangular isotherm, the model was fitted to further breakthrough data at multiple flowrates to estimate the transport limitations. As the model is desired to be a predictive model, to simulate breakthrough at a range of flowrates, the data was split into calibration and validation sets, 160 s and 480 s

chosen as they spanned the current process residence time, with 130 s and 240 s chosen as validation such that one could interpolate and extrapolate for a single residence time. These were first fitted with the parameters determined above, with q_{max} set by the EBC, determined by saturation breakthrough experiments, and the most significant mass transfer resistance (D_p) given freedom to fit to any value.

A

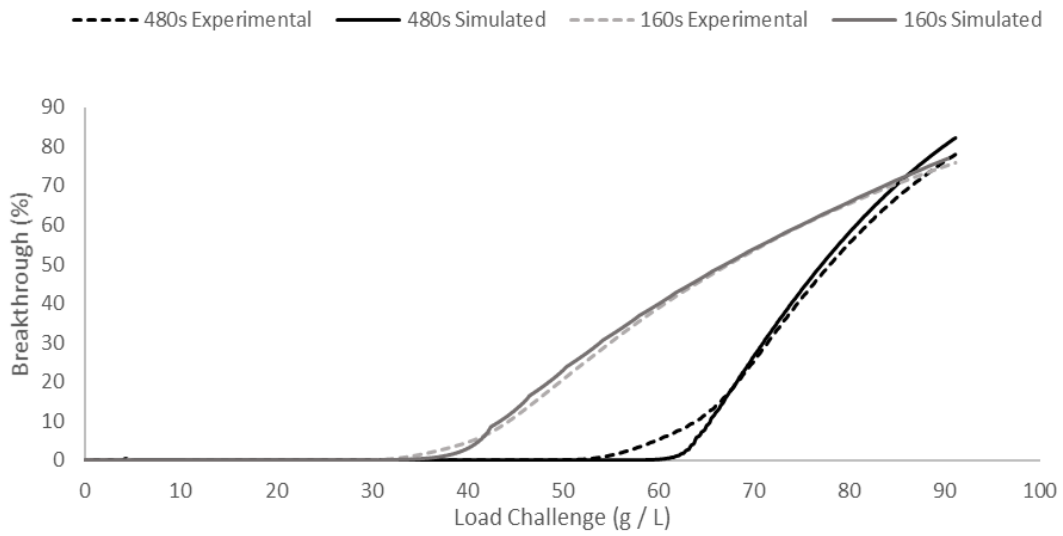

B

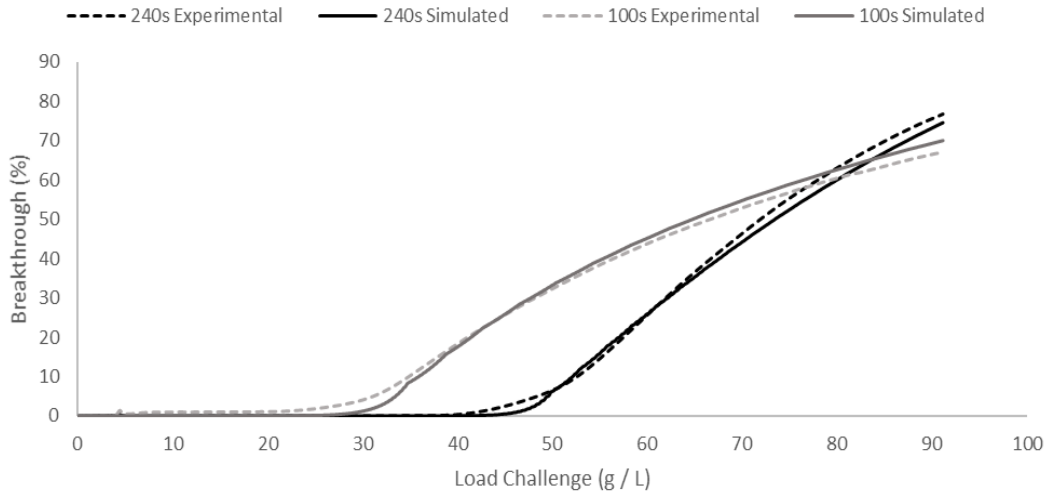

*Figure 6.20- The simulated and experimental breakthrough of the protein a breakthrough for the **A** – calibration (160 and 480 s) and **B** - validation (130 and 240 s) residence times, demonstrating predictive ability of the model*

Acceptable quality of model fit was observed, and good predictive ability was exhibited for the remaining, validation residence times, both in the 10% breakthrough values (Table 6.12), and for overall breakthrough profile (Figure 6.20). The validation dataset (100 s and 240 s) demonstrated similar fitting quality to the calibration dataset (240 s and 480 s) . An average deviation of 4.0% for $DBC_{10\%}$ values, and an MSE of 3.6 $\%^2$ suggests the model is of reasonable quality for prediction between the flowrates the model was calibrated with, though the remaining error is likely due to the assumptions with regard to the adsorption model.

Table 6.12- The derived $DBC_{10\%}$ values from the model and experimental DBC values

Residence Time	100 s	160 s	240 s	480 s
$DBC_{10\%}$ (Experimental)	34 ± 0.1	44 ± 0.1	53 ± 0.1	64 ± 0.1
$DBC_{10\%}$ (Simulated)	31	44	54	66

6.6.4.2 Concentration of feed material

An expected influence on breakthrough behaviour on this system is the impact of feed concentration on resistance to pore diffusion as there are several reports in the literature that the rate of pore diffusion is inversely proportional to mobile phase concentration (McCue et al., 2003, Hahn et al., 2003 Horstmann & Chase 1989). The breakthrough experiments performed at a variety of feed concentrations are used provide an estimation of how this value varies with respect to feed concentration. To investigate whether this was the case with data generated here, unlikely to be the case due to the similar breakthrough profile when accounting for column and system hold-up (Figure 6.18), the three feed concentration runs were set to estimate the pore diffusion coefficient only, with the remaining parameters set the same between runs.

There was no significant trend in the pore diffusion coefficient with increasing concentration, both from the breakthrough profile (Figure 6.18) and the fitted model (Table 6.13), as reported in literature when testing for a wider range of feed concentrations, suggesting this model is viable for the full range of concentrations of IgG likely to be encountered during this capture step considering expected titres of 2-10 mg mL^{-1}, at least for predicting early breakthrough. This does not, however, mean that the pore diffusion is well modelled for the full ranges of load challenges, nor for saturation behaviour, as binding sites become occupied, pore diffusion may become restricted, hindering pore diffusion (Gutenwik *et al*., 2004, McCoy & Liapis, 1991, Clark *et al.*, 1985), nor that the pore diffusion is comporable to that expected with crude feedstock, which may well vary with titre and will have higher viscocity than pure target protein. Additionally, the inability to explain saturation effects, and the significant tailing of the breakthrough, which others have explained by introducing a kinetic isotherm with multiples binding sites (Boi *et* al., 2007, Perez-Almodovar & Carta, 2009a), does introduce error into this estimation and limit the suitability to describe early breakthrough alone, and for separations in which pore diffusion is the dominant resistance.

Table 6.13- The fitted pore diffusion coefficient at multiple feed concentrations

Concentration of Feed (g L^{-1})	D_p (x 10^{-12} m^2 s^{-1})	Error (MSE, $\%^2$)
7.5	3.67	3.17
4.7	3.72	4.73
2.3	3.58	3.21

6.7 Model Parameters of IgG Breakthrough at Lab-scale

Having established the predictive nature of the model, by using two breakthrough curves to fit the pore diffusion resistance, and a saturation run to fit the maximum capacity, and predicting the breakthrough behaviour of two untested residence times, it was investigated whether one could forego the saturation experiment. This was considered as running breakthrough to full saturation consumes significantly more material, with loading to 200 g L^{-1} for saturation compared loading to under 100 g L^{-1} for conventional breakthrough experiments, as well as poor description of saturation behavior with this model. Though this would likely improve model fidelity for early breakthrough, which is more important for batch chromatography, a limitation would be that this would make the model less powerful when predicting multiple column chromatography, where high degree of column saturation is met. With this approach, focussed on describing early breakthrough and omitting saturation data, the model was then calibrated by introducing another breakthrough residence time (240 s), with an initial estimate of the capacity term back to 70 g L^{-1}_{column} as per the resin manufacturer's claim, to evaluate whether one could forgo both saturation and batch adsorption experiments, based upon the assumption that a rectangular isotherm would be appropriate. The model was then set to calibrate as before, though with the breakthrough curves also set to estimate maximum binding capacity as well as pore diffusion. A q_{max} of 80.45 g L^{-1}_{Column} was determined, compared 85.21 g L^{-1}_{column} determined from the saturation runs (Table 6.14), potentially due to no longer fitting saturation behaviour which increases effecting binding capacity at very high load challenges.

Table 6.14- The model parameters for simulating breakthrough at a range of residence times, and the methods of parameter determination

Parameter	Value	Method of Determination
Bed porosity (ε_b)	0.43 ± 0.00	Pulse Tests (Dextran)
Particle porosity (ε_p)	0.97 ± 0.00	Pulse Tests (PABA)
Effective particle porosity for IgG (ε_{eff})	0.65 ± 0.01	Pulse Tests (IgG)
Maximum binding capacity of column (q_{max})	80.45 g L^{-1}_{column}	Breakthrough
Langmuir Equilibrium Constant (K_{eq})	Rectangular	Batch Adsorption, Breakthrough
Pore Diffusion Coefficient (D_p)	3.61 ± 0.12 x 10^{-12} m^2 s^{-1}	Breakthrough
Axial Dispersion correlation constant (γ_2)	2.8 ± 0.1	PABA Pulse
Axial Dispersion Coefficient (D_{ax})	1.1 to 8.0 x 10^{-7} m^2 s^{-1}	Correlation with γ_2
Film Diffusion Coefficient (k_f)	6 to 12 x 10^{-6} m s^{-1}	Correlation
Column Length	0.1 m	Product Data
Particle Diameter	85 µm	Product Data
Feed Concentration	2.3 to 10 g L^{-1}	280 nm UV absorbance
Residence Time	160 to 480 s	Flowrate
Model error (MSE, $\%^2$)	4.45	Experimental vs Simulated data

6.7.1 Parameter Sensitivities

Having fitted a model, it was decided to assess which parameters are most sensitive to change, as well as whether any other parameter sets within the estimation space could also fit the data with similar quality. The fitted parameters are varied singularly with the change in error measured, which has been widely employed to evaluate critical and sensitive parameters in a process (Gu, 1995), without the mathematical rigour of determining the Fisher Information Matrix and determining confidence intervals, which can also be used to determine the significance of each parameter (Engell & Toumi, 2004). This was performed on both IgG pulse and breakthrough tests, at all experimental flowrates.

For pulse tests of non-binding IgG, the pore diffusion coefficient is the most sensitive to change (Figure 6.21A), further demonstrating its significance. Film diffusion had negligible effect on model quality for pulse tests, if it was above a critical value, corresponding to a value when this mechanism becomes rate limiting. Axial dispersion had very modest impact on pulse model quality beneath a value for which it became dominant. The K_{eq} and k_{ads} values were previously shown to be insignificant to model quality if bounded by reasonable values, with no impact by assuming equilibrium is reached instantaneously and adsorption is approximated as a rectangular isotherm (Table 6.11).

With the same methodology applied to the breakthrough models at all residence times, q_{max} is clearly a highly sensitive parameter (Figure 6.21B), with only modest changes impacting model quality significantly. Again, pore diffusion is also highly sensitive, with film diffusion having a negligible impact on model quality above a critical value. Axial dispersion had a slight effect on the model, with a relatively modest increase in error by neglecting it completely. The model sensitivity to porosity was also high, with particle porosity having a slightly greater impact on model quality than column porosity (Figure 6.21C), likely due to the dominance of pore diffusion on model quality, which has also been supported by assessing the characteristic times as above, in which pore diffusion and convection are the rate limiting transport step, and film transfer and binding are relatively insignificant. As changes to both q_{max} and D_p reduced model quality and could not be compensated by allowing the remaining parameters to fit within a reasonable range, there is confidence that these are reliable estimates for these parameters.

A

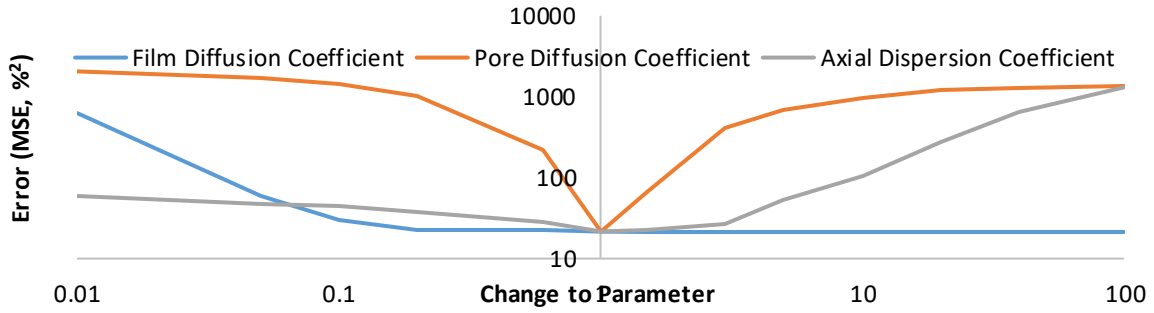

B

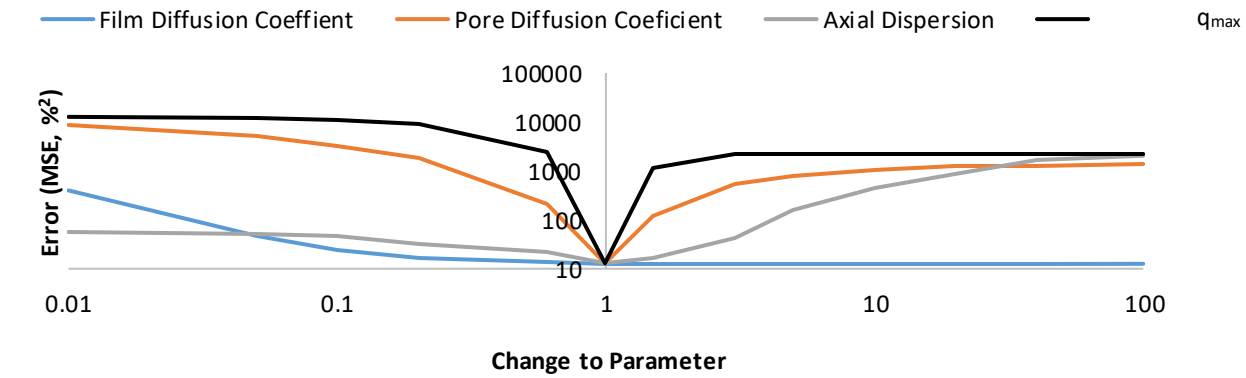

C

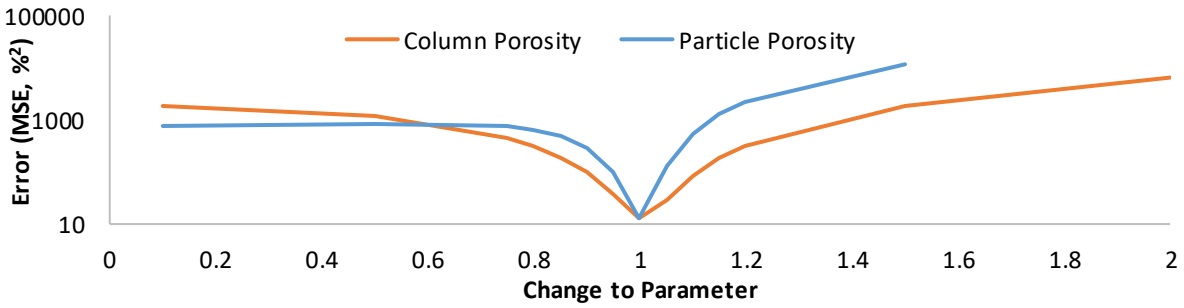

Figure 6.21 – Parameter sensitivities for the IgG – Protein A model at lab scale ***A –*** *For non-binding IgG pulse model.* ***B –*** *Kinetic and thermodynamic parameters on the breakthrough model.* ***C –*** *Bed and particle porosity on both pulse and breakthrough quality*

6.8 Conclusions

A model describing the capture of IgG by Protein A chromatography has been calibrated and parameters determined (Table 6.14). It has demonstrated ability to describe breakthrough behaviour at a variety of residence times and feed concentrations by using a general rate model in tandem with mass transfer correlations to reduce the estimation space and account for flow dependencies. Models describing the system contribution to peak position and broadening at numerous flowrates have been calibrated to supplement this, through both the EMG-method of moments approach, and through modelling PFR and CSTRs, enabling the model to better account for system contributions, which are of particular importance for pulse studies on small columns.

Mass transfer parameters were determined by the inverse method, and through fitting for multiple experiments with known correlations allowed one to mitigate the risks of optimising for a local minimum, or overfitting error. Two widely used correlations for axial dispersion relation to linear velocity, de Ligny and Van Deemter, correlate axial dispersion linearly with flow velocity, which described both pulse and breakthrough data well. The small magnitude of axial dispersion and shallow sensitivity demonstrates this mechanism is not as important to describing and predicting breakthrough behaviour at this scale and system compared to the other parameters, D_P and q_{max}. D_L was determined through a method of moments approach, whereas D_{ax} was determined through an inverse method, both using pulse response of a tracer, and using non-binding IgG pulses to verify the fitting.

Film diffusion was estimated using a widely used correlation (Wilson & Geankoplis, 1966), and described both IgG pulse and breakthrough data well when constrained to this correlation, with negligible improvements to model quality by constraining this during parameter estimation at the flowrates on interest. The pore diffusion coefficient converged to a higher value for pulse responses compared to breakthrough studies, possibly an artefact of the dilute material during pulse experiments diffusing more rapidly compared to the breakthrough studies using constant injection of concentrated feed, or possibly due to errors in accounting for dead volume and fluid handling and inaccuracies in the determination of the statistical moments.

The relative insignificance of the equilibrium constant (K_{eq}) and the impact of the adsorption rate (k_{ads}) enabled the assumption of a rectangular, equilibrium adsorption model. This simplified the model to a transport dispersive model, rather than the full general rate model, whereas the relative dominance of pore diffusion compared to other mass transfer resistances suggests the model may be reduced further to a shrinking core model for this scale.

This approach allows one to probe the flowrates between the calibration flowrates accurately, allowing one to both predict breakthrough behaviour, but to also understand the impact of the physical processes behind this chromatographic operation, the significant mass transfer parameters, and probe how changing the residence time can impact performance. The model is valid for suitable range of flowrates and concentrations likely to be employed on an industrial IgG- Protein A capture operation.

6.8.1 Model Limitations and Assumptions

Unlike the typical, preparative process of IgG capture, these experiments were performed with purified material for ease of interpretation, though a robust model describing capture of crude material should be calibrated with crude material. Deviations in the mass transfer resistances, such as film, molecular and pore diffusion are likely to be observed between purified and raw feed capture, though the magnitude of this has not been assessed. These could be determined through repeating a subset of experiments to evaluate for changes in parameters.

Another source of error is the choice of binding model. As mentioned, proteins often violate the assumptions of Langmuir isotherms, and that the isotherm employed here is valid for a single component; for affinity separations, this is less of a complication, considering the highly favourable isotherm means the IgG will rarely be outcompeted for a binding site. However, if contaminants exhibit high affinity for the ligand or irreversible binding and seen with column fouling (Pathak & Rathore, 2016) , or exist in a high concentration, one may have to determine the isotherm in the presence of contaminants. If important for the separation, determining the mass transfer parameters for these contaminants may need to be performed; all of these experiments increase the material, time and analytical requirement significantly, and therefore being able to scale down this methodology could be very powerful avenue for process understanding. Additionally, with high load challenges, IgG-IgG interactions may lead to a significantly higher effective binding capacity, which has not been included in the model but has been alluded to in the data, in which significant tailing of the saturation may be explained by such a phenomenon, though others have also explained this phenomena by accounting for heterogeneous binding mechanisms and finite rates between Protein A and IgG (Boi *et al*, 2007, Perez-Almodóvar & Carta, 2009a) and various other mechanisms for other adsorber chemistries (see section 6.6.3.1).

As film diffusion has only a small effect on total error above the Wilson and Geankoplis (1966) value with increase in model error of 5% at 100-fold increase in value, but significantly beneath this value at 2,400% increase in error at 1% of the correlated value for both pulse and breakthrough responses. This demonstrates that for these tested flowrates, one can omit film diffusion resistance from the model with only small impact to model quality and approximating all particle mass transfer resistances into pore diffusion alone. In conditions where film diffusion is likely to be more significant, such as low feed concentration or linear velocity, this would be an inappropriate approach (Lacki 2018, Macek *et al*., 2011).

It is clear that determining the pore diffusion coefficient accurately is of utmost importance to calibrating an accurate model for this system, with the column porosity, particle porosity and maximum binding capacity also highly sensitive. The correlation of Mackie and Mears (1955) overestimated the fitted value of this by four-fold (1.43×10^{-11} m^2 s^{-1} vs 3.6×10^{-12} m^2 s^{-1}), highlighting that estimation of the resistance generated by a tortuous pore network requires calibration experiments to determine effective diffusion rates.

Using batch adsorption data for the binding capacity provided an estimate of the column capacity, though the small volumes and variable data inhibited an accurate estimation, though did provide an estimate of K_{eq}; saturation experiments provided the best model fit and accurate q_{max} values but used a significant amount of material, with load challenges of 200 g L^{-1}, and overestimated the column capacity, possibly due to the aforementioned simplifications to the binding model. Calibrating the model with three partial breakthrough experiments enabled a reasonably reliable estimate for both the q_{max}, and D_P values, whilst consuming a small fraction of the material as consumed during saturation experiments.

7 Scale Prediction from Microscale Data

7.1 Introduction

A model has been calibrated describing and predicting IgG breakthrough behaviour at lab-scale, with an understanding of the critical model parameters and suitable workflow for determination. An attempt will be made to adapt the model for microscale chromatography to see whether one could scale the model formulation, calibration and account for the impact of intermittent flow and other scaling artefacts, and ideally, use this to predict behaviour at large scale. This will allow one to optimise, understand and better control chromatographic operations at large scale, by evaluating conditions with the reduced material consumption at microscale.

There have been a number of studies that have calibrated mechanistic models using microscale data; a study used microscale columns integrated into a conventional FPLC to determine breakthrough and pulse studies (Susanto *et al.* 2008), with isotherms determined using a robotic platform in conjunction with resin plates. This was then compared with models calibrated using a conventional scale column, with the models demonstrating notable parameter differences across scales, with an increase in axial dispersion, potentially caused by the wall effect, and an increase in the kinetic rate coefficient apparent at microscale, which was less well understood, though suggested packing differences as the cause. They also employed system volume characterisation to decouple the impact of external band broadening and assumed a bed porosity of 0.37.

Keller *et al.* (2015) have also employed a dispersive model to estimate parameters of a microscale cation exchange process, using a steric mass action isotherm, coupled with moment analysis and calibration data including a series of linear salt gradient (20 to 100 CV in length) to calibrate the isotherm parameters, characteristic charge and equilibrium constant, with the Yamamoto approach (Rudt *et al*. 2015, Yamamoto *et al*., 1983a & 1983b). They employed an understanding of the system differences, including hold-up volumes of an FPLC system, the lessened signal to noise ratio of the microscale system, and compared a lab scale column - FPLC (1 mL) and microscale column – LHS (600 µL) separation. This demonstrated good similarity between scales, with retention volumes differing under 5% for all model proteins across scales, though they highlighted the importance of accounting of all sources of offset. However, despite acceptable differences in retention volumes of the peaks, determined through moments analysis, significant differences in the linear isotherm parameters were highlighted, without further explanation. Additionally, the Peclet number varied across scale with no consistent pattern, suggesting the axial dispersion coefficient was both increased and reduced, depending on gradient length, between systems, though this may be an artefact of the lumped nature of their model. The authors confirmed the microscale system was a useful tool for predicting benchtop performance, though also mentioned model quality was poorer for the microscale system, when simulated experimental data and experimental data were compared, but was adequate for acceptable lab-scale predictions to be made for their purposes.

The same group furthered their work (Keller *et al.* 2017) by further evaluating system differences; namely the nature of detection, with fractions subjected to batch UV absorbance measurements compared to online UV absorbance measurements, the nature of the gradient formation (multistep and true linear gradient) and the increased axial dispersion evident on the microscale domain, based upon the previously described model. Again, the lumped kinetic model was used to account for all resistances to mass transfer, with porosities of the columns assumed rather than measured, and dispersion was determined to be greater on the FPLC system.

A general rate model has been used to describe separations, with model calibration with the inverse method using a genetic algorithm, with a 1 mL column, and demonstrated one could predict behaviour at 160 L using the described strategy. This work used conventional FPLC systems, rather than a robotic LHS (Gerontas *et al* 2010) and evaluated the system across three resins, and successfully predicted retention times at scale. Heterogeneity in the feed proteins, however, was highlighted as an issue that prevented better model fidelity. Axial dispersion and film transfer were estimated by correlation only.

Others have taken this approach further, and used a liquid handling system for breakthrough experiments, also calibrating a mechanistic model to predict large scale behaviour from microscale data and used this to optimise the larger scale operation with success (Osberghaus *et al.,* 2012). However, they mentioned that robotic induced effects, such as the saw-tooth motif previously described, as well as poor resolution, inhibited greater interpretation of this data. They employed a novel technique during pulse tests by repeating the pulse test, the second time with an offset, and combining the data, enabling one to improve the working-volume determined resolution by a factor of two, (67 µL to 33.5 µL) and employed spectral analysis to determine protein identity and concentration. They employed both dextran and acetone pulses, but the relative size of the columns (200 µL), even with the novel offset method for improving resolution meant bed porosity determination had a minimum expected error of 23% and was therefore not used for model calibration. Axial dispersion, lumped kinetic resistance and ionic capacity values were not determined from elution/pulse peaks, but were instead estimated from FPLC experiments due to the improved resolution.

Pirrung *et al.*, (2018) explored the use of 200 µL Robocolumns when developing a model for IgG purification from a crude feedstock. They also used an adaptor to use a microscale column on a conventional chromatography system, though employed a HPLC system with low dead volume (estimated at 30 µL). They also employed UV absorbance measurements at multiple points on the well surface, enabling characterisation of meniscus topology and therefore more reliable volume determination. They employed this approach to both a mixed-mode and cation exchange resin with crude feedstock and accounted for IgG self-association within the adsorption model. Interestingly, the large macropores of one of the bimodal adsorbers precluded bed porosity determination even by very large dextran standards, so instead they used the Blake-Kozeny equation and measured pressure drop across the bed to determine bed porosity.

Khalaf *et al*., (2016) used a different approach for determining retention behaviour of a monoclonal antibody and Fc fusion protein on a cation adsorber with Derjaguin-Landau-Verwey-Overbeek (DLVO) theory, a colloidal theory in which the structure of the protein is used to estimate the thermodynamics of binding. Experiments performed at 600 µL column volume with a LHS and 1 mL column with a conventional system were used to further calibrate a lumped rate model and validate the model-based design space.

Benner *et al*., (2019) investigated parameter estimation with microscale columns for both a cation exchange and Protein A affinity chromatography with a lumped rate model. They performed penetrating tracer tests on 4 mL scale with FPLC's, and performed non-binding product pulse tests at this scale at a single flowrate to quantify the accessible particle porosity and lumped kinetic parameter for each component, and evaluated scales of 7 mL, 4 mL and 600 µL with conventional FPLCs, and 600 µL column on a LHS. They scaled for residence time and focused on better understanding differences in elution pool volumes. They ruled out system effects and column geometries and posited that it was the linear flow velocity dependence of the axial dispersion coefficient that is responsible for an increase in pool volume in the microscale domain. This is in agreement with our own data, in which the HETP between microscale columns and lab scale columns was comparable (with some increase in dispersion on the microscale domain on both FPLC and LHS) when operating at the same linear flow velocity, and that a linear dependence of axial dispersion to flowrate described interparticle dispersion.

While calibrating mechanistic models of small or microscale chromatography is increasingly routine, the system effects plague the accuracy of the resultant models. While work has been performed to mitigate these differences, including increasing the resolution of the data with novel strategies such as repeating runs with offsets, incorporating microscale columns on conventional FPLCS and identifying how dispersive effects differ at scale, there is an unexplored opportunity to investigate, model and mitigate the effects of system and scale with a focus on intermittent flow. It is the focus of this chapter to further investigate the impact of these system effects, and ascertain whether one can account, and mitigate them through mechanistic modelling by accounting for the most significant mass transfer resistances by first investigating a microscale model using the same feed stream as used in above chapters, and then using the learnings form this to predict breakthrough behaviour for a new feed stream (IgG B) at lab-scale, based upon microscale breakthrough experiments.

7.1.1 Impact of Intermittent Flow

In the previous chapter, the impact of intermittent flow has been probed experimentally; it is clear that the impact of halting upon binding for high residence times is insignificant; a sawtooth motif is present, but the majority of the chromatogram, ignoring the small trough region, is indistinguishable between continuous and intermittent flow for slow flowrates. For lower residence times however, there are significant differences in that the intermittent flow lags behind continuous flow in breakthrough. This is likely to inhibit ascertaining accurate mass transfer parameters if using this data to develop a mechanistic model, unless these discrepancies are accounted for.

If taking the mass transfer correlations used in chapter 6, one can see that axial dispersion, at times where superficial flow becomes zero, tends towards the molecular diffusion coefficient, multiplied by some geometric constant. This follows logically, the second term of the correlations correspond to eddy dispersion, which is a phenomenon occurring during flow only, and should not occur for static fluid, whereas molecular diffusivity would continue unhindered. Considering the relatively small magnitude of the contribution of molecular diffusion ($<10^{-10}$ m^2s^{-1}), this is unlikely to be a significant effect.

Stopped, or interrupted, flow during chromatographic operations has been used for investigating mass transfer resistances during HPLC and UPLC, called the 'peak parking' method (Li *et al*. 2008, Gritti & Guiochon, 2011, Miyabe *et al.,* 2007). Using this strategy, a peak of material is pumped down a column, and held for a set amount of time during the experiment, set for when the pulse is about midway down the column. Probing the separation with a set of defined pauses across a range of experiments allows one to determine the molecular diffusivity of components (Miyabe *et al.,* 2007), and to improve the data quality by avoiding signal saturation (Li *et al.,* 2008). The pauses used for this type of study usually are significantly longer than experienced during LHS operation (30-600 minutes for 'peak parking', compared to 40-60 seconds of intermittent flow), though the underlying assumptions should hold true; that during static flow, axial dispersion tends towards molecular diffusivity. Gritti and Guiochon (2011) furthered the peak parking approach by including a location element, in which the peaks were parked at different positions along the length of the column, called multiple location peak parking. They employed this to evaluate column homogeneity in the axial dimension and advised caution due to the propagation of pressure spikes, due to the rapid changes in flowrates, impacting results.

Diederich and Hubbuch (2017) performed an extensive error analysis on microscale chromatography, including a focus on the impact of fractionation and the intermittent flow on liquid handlers, demonstrating that it was associated with an increase in retention time and elution peak width for large proteins, though not consistently for all proteins, and advised taking this phenomenon into account when calibrating mechanistic models for the purposes of scaling-up.

Effective pore diffusion, whether mediated by surface or bulk diffusion, will be invariant to flow, and therefore the associated coefficient will have the same value for the periods without flow as for the periods with flow. Convective flow within the pores is not considered, as this is negligible for microporous beads (Carta & Jungbauer, 2010). Film diffusion, no matter which correlation is followed, tends to zero at zero flow; this is unlikely to be the case as the correlations are valid at low flow velocities, but not for static fluid. The limit of this correlation is $55 > Re > 0.0015$, which corresponds to superficial flow velocities of 0.65 m s^{-1} to 1.76 x 10^{-5} m s^{-1} for this system (assuming a kinematic viscosity of protein solution at 10^{-6} m^2s^{-1}). With microscale chromatography at low bed heights and high residence time, this means the limit where this correlation is valid is 200 µL columns at 480 s residence time, where further reduced bed heights will fall outside of this range. For stagnant flow, material is likely to diffuse across the film, though at a reduced rate, though it is unknown how

important this is to describe the sawtooth motif. Considering the small contribution of molecular diffusivity, and the sharp change in concentration exhibited after interrupted flow, this suggests that even during stopped flow, pore diffusion is rate limiting (SenGupta, 2017). This is further supported by [6.23] in which even at the lowest valid Reynolds number (0.0015) for the Wilson and Geankoplis correlation, with the above modelled pore diffusion (3.6×10^{-12} m^2s^{-1}) provides almost tenfold the resistance to mass transfer compared to film diffusion (3.73×10^{-6} $m\ s^{-1}$) for resin particles of 85 µm diameter (37.5 s vs 4.02 s).

This chapter will focus on determining the magnitude of the mass transfer resistances during static flow and other differences arising from scale on IgG breakthrough. The intention is to use this understanding to build a model accounting for intermittent flow, microscale resolution and low linear flow velocities and any differences with respect to packing quality, and better interpret microscale data.

7.2 Model Calibration

7.2.1 Accounting for Intermittent Flow

To determine the mass transfer resistance during stopped flow, the models describing the continuous large-scale flow determined in the previous chapter are taken, with additional parameters describing transport during stopped flow. This model is identical to the continuous model, though with alterations; two new mass transfer parameters are introduced, $D_{ax(0)}$ and $k_{f(0)}$, corresponding to the axial dispersion, and the film diffusion coefficient of static flow, respectively. When the model simulated stopped flow, these parameters replaced the conventional axial dispersion and film diffusion parameters, and convective transport was halted, with pore diffusion continuing unhindered.

To determine these parameters most accurately, the model describing continuous flow, calibrated on continuous data as in Chapter 6 was used. This model had these two new parameters introduced and the model was formulated to follow the experimental flow regime, with defined flow interruptions. The output of the model was transformed to omit stopped flow from the resulting chromatogram, to mimic the chromatogram generated experimentally. As with the previous work, dead volumes are simulated in addition to the column models; the effect of post-column dead volumes is likely to be far more significant for intermittent flow considering the fine structure of the sawtooth motif. A benchmark was performed for comparison of models with and without intermittent flow and the impact on model quality.

7.2.1.1 Breakthrough Simulation with and without Intermittent Flow

By calibrating the continuous model with the intermittent flow data, small deviations in the fitted mass transfer parameters are observed; the pore diffusion coefficient increases to account for the additional time for diffusion not accounted for with a continuous model. The error is significantly higher for the discontinuous data (Table

7.1) compared to continuous when applied to the continuous model, likely due to the delayed breakthrough of discontinuous runs, the inaccurate mass transfer resistances being fitted, and the saw-tooth motif which is absent from the model formulation all contributing towards the increase in model error. Three residence time (160 s, 240 s, and 480 s) were used as calibration, as they represented the most industrially relevant flowrates for this system.

Table 7.1 - Pore diffusion coefficients and quality of fit, comparing continuous and intermittent flow on model calibration at lab scale, with and without a model formulated for intermittent flow, demonstrating the significance of intermittent flow to model quality

Data	Model	Pore Diffusion Coefficient (D_p)	Error (MSE, %^{2})
Continuous	Continuous	$3.61 \pm 0.12 \times 10^{-12}$ m^2 s^{-1}	4.28
Intermittent	Continuous	$4.00 \pm 0.23 \times 10^{-12}$ m^2 s^{-1}	11.56
Intermittent	Intermittent	$3.42 \times \pm 0.14 \times 10^{-12}$ m^2 s^{-1}	5.37

$D_{ax(0)}$ was found to be insignificant at any value, when bounded between the molecular diffusivity (D_M) and zero, as predicted by the simplified correlation used in Chapter 6, whereas $k_{f(0)}$ was found to not be significant to model quality, no matter which value was employed ($0 \leq k_{f(0)} \leq k_f$) . The post column dead-volume simulation, developed in Chapter 6, is applied to the simulated breakthrough curves, as the rapid changes in outlet concentration means mixing would have a more significant effect and explained both the slight offset and smoothing of the sawtooth motif well for the 160 s data (Figure 7.1).

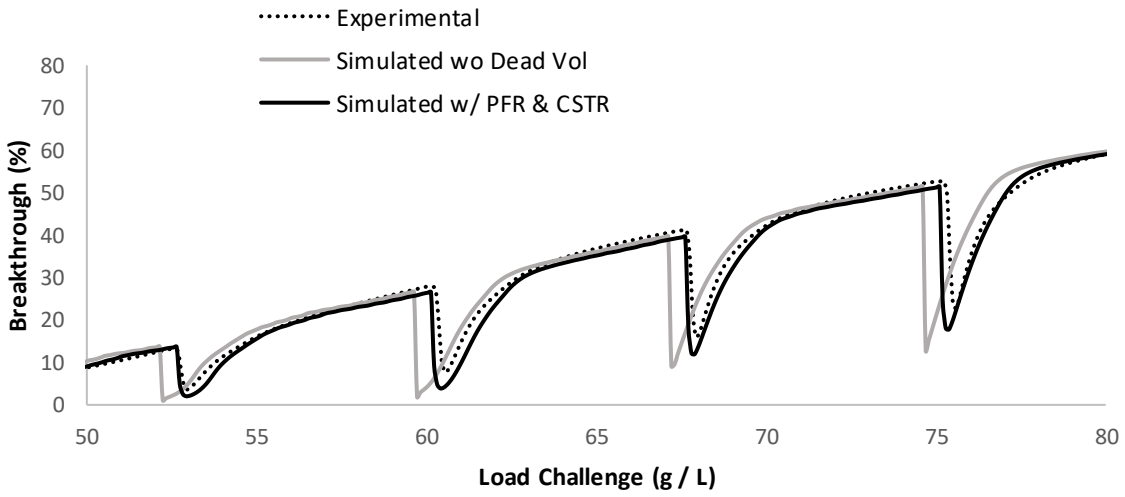

Figure 7.1 - Demonstration of the importance of post-column volume simulation, established in chapter 6 through fitting wash-out curved from a saturated column, demonstrating the smoothing and offset enabling better description of the sawtooth motif then the column model alone.

It is clear that one can model this intermittent flow, and that the general rate model and shrinking core model, when formulated for this flow regime, accurately described the data in correcting for the offset breakthrough, and the magnitude of the sawtooth effect (Figure 7.2). No additional parameters are needed to describe this intermittent flow, so the rectangular equilibrium isotherm is maintained and both $D_{ax(0)}$ and $k_{f(0)}$ are set as 0, and the fitted value of D_P does not vary significantly between continuous data and model, and intermittent data and intermittent model, suggesting this is the correct model for traversing between the microscale and lab scale breakthrough.

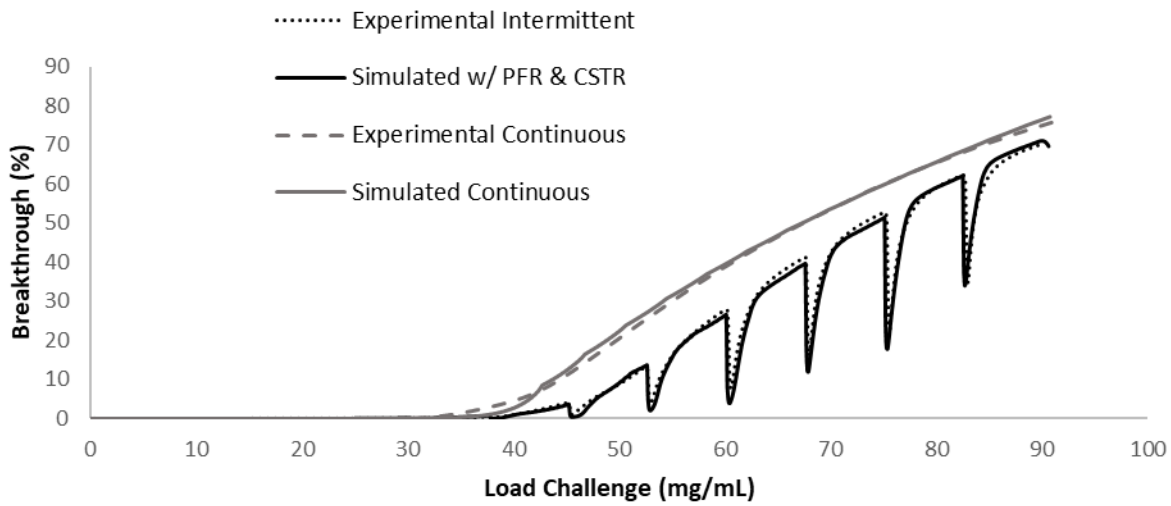

Figure 7.2 – Intermittent and continuous flow model fit for 160 s residence time, with dead volume simulation, demonstrating model description of both the offset in breakthrough and subsequent saw-tooth motif apparent after stopped flow

7.2.2 Scaling Model Formulation

A model is calibrated from microscale data as before; pulse data achieved with the pre dilution method was applied to calibrate bed parameters, using Dextran, IgG and PABA, though at a single residence time (240 s) considering the method of moments and inverse method, no matter which flowrate was assessed, were consistent in pulse test porosity determination (Chapter 6). The precision of these pulse tests, while an improvement over the manufacturer's data, is still poor, with an average of 20 points per column volume, allows a fitting or porosity with poor precision, though the use of an EMG distribution was hoped to improve this, poor resolution is a concern due to the sensitivity of the model to this parameter (Figure 6.21). Additionally, errors in volume determination may impact parameter estimation. Combining multiple pulse tests provided no increase in resolution as the small errors in measuring effluent volume meant the individual columns are not immediately comparable, unlike the more promising results of Osberghaus *et al*., (2012) in which they deliberately introduced an offset between runs, doubling data density.

7.2.3 Determining Column Porosities with PABA, IgG and Dextran 2,000,000. n = 8

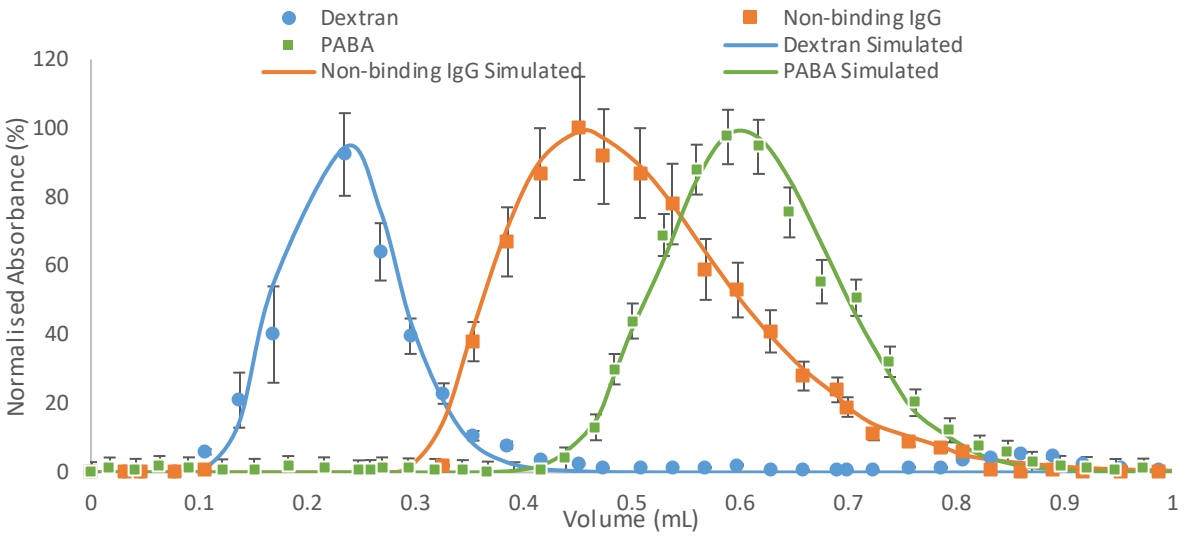

Figure 7.3 - Pulse experiment Performed on a 600uL column with Dextran, PABA and IgG with the model fits

Using pulse experimental data for porosity determination was only practical for 600 µL columns; a 20 µL fraction volume for a 50 µL column corresponded to a precision of 40% CV, and 10% CV for 200 µL columns (Figure 7.3). As the microscale column had the same internal bed diameter, it is hoped the values for bed porosities for 600 µL will be valid for the lower column volumes, though this is an untested assumption.

Table 7.2 - Comparison of Porosities and Axial Dispersion Values for a Microscale Column on a LHS and a conventional column on a FPLC. Errors are provided based upon the standard deviations of independent fits per column, 240 s residence time.

Parameter	600 µL column on a LHS	4.7mL HiScreen on a FPLC
Bed porosity (ε_b)	0.34 ± 0.09	0.43 ± 0.00
Particle porosity (ε_p)	0.97 ± 0.23	0.97 ± 0.00
Effective Particle Porosity for IgG ($\varepsilon_{p,eff}$)	0.57 ± 0.19	0.65 ± 0.01
Axial dispersion correlation constant (γ_2)	3.6 ± 1.1	2.8 ± 0.1
Number of repeats	8	3

A decrease in porosity and increase in axial dispersion correlation coefficient (γ_2) as compared to the large scale calibrations correlation (Table 7.2) is observed, though due to the variable nature of these tests, the significance of this difference is not reliable. Repeats of the larger scale system showed no such variability, as has been demonstrated with prior HETP and DBC work, showing that the results are repeatable with minimal variation. The increased in dispersion and reduction in porosity is in line with reports from Susanto *et al.* (2008) of an

increase of over 50% of their derived dispersion coefficients, corresponding to an increase in y_2 from 8.49 to 12.82. They suggested this was likely caused by the wall effect impacting packing efficiency, a phenomenon that is amplified at the very small bed diameters microscale columns possess (Guiochon *et al*., 1997).

7.2.4 Breakthrough Data

Breakthrough data, obtained in chapter 5 was used for model calibration, also using the inverse method, and the bed parameters fitted above. The model was formulated like the full scale intermittent flow model, though with fractions taken by averaging a continuous chromatogram between the fraction volumes, rather than using its single point as being an accurate representation of the concentration at that particular time or volume, a similar approach to Keller *et al*., (2017). Additionally, the intermittent flow, deliberately introduced to maintain a suitable residence time for the 50 µL and 200 µL columns (Chapter 4), was also introduced for these simulations. The fractionation averaging was not applied to the FPLC system in the previous chapter, as the high data density meant this was not an important consideration, as very little mixing occurs within the small UV flow cell. Whilst axial dispersion at static flow was unimportant for describe lab scale intermittent flow, this is evaluated with half the value of the molecular diffusivity of IgG's in aqueous solution (Guiochon, 2006), a value of 3.7 x 10^{-11} m^2s^{-1} (Tyn & Gusek, 1990), as the reduced length of the micoscale columns, as little as 2.5 mm for the 50 µL column (1% of a typical lab scale column), will amplify the impact of this band broadening. All fits were performed by allowing q_{max} and D_p to vary, and the D_{ax} and ε values as established with the pulse tests of the 600 µL columns, with D_{ax} following a linear flow-rate dependency with y_2 determined through fitting of the PABA peak. Film diffusion followed the correlations of Wilson & Geankoplis with no adjustment, and column length was adjusted for each scale. Models were fitted with an averaged porosity from pulse data, but individually fitted to each columns' breakthrough profile, generating 8 models, each describing a single column. Model parameters are given as the average and standard deviation across all of these models (Table 7-3), and 600 µL columns connected to the FPLC were omitted due to the oscillatory behaviour seen at longer residence times.

A

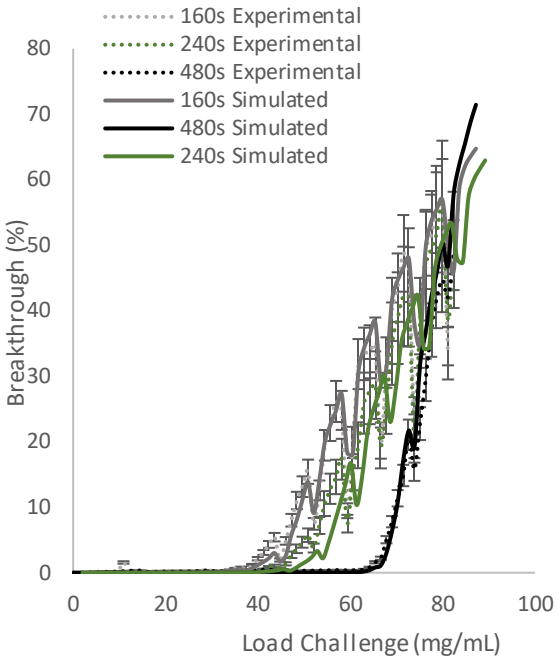

B

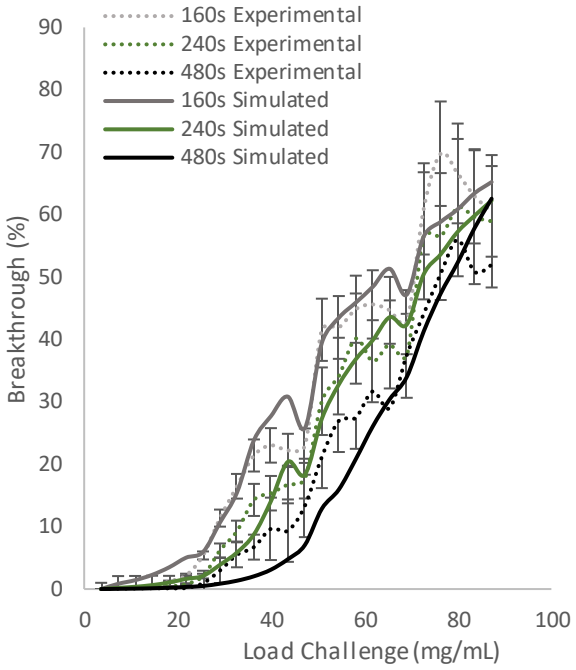

C

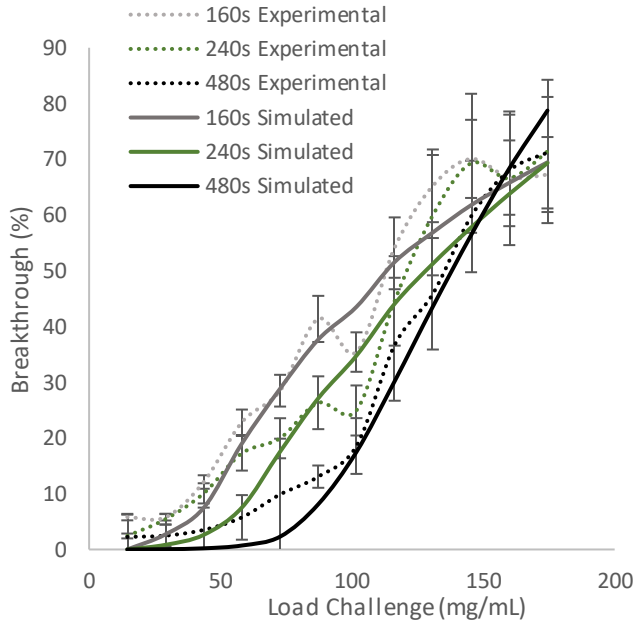

Figure 7.4 – The breakthrough model fits for microscale columns. The simulated profile is given as the average of all 8 fitted breakthrough profiles

A - 600µL columns

B - 200 µL columns

C -50 µL columns,

All three experiments were performed at three residence times in 8-fold replicate, with each column for all residence times described by a single model formulation. The average of determined model parameters is plotted (q_{max}, D_P).

As expected, the 600 µL scale models demonstrated the best fitting to the experimental data, with quality of fit worsening for the 200 µL column, and 50 µL columns, though the sawtooth motif present at the 200 µL scale described well also (Figure 7.4). Additionally, the parameters fitted showed reduced variability between columns compared to the smaller volumes, therefore a more robust fit achievable with 600 µL columns. For the larger

scale system, as repeats had very little variation between runs (a difference in $DBC_{10\%}$ values of less than 0.5 g L as determined in Chapter 5, within model error), the variation in model parameters is determined through individual fits per experiment across every residence time simultaneously (n = 3), with 8 fold repeats in microscale. All of these repeats were performed on a single column at lab scale, and with all columns at microscale, and therefore cannot account for lot to lot variability between resin batches. Other have reported lot-to-lot variability on similar protein A resins as having negligible impact on capacity (Trexler-Schmidt *et al*. 2009), though this is a significant consideration in other adsorber types, such as ion exchangers (Aono *et al*., 2013, Wahome *et al*., 2008).

Table 7.3- Model Parameters for the 3 microscale column volumes, compared to the lab-scale model for IgG A

Parameter	Value				Method of Determination
Column Volume	4.7 mL	600 µL	200 µL	50 µL	
System Used	FPLC	LHS			
Bed porosity (ε_b)	0.43	0.36 ± 0.09 (determined with 600 µL columns)			Pulse Test
Particle porosity (ε_p)	0.97	0.96 ± 0.13 (determined with 600 µL columns)			Pulse Test (PABA)
Effective particle porosity for IgG (ε_{eff})	0.65	0.57 ± 0.11 (determined with 600 µL columns)			Pulse test (IgG, nonbinding conditions)
Maximum binding capacity of column (Q_{max}, g L^{-1}_{column})	80.77	86.11 ± 2.17	67.33 ± 4.93	103.08 ± 21.84	Initial estimate from batch adsorption, refined with breakthrough
Axial dispersion correlation constant (y_2)	2. 8	3.6 ± 1.1			Pulse tests (PABA) to fit Ruthven's (1984) correlation
Film Diffusion Coefficient (k_f)	1.3 x 10^{-5} m s^{-1} to 2.7 x 10^{-6} m s^{-1}				Correlation (Wilson and Geankoplis, 1966)
Pore Diffusion Coefficient ($D_{p,}$ x 10^{-12} m^2 s^{-1})	3.6	3.4 ± 0.3	2.7 ± 0.6	1.6 ± 0.9	Breakthrough Data
MSE ($\%^2$)	4.28	8.31	11.30	19.60	Experimental data vs Simulation (at the same scale)
Column Length	0.1 m	0.03 m	0.01m	0.0025 m	Product data
Column Diameter	7.7 mm	5 mm			Product data
Particle Diameter	85 µm				Product data
Residence Time	160 s, 240 s and 480 s				Set by experiment

With a mechanistic model describing both the lab scale and microscale breakthrough behaviour, an understanding of column characteristics (bed height, porosity, axial dispersion), system contributions (fractionation, intermittent flow, dead volume) and adsorption behaviour, one can isolate and transform each of these phenomena, with the aim to better predict and account for differences across scale and system. All parameters at the larger scale match reasonably well with 600 µL column derived parameters. The notable exception was axial dispersion, which is amplified at the microscale, in agreement with literature reports (Osberghaus *et al*., 2012) and prior HETP work (Chapter 4), whereas even at constant axial dispersion correlation (γ_2) value, greater band broadening is to be expected considering the reduced bed height, though, as discussed, experimental limitations reduce confidence in this assertion. Additionally, differences in column geometry and construction may likely influence this rather than packing quality alone, as flow distributors and tip-placement within the column could neither be determined nor controlled. Film mass transfer may well be significant for the smallest bed heights (2.5 mm) considering the parameter sensitivities established in the previous chapter and the fact that the Wilson and Geankoplis correlation cannot describe this parameter at such low flow velocities (Re < 0.0015) though has not been explored further as the data density was not sufficient to better assess this contribution. A significant limitation in the workflow is the model sensitivity to bed porosity, and the error prone method of determination. The impact of axial dispersion on microscale breakthrough is more pronounced, considering the reduced bed height alone even if the linear dependence of the coefficient remains identical, and the flowrate scaled for residence time. Though this has a relatively small impact on breakthrough profile at lab scale, it is important in describing the saw-tooth motif. The main contributors to any scale dependant offset in breakthrough is the bed porosity, and to a lesser extent film diffusion. The bed porosity is consistently lower than at labscale, though the variable nature of the data means this difference is not statistically significant from pulse tests alone but will be further evaluated.

7.2.5 Transforming the Model Between Scales

An evaluation of the impact of D_{ax} and k_f to scale performance was performed, in which the 4.7 mL scale breakthrough model was transformed to predict breakthrough profile at a range of column lengths, at constant residence time (Figure 7.5). The parameters k_f, D_{ax} were evaluated with respect to bed height and whether following correlations y_2 to axial dispersion, and X for a multiplicative factor applied to the Wilson and Geankoplis (1966) correlation [6.23], was appropriate. With respect to k_f, no significant change in model quality was seen when allowing this to fit to reasonable values ($0.5 < X < 10$), with relatively minor increase in model error at $X < 0.1$ on the lab scale model, so a non-corrected Wilson and Geankoplis correlations has been assumed to be accurate enough, which is supported by both the sensitivity analysis and characteristic time determination in the previous chapter.

For axial dispersion, one can see a clear Impact on breakthrough profiles whether using the y_2 factor determined with the 600 µL columns (3.6), or the 4.7 mL scale (2.8), with a greater effect with the axial dispersion scaling factor determined with the microscale experiments. k_f alone has a modest impact on breakthrough profile when

ignoring axial dispersion completely, with a minimal difference between 100 cm to 3 cm, though this effect is pronounced at the smallest column lengths (2.5 mm). Whilst still not as significant as the pore diffusion or axial dispersion, this resistance does lead towards additional column length dependant broadening.

Assuming the D_{ax} ascertained with a 10 cm column at 240 s residence time is universally applicable for all bed heights led towards the greatest degree of column length dependant band broadening and demonstrates that this value should be estimated at each flowrate, or neglected entirely, but not assumed to be constant for this system as the greatest component of axial dispersion is likely to be eddy dispersion, also supported by the linear relationship demonstrated in the previous chapter.

For each parameter tested, minimal differences were seen between a 10 cm and 1 m bed height (data not shown for clarity, though overlaid the 10 cm column in all conditions), which is unsurprising as at high column length and constant residence time, the impact of pore diffusion and convection remains unchanged, whereas the impact of film diffusion and axial dispersion is reduced. The largest contribution for column length dependant breakthrough shape was axial dispersion alone, highlighting the importance of determining this as accurately as possible, whereas k_f is an important consideration for especially small bed heights. If both of these phenomena are ignored, there is no difference whatsoever for scaling bed height, suggesting that these other mass transfer resistances are of concern due to the requirement for scaling for very low bed heights within this project, and therefore demanding the use of such a model comprising of multiple transport resistances.

The microscale model was transitioned by considering the reduced axial dispersion and porosity, achievable with small material consumption on pulse tests at either scale, with the model describing fractionation, flow regime and any contribution of dead volume (Figure 7.6). The film dispersion coefficient was set to the correlation flow rate dependencies of Wilson and Geankoplis (1966) with no adjustment, with adsorption modelled by rectangular isotherm, with q_{max} and D_p determined at each scale through inverse fitting of breakthrough, enabling prediction at either scale based upon pulse experimental data alone. For prediction purposes, q_{max} was therefore determined as a function of resin particle volume as determined with dextran pulses, rather than for the entire column, enabling the impact of column porosity to q_{max} to be described explicitly. Particle porosity was set to be constant regardless of scale, and therefore used lab scale parameters, with axial dispersion was set to the value determined by the PABA pulse responses of the predicted scale. Therefore q_{max} of the particle and D_P were the only experimentally determined parameters kept constant between scales.

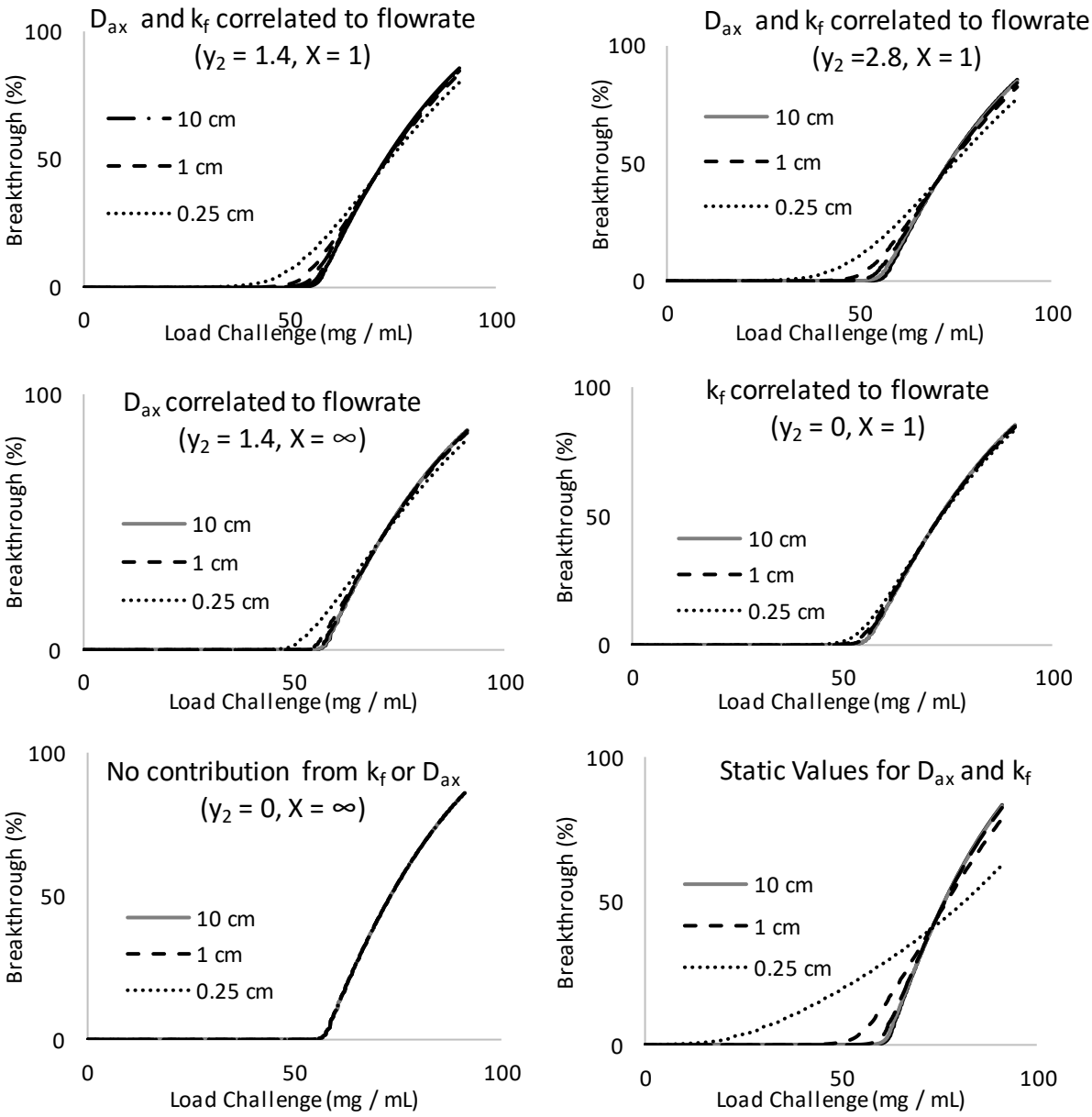

Figure 7.5 - Comparison of the impact of the flow dependant mass transfer resistances, Axial dispersion (D_{ax}) and film diffusion (k_f) on breakthrough profiles at constant residence time with varying bed height based upon the 240 s residence time, 10 cm bed height model.

This variation in bed porosity was supported by refitting the microscale model with large scale parameters, accounting for flowrate dependencies, leaving bed porosity as the only free variable, which also then converged to a reduced value compared to the larger scale fit, with a comparable model residual (ε_b = 0.33, MSE = 9.05 %^{2}, an increase from 8.31%^{2} when given freedom of all parameters though still a reasonable fit), supporting reducing the bed porosity for the microscale system. This porosity value is rather low, but within ranges reported by others (Liu *et al.*, 2017, López *et al.*, 1997, de Neuville *et al.*, 2013, Diederich & Hubbuch, 2017) and may be indicative of excessive compression compared to labscale columns (Kong *et al.*, 2017). Roberts & Carta (2020) recommended using such a strongly binding tracer for characterisation of microscale columns, which has

supported the reduction in porosity. Considering the variability in ascertaining the porosity on the microscale with dextran pulses and relatively poor data density, and the prevalence of assuming the bed porosity at microscale to be similar value rather than directly measuring (Susanto *et al.*, 2008, Keller *et al*., 2015 & 2017, Benner *et al*., 2019,) and others reporting a reduction in porosity compared to larger columns (Osberghaus *et al.,* 2012, Pirrung *et al*., 2018), this transformation appears to be appropriate, though as discussed, could be a significant source of error.

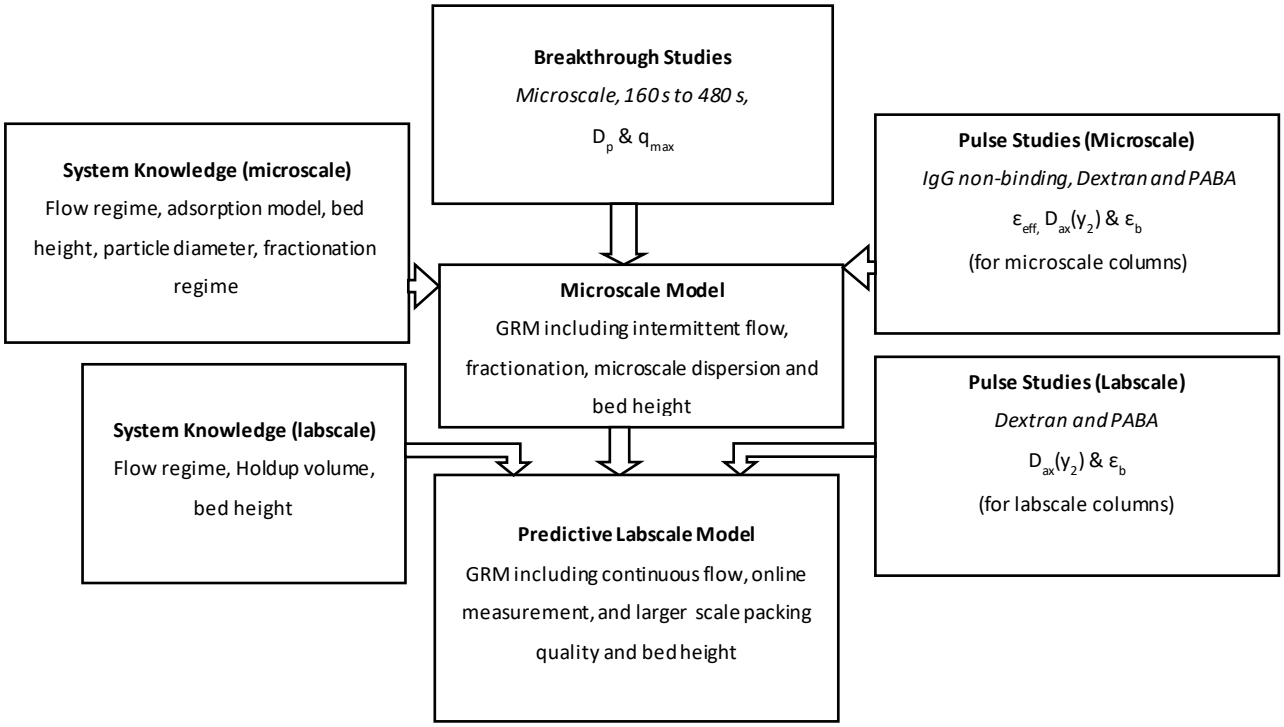

Figure 7.6 - Process of transforming the model between scales, in which the column geometries are determined at both scales with pulse responses. The large scale system is used to determine the particle porosity, due to better resolution, and that this parameter is assumed invariant to scale, whereas the small scale system's pulse tests determine both axial dispersion and bed porosity, which is then used to calibrate the model with microscale breakthrough responses. The model, describing the microscale column and system, could then be transformed into predicting large scale by correcting for dispersion, porosity, bed height removing intermittent flow and fractionation and introducing dead volume simulation

Using the microscale determined axial dispersion correlation coefficient and the reduced porosity, the models describing microscale breakthrough were transformed to predict larger scale breakthrough. Unsurprisingly, the 600 µL columns predicted large scale behaviour best, significantly better than the small column volumes (Table 7.4). The 200 µL columns provided a poor description of labscale breakthrough, with the worst $DBC_{10\%}$ prediction of the set, whereas the 50 µL columns did provide a more accurate prediction of $DBC_{10\%}$ value, but worse estimation of lab scale model parameters – it is likely the underestimation of pore diffusion combined with the overestimation of q_{max} opposed one another and lead towards more equivalent $DBC_{10\%}$ values, though a poorly representative model. The poor description of large scale behaviour is likely due to the poor data quality and fluid effects not modelled, considering that axial dispersion was assumed to be identical as for the 600 µL columns, likely a poor assumption as this mechanism is especially important with such small bed heights. A further concern to this is the fluid regimes specified during the experiment; the flowrates required to meet the

residence times at scale were beneath the minimum flowrate of the system, so a deliberate intermittent flow regimes was introduced (Table 5.1), and though this was incorporated into the mechanistic model, it may have introduced further artefacts. Small differences in column volumes, or hold-up volumes within the column housing are particularly impactful here and were not assessed. The film diffusion coefficient was not fitted, but instead followed Wilson and Geankoplis's (1966) correlation with no correction factor, this is likely to be error prone, but could not be estimated with a greater degree of accuracy as it appeared to not impact larger scale behaviour.

Table 7.4 - Experimental, Modelled and Predicted $DBC_{10\%}$ values for 4.7 mL, 600 µL, 200 µL and 50 µL columns, at 160 s, 240 s and 480 s residence time, demonstrating an improved description of 4.7mL scale breakthrough with 600 µL columns by calibrating a mechanistic model

Column Volume	4.7mL	50 µL	200 µL	600 µL	Source
System	FPLC	LHS	LHS	LHS	
Retention Time (s)	$DBC_{10\%}$ (mg/mL_{column})				
480	64 ± 0.1	85 ± 14.3	44 ± 8.7	70 ± 1.9	Experimental
240	53 ± 0.3	55 ± 9.2	30 ± 7.4	55 ± 2.4	
160	44 ± 0.2	39 ± 11.6	28 ± 10.5	48 ± 2.3	
480	66± 0.2	89± 16.6	49 ± 9.5	70 ± 3.7	Model
240	54± 0.2	58 ± 14.3	36 ± 9.1	57 ± 3.0	
160	44± 0.2	48 ± 10.1	29 ± 8.6	50 ± 2.7	
480	71 ± 0.2[a]	88 ± 16.1 [b]	44± 9.5 [b]	66 ± 2.5 [b]	Scale corrected model
240	57 ± 0.2 [a]	55 ± 12.7 [b]	34 ± 9.0 [b]	54 ± 2.4[b]	
160	47 ± 0.2 [a]	36 ± 8.3 [b]	24± 8.1 [b]	45 ± 2.4[b]	
a = scaled to 600 µL column on LHS, b = scaled to 4.7 mL column on FPLC					

Regardless of the issues facing the smaller column volumes, the model based prediction of 4.7 mL scale derived from the 600 µL column data was very good, describing early breakthrough well for 160 s and 240 s, with the 480 s residence time formulation still failing to describe early breakthrough (Figure 7.7). All $DBC_{10\%}$ values from this prediction were within 1 standard deviation of the experimental data, with generally good fitting across the profile, supporting the workflow that mechanistic model facilitated interpretation of scale up can account for many of these apparent differences.

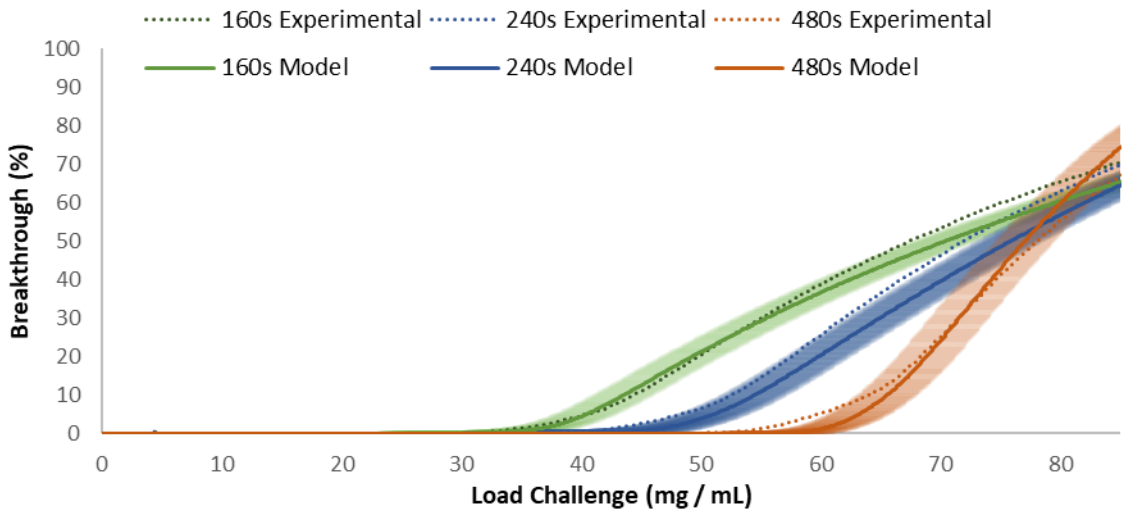

Figure 7.7 - Microscale prediction of larger scale breakthrough, demonstrating good description of the larger scale breakthrough behaviour. The standard deviations of each model prediction are shown in shade, by calibrating a model for each column breakthrough (n = 8)

This approach of using microscale breakthrough to predict lab scale breakthrough will be validated through calibrating a model with microscale data at 600 µL to establish the kinetic and equilibrium parameters with pulse data on the microscale columns for bed characterisation, for a separate drug candidate, IgG B. The resultant model will then be used to predict large scale behaviour through ascertaining mass transfer parameters, altering as needed for the differences in scale.

7.3 Predicting Lab Scale Breakthrough with Microscale Data

IgG B concentration calibration and standard curved were generated in the same way as for the previous IgG. As the batch breakthrough married with sensitivity analysis demonstrated the adsorption model could be adequately reduced to an equilibrium, rectangular isotherm, only q_{max} needs determination to adequately describe the adsorption behaviour, which may be performed as above with partial breakthrough studies, along with the primary mass transfer resistance, D_P. D_{ax} was assumed to follow the same flowrate dependency as for IgG A, with Ruthven's (1984) flowrate dependency and a value of y_2 of 3.6 at microscale and 2.8 at labscale, with bed porosities of 0.36 and 0.43 respectively.

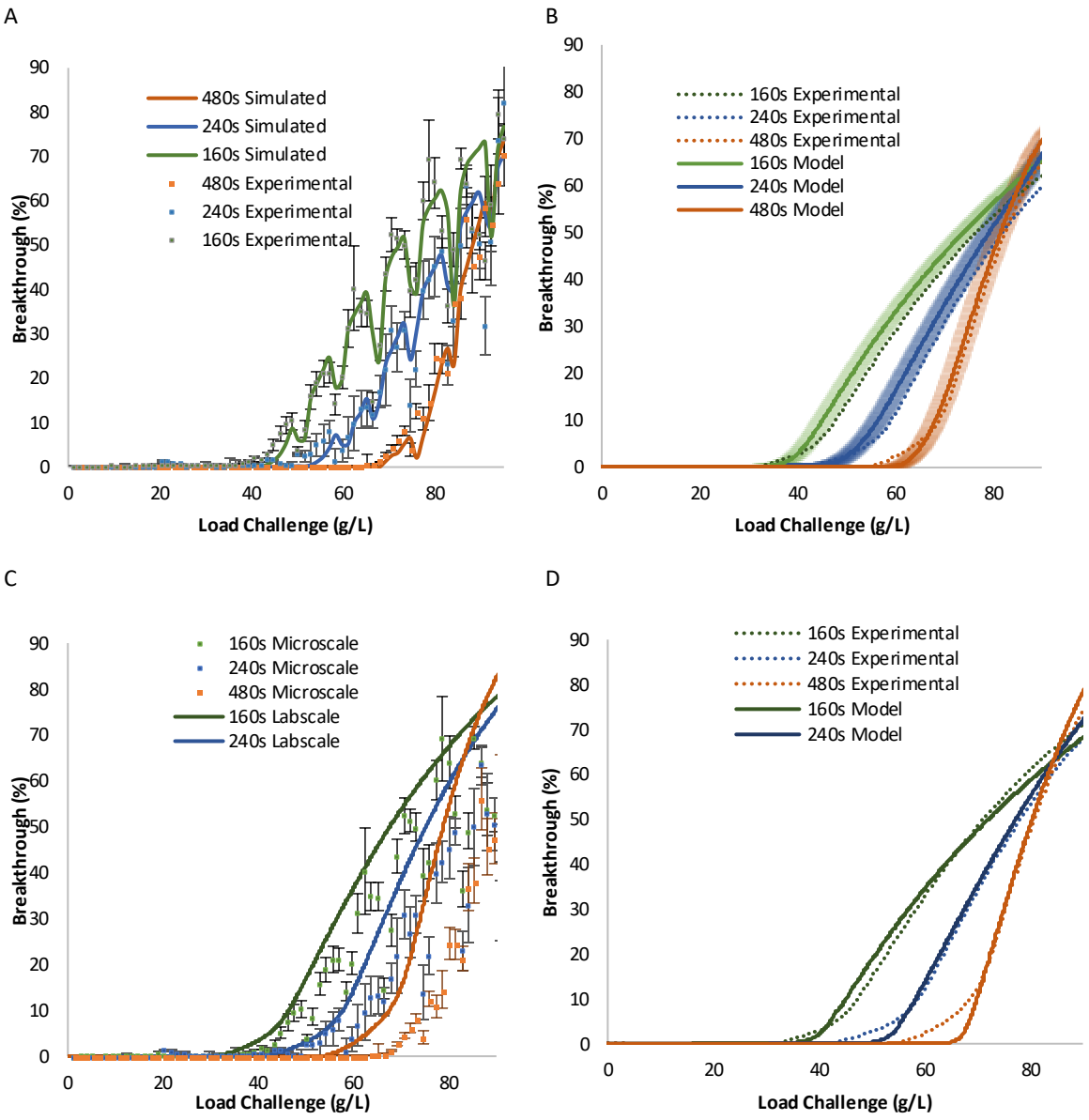

Figure 7.8- Modelled and measured breakthrough profiles for IgG B. ***A*** *– The 600 µL experimental breakthroughs and model fit (single model describing 160 s, 240 s and 480 s residence times),* ***B*** *– The model prediction of large scale behaviour and experimental breakthrough of large scale,* ***C*** *– Comparison of the experimentally determined breakthrough for both 600 µL and 4.7 mL scale,* ***D*** *– Lab scale breakthrough model calibrated with lab scale data*

Having calibrated model describing the microscale operation (Figure 7.8A) with an acceptable quality of fit, the model is transformed in the same manner as for IgG A, in which pulse response data is used to determine the column dispersion at either scale. In this case, the columns were the same as used for IgG A, so the same parameters for porosity and axial dispersion were used. q_{max} was again scaled based upon the phase ratio of the adsorber. As before, experimental 4.7 mL breakthrough curves were generated and were compared to the model predictions (Figure 7.8B), with confidence intervals plotted based upon the standard deviation in model parameters across 8 columns, with these lab-scale breakthrough curves further used to generate a large-scale model. These were used to compare model parameters between prediction and experimentally validated

performance at lab scale, as for IgG A. One can see a clear offset between scales, modelled by the change in bed porosity, and broader breakthrough in the microscale domain (Figure 7.8C), an artefact of the reduced efficiency considering the difference in length and greater contribution of axial dispersion. As with the first IgG, the labscale model calibrated with labscale data had a better quality of fit, though slight deviations in describing early breakthrough (Figure 7.8D).

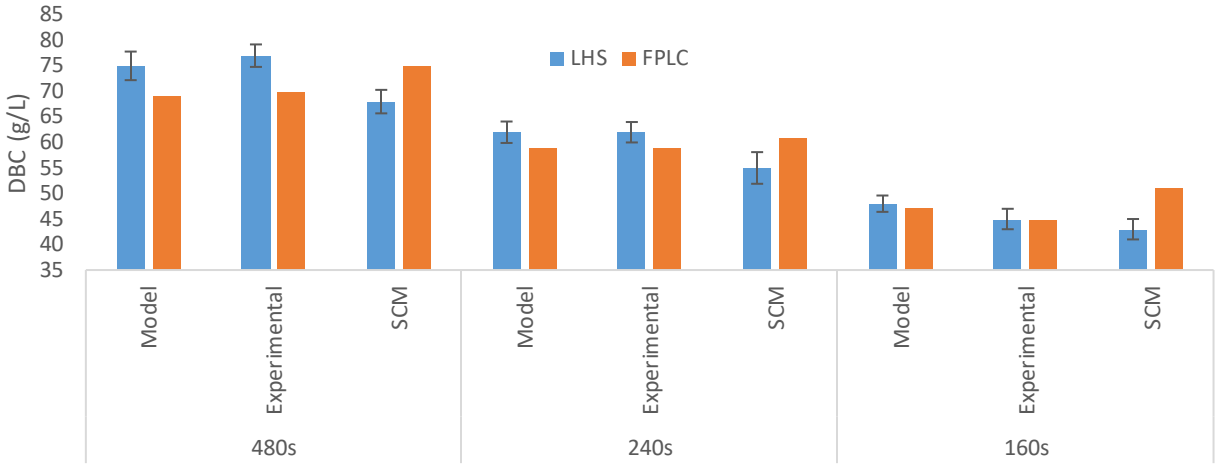

Figure 7.9 Experimental, Modelled and Scale Corrected Model (SCM) $DBC_{10\%}$ values for IgG B on 4.7 m L and 600 µL columns, at 160 s, 240 s and 480 s residence time, demonstrating an improved description of 4.7mL scale breakthrough with 600 µL columns by calibrating a mechanistic model, seen here with the SCM bars (in which one scale, FPLC (4.7 mL) or LHS (600 µL) were used to predict the other scale), as per the workflow in Figure 7.6) Error bars for the microscale system are determined across 8 fold replicates; singlicate experiments were used for labscale studies.

For the predicted $DBC_{10\%}$ values, again better comparability between results is seen when accounting for the system and scale effects by using a mechanistic model. As expected, the 600 µL models exhibit far more variability than their lab scale counterparts. The reduction in $DBC_{10\%}$ differences between scales has not been as effective as with IgG A, as over half of the initial difference between scales remains whilst employing this approach (Figure 7.9). However, as with the IgG A, relatively good comparability is seen with the determined model parameters (Table 7.5).

Table 7.5 - Model parameters for IgG A and IgG B at 600 uL and 4.7 mL scale

Parameter	Value				Method of Determination
Protein	IgG A (IgG_1)		IgG B (IgG_4)		
Column Volume	**4.7 mL**	**600 µL**	**4.7 mL**	**600 µL**	
System Used	**FPLC**	**LHS**	**FPLC**	**LHS**	
Bed porosity (ε_b)	0.43	0.36 ± 0.05	0.43	0.36 ± 0.05	Pulse Test (Dextran)
Particle porosity (ε_p)	0.97	0.98 ± 0.13	0.97	0.98 ± 0.13	Pulse Test (PABA, Assumed to be identical between scales at 0.97)
Effective particle porosity for IgG (ε_{eff})	0.65	0.57 ± 0.11	0.65	0.57 ± 0.11	Pulse test (IgG A, nonbinding conditions. Assumed to be identical between scales at 0.65)
Maximum binding capacity of column (Q_{max}, g L^{-1}_{column})	80.77	86.11 ± 2.17	84.11	90.83 ± 2.94	Initial estimate from batch adsorption, refined with breakthrough
Axial dispersion correlation constant (y_2)	2.8	3.6	2.8	3.6	Pulse tests (Dextran) to fit Ruthven's (1984) correlations
Adsorption model	Rectangular				Batch Adsorption, sensitivity analysis
Film Diffusion Coefficient (k_f)	1.3 x 10^{-5} m s^{-1} to 2.7 x 10^{-6} m s^{-1}				Correlation (Wilson and Geankoplis, 1966)
Pore Diffusion Coefficient (D_p, x 10^{-12} m^2 s^{-1})	3.6	3.4 ± 0.3	3.3	3.0 ± 0.3	Partial Breakthrough (three residence times)
MSE (%^{2})	4.28	8.31	3.62	10.21	Experimental data vs Simulation
Column Length (m)	0.1	0.03	0.1	0.03	Product data
Column Diameter (m)	0.0077	0.005	0.0077	0.005	Product data
Particle Diameter	85 µm				Product data
Residence Time	160 s, 240 s and 480 s				Set by experiment

7.4 Discussion

There are a large number of assumptions within the approach taken above, considering the model formulation, experimental design and analysis, and as clear by the remaining differences in both predicted $DBC_{10\%}$ values and in model parameters, this approach has failed to provide an entirely accurate description of breakthrough behaviour at either scale when testing with another IgG, though has made a prediction closer to the experimental $DBC_{10\%}$ values compared to raw data alone, as well as converging on similar mass transfer parameters to the lab scale model.

Whilst a modelling approach has been able to describe each of the deviations with respect to scale (including reduced column efficiency at small bed heights, fractionation, intermittent flow, dead volumes and flowrate dependency of some mass transfer resistances), the experimental set-up has introduced a significant variability, which has been apparent in raw data. Whilst work has been performed to minimise this as much as possible, the method of running microscale experiments on an LHS has several sources of error that modelling could not mitigate. Variable tip placement on the system was not assessed, the open nature of the experiment in that effluent was not entirely contained, the resolution and method of determining effluent concentration with variable UV pathlengths all introduce further variability. Small deviations in column packing , considering the miniscule working volume of the columns, is likely to be significant, as others have highlighted (Roberts & Carta, 2020). This was particularly important for porosity measurements, which have been shown to be critical to model quality but limited in the precision obtainable. The most impactful deviations between scale were highlighted as a difference in this measured porosity, and better comparability between large and small column's model parameters when this was left to vary, however a large amount of uncertainty remains over this parameter's value, and the evidence this has varied may not be robust, though has also been reported by others on these columns when comparing to labscale (Susanto *et al*., 2008).

It is possible that it is the radial heterogeneity present in such small diameter columns that have led towards this supposed reduction in porosity, as the wall effect has been previously reported to increase packing density at the radial boundary (Shalliker *et al*., 2000), with the interstitial velocity, determined by the bed porosity and flowrate, directly impacting the efficiency of the remaining mass transfer phenomena. Only through further experiments on other IgG candidates, perhaps resin chemistries, or through other means of testing for this discrepancy, may more confidence in this transformation be acquired. Other ways of determining bed porosity include through measuring pressure drops across the bed and using the Blake-Kozeny equation or performing dextran exclusion experiments on a more extensive or precise manner. Both of these approaches may have been possible with further optimising the manner of attaching a microscale column to a FPLC and using the wider range of sensors and resolution available, which also would have paired well with the dead volume corrections used in this work. Roberts and Carta (2020) suggested using breakthrough curves of a strongly bound tracer for column qualification, which has been performed in this work, and has further supported the reduction in porosity based upon retroactive fitting of the labscale model to the microscale data.

Many of the previous experiments were not optimal for the purposes of mechanistic modelling. Saturation runs of the microscale columns and on the lab scale column at more residence times would have been beneficial, for both an insight into saturation behaviour and as additional quality checks on the models. Interestingly, for the saturations run available, the model failed to describe saturation behaviour well, which has previously been described. Others have better described this when accounting for multiple binding sites (Boi *et al*, 2007, Perez-Almodóvar, 2009a), which may have improved model quality, though model calibration with saturated breakthrough experiments, or through kinetic batch adsorption experiments. By implementing the Langmuir adsorption isotherm, rather than the rectangular isotherm, would extend the model's capability to describe binding by dilute feed material, though this was not a consideration for the industrial process with expected high feed titre.

This work has demonstrated that microscale columns perform similarly to lab-scale counterparts with regards to mass transfer resistance, and binding capacity per solid phase, with the notable exception of axial dispersion and bed porosity, and of course, typical mode of operation relying on low linear flow velocities. This also serves to illustrate that using a complex model such as the general rate model, is important. Simulating many transport resistances can in some way improve interpretation of results at microscale, with explicit simulation of film diffusion, pore diffusion and axial dispersion and the flowrate dependencies thereof has enabled an insight into the impact of flowrate on mass transfer resistances and process performance. This is the first application of such a comprehensive mechanistic model, accounting for all significant transport resistances, being applied to interpret microscale data, and also the first of its kind looking at multiple volumes of microscale columns across multiple feed types.

Perhaps using a small column suitable for use on an FPLC, considering the improved data quality with a relatively minor increase in material consumption, would be an improvement when used with a FPLC designed for such small flowrates, though this would be at the cost of throughput. Even with large scale columns, and high resolution and high completeness data, there have been some behaviours not adequately described by the models, most notable both early and late breakthrough profile likely due to the assumptions of the rectangular isotherm incorrectly describing both low concentration adsorption and saturation, and imperfect description of the flowrate-breakthrough relationship with a single model formulation. With respect to the model framework itself, several sources of error have been identified.

Firstly, the model used assumes all parameters do not change during the experiment, in that pore diffusion and axial dispersion coefficients and bed characteristics do not vary with respect to time, concentration of protein or any other factor. This is likely to be incorrect; we know that at high concentrations, pore diffusion is restricted in the literature (Schultze-Jena *et al*., 2020), that axial dispersion and pore diffusion will be reduced within the more viscous fluid at high concentrations, though this dependence has not been suggested by data here of breakthrough at various feed concentrations, which a feed concentration of less than 10 g L^{-1} was tested, far

beneath binding capacity. Another consideration is that the resin particles pore network will also be increasingly restricted as more protein binds within it, further hindering pore diffusion (Boyer & Hsu, 1992). Others have reported notable differences in mass transfer of protein A resins after several reuses (Pathak & Rathore, 2016). The columns used during this study had been subject to several experiments, and there is a very real possibility that the actual pore diffusion and capacity has diminished over both the duration of a single load event, and multiple reuses of the same columns.

The model also assumes that the columns are radially and axially homogenous in adsorber distribution and flow regime, and radially homogenous also with respect to protein concentration. This is not a robust assumption, it is known that the wall effect, leading to radial heterogeneity, is significant at small column diameters (Abia *et al.,* 2009), and there is a significant risk of axial heterogeneity considering that the resin is compressed within the column during manufacture. It is assumed this leads to the variations in axial dispersions as reported here and elsewhere (Susanto *et al*. 2008, Benner *et al*., 2019), in which even small deviations in packing efficiency lead to significant deviations from expected behaviour (Roberts & Carta, 2020).

The rectangular adsorption model is likely a poor assumption, with even the Langmuir model shown to be a simplification of the true behaviour, considering that proteins are highly heterogeneous, with a great variety of binding mechanisms, and do interact with themselves frequently, all assumed to not happen within the Langmuir framework. This would be of considerable concern if the purpose of this study were to assess the impact of saturation, in which these non-ideal effects are apparent. Others have better described this when accounting for heterogeneous binding (Perez-Almodóvar & Carta, 2009a, Boi *et al*., 2007) within a Langmuir framework. The single component Langmuir model assumes all proteins and binding sites are equivalent, and considering the structural freedom of proteins, this is incorrect. The Langmuir isotherm here was further simplified to a rectangular isotherm with infinite binding rates, which as others have demonstrated fails to describe saturation behaviour (Perez-Almodovar & Carta, 2009a), though has been widely used to simplify the complex behaviour to a single model parameter, though a difference in binding kinetics has been previously reported on these systems by Sustanto *et al*., (2008). Additionally, this model used in this work is inappropriate for all but the load phase of the separation; elution, washing and clearance of impurities has not been included, greatly limiting its potential as this is the actual utility of such a step.

Another consideration is within the experimental design; the experiments used to calibrate the model were performed with semi-purified (post protein A capture) material for the purpose of direct protein quantification through UV absorbance, rather than using raw feed material with a plethora of different proteins, lipids and DNA which could also absorb UV radiation, which would need to be measured using Protein A HPLC or other quantitative methods. Purified material will be less viscous than crude feed, likely affecting the mass transfer resistances, and will not be subject to competitive binding by contaminants. This means that for any truly rigorous model describing Protein A capture of antibodies from complex feedstock would need to be calibrated

using complex feedstock; the same strategy could be used, but with considerably more analysis. This has been performed by others, notable Bak *et al*., (2007), and using microscale column with Pirrung, *et al*., (2018). This variation would have been worsened by the method of determining protein concentration and volume introducing error, which has likely propagated into the model.

It is clear one can successfully use microscale data, if of suitably high quality, to predict behaviour at larger scales, though more error prone than using labscale columns alone, or using lab scale columns to calibrate a model to predict behaviour of untested residence times. In order to perform each breakthrough experiment at lab-scale, up to 500 mg of product must be used, whereas at microscale as little as 50 mg of product is consumed. With three breakthrough curves, and small volumes of material for pulse tests at scale, one can calibrate a model with under 200 mg of product, less that that consumed for a single breakthrough experiment at lab scale. Additionally, with this approach, up to 8 individual experiments can be performed simultaneously; one could calibrate 8 models each describing a different IgG, resin, or load composition. Whilst not as accurate as models generated using lab-scale data and is not of comparable quality to predict lab scale behaviour as a lab-scale derived model, this approach is suited for early drug development where material and time must be optimised to gain as much information about as many candidates as possible.

A benefit of using a mechanistic modelling approach to facilitate improved data interpretation in early-stage process development would be for the purposes of process optimisation, assessing process robustness, or has been achieved here, predicting the performance of the process on a different scale and system. Adsorber screening, a very early stage activity (Liu *et al*., 2017b) also well suited to microscale chromatography, in which the process may be effectively locked in to a particular type of resin, could benefit from improved prediction of large scale behaviour; With a mechanistic model, resins could therefore be ranked by the performance expected at commercial scale, rather than what was observed at lab scale. Additionally, upstream development often occurs simultaneously, the feed stream is likely to also be subject to changes, with expected improvement in titre and quality between early development and commercialisation, the performance of an improved feedstock may also be predicted with a lean dataset and limited material consumption, and enable extrapolation to different feed titres, column scale and operation.

8 Conclusions

The project focussed on enabling a better understanding of microscale chromatography in an industrial setting, which has been achieved in part. At the beginning of the project, several ways of operating these columns, such as increasing wash lengths, were being performed routinely based upon prior observations and anecdotal evidence. To find better ways of interpreting microscale data, a project of assessing a microscale separation on two IgG's for improved resolution, means of characterising the columns with conventional metrics such as HETP and DBC, and a mechanistic modelling approach were undertaken.

With microscale columns on a high throughput platform, a number of differences were identified when compared to conventional lab-scale columns, chiefly the operational differences (intermittent flow, fractionation, dead volumes) the scale differences (wall effect, low superficial flow velocities at a given residence time) and the poorer data quality (fewer data points, no online UV, conductivity, pressure, volume or pH measurement) meant interpreting results across scale could benefit from a mechanistic understanding of the process.

Work was performed initially to observe the data quality from these columns in a standard Protein A capture, which demonstrated that there was a hard limit to increasing resolution; the minimum working volume of the collection vessel. Smaller vessels reduced this minimum volume but allowed more drops of effluent to miss the well, and therefore not be measured. Whilst a low resolution could be suitable for screening adsorbers or IgG candidates, in order to qualify these columns, and measure porosities or HETP, a more sensitive approach was developed.

The pre-filling of collection plates allowed one to resolve individual drops from microscale columns, a novel approach that has greatly improved resolution to dropwise levels when paired with a suitable tracer. HETP tracer screening at large scale found PABA to be an acceptable compromise considering available materials, considering favourable safety profile, strong UV absorbance and stability in solution at room temperature, though also highlighted slight deviations in HETP values. Potentially collating any retention by PABA to a typical standard, such as acetone, would have been a suitable route forward, and therefore allowed one to correct for any adsorption. An effort was made to improve the resolution further, and allow pH, conductivity and pressure measurements by rigging a microscale column onto a conventional FPLC system. This was possible, but problems with leaking fluid, the low throughput when compared with the robotic system, the excessive dead volumes and variable positioning limited the utility of this approach and highlighted that using the conventional LHS for such a study may be a better solution Using the prefilling method, HETP results of adequate quality for fitting a widely used probability distribution function, the Exponentially Modified Gaussian (EMG) distribution, were generated, and facilitated determination of the statistical moments, interpolation of the peaks and the HETP parameters. This approach was also compared against the full width at half height approach which was the conventional

approach used in-house. This approach also allowed estimations of bed porosities for mechanistic modelling, as well as measuring the drop volume and mass retention in order to better assess fraction volumes.

Dynamic breakthrough studies were performed at several residence times with 50 µL, 200 µL, 600 µL and 4.7 mL columns to evaluate consistency across and between scales and was paired with the method of moments and system volume tests to separate column and system effects on breakthrough for the smaller columns. As expected, the larger microscale columns demonstrated better scaling, data quality and consistency between runs. The intermittent flow was the most noticeable difference across scale and was therefore screened on a lab-scale column with a system programmed to mimic this intermittent flow regime. It was clear that intermittent flow had a significant effect at lower residence times with regards to breakthrough position, which was intuitive. Significant differences in measured dynamic binding capacity was observed across all columns and scales, and therefore mechanistic modelling was explored in order to attempt to mitigate the scale and system effects.

Mechanistic modelling was first applied to the lab-scale system, allowing prediction of the residence time-breakthrough relationship of IgG A binding to a column, after calibrating with two residence times. Breakthrough experiments were used to estimate the kinetic parameters of the General Rate Model, with batch adsorption for the thermodynamic parameters to initially estimate a Langmuir, later rectangular, isotherm, and pulse studies used to estimate the bed and particle porosity of the system and axial dispersion across multiple flowrates. Dead volume simulation was employed to better interpret pulse experiments and showed modest improvements in fitting porosities at a range of flowrates. The correlations used fitted the data well, with pore diffusion appearing to be the most critical of the kinetic parameters to fit. Additionally, the intermittent flow was simulated, and found that the pore diffusion alone explained the saw-tooth motif, apparent in microscale breakthrough experiments, well, with no further mass transport parameters needed.

This approach was then further adapted to microscale chromatography, with a model describing the intermittent flow calibrated with breakthrough, pulse and batch adsorption data. This intermittent flow model was then corrected for a greater bed height, large scale bed parameters, the intermittent flow, fractionation and dead volume. This allowed prediction of large-scale behaviour at a range of residence times, and was a significant improvement merely comparing the raw data alone, in terms of measured $DBC_{10\%}$ values, allowing a better understanding of the scale separation, whilst using microscale volumes of material. However, better interpretation of the problem at hand, accounting for artefacts of scale and system to better interpret microscale chromatography may have been achievable with modifications to both the experimental and modelling workflow, though the work does represent a better interpretation of microscale breakthrough data than was initially being performed.

8.1 Future directions

8.1.1 Further Applications

The data and models as they stand could be further expanded to explore a variety of other applications. Capture of biomolecules by other chemistries, including ion exchange, hydrophobic interaction and other affinity formats would be straightforward with the approach described in this work for scaling models. However. modifications would need to be made to the workflow, including using a more extensive binding model, such as SMA and calibrating with elution data, such that elution behaviour could also be simulated. Interestingly, the published cases of microscale IgG breakthrough on ion exchange resins (Welsh *et* al., 2014, Wiendahl *et al.*, 2008, Osberghaus *et al.*, 2012) did not demonstrate such a strong saw-tooth motif than seen in our Protein A data, suggesting intermittent flow is less of an issue for their adsorbers at the tested residence time. The high-throughput workflow and methods would apply well for more complex isotherms such as SMA, or multicomponent Langmuir, or to simulate impurity clearance, all of which would need a greater amount of calibration data, easily achievable with the high throughput LHS.

Continuous operation of chromatography, such as simulated moving bed and periodic counter-current chromatography, can be easily modelled from this as well; a core advantage of these models is that the distribution of material in the column is modelled, not just the effluent, meaning one can account for the material distribution and concentration at all lengths of the column for the same simulation, and therefore better predict the load concentration of subsequent columns. One can optimise loading block length, flow rates and strategy of column recycling quicker, cheaper and more easily than performing experiments with multiple columns. Additionally, all calibration experiments may be performed with a single column and simpler equipment, (Kaltenbrunner *et al*., 2016 and Pagkaliwangan *et al*., 2018), considerably simpler and cheaper than using multiple-column systems, with simulations performed by linking each of the column models in series *in silico*. Another benefit of a mechanistic understanding is that one can search well outside of the conventional search space for a process optimum, including looking at novel elution modes (Joshi *et al.,* 2017), or interconnected steps (Nfor et al., 2013, Pirrung et al., 2017 & 2019, Huuk et al., 2014).

Pairing with microscale bioreactors could be an interesting approach for a more integrated process development strategy; the volumes of microscale bioreactors (15 mL to 250 mL) pair well with microscale column volumes; 15mL of CCCF at a typical titre of 3-5gL^{-1} will provide two to three cycles of Protein A capture on a 600 µL column, allowing one to rapidly measure the upstream effect on capture of IgG, or to rapidly generate small volumes of purified material (Kiss *et al*., 2018). Baumann *et al*., (2015) used mechanistic modelling to evaluate and optimise a downstream process, and used this to determine optimal upstream conditions, demonstrating a high degree of synergy between these technologies and a holistic approach to bioprocess development.

It is hoped that the method described for improving resolution by dilution of the collection plates will provide another tool for high throughput method development. For the purposes this was employed for in this study, dilution of material was not a problem, as the UV absorption of the material was the only important metric, though assuming the diluent does not affect the material other than reducing concentration, this strategy may present difficulties where such manipulations are unsuitable, such as evaluating stability of eluate.

8.1.2 Model Framework Improvement

Model improvements would include having the ability to specify pore diffusion coefficients varying with the stationary phase concentration during loading, to account for pore constriction, as per the work of Hagemann *et al*., (2020) Significant differences in pore diffusion were described in literature, and the models failed to account for the saturation segment of the breakthrough curves, inhibiting accurate model behaviour as the product concentration increases, which is an intrinsic property of breakthrough studies. This means estimates for the kinetic resistance, notable D_p, will be inaccurate when this behaviour is seen, which has been highlighted by others when evaluating this resin mechanistically (Baur *et al*., 2018, Pabst *et al*., 2018). As discussed, by introducing a more complex adsorption model this behaviour may have been explained.

A better understanding of model robustness could have been performed with further experimental validations, assessing the confidence interval of the parameters through synthesising the Fisher information matrix, a search for parameter correlations, and a more thorough analysis of how model uncertainty propagates to process uncertainty with sampling (Borg *et al*.2013)., Considering the relatively few parameters needed in this model and calibration strategy using both the inverse method and method of moments, it is likely the parameters are well fitted, but a better statistical framework would have been best practice.

Model calibration could be improved with other algorithms; artificial neural networks have shown much utility, especially when forming hybrid mechanistic-statistical models (Wang *et al*., 2017a & 2017b) . Artificial neural network based approaches have allowed one to determine model parameters from operational runs, rather than dedicated calibration experiments, with parameter estimation occurring in milliseconds, rather than the significantly longer time taken by conventional, inverse model calibration, with the models here often taking several hours to several days. A drawback, however, is that many model simulations must be run to calibrate the artificial neutral network, though this is purely *in silico,* and would not consume valuable product, just computation and time.

The effect of interrupted flow could be further explored, perhaps as a means of calibrating the models with fewer residence times being used, as the stopped flow will allow one to distinguish between band broadening caused by thermodynamic effects, such as an unfavourable isotherm or capacity being challenged, when compared to kinetic effects, such as dispersion and diffusion. The former would not be affected by the flow interruptions, whereas the latter would, perhaps enabling simultaneous determination of isotherm and kinetic

parameters. In this study, the intermittent flow was considered an obstacle, though did allow further model quality assessment as the troughs in the resulting chromatogram became an opportunity for model training. Perhaps using the drawback of the LHS system to better probe the transport and binding within a column without a dedicated separate experiment would have been a valuable avenue for improved understanding.

Additionally, other types of model could show much benefit. Models employing computational fluid dynamics could enable a better understanding of the flow regimes within the microscale columns. The wall effect has been alluded to, and in our data seems to be best described by the axial dispersion and bed porosities being significantly different compared to conventional scale columns, but computational fluid dynamics, coupled with suitable calibration experiments, could provide a stronger understanding the impact, and to better simulate radial heterogeneity and any differences in packing efficiency. Any further insight into column geometry would have greatly helped interpretation of results at microscale mechanistically. Roberts & Carta (2020) better described breakthrough data by implementing a non-uniform flow model compared with the conventional approach used in this work.

Modelling of chromatography will become ever more important due to the increasing complexity, variety and required understanding of bioprocesses, and facilitated by better software and equipment, model formulations and expertise. It is hoped that this work will aid those seeking to mitigate the differences experienced with microscale chromatography and looking to improve data quality and predictive ability of their microscale process development, to deliver better, more robust and more economical processes, quickly.

Bibliography

Abia, J. A., Mriziq, K. S., & Guiochon, G. A. (2009). Radial heterogeneity of some analytical columns used in high-performance liquid chromatography. Journal of Chromatography A, 1216(15), 3185-3191.

Aono, H., Iliescu, I., Cecchini, D., Wood, S., & McCue, J. T. (2013). Mitigation of chromatography adsorbent lot performance variability through control of buffer solution design space. Journal of Chromatography A, 1318, 198-206.

Attene-Ramos, M. S., Austin, C. P., & Xia, M. (2014). High Throughput Screening. Encyclopedia of Toxicology, 916–917.

Atoll. (2013). MediaScout® RoboColumn®., from Atoll: http://www.atoll-bio.com/products/minicolumn/mediascout-robocolumn accessed 17Sep17, 16:16

Bader, A., Meiners, F., & Tracht, K. (2018). Accelerating High-Throughput Screening for Structural Materials with Production Management Methods. Materials, 11(8), 1330.

Bak, H., Thomas, O. R., & Abildskov, J. (2007). Lumped parameter model for prediction of initial breakthrough profiles for the chromatographic capture of antibodies from a complex feedstock. Journal of chromatography B, 848(1), 131-141.

Bankston, T. E., Stone, M. C., & Carta, G. (2008). Theory and applications of refractive index-based optical microscopy to measure protein mass transfer in spherical adsorbent particles. Journal of Chromatography A, 1188(2), 242-254.

Baumann, P., Hahn, T., & Hubbuch, J. (2015). High-throughput micro-scale cultivations and chromatography modeling: Powerful tools for integrated process development. Biotechnology and bioengineering, 112(10), 2123-2133.

Baumann, P., & Hubbuch, J. (2017). Downstream process development strategies for effective bioprocesses: trends, progress, and combinatorial approaches. Engineering in Life Sciences, 17(11), 1142-1158.

Baur, D., Angelo, J. M., Chollangi, S., Xu, X., Müller-Späth, T., Zhang, N., & Morbidelli, M. (2018). Model assisted comparison of Protein A resins and multi-column chromatography for capture processes. Journal of Biotechnology.

Behere, K., Cha, B., & Yoon, S. (2018). Protein a resin lifetime study: Evaluation of protein a resin performance with a model-based approach in continuous capture. Preparative Biochemistry and Biotechnology, 48(3), 242-256.

Bekke-Hansen S, Trockel M, Burg M, &Taylor C. (2011). Depressive symptom dimensions and cardiac prognosis following myocardial infarction: Results from the ENRICHD clinical trial. Psychological medicine. 42. 51-60.

Benner, S. W., Welsh, J. P., Rauscher, M. A., & Pollard, J. M. (2019). Prediction of lab and manufacturing scale chromatography performance using mini-columns and mechanistic modeling. Journal of Chromatography A, 1593, 54-62.

Bergander, T., Nilsson-Välimaa, K., Öberg, K., & Lacki, K. M. (2008). High-throughput process development: determination of dynamic binding capacity using microtiter filter plates filled with chromatography resin. Biotechnology progress, 24(3), 632-639.

Bergander T & Lacki K (2016). High-throughput process development: Chromatography media volume definition. Engineering in Life Sciences 16(2): 185-189.

Bird, P. (1933). A derivation of Langmuir's adsorption isotherm. Journal of Chemical Education 10(4): 237.

Bird, R. B., Stewart, W. E., & Lightfoot, E. N. (2006). Transport Phenomena, revised 2 nd edition.

Bohart, G. S., & Adams, E. Q. (1920). Some aspects of the behavior of charcoal with respect to chlorine. Journal of the American Chemical Society, 42(3), 523-544.

Boi, C., Dimartino, S., & Sarti, G. C. (2007). Modelling and simulation of affinity membrane adsorption. Journal of Chromatography A, 1162(1), 24-33.

Boi, C., Dimartino, S., & Sarti, G. C. (2008). Performance of a new protein a affinity membrane for the primary recovery of antibodies. Biotechnology progress, 24(3), 640-647.

Borg, N., Westerberg, K., Andersson, N., von Lieres, E., & Nilsson, B. (2013). E ffects of uncertainties in experimental conditions on the estimation of adsorption model parameters in preparative chromatography . Computers & Chemical Engineering, 55, 148–157.

Borg, N., Brodsky, Y., Moscariello, J., Vunnum, S., Vedantham, G., Westerberg, K., & Nilsson, B. (2014). Modeling and robust pooling design of a preparative cation-exchange chromatography step for purification of monoclonal antibody monomer from aggregates. Journal of Chromatography A, 1359, 170-181.

Bowes, B. D., Koku, H., Czymmek, K. J., & Lenhoff, A. M. (2009). Protein adsorption and transport in dextran-modified ion-exchange media. I: Adsorption. Journal of Chromatography A, 1216(45), 7774-7784.

Bowes, B. D., & Lenhoff, A. M. (2011). Protein adsorption and transport in dextran-modified ion-exchange media. II. Intraparticle uptake and column breakthrough. Journal of Chromatography A, 1218(29), 4698-4708.

Boyer P &Hsu T. (1992). Experimental studies of restricted protein diffusion in an agarose matrix. AIChE Journal 38(2): 259-272.

Brekke O, Sandlie I (2003). Therapeutic antibodies for human diseases at the dawn of the twenty-first century. Nature Reviews Drug Discovery 2: 52.

Brenner H & Gaydos J. (1977). The constrained brownian movement of spherical particles in cylindrical pores of comparable radius: Models of the diffusive and convective transport of solute molecules in membranes and porous media. Journal of Colloid and Interface Science 58(2): 312-356.

Brian, K. (2007). Very Large Scale Monoclonal Antibody Purification: The Case for Conventional Unit Operations. Biotechnology Progress 23(5): 995-1008.

Britsch, L., Schroeder, T., & Friedle, J. (2008). Automated, High-Throughput chromatographic separation of biological compounds. American Biotechnology Laboratory®, 26(6), 20.

Brooks S, Leff D, Hernandez Torres M, Dorsey J (1988). Dispersion coefficient and moment analysis of flow injection analysis peaks. Analytical Chemistry 60(24): 2737-2744.

Brooks, C. A., & Cramer, S. M. (1992). Steric mass-action ion exchange: displacement profiles and induced salt gradients. AIChE Journal, 38(12), 1969-1978.

Bruce, L. & Chase H .(2001). Hydrodynamics and adsorption behaviour within an expanded bed adsorption column studied using in-bed sampling. Chemical Engineering Science 56(10): 3149-3162.

Bud, R. (2007). Penicillin: Triumph and Tragedy, Oxford University Press.

Buss N (2012). Monoclonal antibody therapeutics: history and future. Current Opinion in Pharmacology, 12(5), 615-622.

Byrd, R, Hribar M, Nocedal J (1999). An Interior Point Algorithm for Large-Scale Nonlinear Programming. SIAM Journal on Optimization 9(4): 877-900.

Carta, G., Ubiera, A. R., & Pabst, T. M. (2005). Protein Mass Transfer Kinetics in Ion Exchange Media: Measurements and Interpretations. Chemical Engineering & Technology , 28(11), 1252–1264.

Carta, G. & Jungbauer A (2010). Protein Chromatography: Process Development and Scale-Up, John Wiley & Sons.

Carta, G. (2012). Predicting protein dynamic binding capacity from batch adsorption tests. Biotechnology Journal 7(10): 1216-1220.

Carter-Franklin, J. N., Victa, C., McDonald, P., & Fahrner, R. (2007). Fragments of protein A eluted during protein A affinity chromatography. Journal of Chromatography A, 1163(1-2), 105-111.

Chaparro M.., Saaltink, M, Soler . M Slooten J., & Mäder, U. (2015). Modelling of Matrix Diffusion in a Tracer Test in Concrete. Transport in Porous Media, 111(1), 27–40.

Chattre C, Titchener-Hooker N (2009). Review: Microscale methods for high-throughput chromatography development in the pharmaceutical industry. Journal of Chemical Technology & Biotechnology 84(7): 927-940.

Chhatre, S. (2012). Extreme Scale-Down Approaches for Rapid Chromatography Column Design and Scale-Up During Bioprocess Development . Measurement, Monitoring, Modelling and Control of Bioprocesses, 109–135.

Chen W, Hu H, Wang Y.(2006). Analysis of steric mass-action model for Protein Adsorption equilibrium onto porous anion-exchange adsorbent. Chemical Engineering Science 61(21): 7068-7076.

Chung S & Wen C (1968). Longitudinal dispersion of liquid flowing through fixed and fluidized beds. AIChE Journal 14(6): 857-866.

Clark, D. S., Bailey, J. E., & Do, D. D. (1985). A mathematical model for restricted diffusion effects on macromolecule impregnation in porous supports. Biotechnology and Bioengineering, 27(2), 208–213.

Close E, Salm J, Bracewell D, Sorensen E (2014a). Modelling of industrial biopharmaceutical multicomponent chromatography. Chemical Engineering Research and Design 92(7): 1304-1314.

Close, E. J., Salm, J. R., Bracewell, D. G., & Sorensen, E. (2014b). A model based approach for identifying robust operating conditions for industrial chromatography with process variability. Chemical Engineering Science, 116, 284–295.

CMC Biotech Working Group. (2009). A-Mab case study . CASSS

Code of Federal Regulations US, 21 CFR Part 600. Subpart A. Sec. 600.3(2018).

Collins, W. E. (1997). Protein Separation with Flow-Through Chromatography. Separation and Purification Methods , 26(2), 215–253

Coning, P. & Swinley, J. (2019). A practical guide to gas analysis by gas chromatography. Amsterdam: Elsevier.

Cooper, R. S., & Liberman, D. A. (1970). Fixed-Bed Adsorption Kinetics with Pore Diffusion Control . Industrial & Engineering Chemistry Fundamentals, 9(4), 620–623.

Costa, C, Cabral J. (1991). Chromatographic and Membrane Processes in Biotechnology , Kluwer Academic Publishers.

da Silva G, Plewka J, Tscheließnig R, Lichtenegger H, Jungbauer A, Dias-Cabral A, Ana C. (2019). Antibody Binding Heterogeneity of Protein A Resins. Biotechnology Journal 14(8): 1800632.

Dancette, O. P., Taboureau, J. L., Tournier, E., Charcosset, C., & Blond, P. (1999). Purification of immunoglobulins G by protein A/G affinity membrane chromatography. Journal of Chromatography B: Biomedical Sciences and Applications, 723(1-2), 61-68.

Danckwerts, P. V. (1953). Continuous flow systems: Distribution of residence times. Chemical Engineering Science 2(1): 1-13.

Dean, J. & Lange, N. (1999). Lange's handbook of chemistry. New York: McGraw-Hill.

de Ligny, C. L. (1970). Coupling between diffusion and convection in radial dispersion of matter by fluid flow through packed beds. Chemical Engineering Science 25(7): 1177-1181.

Degerman, M., Jakobsson N, Nilsson N. (2006). Constrained optimization of a preparative ion-exchange step for antibody purification. Journal of Chromatography A 1113(1): 92-100.

Degerman, M., Westerberg, K., & Nilsson, B. (2009). Determining Critical Process Parameters and Process Robustness in Preparative Chromatography - A Model-Based Approach . Chemical Engineering & Technology, 32(6), 903–911.

Deyl, Z., Janak J, Macek K. (1975). Liquid Column Chromatography: A Survey of Modern Techniques and Applications , Elsevier Scientific Publishing Company.

Diederich P, Hubbuch J (2017). High-Throughput Column Chromatography Performed on Liquid Handling Stations: Process Characterization and Error Analysis : 293-332.

Di Marco, Bombi G. (2001). Mathematical functions for the representation of chromatographic peaks. Journal of Chromatography A 931(1-2): 1-30.

de Neuville, B. C., Tarafder, A., & Morbidelli, M. (2013). Distributed pore model for bio-molecule chromatography. Journal of Chromatography A, 1298, 26-34.

Dimartino S, Boi C, Sarti G (2011a). A validated model for the simulation of protein purification through affinity membrane chromatography. Journal of Chromatography A 1218(13): 1677-1690.

Dimartino S, Boi C, Sarti G (2011b). Influence of protein adsorption kinetics on breakthrough broadening in membrane affinity chromatography. Journal of Chromatography A 1218(26): 3966-3972.

Dimartino, S., Boi, C., & Sarti, G. C. (2015). Scale-up of affinity membrane modules: comparison between lumped and physical models. Journal of Molecular Recognition, 28(3), 180–190.

Do D, Herrera L, Nicholson D., (2011). A method for the determination of accessible surface area, pore volume, pore size and its volume distribution for homogeneous pores of different shapes. Adsorption 17(2): 325-335.

Dozier J ,Distefano M (2015). Site-Specific PEGylation of Therapeutic Proteins. International Journal of Molecular Sciences 16(10): 25831.

Dyson, N. (1998). Chromatographic integration methods. Cambridge: Royal Society of Chemistry, Information Services.

Ecker M, Jones S, Levine H, (2015). The therapeutic monoclonal antibody market. mAbs 7(1): 9-14.

Engell, S, Toumi A (2004). Optimization and control of chromatography. Computer Aided Chemical Engineering. A. Barbosa - Póvoa and H. Matos, Elsevier. 18: 9-22.

European Medicines Evaluation Agency. Revised CPMP Guideline on Virus Validation Studies. CPMP/268/95, 1995

Evans S, Afdahl C, Patel R, Newell K (2017). Optimization of a micro-scale, high throughput process development tool and the demonstration of comparable process performance and product quality with biopharmaceutical manufacturing processes. Journal of Chromatography A 1506(Supplement C): 73-81.

Fang, Z. (2009). Large-scale chromatography columns, modeling flow distribution. Encyclopedia of Industrial Biotechnology: Bioprocess, Bioseparation, and Cell Technology, 1-18.

Farid, S. (2007). Process economics of industrial monoclonal antibody manufacture. Journal of Chromatography B 848(1): 8-18.

Farkas, T., & Guiochon, G. (1997). Contribution of the Radial Distribution of the Flow Velocity to Band Broadening in HPLC Columns. Analytical Chemistry , 69(22), 4592–4600.

Feidl, F., Luna, M. F., Podobnik, M., Vogg, S., Angelo, J., Potter, K., … Butté, A. (2020). Model based strategies towards protein A resin lifetime optimization and supervision . Journal of Chromatography A, 461261.

Feliciano, J., Berrill, A., Ahnfelt, M., Brekkan, E., Evans, B., Fung, Z., Lacki, K. (2016). Evaluating high-throughput scale-down chromatography platforms for increased process understanding . Engineering in Life Sciences, 16(2), 169–178

Felinger A, Guiochon G (1995). Computer simulations in non-linear chromatography. TrAC Trends in Analytical Chemistry 14(1): 6-10.

Felinger A, Guiochon G (2004). Comparison of the Kinetic Models of Linear Chromatography. Chromatographia 60(1): S175-S180.

Fishbaum S, (2011). Translational research: improving the efficiency of drug development from bench to bedside and back again , Health News 9,

Flajnik M, Kasahara K (2010). Origin and evolution of the adaptive immune system: genetic events and selective pressures. Nature reviews. Genetics 11(1): 47-59.

Foley P (1987). Equations for chromatographic peak modeling and calculation of peak area. Analytical Chemistry 59(15): 1984-1987.

Follman D, Fahrner R. (2004), Factorial Screening of Antibody Purification Processes Using Three Chromatography Steps without Protein A . Journal of Chromatography A 1024.1-2

Food and Drug Administration. Guidance for industry, Q8(R1) Pharmaceutical Development. 2009. Nov, Available from: http://www.fda.gov/downloads/Drugs/.../Guidances/ucm073507.pdf . Accessed 16Sep17, 16:00

Fornstedt T, Forssén, P., Samuelsson, J. (2017). Modelling of preparative liquid chromatography. Liquid Chromatography , 573–592.

Frigon R, Leypoldt J, Uyeji S, Henderson L (1983). Disparity between Stokes radii of dextrans and proteins as determined by retention volume in gel permeation chromatography. Analytical Chemistry 55(8): 1349-1354.

Gagnon, P (1996)., Purification tools for monoclonal antibodies. Validated Biosystems,

Ganetsos G, Barker P (1993). Preparative and production scale chromatography. New York, Marcel Dekker.

GE Healthcare, (2011a), MabSelect SuRe Instructions, Application note 11-0026-01 AD

GE. Healthcare (2012a). Extended reports from the second international conference on high-throughput process development. Process Development Forum.

GE Healthcare, (2011b), Dynamic binding capacity study on MabSelect SuRe™ LX for capturing high-titre monoclonal antibodies, 11-0026-01 AD, Application note 28-9875-25 AA

GE Healthcare. (2014a) Resins & Protein Binding Capacities. Retrieved from GE Protein Skills: http://geproteinskills.blogspot.co.uk/2014/10/resins-protein-binding-capacities.html

GE Healthcare, (2014b) Capto™ S ImpAct, Data file 29-0670-18 AC

Gerontas, S., Asplund, M., Hjorth, R., & Bracewell, D. G. (2010). Integration of scale-down experimentation and general rate modelling to predict manufacturing scale chromatographic separations. Journal of Chromatography A 1217(44), 6917–6926.

Gétaz, D., Stroehlein, G., Butté, A., & Morbidelli, M. (2013). Model-based design of peptide chromatographic purification processes . Journal of Chromatography A, 1284, 69–79.

Ghose, S., Nagrath, D., Hubbard, B., Brooks, C., & Cramer, S. M. (2004). Use and Optimization of a Dual-Flowrate Loading Strategy To Maximize Throughput in Protein-A Affinity Chromatography . Biotechnology Progress, 20(3), 830–840.

Ghosh P, Vahedipour K, Lin M, Vogel J, Haynes C, von Lieres E,(2013). Computational fluid dynamic simulation of axial and radial flow membrane chromatography: Mechanisms of non-ideality and validation of the zonal rate model. Journal of Chromatography A 1305: 114-122.

Ghosh, P., Lin, M., Vogel, J. H., Choy, D., Haynes, C., & von Lieres, E. (2014a). Zonal rate model for axial and radial flow membrane chromatography, part II: Model-based scale-up. Biotechnology and bioengineering , 111(8), 1587-1594.

Ghosh, P., Vahedipour, K., Leuthold, M., & von Lieres, E. (2014b). Model-based analysis and quantitative prediction of membrane chromatography: Extreme scale-up from 0.08 ml to 1200 ml . Journal of Chromatography A, 1332, 8-13.

Giddings, J. C. (1959). 'Eddy'diffusion in chromatography. Nature, 184(4683), 357-358.

Gottschalk, U. (2017). Process scale purification of antibodies. Hoboken, NJ: Wiley.

Graham E, Dranoff J (1982). Application of the Stefan-Maxwell equations to diffusion in ion exchangers. 1. Theory. Industrial & Engineering Chemistry Fundamentals 21(4): 360-365.

Grammaticakis P.(1951), Contribution a l'etude de l'absorption dans l'ultraviolet moyen et le visible des arylamines isomeres et de leurs derives N substitues (Premier memoire), Bull. Soc. Chim. Fr, , 18, 220-226.

Green D, Perry R (2007). Perry's Chemical Engineers' Handbook, Eighth Edition, McGraw-Hill Education.

Grilo A, Mantalaris A The Increasingly Human and Profitable Monoclonal Antibody Market. Trends in Biotechnology.

Grinias, J., Bunner, B., Gilar, M., & Jorgenson, J. (2015). Measurement and Modeling of Extra-Column Effects Due to Injection and Connections in Capillary Liquid Chromatography. Chromatography, 2(4), 669–690.

Gronemeyer, P, Ditz R, Strube J (2014). Trends in upstream and downstream process development for antibody manufacturing. Bioengineering 1(4): 188-212.

Grushka, E. (1972). Characterization of exponentially modified Gaussian peaks in chromatography. Analytical Chemistry, 44(11), 1733-1738.

Gu T (1991). Multicomponent adsorption and chromatography with uneven saturation capacities. AIChE Journal 37(9): 1333-1340.

Gu T. (1995). Mathematical Modeling and Scale-up of Liquid Chromatography , Springer.

Gu T, Iyer G, Chen K.(2013). Parameter estimation and rate model simulation of partial breakthrough of bovine serum albumin on a column packed with large Q Sepharose anion-exchange particles. Separation and Purification Technology 116: 319-326.

Guan, H. and Guiochon, G., 1996. Study of physico-chemical properties of some packing materials: I. Measurements of the external porosity of packed columns by inverse size-exclusion chromatography. Journal of Chromatography A, 731(1-2), pp.27-40.

Guélat B, Ströhlein G, Lattuada M, Delegrange L, Valax P, Morbidelli M. (2012). Simulation model for overloaded monoclonal antibody variants separations in ion-exchange chromatography. Journal of Chromatography A 1253: 32-43.

Guiochon, G., Farkas, T., Guan-Sajonz, H., Koh, J.-H., Sarker, M., Stanley, B. J., & Yun, T. (1997). Consolidation of particle beds and packing of chromatographic columns. Journal of Chromatography A, 762(1-2), 83–88.

Guiochon G. (2002). Preparative liquid chromatography. Journal of Chromatography A 965(1-2): 129-161.

Guiochon G, Felinger A, Shirazi D. (2006). Fundamentals of Preparative and Nonlinear Chromatography , Elsevier Science.

Gritti, F., & Guiochon, G. (2006). General HETP Equation for the Study of Mass-Transfer Mechanisms in RPLC . Analytical Chemistry, 78(15), 5329–5347.

Gritti, F., & Guiochon, G. (2011). Multi-location peak parking method: An important new tool for the study of mass transfer kinetics in liquid chromatography . Journal of Chromatography A, 1218(7), 896–906.

Gritti, F., & Guiochon, G. (2012). Mass transfer kinetics, band broadening and column efficiency . Journal of Chromatography A, 1221, 2–40.

Gunst R, Mason R (2009). Fractional factorial design. Wiley Interdisciplinary Reviews: Computational Statistics 1(2): 234-244.

Gutenwik, J., Nilsson, B., & Axelsson, A. (2004). „Coupled diffusion and adsorption effects for multiple proteins in agarose gel . AIChE Journal, 50(12), 3006–3018.

Hagel L, Osterberg M, Andersson T (1996). Apparent pore size distributions of chromatography media. Journal of Chromatography A 743(1): 33-42.

Hagemann, F., Adametz, P., Wessling, M. and Thom, V., (2020). Modeling hindered diffusion of antibodies in agarose beads considering pore size reduction due to adsorption. Journal of Chromatography A, 1626, p.461319.

Hahn, R., Bauerhansl, P., Shimahara, K., Wizniewski, C., Tscheliessnig, A., & Jungbauer, A. (2005). Comparison of protein A affinity sorbents: II. Mass transfer properties . Journal of chromatography A, 1093(1-2), 98-110.

Hahn R (2012). Methods for characterization of biochromatography media. Journal of Separation Science 35(22): 3001-3032.

Hahn, T., Sommer, A., Osberghaus, A., Heuveline, V., & Hubbuch, J. (2014). Adjoint-based estimation and optimization for column liquid chromatography models . Computers & Chemical Engineering, 64, 41–54.

Hanes, C. S. (1932). Studies on plant amylases . Biochemical Journal, 26(5), 1406–1421

Hanke A, Ottens M. (2014). Purifying biopharmaceuticals: knowledge-based chromatographic process development. Trends in Biotechnology 32(4): 210-220.

Harrison, R. K. (2016). Phase II and phase III failures: 2013-2015. Nature Reviews Drug Discovery 15: 817.

Haynes, W. (2014). CRC handbook of chemistry and physics : a ready-reference book of chemical and physical data . Boca Raton, Florida: CRC Press.

He L, Niemeyer B. (2003). A Novel Correlation for Protein Diffusion Coefficients Based on Molecular Weight and Radius of Gyration. Biotechnology Progress 19(2): 544-548.

Heeter G, Liapis A. (1998). Frontal chromatography of proteins: Effect of axial dispersion on column performance. Journal of Chromatography A 796(1): 157-164.

Helling C, Dams T, Gerwat B, Belousov A Strube J. (2013). Physical characterization of column chromatography: stringent control over equipment performance in biopharmaceutical production. Trends in Chromatography 8: 55-71.

Hill A, Barber M, Gotham D. (2018). Estimated costs of production and potential prices for the WHO Essential Medicines List. BMJ Global Health 3(1).

Horstmann B, Chase H (1989). Modeling the affinity adsorption of immunoglobulin G to Protein A immobilised to agarose matrices. Chemical engineering research & design 67(3): 243-254.

Houp R (2009). Ultrafiltration and Diafiltration. Journal of Validation Technology, 40 -45.

Hubbuch, J., Linden, T., Knieps, E., Ljunglöf, A., Thömmes, J., & Kula, M.-R. (2003). „Mechanism and kinetics of protein transport in chromatographic media studied by confocal laser scanning microscopy . Journal of Chromatography A, 1021(1-2), 93–104.

Hubbuch, J. (2012). Editorial: High-throughput process development . Biotechnology Journal, 7(10), 1185–1185.

Hunter, A, Carta, G. (2001). Effects of bovine serum albumin heterogeneity on frontal analysis with anion-exchange media. Journal of chromatography. A, 937(1-2), 13–19.

Hutchinson, N. (2014). Understanding and Controlling Sources of Process Variation: Risks to Achieving Product Critical Quality Attributes . Enabling Cell Therapy Manufacturing.

Huuk, T. C., Hahn, T., Osberghaus, A., & Hubbuch, J. (2014). Model-based integrated optimization and evaluation of a multi-step ion exchange chromatography . Separation and Purification Technology, 136, 207–222.

Ishihara, T., Kadoya, T., Yoshida, H., Tamada, T., & Yamamoto, S. (2005). Rational methods for predicting human monoclonal antibodies retention in protein A affinity chromatography and cation exchange chromatography: Structure-based chromatography design for monoclonal antibodies. Journal of Chromatography A, 1093(1-2), 126-138.

Jakobsson, N., Degerman, M., Nilsson, B. (2005). Optimization and robustness analysis of a hydrophobic interaction chromatography step . J. Chromatogr. A., 1063: 99 – 109

Jakobsson, N., Degerman, M., Stenborg, E., & Nilsson, B. (2007). „Model based robustness analysis of an ion-exchange chromatography step . Journal of Chromatography A, 1138(1-2), 109–119

Jansson, B., Uhlén, M., & Nygren, P.-Å. (2006). All individual domains of staphylococcal protein A show Fab binding . FEMS Immunology & Medical Microbiology, 20(1), 69–78.

Jeansonne, M,S, Chromatographic Peak Shape Analysis and Modeling. (1990). LSU Historical Dissertations and Theses. 5061. https://digitalcommons.lsu.edu/gradschool_disstheses/5061

Joshi VS, Kumar V, Rathore AS. (2017). Optimization of ion exchange sigmoidal gradients using hybrid models: Implementation of quality by design in analytical method development. Journal of Chromatography A 1491: 145-152.

Jungreuthmayer C, Steppert P, Sekot G, Zankel A, Reingruber H, Zanghellini J, Jungbauer A. (2015). The 3D pore structure and fluid dynamics simulation of macroporous monoliths: High permeability due to alternating channel width. Journal of Chromatography A 1425: 141-149.

Kadjo, A. F., Dasgupta, P. K., Su, J., Liu, S., & Kraiczek, K. G. (2017). Width Based Quantitation of Chromatographic Peaks: Principles and Principal Characteristics. Analytical Chemistry, 89(7), 3884–3892.

Kalambet, Y., Kozmin, Y., & Samokhin, A. (2018)Comparison of integration rules in the case of very narrow chromatographic peaks . Chemometrics and Intelligent Laboratory Systems, 179, 22–30.

Kaltenbrunner, O., Jungbauer, A., & Yamamoto, S. (1997). Prediction of the preparative chromatography performance with a very small column . Journal of Chromatography A, 760(1), 41–53.

Kaltenbrunner, O., Giaverini, O., Woehle, D., & Asenjo, J. A. (2007). Application of chromatographic theory for process characterization towards validation of an ion-exchange operation . Biotechnology and Bioengineering, 98(1), 201–210.

Kaltenbrunner, O., Diaz, L., Hu, X., & Shearer, M. (2016). Continuous bind-and-elute protein A capture chromatography: Optimization under process scale column constraints and comparison to batch operation . Biotechnology Progress, 32(4), 938–948.

Karlsson D, Jakobsson N, Brink K, Axelsson A, Nilsson B. (2004a). Methodologies for model calibration to assist the design of a preparative ion-exchange step for antibody purification. Journal of Chromatography A 033(1): 71-82.

Karlsson, D., Jakobsson, N., Axelsson, A., & Nilsson, B. (2004b). Model-based optimization of a preparative ion-exchange step for antibody purification. Journal of Chromatography A , 1055(1-2), 29–39.

Kasche V, de Boer M, Lazo C, Gad M. (2003). Direct observation of intraparticle equilibration and the rate-limiting step in adsorption of proteins in chromatographic adsorbents with confocal laser scanning microscopy. Journal of Chromatography B 790(1-2): 115-129.

Kataoka T, Yoshida H, Koretsune U (1972). Mass Transfer In Laminar Region Between Liquid And Packing Material Surface In The Packed Bed. Journal of Chemical Engineering of Japan 5(2): 132-136.

Katoh S, Imada M, Takeda N, Katsuda T, Miyahara H, Inoue M, Nakamura S. (2007). Optimization of silica-based media for antibody purification by protein A affinity chromatography. Journal of Chromatography A 1161(1-2): 36-40.

Kempe H, Persson P, Axelsson A, Nilsson B, Zacchi G. (2006). Determination of diffusion coefficients of proteins in stationary phases by frontal chromatography. Biotechnology and Bioengineering 93(4): 656-664.

Keller, W. R., Evans, S. T., Ferreira, G., Robbins, D., & Cramer, S. M. (2015). Use of MiniColumns for linear isotherm parameter estimation and prediction of benchtop column performance. Journal of Chromatography A, 1418, 94–102.

Keller, W. R., Evans, S. T., Ferreira, G., Robbins, D., & Cramer, S. M. (2017). Understanding operational system differences for transfer of miniaturized chromatography column data using simulations. Journal of Chromatography A, 1515, 154–163.

Khalaf, R., Heymann, J., LeSaout, X., Monard, F., Costioli, M., & Morbidelli, M. (2016). Model-based high-throughput design of ion exchange protein chromatography. Journal of Chromatography A, 1459, 67–77.

Kidal, S., Jensen, O.. (2006). Using volumetric flow to scaleup chromatographic processes. Biopharm international, 19(3).

Kiesewetter, A., Menstell, P., Peeck, L. H., & Stein, A. (2016). Development of pseudo-linear gradient elution for high-throughput resin selectivity screening in RoboColumn® Format. Biotechnology Progress, 32(6), 1503–1519.

Kim T, Kim S (2011). Clinical Outcomes of Occupational Exposure to N,N-Dimethylformamide: Perspectives from Experimental Toxicology. Safety and Health at Work 2(2): 97-104.

Kiss, B., Gottschalk, U. & Pohlscheidt, M. (2018). New bioprocessing strategies : development and manufacturing of recombinant antibodies and proteins. Cham, Switzerland: Springer.

Knox, J. H., & Parcher, J. F. (1969). Effect of the column to particle diameter ratio on the dispersion of unsorbed solutes in chromatography. Analytical Chemistry, 41(12), 1599–1606.

Knox, J. H., Laird, G. R., & Raven, P. A. (1976). Interaction of radial and axial dispersion in liquid chromatography in relation to the infinite diameter effect. Journal of Chromatography A, 122, 129–145.

Kong, D. Y., Gerontas, S., McCluckie, R. A., Mewies, M., Gruber, D., & Titchener-Hooker, N. J. (2018). Effects of bed compression on protein separation on gel filtration chromatography at bench and pilot scale. Journal of Chemical Technology & Biotechnology, 93(7), 1959-1965.

Kong, D. Y. C. (2019). Influence of different methods of bed compression on protein separation in process chromatography (Doctoral dissertation, UCL (University College London)).

Koppejan, V., Ferreira, G., Lin, D.-Q., & Ottens, M. (2018). Mathematical modelling of expanded bed adsorption - a perspective on in silico process design. Journal of Chemical Technology & Biotechnology, 93(7), 1815–1826.

Kolitcheff, S., Jolimaitre, E., Hugon, A., Verstraete, J., Carrette, P. L., & Tayakout-Fayolle, M. (2017). Tortuosity of mesoporous alumina catalyst supports: Influence of the pore network organization. Microporous and Mesoporous Materials, 248, 91-98.

Kumar V, Leweke S, von Lieres E, Rathore AS. (2015). Mechanistic modeling of ion-exchange process chromatography of charge variants of monoclonal antibody products. Journal of Chromatography A 1426: 140-153.

Kumar, V., & Lenhoff, A. M. (2020). Mechanistic Modeling of Preparative Column Chromatography for Biotherapeutics. Annual Review of Chemical and Biomolecular Engineering, 11(1), 235–255.

Łącki, K. M. (2012). High-throughput process development of chromatography steps: Advantages and limitations of different formats used. Biotechnology Journal, 7(10), 1192–1202.

Łącki, K. M. (2018). Chapter 16 - Introduction to Preparative Protein Chromatography. Biopharmaceutical Processing. G. Jagschies, E. Lindskog, K. Łącki and P. Galliher, Elsevier: 319-366.

Ladiwala, A., Rege, K., Breneman, C. M., & Cramer, S. M. (2005). A priori prediction of adsorption isotherm parameters and chromatographic behavior in ion-exchange systems. Proceedings of the National Academy of Sciences, 102(33), 11710–11715.

Lain B. 2013. Protein A: The Life of a Disruptive Technology. Bioprocess Intl. 11:28-38.

Larson, T. M., Davis, J., Lam, H., & Cacia, J. (2003). Use of Process Data To Assess Chromatographic Performance in Production-Scale Protein Purification Columns . Biotechnology Progress, 19(2), 485–492

Latour R (2014). The langmuir isotherm: A commonly applied but misleading approach for the analysis of Protein Adsorption behavior. Journal of Biomedical Materials Research Part A 103(3): 949-958.

Lebrun L, Junter G(1993). Diffusion of sucrose and dextran through agar gel membranes. Enzyme and Microbial Technology 15(12): 1057-1062.

Lettner H, Kaltenrunner O, Jungbauer A (1995). HETP in Process Ion-Exchange Chromatography. Journal of Chromatographic Science 33(8): 451-457.

Li, F., Maguigad, J., Pelzer, M., Jiang, X, Ji C. (2008). A novel peak parking strategy for ultra-performance liquid chromatography/tandem mass spectrometric detection for enhanced performance of bioanalytical assays. Rapid Communications in Mass Spectrometry, 22(4), 486–494.

Li F, Vijayasankaran N, Shen A, Kiss R, Amanullah A. (2010). Cell culture processes for monoclonal antibody production. mAbs 2(5): 466-477.

Lichty J, Malecki J, Agnew H, Michelson-Horowitz D & Tan S. (2005). Comparison of affinity tags for protein purification. Protein Expr Purif 41(1): 98-105.

Lienqueo, M. E., Shene, C., & Asenjo, J. (2009). Optimization of hydrophobic interaction chromatography using a mathematical model of elution curves of a protein mixture. Journal of Molecular Recognition, 22(2), 110–120.

Liu J (2014). The history of monoclonal antibody development - Progress, remaining challenges and future innovations. Annals of Medicine and Surgery 3(4): 113-116.

Liu Z, Mostafa S, Shukla A. (2015). A comparison of Protein A chromatographic stationary phases: Performance characteristics for monoclonal antibody purification. Biotechnology and Applied Biochemistry 62(1): 37-47.

Liu, T., Angelo, J.M., Lin, D.Q., Lenhoff, A.M. & Yao, S.J., (2017). Characterization of dextran-grafted hydrophobic charge-induction resins: Structural properties, protein adsorption and transport. Journal of Chromatography A, 1517, pp.44-53.

Liu, S., Gerontas, S., Gruber, D., Turner, R., Titchener-Hooker, N. J., & Papageorgiou, L. G. (2017b). Optimization-based framework for resin selection strategies in biopharmaceutical purification process development. Biotechnology progress, 33(4), 1116-1126.

Lopes da Silva, G. F., Plewka, J., Tscheließnig, R., Lichtenegger, H., Jungbauer, A., & Dias-Cabral, A. C. M. (2019). Antibody binding heterogeneity of Protein A resins. Biotechnology Journal, 1800632

López, Z. K., Tejeda, A., Montesinos, R. M., Magana, I., & Guzman, R. (1997). Modeling column regeneration effects on ion-exchange chromatography. Journal of Chromatography A, 791(1-2), 99-107.

Macek K, Deyl Z, Janak J (2011). Liquid Column Chromatography: A Survey of Modern Techniques and Applications, Elsevier Science.

Mackie J, Meares P (1955). The Diffusion of Electrolytes in a Cation-Exchange Resin Membrane. I. Theoretical. Proceedings of the Royal Society of London. Series A. Mathematical and Physical Sciences 232(1191): 498-509.

Maitra J (2008). Principle Component Analysis and Partial Least Squares: Two Dimension Reduction Techniques for Regression. Casualty Actuarial Society, 79-90.

Malmquist G, Danielsson R (1994). Alignment of chromatographic profiles for principal component analysis: a prerequisite for fingerprinting methods. Journal of Chromatography A 687(1): 71-88.

Mandenius, C.-F., & Brundin, A. (2008). Bioprocess optimization using design-of-experiments methodology. Biotechnology Progress, 24(6), 1191–1203.

Marchetti N, Cavazzini A, Past, L, Dondi F. (2009). Determination of adsorption isotherms by means of HPLC: Adsorption mechanism elucidation and separation optimization. Journal of Separation Science 32(5-6): 727-741.

Marek, W. K., Sauer, D., Dürauer, A., Jungbauer, A., Piątkowski, W., & Antos, D. (2018). Prediction tool for loading, isocratic elution, gradient elution and scaling up of ion exchange chromatography of proteins. Journal of Chromatography A, 1566, 89–101.

McCaw T, Koepf E, Conley L. (2014). Evaluation of a novel methacrylate-based Protein A resin for the purification of immunoglobulins and Fc-fusion proteins. Biotechnology Progress 30(5): 1125-1136.

McCoy, M. A., & Liapis, A. I. (1991). Evaluation of kinetic models for biospecific adsorption and its implications for finite bath and column performance. Journal of Chromatography A, 548, 25–60.

McCue J, Kemp G, Low D, Quiñones-García I. (2003). Evaluation of protein-A chromatography media. Journal of Chromatography A 989(1): 139-153.

McCue JT, Engel P, Ng A, Macniven R, Thömmes J. (2008) Modeling of protein monomer/aggregate purification and separation using hydrophobic interaction chromatography . Bioprocess Biosyst Eng.;31(3):261-275

McGown K (1998). Verification of Multichannel Liquid Dispenser Performance in the 4-30 µL Range by Using Optical Pathlength Measurements in Microplates. Clinical Chemistry, 44(10), 2206-2208.

Mcgown E, Hafeman D. (1998): Multichannel Pipettor Performance Verified by Measuring Pathlength of Reagent Dispensed into a Microplate. Analytical Biochemistry 258.1 155-57. Web.

Meijer, R. T., Surachno, S., Yong, S. L., Bemelman, F. J., Florquin, S., Ten Berge, I. J. M., & Schellekens, P. T. A. (2003). Treatment of acute kidney allograft rejection with a non-mitogenic CD3 antibody. Clinical and Experimental Immunology, 133(3), 485–492

Misra, S, Wahab, M, Patel, D, Armstrong D (2019). The utility of statistical moments in chromatography using trapezoidal and Simpson's rules of peak integration . Journal of Separation Science, 42(8)

Miyabe, K., Matsumoto, Y., & Guiochon, G. (2007). Peak Parking– Moment Analysis. A Strategy for the Study of the Mass-Transfer Kinetics in the Stationary Phase. Analytical chemistry, 79(5), 1970-1982.

Mo Y, Jensen K (2016). A miniature CSTR cascade for continuous flow of reactions containing solids. Reaction Chemistry & Engineering 1(5): 501-507.

Mohs R, Greig N (2017). Drug discovery and development: Role of basic biological research. Alzheimer's & Dementia : Translational Research & Clinical Interventions 3(4): 651-657.

Mollerup, J (2008). A Review of the Thermodynamics of Protein Association to Ligands, Protein Adsorption, and Adsorption Isotherms. Chemical Engineering & Technology 31(6): 864-874.

Montesinos-Cisneros R, Lucero-Acuña A, Ortega J, Guzmán R, Tejeda-Mansir A. (2007). Breakthrough performance of large proteins on ion-exchange membrane columns. Biotechnology and Applied Biochemistry 48(2): 117-125.

Müller-Späth T, Ströhlein G, Aumann L, Kornmann H, Valax P, Delegrange L, Charbaut E, Baer G, Lamproye A, Jöhnck M, Schulte M, Morbidelli M. (2011). Model simulation and experimental verification of a cation-exchange IgG capture step in batch and continuous chromatography. Journal of Chromatography A 1218(31): 5195-5204.

Ndocko, E. N., Ditz, R., Josch, J. P., & Strube, J. (2011). New Material Design Strategy for Chromatographic Separation Steps in Bio-Recovery and Downstream Processing. Chemie Ingenieur Technik, 1(83), 113-129.

Nelson, A. (2010). Antibody Fragments - Hope and Hype. mAbs, 77-83.

Nfor, B, Verheijen, P., Verhaert, P.., van der Wielen, L. Ottens, M. (2011). Model-based rational strategy for chromatographic resin selection. Biotechnology Progress, 27(6), 1629–1643.

Nfor, B. K., Ahamed, T., Pinkse, M. W. H., van der Wielen, L. A. M., Verhaert, P. D. E. M., van Dedem, G Ottens, M. (2012). Multi-dimensional fractionation and characterization of crude protein mixtures: Toward establishment of a database of protein purification process development parameters. Biotechnology and Bioengineering, 109(12), 3070–3083.

Nfor,B, Ahamed, T., van Dedem, G, Verhaert, P, van der Wielen, L., Eppink M Ottens, M. (2013). Model-based rational methodology for protein purification process synthesis. Chemical Engineering Science, 89, 185–195.

Ng C, Osuna-Sanchez H, Valéry E, Sørensen E, Bracewell D. (2012). Design of high productivity antibody capture by Protein A chromatography using an integrated experimental and modeling approach. Journal of Chromatography B 899: 116-126.

Ng, C., Rousset, F., Valery, E., Bracewell, D. G., & Sorensen, E. (2014). Design of high productivity sequential multi-column chromatography for antibody capture. Food and Bioproducts Processing, 92(2), 233–241.

Nicoud, R (2015). Chromatographic Processes: Modeling, Simulation, and Design, Cambridge University Press.

Nilsson B, Soellner M, Raines R (2005). Chemical Synthesis of Proteins. Annual review of biophysics and biomolecular structure 34: 91-118.

Nilsson, B. (2005). Aspects of modeling a preparative ion-exchange step for antibody purification. Chemical Engineering & Technology: Industrial Chemistry-Plant Equipment-Process Engineering-Biotechnology, 28(11), 1367-1374.

Norde W. (1996). Driving forces for Protein Adsorption at solid surfaces. Macromolecular Symposia 103(1): 5-18.

Ogasawara, K., & Alexander, G. C. (2019). Use of Population Pharmacokinetic Analyses Among FDA-Approved Biologics. Clinical Pharmacology in Drug Development.Orellana C , Shene C, Asenjo J. (2009). Mathematical modeling of elution curves for a protein mixture in ion exchange chromatography applied to high protein concentration. Biotechnology and Bioengineering 104(3): 572-581.

Orr V. Zhong L, Moo-Young M, Chou C. (2013). Recent advances in bioprocessing application of membrane chromatography. Biotechnology Advances 31(4): 450-465.

Osberghaus A., Drechsel, K, Hansen S., Hepbildikler S, Nath S, Haind, M., Hubbuch J. (2012). Model-integrated process development demonstrated on the optimization of a robotic cation exchange step. Chemical Engineering Science, 76, 129–139.

Özdural, A. R., Alkan, A., & Kerkhof, P. J. (2004). Modeling chromatographic columns: Non-equilibrium packed-bed adsorption with non-linear adsorption isotherms. Journal of Chromatography A, 1041(1-2), 77-85.

Pabst T, Thai J, Hunter A. (2018). Evaluation of recent Protein A stationary phase innovations for capture of biotherapeutics. Journal of Chromatography A, 1554, 45–60.

Pagkaliwangan, M., Hummel, J., Gjoka, X., Bisschops, M., & Schofield, M. (2018). Optimized continuous multi-column chromatography enables increased productivities and cost savings by employing more columns. Biotechnology Journal.

Palmqvist, N., Foster, T., Tarkowski, A., & Josefsson, E. (2002). Protein A is a virulence factor in Staphylococcus aureus arthritis and septic death. Microbial Pathogenesis, 33(5), 239–249

Pan B, Meng F, Chen X (2005). Application of an effective method in predicting breakthrough curves of fixed-bed adsorption onto resin adsorbent. Journal of hazardous materials 124(1-3): 74-80.

Pandey P, Bharadwaj R, Chen X. (2017). Modeling of drug product manufacturing processes in the pharmaceutical industry. Predictive Modeling of Pharmaceutical Unit Operations, Woodhead Publishing: 1-13.

Pasti L., Marchetti N., Guzzinati R., Catani M., Bosi V., Dondi F., Cavazzini A. (2016). Microscopic models of liquid chromatography: From ensemble-averaged information to resolution of fundamental viewpoint at single-molecule level. TrAC Trends in Analytical Chemistry, 81, 63–68.

Patel, N. P., Highton, A. Moy, R. L. (1992). Properties of Topical Sunscreen Formulations: A Review. The Journal of Dermatologic Surgery and Oncology, 18(4), 316–320

Patiha, Firdaus M, Wahyeningsah S (2018). Derivation and constants determination of the Freundlich and (fractal) Langmuir adsorption isotherms from kinetics. IOP Conference Series: Materials Science and Engineering 333: 012010.

Pathak M, Rathore A (2016). Mechanistic understanding of fouling of Protein A chromatography resin. Journal of Chromatography A 1459: 78-88.

Perez-Almodovar E, Carta G. (2009a). IgG adsorption on a new protein A adsorbent based on macroporous hydrophilic polymers. I. Adsorption equilibrium and kinetics. Journal of Chromatography A 1216(47): 8339-8347.

Perez-Almodovar E, Carta G. (2009b). IgG adsorption on a new protein A adsorbent based on macroporous hydrophilic polymers II. Pressure-flow curves and optimization for capture. Journal of Chromatography A 1216(47): 8348-8354.

Peters, Jr, W. A. (1922). The efficiency and capacity of fractionating columns. Industrial & Engineering Chemistry, 14(6), 476-479.

Pfister, D., David, L., Holzer, M., & Nicoud, R.-M. (2017). Designing affinity chromatographic processes for the capture of antibodies. Part I: A simplified approach. Journal of Chromatography A, 1494, 27–39.

Pfister D, Niclous L, Morbidelli M (2018). Continuous Biopharmaceutical Processes: Chromatography, Bioconjugation, and Protein Stability, Cambridge University Press.

PhRMA (2016), Pharmaceutical Research and Manufacturers of America. 2016 biopharmaceutical research industry profile. Washington, DC: PhRMA; April 2016.

Pirrung, S. M., van der Wielen, L. A. M., van Beckhoven, R. F. W. C., van de Sandt, E. J. A. X., Eppink, M. H. M., & Ottens, M. (2017). Optimization of biopharmaceutical downstream processes supported by mechanistic models and artificial neural networks . Biotechnology Progress, 33(3), 696–707.

Pirrung, S. M., Parruca da Cruz, D., Hanke, A. T., Berends, C., Van Beckhoven, R. F. W. C., Eppink, M. H. M., & Ottens, M. (2018). Chromatographic parameter determination for complex biological feedstocks. Biotechnology Progress.

Pirrung, S. M., Berends, C., Backx, A. H., van Beckhoven, R. F. W. C., Eppink, M. H. M., & Ottens, M. (2019). Model-based optimization of integrated purification sequences for biopharmaceuticals. Chemical Engineering Science: X, 100025.

Polson A (1950). The Some Aspects of Diffusion in Solution and a Definition of a Colloidal Particle. The Journal of Physical and Colloid Chemistry 54(5): 649-652.

Qader S, Aman A, Azhar A. (2011). Continuous Production of Dextran from Immobilized Cells of Leuconostoc mesenteroides KIBGE HA1 Using Acrylamide as a Support. Indian journal of microbiology 51(3): 279-282.

Qamer S, Bashir S, Perveen S, Seidel-Morgenstern A. (2019). Relations between kinetic parameters of different column models for liquid chromatography applying core-shell particles. Journal of Liquid Chromatography & Related Technologies 42(1-2): 16-30.

Rabe M, Verdes D, Seeger S. (2011). Understanding Protein Adsorption phenomena at solid surfaces. Advances in Colloid and Interface Science 162(1-2): 87-106.

Rader R (2008). (Re)defining biopharmaceutical. Nature Biotechnology 26: 743.

Raedler L (2016). Zarxio (Filgrastim-sndz): First Biosimilar Approved in the United States. American Health & Drug Benefits 9(Spec Feature): 150-154.

Rathore A, Velayudhan A (2002). Scale-Up and Optimization in Preparative Chromatography: Principles and Biopharmaceutical Applications, Taylor & Francis.

Rathore A, Kennedy R, O'Donnell J, Memberis L, Kaltenbrunner O (2003). Qualification of a chromatographic column: Why and how to do it. Biopharm Int, 16 30-40

Rathore A, Winkle H (2009). Quality by design for biopharmaceuticals. Nature Biotechnology 27: 26.

Rathore A, Pathak M., Ma G, Bracewell D (2015). Re-use of Protein A resin: fouling and economics. Biopharm Int, 28, 28-33.

Reader P, Shaw M (2017). Kinetic Analysis of the Multivalent Ligand Binding Interaction between Protein A/G and IgG: A Standard System Setting. J Phys Chem B. 121(38): 8919-8925.

Register, U. S. O. o. t. F. (1969). Code of Federal Regulations: 1949-1984, U.S. General Services Administration, National Archives and Records Service, Office of the Federal Register.

Rischawy, F., Saleh, D., Hahn, T., Oelmeier, S., Spitz, J., & Kluters, S. (2019). Good modeling practice for industrial chromatography: Mechanistic modeling of ion exchange chromatography of a bispecific antibody. Computers & Chemical Engineering, 106532.

Roberts, J. A., & Carta, G. (2020). Relationship between HETP measurements and breakthrough curves in short chromatography columns. Biotechnology Progress.

Rüdt, M., Gillet, F., Heege, S., Hitzler, J., Kalbfuss, B., & Guélat, B. (2015). Combined Yamamoto approach for simultaneous estimation of adsorption isotherm and kinetic parameters in ion-exchange chromatography. Journal of Chromatography A, 1413, 68-76.

Ruthven, D. M. (1984). Principles of Adsorption and Adsorption Processes, Wiley.

Ruthven, D. M. (2000). The Rectangular Isotherm Model for Adsorption Kinetics. Adsorption 6(4): 287-291.

Sakoda, A. & Wang H (1989). A new isolation and purification method for staphylococcal protein A using membrane encapsulated rabbit IgG-agarose. Biotechnology and Bioengineering 34(8): 1098-1103.

Saha, K., Bender, F., & Gizeli, E. (2003). Comparative study of IgG binding to proteins G and A: nonequilibrium kinetic and binding constant determination with the acoustic waveguide device. Analytical chemistry, 75(4), 835-842.

Said, A. S., Al-Nafea, M., Al-Ali, H., & Hamad, E. (1982). Concentration profiles and breakthrough curves in non-linear chromatography. Journal of High Resolution Chromatography, 5(12), 674–680.

Sandoval, G., Andrews, B. A., & Asenjo, J. A. (2012). Elution relationships to model affinity chromatography using a general rate model. Journal of Molecular Recognition, 25(11), 571-579.

Sarfert, F. T. & Etzel M R(1997). Mass transfer limitations in protein separations using ion-exchange membranes. Journal of Chromatography A 764(1): 3-20.

Schmidt-Traub, H. (2006). Preparative Chromatography: of Fine Chemicals and Pharmaceutical Agents, Wiley.

Schroeder, T (2006) Method for Depositing Samples in Modules and an Adapter. Patent US 20100242634 A1.

Schulte, M. & Epping , A (2005). Fundamentals and General Terminology. Preparative Chromatography, Wiley-VCH Verlag GmbH & Co. KGaA: 9-49

Schultze-Jena, A., Boon, M. A., de Winter, D. A. M., Bussmann, P. J. T., Janssen, A. E. M., & van der Padt, A. (2019). Predicting intraparticle diffusivity as function of stationary phase characteristics in preparative chromatography. Journal of Chromatography A, 460688

Schweiger, S., Hinterberger, S., & Jungbauer, A. (2017). Column-to-column packing variation of disposable pre-packed columns for protein chromatography. Journal of Chromatography A, 1527, 70–79

Seidel-Morgenstern A. (2004). Experimental determination of single solute and competitive adsorption isotherms. Journal of Chromatography A 1037(1): 255-272.

Sellers SP, Y. M. (2005). Principles of Biopharmaceutical Protein Formulation. Methods in Molecular Biology, 308, 243-263.

SenGupta, A. (2017). Ion exchange in environmental processes : fundamentals, applications and sustainable technology. Hoboken, NJ: Wiley.

Shalliker, R. A., Broyles, B. S., & Guiochon, G. (2000). Physical evidence of two wall effects in liquid chromatography. Journal of Chromatography A, 888(1-2), 1-12.

Sharma, C., Malhotra, D., & Rathore, A. S. (2011). Review of Computational fluid dynamics applications in biotechnology processes. Biotechnology Progress, 27(6), 1497–1510

Shaughnessy, A. F. (2012). Monoclonal antibodies: magic bullets with a hefty price tag. BMJ : British Medical Journal 345.

Shaw, M., & Schy, A. (1981). Diffusion coefficient measurement by the stop-flow method in a 5% collagen gel. Biophysical Journal, 34(3), 375–381. d

Shekhawat, L. K., Manvar, A. P., & Rathore, A. S. (2016). Enablers for QbD implementation: Mechanistic modeling for ion-exchange membrane chromatography. Journal of Membrane Science, 500, 86-98.

Shekhawat, L. K., Pathak, M., Sakar, J., & Rathore, A. S. (2018). Process development in the Quality by Design paradigm: Modeling of Protein A chromatography resin fouling. Journal of Chromatography A.

Shekhawat, L. K., & Rathore, A. S. (2019). An overview of mechanistic modeling of liquid chromatography. Preparative Biochemistry and Biotechnology, 1–16.

Shene, C., Lucero, A., Andrews, B. A., & Asenjo, J. A. (2006). Mathematical modeling of elution curves for a protein mixture in ion exchange chromatography and for the optimal selection of operational conditions. Biotechnology and Bioengineering, 95(4), 704–713.

Sheth, B. (2009). Characterisation of chromatography adsorbents for antibody bioprocessing (Doctoral dissertation, UCL (University College London)).

Shi, C., Gao, Z.-Y., Zhang, Q.-L., Yao, S.-J., Slater, N. K. H., & Lin, D.-Q. (2020). Model-based process development of continuous chromatography for antibody capture: a case study with twin-column system. Journal of Chromatography A, 460936.

Shukla, A. A., Hubbard, B., Tressel, T., Guhan, S., & Low, D. (2007). Downstream processing of monoclonal antibodies — application of platform approaches. Journal of Chromatography B, 848(1), 28-39.

Skidmore, G. L., Hortsmann, B. J., & Chase, H. A. (1990). Modelling single-component protein adsorption to the cation exchanger S Sepharose® FF. Journal of Chromatography A, 498, 113-128.

Sofer, G. & Hagel, L. (1997). Handbook of process chromatography : a guide to optimization, scale up, and validation. San Diego: Academic Press.

Spadiut, O., Capone, S., Krainer, F., Glieder, A., & Herwig, C. (2014). Microbials for the production of monoclonal antibodies and antibody fragments. Trends in Biotechnology, 32(1), 54–60.

Staby A, Rathore A, Ahuja S (2017). Preparative Chromatography for Separation of Proteins, Wiley.

Starzl, T. E., & Fung, J. J. (1986, August). Orthoclone OKT3 in treatment of allografts rejected under cyclosporine-steroid therapy. In Transplantation proceedings (Vol. 18, No. 4, p. 937). NIH Public Access.

Steinebach, F., Angarita, M., Karst, D. J., Müller-Späth, T., & Morbidelli, M. (2016). Model based adaptive control of a continuous capture process for monoclonal antibodies production. Journal of Chromatography A, 1444, 50-56.

Stone M, Carta G (2007). Protein adsorption and transport in agarose and dextran-grafted agarose media for ion exchange chromatography. J Chromatogr A.;1146(2):202-215.

Subramanian, G. (2013). Antibodies: Volume 1: Production and Purification, Springer US.

Sun, Y. & Yang K (2008). Analysis of mass transport models based on Maxwell-Stefan theory and Fick's law for protein uptake to porous anion exchanger. Separation and Purification Technology 60(2): 180-189.

Sunil, C. Tichener-Hooker. N. J. (2009). Review: Microscale methods for high-throughput chromatography development in the pharmaceutical industry. Journal of Chemical Technology & Biotechnology 84(7): 927-940.

Susanto A, Herrmann T, von Lieres E, Hubbuch J (2007). Investigation of pore diffusion hindrance of monoclonal antibody in hydrophobic interaction chromatography using confocal laser scanning microscopy. J Chromatogr A.;1149(2):178-188.

Susanto, A., Knieps-Grünhagen, E., von Lieres, E., & Hubbuch, J. (2008). High throughput screening for the design and optimization of chromatographic processes: assessment of model parameter determination from high throughput compatible data. Chemical Engineering & Technology: Industrial Chemistry-Plant Equipment-Process Engineering-Biotechnology, 31(12), 1846-1855.

Tao, Y., Chen, N., Carta, G., Ferreira, G., & Robbins, D. (2011). Modeling multicomponent adsorption of monoclonal antibody charge variants in cation exchange columns. AIChE Journal, 58(8), 2503–2511

Teeters, M., Benner, T., Bezila, D., Shen, H., Velayudhan, A., & Alred, P. (2009). Predictive chromatographic simulations for the optimization of recovery and aggregate clearance during the capture of monoclonal antibodies. Journal of Chromatography A, 1216(33), 6134-6140.

Tran R, Joseph J, Sinclair A, Bracewell D, Zhou Y, Titchener-Hooker N. (2007). A Framework for the Prediction of Scale-Up When Using Compressible Chromatographic Packings. Biotechnology Progress 23(2): 413-422.

Traylor, S. J., Xu, X., Li, Y., Jin, M., & Li, Z. J. (2014). Adaptation of the pore diffusion model to describe multi-addition batch uptake high-throughput screening experiments. Journal of Chromatography A, 1368, 100–106.

Treier, K., Hansen, S., Richter, C., Diederich, P., Hubbuch, J., & Lester, P. (2012a). High-throughput methods for miniaturization and automation of monoclonal antibody purification processes. Biotechnology Progress, 28(3), 723–732.

Treier, K., Berg, A., Diederich, P., Lang, K., Osberghaus, A., Dismer, F., & Hubbuch, J. (2012b). Examination of a genetic algorithm for the application in high-throughput downstream process development. Biotechnology journal, 7(10), 1203-1215.

Trexler-Schmidt, M., Sze-Khoo, S., Cothran, A. R., Thai, B. Q., Sargis, S., Lebreton, B., ... & Blank, G. S. (2009). Purification strategies to process 5 g/L titers of monoclonal antibodies. BioPharm Intl Supplement March, 8-15.

Trygg, J., Holmes, E., & Lundstedt, T. (2007). Chemometrics in metabonomics. Journal of proteome research, 6(2), 469-479.

Tyn, M. T. & T. W. Gusek (1990). Prediction of diffusion coefficients of proteins. Biotechnology and Bioengineering 35(4): 327-338.

UCB. (2014). Our History, Blockbusters and Biopharma. [ONLINE] Available at: http://www.ucb.com/our-company/history. [Accessed 12 October 15].

Vajda, J., Conze, W., & Müller, E. (2015). Kinetic plots in aqueous size exclusion chromatography of monoclonal antibodies and virus particles. Journal of Chromatography A, 1426, 118-125.

Van Deemter, J. J., Zuiderweg, F. J., & Klinkenberg, A. V. (1956). Longitudinal diffusion and resistance to mass transfer as causes of nonideality in chromatography. Chemical Engineering Science, 5(6), 271-289.

Van Loghem, E., Frangione, B., Recht, B., & Franklin, E. C. (1982). Staphylococcal protein A and human IgG subclasses and allotypes. Scandinavian journal of immunology, 15(3), 275-278.

Velayudhan, A. & M. Ladisch (2006). Plate models in chromatography: Analysis and implications for scale-up.

von Lieres, E. & J. Andersson (2010). A fast and accurate solver for the general rate model of column liquid chromatography. Computers & Chemical Engineering 34(8): 1180-1191.

Wahome, J., Weichang, Z., & Kundu, A. (2008). Impact of lot-to-lot variability of cation exchange chromatography resin on process performance. Biopharm international, 21(5).

Walsh, G. (2014). Biopharmaceutical benchmarks 2014. Nature Biotechnology 32: 992.

Wang, G. Q., Yuan, X. G., & Yu, K. T. (2005). Review of Mass-Transfer Correlations for Packed Columns*. Industrial & Engineering Chemistry Research, 44(23), 8715–8729.

Wang, G., Briskot, T., Hahn, T., Baumann, P., & Hubbuch, J. (2017a). Estimation of adsorption isotherm and mass transfer parameters in protein chromatography using artificial neural networks. Journal of Chromatography A, 1487, 211-217.

Wang, G., Briskot, T., Hahn, T., Baumann, P., & Hubbuch, J. (2017b). Root cause investigation of deviations in protein chromatography based on mechanistic models and artificial neural networks. Journal of Chromatography A, 1515, 146–153.

Weinberg, J., Zhang, S., Crews, G., Healy, E., Carta, G., & Przybycien, T. (2017). Polyclonal and monoclonal IgG binding on protein A resins—Evidence of competitive binding effects. Biotechnology and Bioengineering, 114(8), 1803-1812.

Welsh, J. P., Petroff, M. G., Rowicki, P., Bao, H., Linden, T., Roush, D. J., & Pollard, J. M. (2014). A practical strategy for using miniature chromatography columns in a standardized high-throughput workflow for purification development of monoclonal antibodies. Biotechnology Progress, 30(3), 626–635.

Wenger M (2010). Micro-tip chromatography; a route to an integrated strategy for high throughput bioprocess development, UCL (University College London).

Wenger, M. D., DePhillips, P., Price, C. E., & Bracewell, D. G. (2007). An automated microscale chromatographic purification of virus-like particles as a strategy for process development. Biotechnology and applied biochemistry, 47(2), 131-139.

Westerberg, K., Broberg-Hansen, E., Sejergaard, L., & Nilsson, B. (2013). Model-based risk analysis of coupled process steps. Biotechnology and Bioengineering, 110(9), 2462–2470.

Whitcomb, P. J,. Anderson M J (2004). RSM Simplified: Optimizing Processes Using Response Surface Methods for Design of Experiments, Taylor & Francis.

Wiendahl, M., Schulze Wierling, P., Nielsen, J., Fomsgaard Christensen, D., Krarup, J., Staby, A., & Hubbuch, J. (2008). High throughput screening for the design and optimization of chromatographic processes–miniaturization, automation and parallelization of breakthrough and elution studies. Chemical Engineering & Technology: Industrial Chemistry-Plant Equipment-Process Engineering-Biotechnology, 31(6), 893-903.

Wilson, E. J. & Geankoplis C J (1966). Liquid Mass Transfer at Very Low Reynolds Numbers in Packed Beds. Industrial & Engineering Chemistry Fundamentals 5(1): 9-14.

Wilson, J. L., Scott, I. M., & McMurry, J. L. (2010). Optical biosensing: Kinetics of protein A-IGG binding using biolayer interferometry. Biochemistry and Molecular Biology Education, 38(6), 400-407.

Wormell, P., & Rodger, A. (2013). Absorbance Spectroscopy: Overview. Encyclopedia of Biophysics, 23–25.

Yadav, S., Sreedhara, A., Kanai, S., Liu, J., Lien, S., Lowman, H., ... & Shire, S. J. (2011). Establishing a link between amino acid sequences and self-associating and viscoelastic behavior of two closely related monoclonal antibodies. Pharmaceutical research, 28(7), 1750-1764.

Yalkowsky, S. & Yan. (2003). Handbook of aqueous solubility data. Boca Raton, Fla: CRC Press.

Yamamoto, S., Nakanishi, K., Matsuno, R., & Kamikubo, T. (1978). Dispersion mechanism in gel chromatography of proteins. Agricultural and Biological Chemistry, 42(5), 963-970.

Yamamoto, S., Nakanishi, K., Matsuno, R., & Kamikubo, T. (1983a). Ion exchange chromatography of proteins?prediction of elution curves and operating conditions. I. Theoretical considerations. Biotechnology and Bioengineering, 25(6), 1465–1483.

Yamamoto, S., Nakanishi, K., Matsuno, R., & Kamijubo, T. (1983b). Ion exchange chromatography of proteins?predictions of elution curves and operating conditions. II. Experimental verification. Biotechnology and Bioengineering, 25(5), 1373–1391.

Yang, L., Biswas, M. E., & Chen, P. (2003). Study of binding between protein A and immunoglobulin G using a surface tension probe. Biophysical journal, 84(1), 509-522.

Yang, H. & Etzel A (2003). Evaluation of Three Kinetic Equations in Models of Protein Purification Using Ion-Exchange Membranes. Industrial & Engineering Chemistry Research 42(4): 890-896.

Yao, Y. &. Lenhoff A (2006). Pore size distributions of ion exchangers and relation to protein binding capacity. Journal of Chromatography A 1126(1-2): 107-119.

Young, M. E., Carroad, P. A., & Bell, R. L. (1980). Estimation of diffusion coefficients of proteins. Biotechnology and bioengineering, 22(5), 947-955.

Zhang, S., Xu, K., Daniels, W., Salm, J., Glynn, J., Martin, J., … Carta, G. (2015). Structural and functional characteristics of virgin and fouled Protein A MabSelect resin cycled in a monoclonal antibody purification process. Biotechnology and Bioengineering, 113(2), 367–375.

Zhang, L., Parasnavis, S., Li, Z., Chen, J., & Cramer, S. (2019). Mechanistic modeling based process development for monoclonal antibody monomer-aggregate separations in multimodal cation exchange chromatography. Journal of Chromatography A.